STRATEGIES TO IMPROVE ELECTROCHEMICAL DETECTION OF NITRIC OXIDE IN BIOLOGICAL ENVIRONMENTS

Micah Daniel Brown

A dissertation submitted to the faculty at the University of North Carolina at Chapel Hill in partial fulfillment of the requirements for the degree of Doctor of Philosophy in the Department of Chemistry (Analytical Chemistry).

Chapel Hill
2018

Approved by:

Mark H. Schoenfisch

James W. Jorgenson

R. Mark Wightman

William A. Marston

Koji Sode

ABSTRACT

Micah Daniel Brown: Strategies to Improve Electrochemical Detection of Nitric Oxide in Biological Environments
(Under the direction of Mark H. Schoenfisch)

Nitric oxide (NO) is a gaseous molecule of vast biological significance whose activity is likely to be concentration-dependent. As our understanding of this molecule becomes more nuanced and precise, so too must detection strategies evolve to detect NO with greater precision and accuracy. Spectroscopic techniques are able to measure NO with high specificity, but the only technique unhindered by complex instrumentation and the requirement for additional reagents, *and* able to measure NO directly in situ, is electrochemistry. However, bare electrodes are unable measure NO with sufficient selectivity and sensitivity, particularly in biological environments, necessitating the use of transducer surface modifiers to improve performance.

Herein, systematic evaluations and comparisons of electrochemical NO sensor modifications were carried out. Electropolymerized films (EPFs) represent a class of selectivity-enhancing membranes favorable for their reproducible and self-terminating depositions. Six different monomers were evaluated for their permselectivity characteristics for NO against a panel of electroactive biological interferents. After tailored optimizations of their deposition parameters, polymers were also evaluated for their anti-fouling properties in simulated wound fluid. In addition to EPFs, another common strategy to improve NO sensor performance is the incorporation of metallophthalocyanine (MPc) electrocatalysts. Four MPc macrocycles (M = iron, cobalt,

nickel, and zinc) previously determined to have the highest electrocatalytic activity towards NO oxidation were evaluated for their selectivity characteristics. The ability to specifically coordinate with NO at the metal center (as opposed to weak physisorption on the aromatic periphery) proved an adequate predictor of selectivity findings.

Based on these evaluations of different modifiers, a solid-state electrochemical NO sensor was designed for long-term use in proteinaceous media. With extensive characterizations of sensocompatibility, the final NO sensor was capable of high sensitivity and selectivity retention with continuous operation in culture media. The sensor was then used to successfully interrogate the temporal (> 24 h) and spatial concentration profiles of macrophage NO release under neutral and pro-inflammatory stimulated conditions. Lastly, hydrogen sulfide (H_2S) is another gasotransmitter responsible for mediating many of the same biological processes as NO, and may either upregulate or inhibit NO production in a manner likely to be concentration-dependent. An EPF-modified, solid-state electrode was therefore developed for selective detection of H_2S for subsequent incorporation into a NO/H_2S dual-sensor.

This work is dedicated to my parents, Kurt and Brenda,
who filled me with curiosity and gave me the tools to explore.

TABLE OF CONTENTS

LIST OF TABLES

LIST OF FIGURES

LIST OF ABBREVIATIONS AND SYMBOLS

%	percent
°	degree(s)
°C	degree(s) Celsius
±	margin of error
<	less than
>	greater than
|	redox couple
~	approximately
≈	approximately equal to
≤	less than or equal to
≥	greater than or equal to
17FTMS	(heptadecafluoro-1,1,2,2,-tetrahydrodecyl)trimethoxysilane
3D	3-dimensional
3DG	3-dimensional graphene
5-HIAA	5-hydroxyindole-3-acetic acid
5-HT	serotonin
5A1N	5-amino-1-naphthol
AA	L-ascorbic acid
AB	acetate buffer; acetylene black
Ach	acetylcholine
aCSF	artificial cerebrospinal fluid
Ag	silver

Ag|AgCl	silver-silver chloride reference electrode
AlbSNO	*S*-nitrosoalbumin
AP	acetaminophen
APBA	3-aminophenylboronic acid
APTES	(3-aminopropyl)triethoxysilane
Ar	argon
ATCC	American Type Culture Collection
Au	gold
BMIMPF6	1-butyl-3-methylimidazolium
BSA	bovine serum albumin
C	coulomb(s)
CA	cellulose acetate
ca.	*circa*; around
Ca^{2+}	calcium cation
CAS	catalase
CC	chronocoulometry
CE	counter electrode
CEC	cyanoethyl cellulose
CF	carbon fiber
cGMP	cyclic guanosine monophosphate
cm	centimeter(s)
CO	carbon monoxide
Co	cobalt

CPA	constant potential amperometry
CS	chitosan
CTAB	hexadecyltrimethylammonium bromide
CV	cyclic voltammetry
cyt *c*	cytochrome c
Cys	cysteine
CysNO	*S*-nitrosocysteine
D	diffusion coefficient
d	day(s)
D.C.	diffusion-controlled
DA	dopamine
DC	direct current
dec	decade(s)
DFT	density functional theory
DHA	dehydroascorbic acid
DI	deionized
dia.	diameter
dim.	dimension(s)
DMEM	Dulbecco's Modified Eagle Medium
DOPAC	3,4-dihydroxyphenylacetic acid
DPV	differential pulse voltammetry
e^-	electron(s)
e.g.	*exempli gratia*; for example

E_a	anodic peak potential
E_{appl}	applied potential
EASA	electroactive surface area
ECF	extracellular fluid
ECM	extracellular matrix
EDC	*N*-(3-dimethylamino-propyl)-*N*'-ethylcarbodiimide
EDTA	ethylenediaminetetraacetic acid
eNOS	endothelial nitric oxide synthase
EPF	electropolymerized film
EPR	electron paramagnetic resonance spectroscopy
Eq.	equation
ET	electron transfer
et al.	*et alii*; and others
etc.	*et cetera*; and so forth
ETH1001	calcium ionophore
EtOH	ethanol
eV	electron-volt(s)
Fb	fibrinogen
FBS	fetal bovine serum
Fe	iron
FeTCP	iron(III)*meso*-tetra(4-carboxyphenyl)porphyrin
G	graphene
g	gram(s)

GC	glassy carbon
Glu	glutamic acid
GO	graphene oxide
GSH	glutathione
GSNO	*S*-nitrosoglutathione
h	hour(s)
H^+	proton
H_2O	water
H_2O_2	hydrogen peroxide
H_2S	hydrogen sulfide
Hb	oxyhemoglobin
HBSS	Hank's Balanced Salt Solution
HCF	hexacyanoferrate
HCl	hydrochloric acid
HL60	human leukemia cell line
HNG	hierarchical nanoporous gold
HNO_2	nitrous acid
HS^-	hydrosulfide
HUVEC	human umbilical vein endothelial cells
HVA	homovanillic acid
i.e.	*id est*; in other words
IFN-γ	interferon-gamma
iNOS	inducible nitric oxide synthase

Ir	iridium
IS	internal solution
ISE	ion-selective electrode
ITO	indium tin oxide
j	interferent
j_{NO}	NO current flux
K^+	potassium cation
k^0	standard heterogeneous electron transfer coefficient
KCl	potassium chloride
K_m	Michaelis-Menton constant
K_m^{app}	apparent Michaelis-Menton constant
KOH	potassium hydroxide
k_s	heterogeneous electron transfer rate constant
L-Arg	L-arginine
L-NAME	*N*-Nitroarginine methyl ester
LOD	limit of detection
log$k_{NO,j}$	selectivity coefficient for NO over interferent j
LPS	lipopolysaccharide
LSV	linear sweep voltammetry
m	meter(s)
M	molar
m-PD	*meta*-phenylenediamine
Mb	myoglobin

MEM	Minimum Essential Media
MeOH	methanol
mg	milligram(s)
min	minute(s)
mM	millimolar
mm	millimeter(s)
mmol	millimole(s)
mol	moles(s)
MoS_2-NH_2	amine-modified molybdenum disulfide
MP	metalloporphyrin; microperoxidase
MPc	metallophthalocyanine
ms	millisecond(s)
MTMOS	methyltrimethoxysilane
mV	millivolt(s)
MWCNT	multiwalled carbon nanotube
MΦ	macrophage
MΩ	megaohm(s)
n	natural number
N	normal
N-G	nitrogen-doped graphene
n.a.	not applicable
n.q.	not quantified
n.r.	not reported

N_2	nitrogen
nA	nanoampere(s)
Na_2S	sodium sulfide
NaCl	sodium chloride
NADPH	nicotinamide adenine dinucleotide phosphate
NaOH	sodium hydroxide
NC	nanocube
NCstr	nanocluster
NED	*N*-(1-naphthyl)ethylenediamine dihydrochloride
NH_3	ammonia
NH_4^+	ammonium cation
NH_4OH	ammonium hydroxide
NHS	*N*-hydro-sulfosuccinimide sodium salt
Ni	nickel
nm	nanometer(s)
nM	nanomolar
nNOS	neuronal nitric oxide synthase
NO	nitric oxide
NO^-	nitroxyl anion
NO^+	nitrosonium cation
NO_2	nitrogen dioxide
NO_2^-	nitrite
NO_3^-	nitrate

NOS	nitric oxide synthase
NO_X	collective nitrogen oxide species
NP	nanoparticle
NR	nanorod
NYPA	naphthalen-1-ylmethylphosphonic acid
Ø	diameter
o-PD	*ortho*-phenylenediamine
O_2	oxygen
O_2^-	superoxide
OH^-	hydroxide
$ONOO^-$	peroxynitrite
p	probability that the null hypothesis is true
P	permeability
p-PD	*para*-phenylenediamine
pA	picoampere(s)
PADA	poly(acrylamide-co-diallyldimethylammonium chloride)
PB	phosphate buffer
PBS	phosphate buffered saline
PBZ	2-(2-pyridyl)benzimidazole
PDMS	poly(dimethylsiloxane)
PEA	palmitoylethanolamide
pH	power of hydrogen
p*K*a	acid dissociation constant

PLEDGE	poly(ethylene glycol) diglycidyl ether
PLL	poly(L-lysine)
pM	picomolar
PMA	*para*-methoxyamphetamine
ppb	parts per billion
ppm	parts per million
Pt	platinum
PTFE	polytetrafluoroethylene
PVD	physical vapor deposition
q.	quantitative
QC	quaternized cellulose
RE	reference electrode
ref.	reference
ret.	retention
RGD	arginylglycylaspartic acid
rGO	reduced graphene oxide
RNS	reactive nitrogen species
ROS	reactive oxygen species
RPMI	Roswell Park Memorial Institute media
RSNO	*S*-nitrosothiol species
RT	room temperature
s	second(s)
S	sensitivity

S-G	sulfur-doped graphene
S.C.	surface-controlled
S/N	signal-to-noise ratio
SA	surface area
salen	bis(2-hydroxy-benzaldehyde) ethylenediimine
SAM	self-assembled monolayer
SECM	scanning electrochemical microscopy
sGC	soluble guanylate cyclase
Sn	tin
SOD	superoxide dismutase
SWF	simulated wound fluid
SWV	squarewave voltammetry
t	time
T-C	transparent carbon
T-CUA	transparent carbon ultramicroelectrode array
TAPc	tetra-amine phthalocyanine
tech.	technique
Ti	titanium
TPDP	tris(2,4,6-tribromophenoxy)dichlorophosphorane
TTCA	5,2':5',2''-terthiophene-3'-carboxylic acid
U.S.	United States
UA	uric acid
UME	ultramicroelectrode

UV	ultraviolet
V	volt(s)
v/v	volume-to-volume ratio
vs.	versus
W	watt(s)
w/v	weight-to-volume ratio
WE	working electrode
XG	xerogel
XPS	X-ray photoelectron spectroscopy
Zn	zinc
α	charge transfer coefficient
Δ	change in
δ	partial charge
μA	microampere(s)
μC	microcoulomb(s)
μg	microgram(s)
μL	microliter(s)
μm	micrometer(s)
μM	micromolar
μmol	micromole(s)
ν	scan rate
π*	antibonding pi-orbital

CHAPTER 1: A CRITICAL OVERVIEW OF RECENT ADVANCES IN ELECTROCHEMICAL NITRIC OXIDE DETECTION[1]

1.1 Introduction

Since the discovery that nitric oxide (NO) was the endothelial derived relaxation factor, knowledge of the true breadth of NO's activity in mammalian physiology has rapidly expanded.[1] With roles to play in mediating the immune response,[2,3] wound healing,[4,5] vasodilation,[1,6] cancer biology,[7] and neurotransmission,[8,9] this diatomic radical species—once only recognized as an environmental pollutant—is in fact vital to homeostasis. As our understanding of NO becomes more nuanced, it has become clear that the many functions of NO are activated in a concentration-dependent manner. In the immune system, low concentrations of NO exhibit anti-inflammatory effects by suppressing T helper cell proliferation,[10] while higher concentrations elicit a robust pro-inflammatory response in the presence of infection.[2,3,11,12] In cutaneous injury, high concentrations of NO can lead to prolonged oxidative stress and wound chronicity,[5,13,14] while low concentrations mediate the transition to proliferative stages of healing, encouraging angiogenesis and tissue regranulation.[15,16] The concentration-dependence of NO's activity and bioavailability is also significant in a number of different pathologies, including sepsis,[17] Alzheimer's,[18] Parkinson's,[19,20] atherosclerosis,[21] hypotension,[22] and ischemia-reperfusion injury.[23]

---

[1] This chapter was adapted in part from an article that has been submitted for publication. The original citation is as follows: Brown, M. D.; Schoenfisch, M. H. Electrochemical nitric oxide sensors: design principles. *submitted.*

[2] This chapter was adapted in part from an article that has already been published. The

Our understanding of the words 'high' and 'low' with respect to NO concentration is admittedly imprecise, commonly based on indirect immunohistochemical analysis of relevant enzymes (i.e., nitric oxide synthases; NOS) or the measurement of stable oxidative byproducts (i.e., NO_x species, nitrite and nitrate) that accumulate in vivo.[24-26] In order to deepen our understanding of NO—its basal concentrations, the roles it plays in specific disease states, and how it can activate seemingly opposing biological processes—direct and precise measurement strategies are essential. Moreover, the ability to harness NO as a biomarker and therapeutic agent necessarily relies on accurate quantitation.

Traditionally, spectroscopy and electrochemistry are the only techniques that have enabled *direct* detection of NO.[27] In chemiluminescent methods, reaction of NO with ozone produces excited-state nitrogen dioxide, which emits a detectable photon upon relaxation to the ground state. Adducts of NO formed with specialized dyes or spin-traps allow fluorescent and electron paramagnetic resonance (EPR) detection, respectively. In total, spectroscopic techniques offer high sensitivity (pM) and inherent selectivity, but are notably constrained by the need for complex instrumentation and additional reagents. Irreversible adduct formation in some cases also prevents monitoring NO fluctuations in real time.[28] Exploiting NO's ability to be oxidized or reduced, electrochemical sensors are better suited to in situ, biological monitoring of NO, benefitting from limited sample perturbation, freedom from exogenous reagents, superior spatial and temporal resolution, and easily miniaturized detection platforms.[29-31]

Though electrochemical techniques are amenable to biological systems, a number of key considerations must inform the design and application of sensors utilizing such techniques. Nitric oxide is a radical species and therefore highly reactive, particularly with

oxygen and superoxide.[32,33] Additional scavenging/inactivation by heme-containing proteins (e.g., hemoglobin), free metals, and thiols limit the half-life of NO in physiological media to an estimated 10 seconds (and diffusion to hundreds of micrometers).[34,35] Coupled with the broad range of biologically relevant NO concentrations (pM-μM), assurances must be made that an electrochemical sensor have suitable response time, sensitivity, and detection limit (LOD) for the given application.[36] Additionally, there are a number of electroactive biological species that can interfere with accurate detection of NO. Electrochemical sensors must therefore be modified to meet these specific challenges of biological NO measurement.

With nearly thirty years since the development of the first electrochemical NO sensor by Shibuki et al.,[37] there have been many incremental improvements to sensor construction and modification.[29-31] The last decade in particular has witnessed the growth of multi-analyte detection platforms, ultramicroelectrode arrays, and microfluidic devices to improve analytical performance and accommodate cellular measurement of NO. Moreover, new transducer modifications (e.g., electrocatalysts, selectively permeable membranes, protective and biocompatible coverings) have recently been discovered or adapted to electrochemical NO sensors. Herein, we provide a critical overview of the last decade of electrochemical NO sensors, their construction, and transducer modification. Focus has been placed on rigorous, quantitative evaluations of analytical performance with respect to selectivity, sensitivity, and application to biological systems.

1.2 Improvements to selectivity

Electrochemical detection of NO is most often achieved through electrooxidative means. Although electroreduction of NO is feasible, low sensitivity at physiological pH and major interference from dissolved oxygen have largely limited its application to NO sensors

modified by heme-containing biomolecules (*see* Section 1.2.2).[29,30,38] Oxidation of NO proceeds first through a transfer of one electron to the electrode sink (Eq. 1).

$$NO \rightarrow NO^+ + e^- \quad \text{(Eq. 1)}$$
$$NO^+ + OH^- \rightarrow HNO_2 \quad \text{(Eq. 2)}$$
$$HNO_2 + H_2O \rightarrow NO_3^- + 2e^- + 3H^+ \quad \text{(Eq. 3)}$$

The transient nitrosonium cation (NO^+) is a relatively strong Lewis acid and in the presence of hydroxide reacts to form nitrous acid (i.e., protonated nitrite; Eq. 2).[31] If the electrode is biased at a sufficiently positive potential, HNO_2 can be further oxidized to nitrate (NO_3^-) in a two-electron reaction (Eq. 3). Depending on the electrode material, oxidation of NO must be driven at potentials generally ranging from +0.7 to +1.0 V *vs*. Ag|AgCl. Such large overpotentials are also capable of oxidizing a number of electroactive biological molecules, posing a significant challenge to sensor selectivity, and therefore accuracy. Table 1 lists common biological interferents and their basal concentrations in vivo.

The choice in electrochemical technique affords some control over selectivity. Potentiodynamic techniques, such as linear sweep voltammetry (LSV), cyclic voltammetry (CV), and differential pulse voltammetry (DPV), aid in discriminating the anodic peak of NO from lower-potential interferents. However, the greater sensitivity and temporal resolution afforded by potentiostatic techniques, including constant potential amperometry (CPA) and chronocoulometry (CC), are more favorable for biological applications. Modification of the electrode design is therefore necessary to eliminate Faradaic contributions of interferent species and improve sensor selectivity.

Table 1.1 Electroactive biological interferents.[a]

Interferent	Charge (pH 7.4)	Concentration[b]	Location	$\log k_{NO,j}$[c]
Acetaminophen (AP)	0	130 μM[d]	Plasma	−5.1
Ammonium/Ammonia (NH_4^+/NH_3)	+1/ 0 (pK_a 9.2)	30 μM	Blood	−4.5
L-Ascorbic acid (AA)	−1	43 μM	Serum	−4.6
Carbon monoxide (CO)	0	1.5 μM	Kidney	−3.2
Dopamine (DA)	+1	2.0 nM	Plasma	−0.3
Hydrogen peroxide (H_2O_2)	0	3 μM	Brain ECF[e]	−3.5
Hydrogen sulfide/Hydrosulfide (H_2S/HS^-)	0 /−1 (pK_a 6.6)	100 nM	Blood	−2.0
Nitrite (NO_2^-)	−1	20 μM	Plasma	−4.3
Peroxynitrite ($ONOO^-$)	−1	30 pM	Endothelium	1.5
Serotonin (5-HT)	+1	1.14 μM	Blood	−3.1
Uric Acid (UA)	−1	470 μM	Serum	−5.7

[a]Adapted from references 29 and 30 and references cited therein. [b]Upper bound of reported range. [c]Selectivity coefficient over interferent *j* calculated from Eq. 4 required to measure 10 nM of NO with 90% accuracy. [d]Therapeutic concentration. [e]Extracellular fluid.

1.2.1 Chemical modification

By far the most common means of imparting selectivity to an electrochemical sensor is chemical modification on or near the transducer surface. These modifications primarily exploit the physical properties of NO (e.g., small size, neutral charge, lipophilicity) to permit NO selective access to the electroactive surface while obstructing interferent species. Selectivity coefficients provide a useful means of quantifying a sensor's selectivity against a particular interferent *j* according to Eq. 4.[39] Expressed as logarithmic ratio of interferent and NO sensitivities (S_j and S_{NO}, respectively), more negative coefficients are indicative of greater selectivity.

$$\log k_{NO,j} = \log\left(\frac{S_j}{S_{NO}}\right) \qquad \text{(Eq. 4)}$$

Given that many biological interferents are present at concentrations orders of magnitude greater than NO, large selectivity coefficients are required to achieve accurate NO measurement (Table 1). For instance, a selectivity coefficient of −4 against nitrite (NO_2^-) is needed to quantify 10 nM of NO with 90% accuracy, corresponding to 10,000-fold greater sensitivity towards NO than NO_2^-. Clearly, *quantitative* measurements of selectivity against pertinent interferents are essential to the overall analytical assessment of a NO sensor, although such measurements are surprisingly rare. Recent electrochemical NO sensors incorporating chemical modification, and for which quantitative evaluations of selectivity were undertaken, are summarized in Table 2.

Electrochemical NO sensors can be broadly divided into two types of construction: Shibuki and solid (Figure 1.1.). The Shibuki-type sensor emerged first, based on the Clark-type O_2 sensor, and comprised a micropipette containing an internal electrolyte solution, a solid platinum (Pt) working electrode, silver reference, and a gas-permeable chloroprene

membrane.[37] Small gaseous species such as NO and O_2 were able to permeate the membrane while larger interferents were blocked. There are only a few examples of Shibuki-type sensors recently developed,[40-42] largely attributable to the difficulties associated with internal solutions (e.g., leakage, evaporation, replacement, and poor miniaturizability). Jensen et al. fabricated a NO sensor with an alkaline internal solution, Pt working electrode, and polytetrafluoroethylene (PTFE) membrane to improve selectivity against carbon monoxide (CO).[43] Discrimination against CO is particularly challenging given its similar physicochemical properties to NO. Polarization at +0.7 V *vs*. Ag|AgCl formed Pt oxides on the transducer surface in the alkaline environment, effectively inhibiting adsorption of CO. Unlike NO, adsorption is a key step in the electrooxidation mechanism of CO on Pt,[44] and prevention of this process allowed the sensor to achieve a −2.1 selectivity coefficient for NO against CO. In this instance, chemical modification *on* (Pt oxide formation) and *near* (PTFE membrane) the transducer were used to enhance selectivity.

The size of the Shibuki-type sensor (>150 μm) was not amenable to single-cell analysis, motivating the construction of solid-type sensors. Applying chemical modifications directly to the electrode surface allowed the internal solution to be eliminated and sensor dimensions to be greatly reduced. Perhaps the most famous example of a solid-type NO sensor was developed by Malinski et al., in whose pivotal work a carbon fiber electrode of ~0.5 μm tip diameter was modified with electropolymerized nickel(II)porphyrin and a Nafion ionomer.[45] With a low detection limit of 10 nM and high selectivity against nitrite (selectivity coefficient of −3.3 based on provided data), they were then able to measure the NO release of single endothelial and smooth muscle cells under stimulation with bradykinin. As a result, chemically modified solid-type sensors have dominated the NO research sphere.

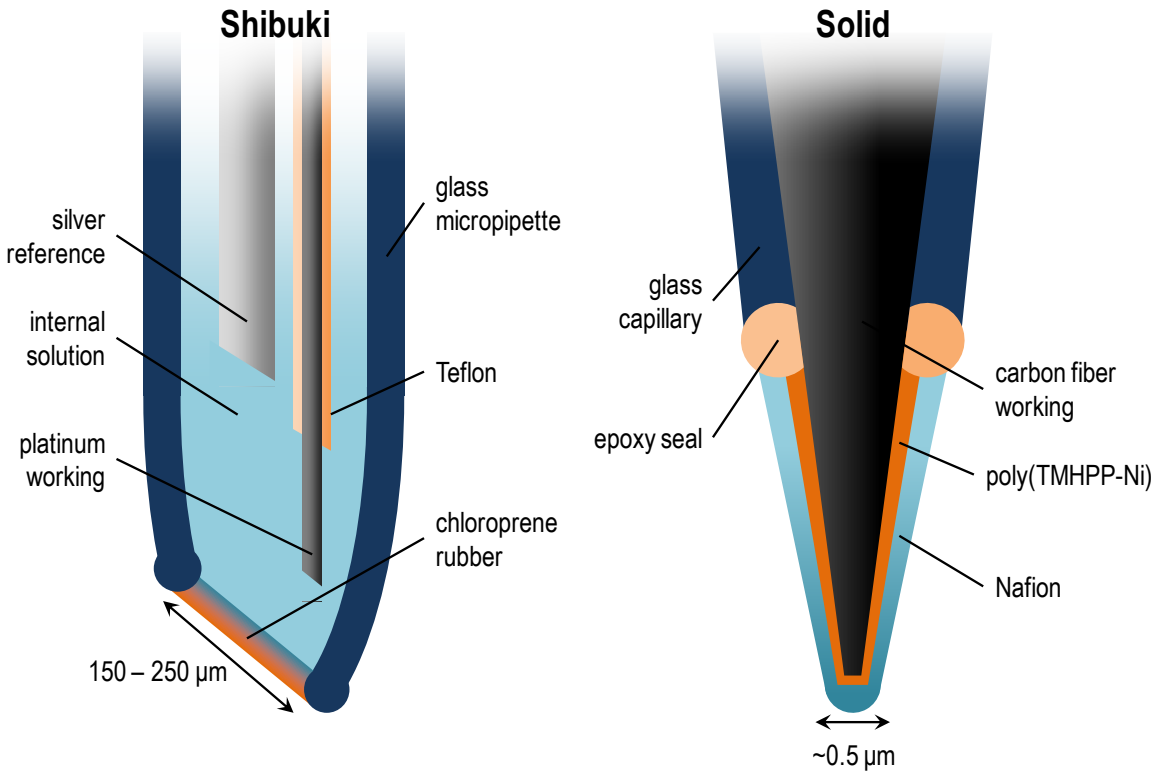

Figure 1.1 Representative Shibuki- and solid-type electrochemical NO sensor designs. TMHPP-Ni: tetrakis(3-methoxy-4-hydroxyphenyl)-nickel porphyrin.

Since its initial use in a solid-type construction, Nafion has proven to be the most commonly applied selectivity-imparting membrane for electrochemical NO sensors.[31,38,46,47] The highly fluorinated, Teflon-like backbone can be permeated by NO while rejecting bulkier interferents, and the negatively-charged sulfonate pendant groups repel critical anionic species (e.g., AA, UA, and NO_2^-; Table 1). Nitrite in particular, in spite of its similar size to NO, is well rejected on the basis of charge-repulsion. Recently, Wynne et al. have meticulously evaluated the selectivity performance of Nafion films as function of different deposition procedures on Pt wires (i.e., pre-coats and annealing) and have achieved moderate selectivity against a wide range of tested interferents (Table 2).[48] Moreover, they noted a phenomenon with ascorbate in which small amounts may permeate the film and be oxidized to dehydroascorbic acid (DHA) at the electrode surface. Once there, DHA remains within the membrane and helps to block further influx of AA, improving selectivity for NO.[48,49] Given the differences in nitrite selectivity reported by Wynne, Malinski, and others, it is clear that the performance of Nafion is highly depended on deposition procedure and underlying electrode substrate (Table 2). Moreover, based on a systematic evaluation of sensor sensitivity and hydrophobicity with different membrane modifications, Pontié et al. have suggested that the hydrophilic sulfonates of Nafion may force NO to concentrate within more hydrophobic domains, limiting diffusion and reducing sensitivity.[50] Lastly, selectivity against neutral and positively-charged interferents remains a significant challenge (Table 1).[51]

In place of Nafion, purely hydrophobic membranes have helped to further improve selectivity for NO in the last decade. A TeflonAF-modified Celgard membrane was used by Cha et al. to allow highly selective diffusion of NO from a microfluidic channel to a gold-hexacyanoferrate-modified electrode in an adapted Shibuki-type arrangement.[52] The resulting

sensor had excellent selectivity coefficients of −5.9 against both NO_2^- and AA and was able to monitor long-term (>16 h) NO release from cultured macrophages stimulated with endotoxin. As with Nafion, the highly fluorinated backbone of TeflonAF is conducive to NO diffusion, but even without sulfonate pendant groups, TeflonAF is still capable of rejecting anionic species. This comparison suggests that size-exclusion and hydrophobic-interactions supersede charge-repulsion as the most impactful NO sieving mechanisms. Work by Shin, Lee, and Schoenfisch and colleagues has pioneered the use of fluorinated xerogel membranes for their NO-permselective traits in several recent electrochemical sensor configurations.[42,53-55] Based on standard sol-gel chemistry, hydrolysis and co-condensation of fluorinated and backbone alkoxysilane precursors under acidic conditions yields a viscous sol solution than can be applied to micro- or planar electrodes. A rigid monolith forms after curing the sol, and excellent selectivity for NO against a range of anionic, cationic, and neutral interferents of different sizes can be achieved (Table 2).

Gas-permeable polymeric and gel membranes can be applied to different electrode geometries through simple casting or dip-coating procedures. However, depositions of this sort are prone to variations in thickness, affecting sensor sensitivity in turn. In contrast, electropolymerized films (EPFs) can be deposited with high uniformity and reproducibility to practically any electroactive surface.[30,38] Briefly, monomers are oxidized to radical cations by placing the electrode in a monomer solution and applying a sufficiently positive potential. Repeated radical coupling and oxidation reactions lead to oligomer formation. Once the size of the oligomer exceeds solubility, precipitation onto the electrode surface occurs, building the EPF. Non-conducting and some semiconducting polymers passivate the electrode surface with precipitation, preventing further oxidations of monomers and effectively self-

terminating film growth. The growth of conducting polymers, which relay charge to the outer reaches of the film and continue to oxidize monomers, can be easily observed (and controlled) with the passage of current under CV or CPA techniques. These mechanisms of EPF formation result in both reproducible deposition and sensor performance.

Electropolymerized films were first optimized and used to impart H_2O_2 selectivity in first generation glucose biosensors,[56-59] but the similar size and neutral charge of NO has since prompted application to electrochemical NO sensors. Recently, a layering of poly(eugenol) and poly(phenol) was used by Quinton et al. to achieve good selectivity against anionic interferents,[60] and polymers resulting from *o*- and *m*-phenylenediamine monomers have been used in several layered sensor designs.[48,61,62] Because EPFs are most commonly used in conjunction with a secondary membrane or co-deposited modifier, it is difficult to isolate the permselectivity traits of a given monomer. Shim et al. undertook a comparative study of poly(*m*-phenylenediamine), poly(5-amino-1-naphthol), and poly(2,3-diaminonaphthalene) EPFs for their NO sieving ability and found that poly(5-amino-1-naphthol) (5A1N) performed best with a −3.7 selectivity coefficient against nitrite.[63] They then demonstrated that a Pt microelectrode modified with Pt-black and poly(5A1N) had stable sensitivity and selectivity performance over 35 h of continuous polarization.

Very often, permselective membranes are applied with other chemical modifiers in either layered or composite fashions (discretely or mixed, respectively). In the literature, an enormous collection of transition metal nanoparticles, carbon nanostructures, metallo-macrocycles, and other chemical modifiers broadly categorized as electrocatalysts has been used to improve NO sensor sensitivity (*see* Section 1.3.1) while suspended within or coated beside permselective membranes. Metalloporphyrins and metallophthalocyanines in

particular represent the most commonly used NO electrocatalysts. Although these catalysts have been proven capable of amplifying the NO signal ca. 3-fold and shifting anodic peak features to lower potentials, notably, there have been no quantitative indications of their specific selectivity benefits.[30]

Table 1.2 Electrochemical NO sensors with selectivity-enhancing modifiers.

Electrode Design[a]	E_{appl}[b] (V)	Media	S_{NO}[c] (pA nM^{-1})	Dim.[d]	LOD	Selectivity[e] (log$k_{NO,i}$)	Year	Ref.
Pt/Pt-black/XG	0.85	PBS (pH 7.4)	0.18	50 µm Ø	6 nM	NO_2^- (−4.63) AA (−5.38) DA (−5.60) UA (−4.18) AP (−3.69) H_2O_2 (−3.25) H_2S (−4.30)	2016	54
ITO/rGO-FeTCP/APBA	0.75	100 mM PBS (pH 7.4)	123.2	100 µm Ø	55 pM	NO_2^- (−2.05) AA (−1.98) DA (−2.20 UA (−2.07)	2015	64
Pt/Nafion(1/2)/poly(*o*-PD)	0.945	40 mM PBS (pH 7.4)	1.07	127 µm Ø	8 nM	NO_2^- (−2.17) AA (−2.24) DA (−2.32) UA (−2.32) H_2O_2 (−2.12) 5-HT (−1.82) DOPAC (−2.24) GSH (−2.72) 5-HIAA (−2.24) HVA (−1.91)	2014	48
Pt/Pt-black/IS(pH 11.7) /PTFE	0.7	10 mM PBS (pH 7.4)	*n.r.*	76 µm Ø	n.r.	CO (−2.1)	2013	43
Pt/APTES/XG	0.7	10 mM PBS (pH 7.4)	1.4	100 µm × 3 mm	840 pM	NO_2^- (−5.3) AA (−4.2) UA (−5.0) AP (−4.0) NH_3 (−3.8) NH_4^+ (−5.8) $ONOO^-$ (−4.0)	2013	53
GC/P-1Co(II)(salen)-MWCNT-CS	0.895	100 mM PBS (pH 7.4)	3870	3 mm Ø	2.99 nM	NO_2^- (−2.66) AA (−4.22) GSH (−2.89)	2012	65
Au/poly(eugenol) /poly(phenol)	0.8	100 mM PBS (pH 7.4)	0.56	50 µm Ø (× 110)	27 nM	NO_2^- (−3.04) AA (−3.15) DA (−1.74) H_2O_2 (−1.41)	2011	60
Pt/Nafion/poly(*m*-PD)-poly(resorcinol)/Nafion	0.74	10 mM PBS (pH 7.4)	17.1	*n.r.*	*n.r.*	NO_2^- (−2.80) AA (−4.06) NH_4^+ (−4.89)	2011	62
Pt/Pt-black/poly(5A1N)	0.75	PBS (pH 7.4)	0.122	25 µm Ø	5.8 nM	NO_2^- (−3.70) CO (−1.54)	2010	63
Pt/MB/poly(*o*-PD)/CS	n.r.	100 mM PBS (pH 7.4)	20	125 µm Ø	1 nM	NO_2^- (−1.62) AA (−2.01) DA (−1.57)	2010	61
ITO/Au/Au-HCF/TeflonAF	0.75	PBS (pH 7.3)	10	1 mm Ø	1 nM	NO_2^- (−5.9) AA (−5.9) NH_4^+ (−5.4) GSH (−4.9)	2010	52

[a]Slashes signify separation between depositions of electrode modifiers; dashes indicate co-deposition. XG: fluorinated xerogel; ITO: indium tin oxide; rGO: reduced graphene oxide; FeTCP: Fe(III) *meso*-tetra (4-carboxyphenyl) porphyrin; APBA: 3-aminophenylboronic acid; *o*-PD: *ortho*-phenylenediamine; IS: internal solution; PTFE: polytetrafluoroethylene; APTES: (3-aminopropyl)triethoxysilane; salen: bis(2-hydroxy-benzaldehyde) ethylenediimine; MWCNT: multiwalled carbon nanotube; 5A1N: 5-amino-1-naphthol; MB: Meldola blue; HCF: hexacyanoferrate.
[b]Applied potential *vs*. Ag|AgCl under constant potential amperometry.
[c]Sensitivity towards NO. *n.r.*: not reported.
[d]Dimensions. Parathetical multipliers indicate the number of short-circuited electrodes of the given dimension.
[e]Tested interferent species with reported selectivity coefficients or those calculated from Eq. 4 with provided data: AA: L-ascorbic acid; DA: dopamine; UA: uric acid; AP: acetaminophen; 5-HT: serotonin; L-Arg: L-arginine; ACh: acetylcholine; DOPAC: 3,4-dihydroxyphenylacetic acid; GSH: glutathione; 5-HIAA: 5-hydroxyindole-3-acetic acid; HVA: homovanillic acid.

1.2.2 Biosensors and biomolecular catalysts

The predominant means of imparting NO selectivity to an electrochemical sensor are chemical modifications of the transducer surface that take advantage of certain passive physical properties of NO, namely its small size and ability to permeate hydrophobic barriers.[38] These properties are what allow NO to easily traverse lipid bilayers and act as an intercellular gasotransmitter. However, once inside the cell, nature has evolved a number of exquisite hemoprotein receptors to target NO, allowing it to exert its specific biological activity. Hemoglobin (Hb), myoglobin (Mb), cyctochrome c (cyt *c*), and soluble guanylate cyclase (sGC) are all known to bind NO to some extent at the Fe(II)|Fe(III) redox center of their heme prosthetic group(s).[66,67] As a result, several electrochemical biosensors have incorporated these proteins to detect NO and potentially improve selectivity by harnessing NO's unique chemistry for metal coordination (as opposed to its diffusional traits).

The electrochemical detection of biomolecule-mediated redox events has traditionally been achieved through three generations of biosensors.[68] The first generation relies on the detection of electroactive co-products, -substrates, or -factors, whereas the second utilizes artificial redox mediators to shuttle electrons to the electrode. Third generation biosensors offer a more elegant means of detection, relying on direct heterogeneous electron transfer (ET) between the metal redox center and the electrode itself. Though simpler and reagentless, direct electron transfer can be hampered if redox centers are buried deep within the protein.[69] For instance, the insulating effects of the peptide backbone are most pronounced for Hb, whose Fe(II)|Fe(III) redox couple exhibits poor electron transfer kinetics consequently.[70] Moreover, immobilization of proteins onto the electrode surface can cause denaturation, alter function, and lead to long-term sensor instability. Although sGC is

the most selective protein for binding NO (particularly over O_2), it is extremely unstable once removed from its physiological environment, precluding the use of even the lightest immobilization techniques.[66] Enhancing electron transfer kinetics and ensuring stability are therefore the most important preliminary considerations for NO biosensor design.

Recent strategies to immobilize different hemoproteins on electrode surfaces for the purpose of NO detection are summarized in Table 3. A notable shift in the latest formulations has been away from thiolated self-assembled monolayer (SAM) on gold schemes to those based on glassy carbon (GC), the latter offering greater flexibility in terms of covalent and electrostatic attachment and a wider potential window.[71] Many of the formulations include either noble metal nanomaterials and/or different allotropes of carbon co-deposited with Hb or Mb. Combined with the choice in supporting matrix (e.g., a polymer, graphene oxide composite, or surfactant), the interfacing of highly electroactive materials such as these with hemoproteins markedly improves electron transfer kinetics, most commonly demonstrated by the appearance of well-known, quasireversible Fe(II)|Fe(III) cathodic and anodic peaks between −0.1 and −0.4 V *vs*. Ag|AgCl under cyclic voltammetry (CV). Voltammetry of a diffusionless system (i.e., surface-confined, as with an immobilized hemoprotein) enables calculation of the surface concentration and heterogeneous electron transfer rate constant (k_s) from Laviron's model.[72] Values of k_s between 1.10 and 60.3 s^{-1} have recently been reported for Hb composites to demonstrate enhanced ET,[73-75] but it is by no means a consistent form of characterization across hemoprotein-based NO biosensors. Moreover, it remains unclear how enhanced ET of the heme group directly impacts electrocatalysis of NO.

After immobilization, most sensors incorporating a biological recognition element for NO yield a detectable signal through electroreductive means, which generally follow Eq. 5-7 when mediated through Fe(II).[31,76]

$$\text{Fe(II)} + \text{NO} \rightarrow \text{Fe(II)-NO} \qquad \text{(Eq. 5)}$$
$$\text{Fe(II)-NO} + e^- \rightarrow \text{Fe(II)-NO}^- \qquad \text{(Eq. 6)}$$
$$2\text{Fe(II)-NO}^- + 2\text{H}^+ \rightarrow 2\text{Fe(II)} + \text{N}_2\text{O} + \text{H}_2\text{O} \qquad \text{(Eq. 7)}$$

Reduction of the Fe(II)-NO complex occurs in the −0.7 to −0.8 V range *vs*. Ag|AgCl, observable under CV. The lifetime of the nitroxyl adduct (Fe(II)-NO^-) is pH-dependent, as seen in the decomposition and catalyst regeneration pathway in Eq. 7. As a result, the pH has been optimized for maximum NO sensitivity in several studies, even though such matrix alterations are not practical for most biological applications. Amperometric calibrations revealed low and, in most cases, sub-micromolar LOD values (Table 3). In some studies, the leveling-off of the calibration curve at high NO concentrations is characteristic of immobilized enzymes, and the Lineweaver-Burk equation was used to determine an apparent Michaelis-Menton constant (K_m^{app}).[77] Values of K_m^{app} ranging from 0.12 to 75.39 μM have been recently reported and offer an indication of the NO binding affinity.[73,75,76] For comparison, sGC selectivity binds NO with a K_m of 10 nM in what may represent an ideal limit to natural receptor-modified NO biosensors.[78]

Artificial biomolecules represent a small, but intriguing category within NO biosensor development. As opposed to altering the surroundings of the hemoprotein to change its electrochemical properties, alterations to the protein itself can be made instead. Microperoxidase (MP) is a small oligopeptide produced from tryptic digestion of cyt *c* and retains a redox active heme center. The smaller, simpler structure is better suited to sensor development as denaturation concerns are reduced.[79] Abdelwahab et al. evaluated MP for NO

electroreductive ability with co-immobilized catalase and superoxide dismutase to improve selectivity (over H_2O_2 and O_2^-, respectively) through competitive binding.[74] The resulting biosensor had a low LOD of 4.3 nM and high purported selectivity, but measurements were performed under biologically irrelevant conditions at pH 4.0. Taking protein design a step further, Musameh et al. developed a sensor based on heme trapped in recombinant silk to loosely emulate the protein shell of sGC.[80] The resulting sensor had a LOD of 2 nM under CV—the choice of technique allowing peak discrimination against O_2 reduction. Ultimately, the authors concluded that the protein scaffold of silk could be easily reengineered to further enhance selectivity against O_2 and mimic sGC while still retaining stability.

Without a consistently reported set of analytical metrics, there is no strong basis of comparison across recent biosensor designs (Table 3). Selectivity is perhaps the main theoretical advantage of NO-binding proteins; however, it is often left unquantified in a meticulous fashion. Instead, what is very often displayed is an amperogram of interferent injections yielding imperceptible changes in current in comparison to injections of an arbitrary concentration of NO. Demonstrations of selectivity of this sort are too prone to misrepresentations stemming from the choice of scale, even if biologically relevant concentrations of interferents are used. And although electroreductive techniques (as with hemoprotein-based sensors) offer greater selectivity over many interferents found biologically (which are sooner oxidized than reduced), oxygen can be easily reduced below −0.6 V *vs.* Ag|AgCl according to Eq. 8.[38]

$$O_2 + 4H^+ + 4e^- \rightarrow 2\ H_2O \qquad \text{(Eq. 8)}$$

Potentiodynamic techniques such as CV, LSV, and DPV are inherently more selective towards NO detection, allowing discrimination between the reduction peaks of O_2 and NO.

However, amperometric techniques will yield a single, cumulative current from all species reduced at the applied potential, including O_2. Future evaluations of hemoprotein-based NO sensors must include either a sensitivity ratio or selectivity coefficient for NO over O_2 to assess the practicality of use in oxygenated milieu. Lastly, very little has been done to quantitatively assess the ability of these electrochemical NO biosensors to perform in complex biological matrices. As notable exceptions, Musameh et al. saw near complete (>90%) sensitivity retention while measuring NO in 10% fetal bovine serum in PBS relative to PBS measurements,[80] and Wen et al. reported 51% sensitivity retention in a solution of 12.5% plant homogenate in PBS.[73] Characterizations of analytical performance in the media of application (or closest simulant thereto) must be carried out to ensure measurement accuracy in the future.

Table 1.3 Recent advances in electrochemical NO biosensor design.

Electrode Design[a]	Tech.[b]	E_{appl}[c] (V)	Media[d]	S_{NO}[e] (nA nM^{-1})	Ø	LOD	Selectivity[f]	Year	Ref.
GC/MWCNT/silk-hemin	CV	*n.a.*	100 mM AB (pH 3.0)	198	*n.r.*	2 nM	DA, NO_2^-, AP, O_2 (*n.q.*)	2018	80
Au/cysteamine /(MoS_2-NH_2)-GO/Mb	CPA	-0.3	PBS	*n.r.*	*n.r.*	3.6 nM	NO_2^-, AA, $NaHCO_3$ (*n.q.*)	2017	81
GC/rGO-(AuNR-Mb)	LSV	*n.a.*	100 mM PB (pH 2.5)	0.0539	*n.r.*	5.5 µM	$NaNO_3$, NaF, KCl, NH_4Cl, $NaCO_3$, AA, DA, glucose, UA, H_2O_2 (*n.q.*)	2016	82
GC/PEGDGE-(QC-AuNP)-Hb	CPA	-0.78	100 mM PBS (pH 7.0)	*n.r.*	3 mm	12 nM	AA, Cys, glucose, DA, L-Arg, NO_2^- (*n.q.*)	2014	76
GC/(MWCNT-NYPA)-Hb/Nafion	CPA	-0.811	100 mM PBS (pH 7.0)	~0.0667	3 mm	15 nM	H_2O_2	2013	71
GC/G-CTAB/CS-Hb	CPA	-0.655	100 mM PBS (pH 7.0)	0.615	3 mm	6.75 nM	HPO_4^{2-}, K^+, NO_3^-, AA, NO_2^-, H_2O_2 (*n.q.*)	2012	73
GC/AuNP/MWCNT-poly(TTCA)/MP /SOD/CAS	CPA	-0.8	100 mM PBS (pH 4.0)	1.20	3 mm	4.3 nM	H_2O_2, O_2^-, AA, L-Arg, GA (*n.q.*)	2010	74
GC/poly(5A1N)/CC /cyt *c*	CPA	-0.4	100 mM PBS (pH 7.4)	0.156 (nA nM^{-1}cm^{-2})	*n.r.*	2.85 µM	*n.r.*	2009	83
GC/CEC-Hb	CPA	-0.755	100 mM PBS (pH 7.0)	0.025	*n.r.*	20 nM	DA, glucose, NO_2^-, L-Arg (*n.q.*)	2009	75

[a]Slashes signify separation between depositions of electrode modifiers; dashes indicate co-deposition. Abbreviations in order of appearance: GC: glassy carbon; MWCNT: multi-walled carbon nanotube; MoS_2-NH_2: amine-modified molybdenum disulfide; GO: graphene oxide; Mb: myoglobin; rGO: reduced graphene oxide; AuNR: gold nanorod; PLEDGE: poly(ethylene glycol) diglycidyl ether; QC: quaternized cellulose; AuNP: gold nanoparticle; Hb: hemoglobin; NYPA: naphthalen-1-ylmethylphosphonic acid; CS: chitosan; G: graphene; CTAB: hexadecyltrimethylammonium bromide; TTCA: 5,2':5',2''-terthiophene-3'-carboxylic acid; MP: microperoxidase; SOD: superoxide dismutase; CAS: catalase; 5A1N: 5-amino-1-naphthol; CC: cyanuric chloride; cyt *c*: cytochrome c; CEC: cyanoethyl cellulose.

[b]Electrochemical measurement technique. CV: cyclic voltammetry; CPA: constant potential amperometry; LSV: linear sweep voltammetry.

[c]Applied potential *vs*. Ag|AgCl. *n.a.*: not applicable.

[d]AB: acetate buffer; PB: phosphate buffer; PBS: phosphate buffered saline.

[e]Sensitivity towards NO. Tildes signify approximations from calibration traces. *n.r.*: not reported.

[f]Tested interferent species: DA: dopamine; AP: acetaminophen; AA: L-ascorbic acid; UA: uric acid; Cys: cysteine; L-Arg: L-arginine; GSH: glutathione; GA: glutamic acid; *n.q.*: not quantified.

1.2.3 Dual and multi-analyte detection

A quickly growing alternative means of imparting selectivity to an electrochemical sensor is dual- or multi-analyte detection.[84-86] In place of blocking a particular electroactive species besides NO from the transducer surface, simultaneous detection allows for quantification of additional species and, if necessary, correction of the NO signal. In order to collect electrochemical information simultaneously for a given number of analytes, there must exist the same number of electrodes, each either biased or chemically modified to preferentially detect a specific analyte over the others. For biological measurements, ultramicroelectrodes (UMEs) positioned in close proximity to one another are ideal to ensure that each electrode samples the same concentration profile. Larger electrodes placed further apart may be used only if assurances are made that each electrode experiences identical chemical/biological phenomena. As an alternative to requiring multiple electrodes, for near-simultaneous detection, the same electrode may be used with different pulsed potentials (e.g., potential-step chronoamperometry), each potential selected based upon the specific redox properties of each analyte. Pulsed techniques reduce fabrication complexity, but variable capacitive currents and pulse lengths place an inherent limit on the sampling rate and ability to measure fast-releasing systems.[87,88]

Theoretically, the selectivity advantages of multi-analyte detection arise primarily from signal deconvolution, which warrants explanation here. Let us consider the simplest scenario of an electrochemical sensor for two analytes: *a* and *b*. The sensor is comprised of two working electrodes: 1 and 2. The Faradaic current measured by electrodes 1 and 2 will depend on their individual sensitivities towards analytes, *a* and *b*, and on the actual concentrations of *a* and *b*. The relationship between these variables can be described as a

system of two linear equations, where $S_{1,a}$ is the sensitivity of electrode 1 towards analyte *a*, C_a is the concentration of analyte *a*, I_1 is the current measured by electrode 1, etc. (Eq. 9, 10).

$$S_{1,a}C_a + S_{1,b}C_b = I_1 \quad \text{(Eq. 9)}$$
$$S_{2,a}C_a + S_{2,b}C_b = I_2 \quad \text{(Eq. 10)}$$

Or, when expressed in matrix formalism (Eq. 11):

$$\begin{bmatrix} S_{1,a} & S_{1,b} \\ S_{2,a} & S_{2,b} \end{bmatrix} \begin{bmatrix} C_a \\ C_b \end{bmatrix} = \begin{bmatrix} I_1 \\ I_2 \end{bmatrix} \quad \text{(Eq. 11)}$$

Currents are measured, and all sensitivity values may be obtained through calibrations of the dual-sensor. The two unknown concentrations may be obtained easily by solving the system of equations (Eq. 12).

$$\begin{bmatrix} C_a \\ C_b \end{bmatrix} = \begin{bmatrix} S_{1,a} & S_{1,b} \\ S_{2,a} & S_{2,b} \end{bmatrix}^{-1} \begin{bmatrix} I_1 \\ I_2 \end{bmatrix} \quad \text{(Eq. 12)}$$

The existence of the reciprocal matrix (i.e., the system of equations' ability to be solved) depends on each electrode having unique sensitivities towards the analytes—which is to say that if electrodes 1 and 2 were identical (or simply different areas, such that their sensitivities were modified by some scalar), Eq. 9 and 10 would be redundant, and there would no longer exist a unique solution for C_a and C_b. Intuitively, it makes sense that a second electrode would have to have an additional modifier or different applied potential to offer any new information from the sample. Perhaps less intuitively, two electrodes that, individually, are not selective for only one analyte can be used in combination to obtain two accurate concentrations (i.e., signal deconvolution). Therein lies the selectivity benefit of multi-analyte detection. Extending from the case of the dual-sensor, so long as *n* unique electrodes are operated to detect *n* analytes, the solution to the system of equations can be generalized to Eq. 13.

$$\begin{bmatrix} C_a \\ \vdots \\ C_n \end{bmatrix} = \begin{bmatrix} S_{1,a} & \cdots & S_{1,n} \\ \vdots & \ddots & \vdots \\ S_{n,a} & \cdots & S_{n,n} \end{bmatrix}^{-1} \begin{bmatrix} I_1 \\ \vdots \\ I_n \end{bmatrix} \quad \text{(Eq. 13)}$$

With having to collect $n \times n$ calibration curves and solve a system of equations for each time-point, the computational complexity can quickly increase with each added analyte. Additionally, a key underlying assumption is that Faradaic current contributions from other electroactive species (besides those specifically targeted by the multi-sensor) are negligible. Programs to assist with data processing and additional selectivity-enhancing electrode modifiers can be used to address these problems, respectively.

The most pertinent application of multi-analyte detection within the context of electrochemical NO measurement is analysis of reactive oxygen and nitrogen species (ROS and RNS, respectively), including peroxynitrite ($ONOO^-$), hydrogen peroxide (H_2O_2), superoxide (O_2^-), and nitrite (NO_2^-). The balance of these species amongst themselves and against antioxidants plays an essential role in mammalian physiology. Low levels of ROS/RNS species may promote cell proliferation, while higher concentrations can induce cell damage/death through oxidative stress and are implicated in a number of degenerative pathologies, such as Parkinson's and Alzheimer's diseases.[20,86] While NO is produced from NOS, partial reduction of oxygen during aerobic respiration results in O_2^-, which may either spontaneously breakdown to H_2O_2 or quickly react with NO to yield $ONOO^-$.[32,89,90] Nitric oxide may also react with oxygen to yield NO_2^-. Given their differing lifetimes and cross-reactivities, the ability to simultaneously monitor ROS/RNS dynamics is critical to fully understanding their individual and collective biological functions.

Over the years, Amatore and colleagues have worked to simultaneously measure the flux of ROS/RNS species originating from a single cell.[87,91] However, the platform has

recently been adapted to facilitate populational measurements to reduce the number of trials required to achieve statistical significance.[88] Macrophages were cultured and stimulated with calcium ionophore in four separate chambers with Pt-black-modified microband electrodes. By applying four different potentials based off the voltammetric profiles of H_2O_2, $ONOO^-$, NO, and NO_2^- and applying appropriate signal deconvolution methods (as outlined above), they were able to distinguish the temporal release profiles of each analyte upon stimulation.[88,92] Integration of the signal allowed mean femtomole quantities of ROS/RNS species per cell to be calculated for comparison to single-cell measurements. A reduction in the per cell amount of NO and $ONOO^-$ measured from populational *vs*. single-cell macrophages was attributed to intercellular interactions affecting the global response. However, poisoning of the Pt-black was also suggested, due to direct culturing of the cells onto the electrodes and lack of any surface protecting modifications.

Other attempts to simultaneously measure NO and other ROS/RNS species are summarized in Table 4. Bedioui and colleagues have demonstrated the utility of ultramicroelectrode (UME) arrays for measurements from cell cultures, and in a recent construction, they were able to detect NO and $ONOO^-$ from HL60 cells stimulated with *p*-methoxyamphetamine (PMA).[93] By applying two different potentials to two different sets of short-circuited UME arrays, they were able to eliminate crosstalk between NO and $ONOO^-$ current responses.[60] The NO electrodes were additionally modified with poly(phenol) and poly(eugenol) to reduce interference from larger electroactive species capable of being oxidized at the high +0.8 V *vs*. Ag|AgCl overpotential.

Lee and colleagues have reported on a number of dual-sensor designs, spanning O_2, CO, Ca^{2+}, and K^+.[40,41,54,94-96] Though these analytes are not ROS/RNS species per se, they are

all in some way tied to the intrinsic biological activity of NO. Coordination of NO with sGC upregulates cyclic guanosine monophosphate (cGMP), which in turn activates K^+ channels to hyperpolarize the cell membrane.[1] Hyperpolarization results in closure of voltage-gated Ca^{2+} channels, reducing intracellular levels of Ca^{2+} in smooth muscle cells, thereby regulating vascular tone. Dual detection of these cations with NO was achieved using specific ionophores to modify the secondary electrode surface: valinomycin for K^+ and ETH1001 for Ca^{2+}.[95,96] Potentiometry was then used in the final ion-selective electrode (ISE) design. Given the vastly different detection strategies, virtually no crosstalk occurred between cation and NO signals, greatly simplifying data processing. The dual-sensors were then applied to real-time, quantitative measurements in rat models. Also critical to NO's activity, O_2 is a required cofactor in the biosynthesis of NO from NOS enzymes[97] and is one of the main physiological scavengers of NO. Park et al. developed a miniaturized Shibuki/Clark-type sensor for simultaneous detection of NO and O_2.[94] The design comprised two working electrodes (polarized at +0.75 and -0.4 V *vs*. Ag|AgCl for NO and O_2, respectively) housed in an internal solution separated from the sample matrix by a PTFE membrane. Although the NO-specific electrode was responsive to NO alone, the O_2-specific electrode was partially sensitive to NO, thus requiring signal deconvolution. Once the electrochemical responses were resolved from one another, they were able to monitor and correlate fluctuations of both analytes in the rat neocortex upon electrical stimulation.[40]

Carbon monoxide is unique in that it has several physicochemical properties in common with NO, including its size, short lifetime, lipopermeability, and affinity for heme binding. Achieving selectivity for NO against CO with chemical modification of the electrode is therefore challenging given these similarities. Both gases have been found to

regulate many of the same processes physiologically, including vasodilation, neurotransmission, platelet aggregation, and the immune response.[98] Overall, there is an incentive both in improving selectivity and unraveling the coupled biology of NO and CO to pursue co-detection. Similar to their NO/O_2 probe, Lee and colleagues developed a miniaturized Shibuki-type sensor for NO and CO using an electroplated layer of tin on the CO electrode to enhance sensitivity.[41] Although the CO-specific electrode was slightly responsive to NO, signal deconvolution allowed both species to be analyzed in real time in an excised rat kidney exposed to the NOS inhibitor, L-NAME. The sensor design was recently revamped to eliminate the internal electrolyte solution and allow for direct insertion into a rat cortex.[54] The new design's CO-specific electrode was modified by electroplated gold and operated at a significantly lower potential (+0.2 *vs*. +0.7 V, *vs*. Ag|AgCl). These changes allowed each electrode to respond to either NO or CO solely, greatly simplifying post-collection data processing. Both electrodes were additionally modified with layers of a highly fluorinated xerogel to enhance selectivity against other interferents unable to permeate the hydrophobic membrane as well as NO and CO.

Table 1.4 Recent advances in multi-analyte electrochemical NO sensor design.

Electrode Design[a]	Analyte	E_{appl}[b] (V)	Analyte Modifiers[c]	S_{NO}[d] pA nM^{-1}	Dim.[e]	LOD	Selectivity[f]	Year	Ref.
Pt/Pt-black /APTES/XG	K^+	+0.85 (ISE)	valinomycin	0.106	50 µm Ø	9.55 nM	NO_2^-, AP, AA, DA, UA, H_2O_2, H_2S (*n.q.*)	2016	96
Pt/Pt-black	H_2O_2, $ONOO^-$, NO_2^-	+0.62 (+0.3, +0.45, +0.85)	*n.a.*	*n.r.*	0.01 cm^2	*n.r.*	H_2O_2, NO_2^-, $ONOO^-$	2016	88
Pt/Pt-black /APTES/XG	Ca^{2+}	+0.85 (ISE)	ETH1001	0.0408	25 µm Ø	20 nM	NO_2^-, AA, UA, AP, DA, H_2S, H_2O_2 (*n.q.*)	2016	95
Pt/Pt-black/XG	CO	+0.85 (+0.20)	electroplated Au	0.180	50 µm Ø	6 nM	NO_2^-, AP, AA, DA, UA, H_2O_2, H_2S	2016	54
Au/poly(eugenol) /poly(phenol)	$ONOO^-$	+0.8 (−0.1)	bare Au	*n.r.*	20 µm Ø (×1234)	*n.r.*	$ONOO^-$, O_2, H_2O_2	2014	93
Pt/Pt-black	H_2O_2, $ONOO^-$, NO_2^-	+0.62 (+0.3, +0.45, +0.85)	*n.a.*	1.3	200 µm × 197 µm	30 nM	$ONOO^-$, H_2O_2, NO_2^-	2014	92
Pt/Pt-black/XG	O_2	+0.8 (−0.4)	*n.a.*	4.207	127 µm Ø	0.5 nM	NO_2^-, AA, UA, AP (*n.q.*)	2013	42
Pt/Pt-Fe(III)NP /(IS pH 1)/PTFE	CO	+0.75 (+0.70)	electroplated Sn	0.65	76 µm Ø	5 nM	CO (*q.*); AP, UA, NO_2^- AA, DA (*n.q.*)	2012	41
Au/poly(eugenol) /poly(phenol)	$ONOO^-$	+0.8 (−0.1)	bare Au	0.56	50 µm Ø (×110)	27 nM	H_2O_2, DA, NO_2^-, AA, $ONOO^-$	2011	60
Pt/Pt-black /(IS pH 7.5)/PTFE	O_2	+0.75 (−0.4)	*n.a.*	0.1781	25 µm Ø	5 nM	O_2, CO (*q.*); NO_2^- UA, AA, AP, DA (*n.q.*)	2009	94

[a]Slashes signify separation between depositions of electrode modifiers; dashes indicate co-deposition. Abbreviations in order of appearance: APTES: (3-aminopropyl)triethoxysilane; Fe(II)NP: iron nanoparticle; IS: internal solution; PTFE: polytetrafluoroethylene.

[b]Applied potential *vs*. Ag|AgCl during constant potential amperometry; parentheses indicate potential or technique used for detection of other analytes.

[c]Additional electrode modifiers used for separate detection of other analytes. *n.a.*: not applicable.

[d]Sensitivity towards NO. *n.r.*: not reported.

[e]Dimensions. Parathetical multipliers indicate the number of short-circuited electrodes of the given dimension.

[f]Tested interferent species: AP: acetaminophen; AA: L-ascorbic acid; DA: dopamine; UA: uric acid; *n.q.* not quantitated; *q.* quantitated.

1.3 Improvements to sensitivity

The sensitivity of an electrochemical NO sensor will depend on the same variables that exert influence on selectivity, including technique, transducer modifications, and electrode material. Generally, lower potentials are more favorable for NO selectivity and improving signal-to-noise (*S*/*N*). Noble metal electrodes like platinum (Pt), platinum-iridium alloys (Pt-Ir), and gold (Au) are suitably electroactive towards NO and benefit from high electrochemical and mechanical stability.[29,31] Carbon allotrope electrodes like glassy carbon (GC), carbon fiber (CF), and graphene (G) are comparably rigid and conductive, also benefitting from a wider potential window (higher potential onset of water oxidation) and greater ease of chemical modification from a high density of oxygen-containing functional groups (e.g., carbonyl, epoxy, carboxylic acid).[99] On the other hand, carbon-based electrodes are more friable and typically require higher overpotentials to oxidize NO.[46] Indium tin oxide (ITO) and transparent carbon (T-C) electrodes are amenable to cell culture, where the integration of transparent electrodes simplifies microscopic/spectroscopic interrogation of adherent cells.[64,100] In certain applications where low levels of NO must be measured, and the bare electrode itself is not adequately sensitive, there are a number of techniques available to enhance sensitivity.

Unlike selectivity, sensitivity scales proportionately with surface area (SA). However, a simple increase in the planar SA comes at the expense of spatial resolution. Alternatively, increasing microscopic surface roughness and porosity increases the electroactive surface area (EASA) and potentially enhances mass transport without increasing the macroscopic SA. Platinum-black deposition (i.e., platinization) on Pt electrode surfaces is a well-established technique and increases NO sensitivity ~10-fold.[101] A recent procedure for the

etching of hierarchical nanoporous gold (HNG) was developed by Liu et al. via an electrochemical alloying/dealloying method, increasing NO sensitivity over bare Au by a factor of 22.9.[102] Unfortunately, if the oxidation of NO continues to occur in a diffusion-controlled (i.e., mass-transport-controlled) manner on roughened surfaces, the capacitive current will often increase in parallel to the desirable Faradaic current.[103] In order to isolate and amplify the NO signal, surface-confined (i.e., surface-controlled) interaction or adsorption of NO must occur.[72] This goal is often achieved with the use of electrocatalysts, relying on specific interaction/coordination with NO.

1.3.1 Electrocatalysts

Heterogeneous electrocatalysts lower the activation energy of an electrochemical reaction at or near (e.g., suspended in a conductive matrix) the electrode surface. Specific catalytic effects can be observed when oxidation wave features are shifted to lower potentials and peak/plateau currents are amplified (reduction-facilitating catalysts are discussed in Section 1.2.2). Table 5 lists recent constructions of electrocatalyst-modified NO sensors. Traditional metalloporphyrin (MP) and metallophthalocyanine (MPc) catalysts specifically coordinate with NO, either at the metal center or aromatic periphery.[104,105] Formation of the nitrosyl adduct facilitates electron transfer, first to the macrocycle, and then to the electrode sink.[106] Different metal centers alter the bond orientation, electronic structure, and oxidation potential; however, iron (Fe), cobalt (Co), and nickel (Ni) are most common due to favorable signal amplification.[107] Though mediated through specific chemical interaction with NO, there has been no attempt to quantify the selectivity benefits of MP and MPc modification.[30]

In the field of electrochemical NO sensing, the recent literature is dominated by electrode modifications with noble metal, transition metal, and semiconductive

nanostructures (Table 5). The high SA-to-volume ratio and density of reactive edge sites are favorable for NO signal amplification and enhancing electron transfer (ET) kinetics.[108] As such, the concentration of nanostructure and choice of suspension matrix (e.g., reduced graphene oxide, chitosan, electropolymerized films) must be carefully optimized to avoid agglomeration and return to bulk properties.[109-111] Of note, the SA-enhancing and electrocatalytic effects of nanostructures are difficult to view in isolation without specific kinetic characterization. Too often, a simple increase in NO sensitivity or current flux (j_{NO}) is attributed to the electrocatalytic properties of the nanostructure without additional evidence. For instance, the wide range of j_{NO} values reported in Table 5 is not at all expected to reliably reflect the electrocatalytic ability of the respective modifier(s) without separation from EASA-enhancing effects. A better indicator of electrocatalytic ability is the change in anodic peak potential (ΔE_a) relative to the bare electrode, but even then, the condition of the starting electrode (e.g., presence of surface oxides, cleanliness) will influence the magnitude of ΔE_a with electrocatalyst modification. As a result, the best comparative investigations of catalytic activity have been carried out within the same study (where non-trivial experimental variability can be minimized more effectively).[107] Notably, there has been no attempt to conduct such a comparison for nanostructure-modified electrochemical NO sensors, perhaps given the great variety of compositions.

A recent study by Xu et al. undertook a more rigorous characterization of the electrocatalytic mechanism of a FePc-modified, nitrogen-doped graphene electrode.[112] Linear correlation between the scan rate and peak anodic current indicated a surface-controlled reaction,[113,114] and variation of the peak potential with scan rate demonstrated the well-known irreversibility of NO oxidation. Further analysis on a rotating disk electrode (RDE)

modeled after a study by Caro et al.[107] returned a Tafel plot of slope ~1.2 V dec^{-1}, demonstrating that transfer of the first electron (Eq. 1) was the rate-determining step. Liu et al. created Tafel plots in the +0.65 to +0.80 V *vs*. Ag|AgCl region and observed slopes of 59.0 and 101 mV dec^{-1} for HNG and bare Au electrodes, respectively.[102] The lower slope for HNG electrodes denoted greater electrocatalysis of NO oxidation. This comparison is a reasonable demonstration of electrocatalytic activity as the Tafel plot slope is proportional to the charge transfer coefficient (α), a dimensionless descriptor of the activation energy barrier at the electrode-electrolyte interface. Sivanesen et al. supplied a measurement of the standard heterogeneous ET rate constant ($k^0 = 4.42 \times 10^{-4}$ cm s^{-1}) on a CoPc-modified GC electrode using Eq. 14,[115] which is only applicable to completely irreversible systems.[116]

$$k^0 = 1.11(D_O v)^{1/2}(E_p - E_{p/2})^{-1/2} \qquad \text{(Eq. 14)}$$

Here, D_O represents the diffusion coefficient of the oxidant, v the scan rate, E_p the peak potential, and $E_{p/2}$ the half-height peak potential. In all, evaluations of electrocatalytic activity for NO oxidation would benefit from standardized reporting of kinetic parameters (e.g., k^0, α, ΔE_a) rather than NO sensitivity. Though requiring more analysis for computation, internal and cross-study comparisons would be greatly aided.

Table 1.5 Electrocatalyst-modified electrochemical NO sensors.

Electrode Design[a]	Tech.[b]	E_{appl}[c] (V)	j_{NO}[d] (nA nM^{-1} cm^{-2})	Ø	LOD	ΔE_a[e] (V)	Add. Meas.[f]	Year	Ref.
N-G/FePc/Nafion/PLL	CPA	+0.945	0.21	*n.r.*	180 nM		S.C., n	2018	112
Au/HNG	CPA	+0.8	14.4	*n.r.*	1.38 nM	-0.09		2017	102
T-CUA/CS-AuNP/CA	SWV	*n.a.*	0.1	3 mm	200 nM			2017	100
GC/(S-G)-AuNP	DPV	*n.a.*	0.02105	2 mm	9 nM	-0.43	D.C., D_{NO}, k_{cat}	2017	117
GC/rGO-AuPtNP	CPA	+0.84	104	3 mm	2.88 nM	-0.184		2016	118
GC/rGO-AgNP	CPA	+0.96	0.1507	3 mm	2.84 µM	+0.14	D.C., D_{NO}	2016	119
GC/AuNP/G	CPA	+0.845	1.090	3 mm	18 nM	-0.22	D.C., n	2015	120
GC/PADA-AuAgNCstr	CPA	+0.945	53.3	3 mm	10 nM	-0.11		2015	121
GC/rGO-Co_3O_4NC-PtNP	CPA	+0.84	0.37	3 mm	1.73 µM	-0.10	D.C., D_{NO}	2015	122
GC/rGO-CeO_2NP	CPA	+0.845	1.676	3 mm	9.6 nM			2015	123
GC/poly(PBZ)-AuNP	CPA	+1.0	6.45	3 mm	3.7 nM	-0.10	D.C., D_{NO}, k_{cat}, α	2014	124
CF/RuO_2NR/Nafion	CPA	+0.65	58.6	8 µm	n.r.	-0.10		2014	125
GC/rGO-AuNR-TPDP	CPA	+0.8	8.46	3 mm	6.5 nM	-0.168	D.C.	2014	126
GC/rGO/AuNP	CPA	+0.8	5.38	*n.r.*	133 nM	-0.085		2013	127
GC/AB/PtNP	CPA	+0.895	4.1	3 mm	50 nM	-0.13		2012	128
GC/AuNP-CS	CPA	+0.895	0.6	3 mm	7.20 nM	-0.37		2011	110
GC/3DG-$BMIMPF_6$ /Nafion	CPA	+0.8	11.2	3 mm	16 nM		D.C	2011	129
GC/CoTAPc	CPA	+1.1	17	3 mm	0.14 nM	-0.31	D.C., D_{NO}, k^0	2010	116
GC/MWCNT-CS-AuNP /Nafion	CPA	+0.895	24.5	3 mm	7.6 nM	-0.25		2010	111

[a]Slashes signify separation between depositions of electrode modifiers; dashes indicate co-deposition. Abbreviations in order of appearance: N-G: nitrogen-doped graphene; FePc: iron(II)phthalocyanine; PLL: poly(L-lysine); HNG: hierarchical nanoporous gold; T-CUA: transparent carbon ultramicroelectrode array; CS: chitosan; NP: nanoparticle; CA: cellulose acetate; S-G: sulfur-doped graphene; rGO: reduced graphene oxide; G: graphene; PADA: poly(acrylamide-*co*-diallyldimethylammonium chloride); NCstr: nanocluster; NC: nanocube; PBZ: 2-(2-pyridyl)benzimidazole; NR: nanorod; TPDP: tris(2,4,6-tribromophenoxy)dichlorophosphorane; AB: acetylene black; 3DG: 3-dimensional graphene; $BMIMPF_6$: 1-butyl-3-methylimidazolium; CoTAPc: cobalt(II)tetra-amine phthalocyanine; MWCNT: multiwalled carbon nanotube.

[b]Electrochemical technique: CPA: constant potential amperometry; SWV: squarewave voltammetry; DPV: differential pulse voltammetry.

[c]Applied potential *vs*. Ag|AgCl; *n.a.*: not applicable; *n.r.*: not reported.

[d]Current flux either as reported or calculated from provided data.

[e]Change in anodic peak potential with electrocatalyst modified relative to the bare electrode.

[f]Additional measurements: S.C.: surface-controlled; n: number of electrons; D.C.: diffusion-controlled; D_{NO}: diffusion coefficient of NO; k_{cat}: catalytic rate constant; α: charge transfer coefficient; k^0: standard heterogeneous electron transfer rate constant.

1.3.2 Ultramicroelectrode arrays

Ultramicroelectrodes (UMEs) have several well-characterized advantages over macroscopic electrodes.[85,130] By shrinking the diameter, the transition from linear to radial diffusion increases the rate of mass transfer, facilitating study of fast kinetic redox processes. The small currents passed (nA-pA) reduce the potential drop across the uncompensated (i.e., solution) resistance between the reference and working electrodes, and thus UMEs tolerate measurement in dilute electrolytes and often eliminate the need for counter electrodes. Lastly, low current passage leads to quick (milliseconds) charging of the electrode double layer, enhancing *S*/*N* in pulsed-potential techniques. In the case of an individual UME, these advantages are often offset by reduced sensitivity; however, microfabrication techniques have assisted the construction of UME arrays. A UME array is able to combine the benefits of a UME with the greater sensitivity of a macroscopic electrode by short-circuiting electrodes, thereby pooling the response.

Elliot et al. developed a UME array of 1.54 μm diameter T-C electrodes modified by gold nanoparticles suspended in a chitosan matrix.[100] With a final coating of cellulose acetate, the array was able to achieve a 200 nM limit of detection towards NO, outperforming the 1.1 μM LOD of a macroelectrode of near-equivalent area. In order to fully exploit the mass transfer benefits of UMEs, Quinton et al. optimized the hexagonal spacing of individual UMEs to prevent double layer overlap.[60] With a ferricyanine redox probe, they determined that the current response trended linearly with the number of short-circuited electrodes when the spacing between the electrodes was ≥10× the electrode diameter. A comparable study optimized the geometry of an arrayed ring-disk UME template: the disk to generate copper ions to catalyze NO release from localized *S*-nitrosoglutathione (GSNO), and the ring to

electrooxidize NO.[131] With seven short-circuited rings, they were able to achieve 15% collector efficiency and a 27 nM LOD towards NO. Arrays of UMEs have also recently been adapted to the measurement of NO from cell cultures, including pig aortic endothelial[132] and HL60 cells.[93] While short-circuiting enhances sensitivity, maintaining UMEs as individually addressable sensors makes possible multi-analyte detection (*see* Section 1.2.3). With the push towards multiplexed measurement from biological systems, the sensitivity and selectivity benefits of UME arrays will be advantageous to future cell culturing platforms.

1.4 Application to measurement in biological systems

The word 'biocompatible' can carry different connotations in different contexts. For example, both an implanted sensor that does not provoke host rejection and a sensor that maintains analytical performance in biological milieu may be referred to as biocompatible. In one case, the sensor avoids negatively affecting the biological system; in the other, the biological system does not negatively impact the sensor's analytical performance. In order to highlight this distinction, we have chosen to adopt the terminology of Reichert and colleagues: 'biocompatibility' for avoiding ill effect to the biological system, and 'sensocompatibility' for avoiding ill effect to sensor analytical performance.[133]

1.4.1 Sensocompatibility

Evaluations of analytical performance in clean, deoxygenated saline solutions assess an electrochemical NO sensor's ideal performance. However, introduction to biological systems introduces biofouling and matrix effects that are likely to affect the sensor's sensitivity and long-term stability. Evaluations of sensocompatibility are therefore necessary to inform the design or at least account for such effects to ensure measurement accuracy. A common means of assessing sensocompatibility is endpoint calibration, used primarily for in

vivo applications. Calibration of the sensor in clean saline before and after use provides an indication of the extent of irreversible damage/fouling undergone. Lee and colleagues have used endpoint calibration to ensure sensor stability for various microsurgery applications.[40,41,95] Fluorinated xerogel-coated, electrooxidative NO dual-sensors of end-plane diameters <0.5 mm were inserted into rat brains, retaining 76-92% of their initial sensitivity after measurement.[54,96] Comparatively, a Nafion-modified Pt microelectrode developed by Finnerty et al. maintained 46% NO sensitivity after perfusate measurements in a rat brain.[134] Reductions in sensitivity are due to a variety of factors, most commonly attributed to irreversible protein adsorption or mechanical strain damage.

Though good for stability assessment, endpoint calibrations fail to take into account matrix effects during use. The greater number of potential scavengers (e.g., free metals, cell-free hemoglobin, and thiol-containing residues) and greater viscosity of proteinaceous media reduce NO sensitivity, irrespective of damage/fouling. A comparative study by Hunter et al. demonstrated that a Pt/XG sensor retained only 37, 25, 10, and 0.1% of its initial NO sensitivity in oxygenated PBS while measuring in simulant wound fluid (10% v/v FBS in PBS), porcine plasma, serum, and blood, respectively.[135] The authors attributed only 3-5% of the sensitivity reduction to biofouling, so clearly the sample matrix can have profound and varied effects on NO sensitivity. Table 6 lists recent electrochemical NO sensors and their sensocompatibilities in different matrices. Of note, the retention in sensitivity (S_{NO} Ret.) will account for both matrix effects and biofouling, as the two cannot be distinguished without specific characterization. Notwithstanding, higher complexity matrices like blood or plasma more negatively impact NO sensitivity than simple simulant or culture media.

With biofouling, protein adsorption at the transducer-sample interface invariably affects mass transport of NO and therefore sensitivity. The primary thermodynamic force driving protein-surface interactions is hydrophobicity.[136] Due to the greater amount of entropic energy required to disrupt an ordered water layer, hydrophilic surfaces are thought to be less susceptible to protein fouling, explaining the wide use of hydrophilic poly(ethylene glycol) and poly(ethylene oxide) modifications to passivate medical and biological surfaces. Little work has sought to quantify/mitigate protein adsorption at NO sensor interfaces, in part because hydrophobic surfaces are so favorable for selective NO diffusion. As a result, the anti-biofouling benefits of hydrophilic coatings may well be counteracted by hampered NO diffusion.[50] Nevertheless, strategies to improve anti-biofouling character in electroanalytical platforms have been recently reviewed and may warrant adaptation to NO sensing.[137] Traditional gravimetric (e.g., electrochemical quartz crystal microbalance) and spectroscopic (e.g., the Bradford assay) quantifications of protein content may furnish future utility as well.[138,139] Rather than seek out transducer modifiers to mitigate biofouling, sensor pretreatment strategies may effectively pre-load the surface with contaminant protein to stabilize performance.[61,140] Assuming protein adsorption does not catastrophically impact sensitivity, soaking or polarizing electrochemical NO sensors in proteinaceous media before calibration has been used to minimize biofouling-related sensitivity fluctuations during eventual use.

Besides sensitivity, additional analytical metrics are rarely evaluated in biological contexts. As a notable exception, Wynne et al. observed a gradual increase in the AA response of Nafion-modified Pt electrodes with extended storage in various proteinaceous media.[48] Such assurances of selectivity maintenance are essential for accurate long-term

measurement of NO. Pekarova et al. observed 20 h evolution of NO release from endotoxin-stimulated macrophages with carbon fiber microelectrodes modified with polymeric nickel(II)tetrakis(3-methoxy-4-hydroxyphenyl)porphyrin and Nafion. Endpoint measurements of AA, DA, and NO_2^- responses assured that the sensors had in fact maintained selectivity for the duration of the experiment.[141]

Table 1.6 Sensocompatibility characterization of electrochemical NO sensors.

Electrode Design[a]	Media	S_{NO}[b] (pA nM^{-1})	LOD	Sensocompatibility		Year	Ref.
				Media[c]	S_{NO} Ret.[d] (%)		
ITO/rGO-FeTCP/APBA	100 mM PBS (pH 7.4)	123.2	55 pM	RPMI	70	2015	64
Pt/APTES/XG	10 mM PBS (pH 7.4)	0.0226 (S_{GSNO}) 0.0255 (S_{CysNO}) 0.0050 (S_{AlbSNO})	60 nM 60 nM 280 nM	Plasma	18 (S_{GSNO}) 27(S_{CysNO}) 13 (S_{AlbSNO})	2015	142
Pt/Nafion(1/2) /poly(*o*-PD)	40 mM PBS (pH 7.4)	1.07	8 nM	10% w/v BSA in PBS 10% w/v PEA in PBS	100 100	2014	48
Pt/APTES/XG	10 mM PBS (pH 7.4)	1.4	840 pM	Blood	<1	2013	53
GC/P-lCo(II)(salen)-MWCNT-CS	100 mM PBS (pH 7.4)	3870	2.99 nM	Peach extract	98	2012	65
GC/G-CTAB/CS-Hb	100 mM PBS (pH 7.0)	615	6.75 nM	Plant homogenate	51	2012	73
Au/poly(eugenol) /poly(phenol)	100 mM PBS (pH 7.4)	0.56	27 nM	RPMI DMEM MEM 50 μg mL^{-1} Fb	75 38 30 80	2011	60
Pt/MB/poly(*o*-PD)/CS	100 mM PBS (pH 7.4)	20	1 nM	MEM/HBSS/FBS aCSF	50 60	2010	61
Pt/Nafion	40 mM PBS (pH 7.4)	1.67	5 nM	10% w/v BSA in PBS 10% w/v PEA in PBS	71 58	2009	140

[a]Slashes signify separation between depositions of electrode modifiers; dashes indicate co-deposition. Abbreviations in order of appearance: ITO: indium tin oxide; rGO: reduced graphene oxide; FeTCP: iron(III) *meso*-tetra(4-carboxyphenyl)porphyrin; APBA: 3-aminophenylboronic acid; APTES: (3-aminopropyl)-triethoxysilane; XG: fluorinated xerogel; *o*-PD: *ortho*-phenylenediamine; P-1: molecularly-imprinted polymer; MWCNT: multiwalled carbon nanotube; CS: chitosan; G: graphene; CTAB: cetrimonium bromide; Hb: hemoglobin; MB: meldola blue.

[b]Sensitivity towards NO (or relevant *S*-nitrosothiol species when indicated).

[c]RPMI: Roswell Park Memorial Institute media; BSA: bovine serum albumin; PEA: palmitoylethanolamide; DMEM: Dulbecco's Modified Eagle Medium; MEM: Minimum Essential Media; Fb: fibrinogen; HBSS: Hank's Balanced Salt Solution; FBS: fetal bovine serum; aCSF: artificial cerebrospinal fluid.

[d]Retention in NO sensitivity (or relevant *S*-nitrosothiol species when indicated) relative to PBS measurement.

1.4.2 Biocompatibility

Biocompatibility concerns arise when detection methodologies perturb the biological system under observation, which may in turn affect the production of relevant analytes. In such instances, it can be exceedingly difficult to decouple artificial and natural stimuli. Electrochemical sensors are already well suited to reducing biological sample perturbation given their ability to be miniaturized and function in situ without additional reagents.[29] Interactions between the biological system and transducer (encompassing the electrode, its modifiers, and the applied potential) can still occur, and biocompatible modifiers have been used to minimize such interactions. Of course, the choice in modifier(s) will depend on the specific application and duration of measurement. For instance, subcutaneous in vivo electrochemical sensors must seek to minimize tissue inflammation at the site of implantation, and long-term measurement must be able to mitigate or account for the foreign body response (FBS).[143] With respect to NO measurement, there has not yet been a push to develop a long-term, implantable electrochemical sensor for which modifications mitigating the FBS would be relevant. Most electrochemical NO sensors applied in vivo conduct measurements over the course of minutes or hours, rather than days.[40,54,96] Under such short durations, the adsorption of proteins is a relevant factor, but only in so far as it affects sensor performance (i.e., sensocompatibility).[133] In general, the use of UMEs (10-50 μm) for in vivo monitoring allows non-invasive and non-destructive implantation of NO sensors at the site of release.[84]

Particularly within the last decade, most modifications specifically seeking to improve electrochemical NO sensor biocompatibility have occurred in the context of in vitro monitoring of cultured cells (i.e., cytocompatibility). In these platforms, a cell line is cultured

directly overtop an integrated planar electrode or UME array, and the basal (i.e., from the base of the cell) concentration of NO can be measured in the unstimulated, stimulated, or co-stimulated/inhibited state. Basal measurement of cellular NO release contrasts with the more common synapse-like arrangement, in which the electrode is placed in close proximity above a single cell or cell cluster.[88,91] However, basal measurement helps to eliminate variability in the cell-to-transducer distance, which can affect the amount of NO measured due to rapid scavenging.[29,144] To ensure biological relevance of basal NO measurements, assurances of cell adhesion, proliferation, healthy morphology, and viability on/above the electrode surface must be made.

As in vitro cell models come closer to mimicking tissue, efforts to develop flexible or bendable electrode substrates have gained attention. Zhao et al. recently created a flexible and stretchable electrode surface for the purpose of cell culturing and NO measurement.[145] A poly(dimethylsiloxane) (PDMS) film was exposed to UV irradiation to generate carboxyl groups, which were then modified with gold nanostructures through exposure to a solution of ethanol (radical reducing agent under UV) and chloroauric acid. Once seeded onto the surface, human umbilical vein endothelial cells (HUVECs) were able to proliferate with good morphology, retaining their normal spindle shape. With the application of a +0.85 V *vs.* Ag|AgCl working potential, NO release in response to L-arginine (L-Arg) stimulation could be measured. Guo et. al. created sheets of rGO modified with pyrenebutyric acid, which when activated by N-(3-dimethylamino-propyl)-N^0-ethylcarbodiimide (EDC) and N-hydro-sulfosuccinimide sodium salt (NHS), could covalently bind with arginylglycylaspartic acid (RGD)-peptide.[146] The RGD-peptide mimics the cell-binding sequence of extracellular matrix proteins, and was thus used to promote cell adhesion. Cultured HUVEC attachment

and growth were significantly improved over bare graphene, with a 2-fold increase in cell density and nearly 50% increase in cell length. The platform was then able to detect concentration-dependent release of NO with acetylcholine (ACh) stimulation. In both studies, the electrode was able to maintain the same NO sensitivity with repeated bending.[145,146]

Similar to the RGD-peptide, the use of small molecule binders to enhance cell adhesion has been a popular transducer modification. Xu et al. recently modified an ITO electrode with nitrogen-doped graphene (N-G), iron(II)phthalocyanine (FePc), and Nafion.[112] A final coat of poly-L-lysine (PLL) was added to improve cell adherence through electrostatic interaction between the positively-charged polymer and negatively-charged moieties on the cell membrane; as such, PLL is common surface modifier to tissue cultureware. Compared to the bare ITO electrode, HUVECs were able to grow with better morphology on the ITO/N-G/FePc/Nafion/PPL electrode. With an applied potential of +0.945 V *vs*. Ag|AgCl, NO release with L-Arg stimulation could be measured. Liu et al. modified an ITO electrode with reduced graphene oxide (rGO), iron(III)*meso*-tetra(4-carboxyphenyl)porphyrin (FeTCP), and 3-amino-phenylboronic acid (APBA).[64] The outermost APBA modification is able to react with 1,2- or 1,3-diols present in cell membrane carbohydrate moieties. Bare ITO and ITO/rGO-FeTCP/APBA electrodes were cultured with HUVECs and rinsed with saline to removed loosely bound cells, the latter retaining more cells due to enhanced adhesion from APBA. Moreover, they were able to track cell proliferation and viability for up to 86 h. Stimulation with L-Arg yielded measurable NO under an applied potential of +0.75 V *vs*. Ag|AgCl.

Depending on the scale of the electrode, assuring attachment of a high density of cells may be necessary to generate a measurable amount of NO. However, many studies verify cell

attachment and proliferation at electrode interfaces in the absence of an applied potential. An early study by Yaoita et al. found that the application of low DC potentials commonly used in electrooxidative electrochemical sensors (0 to +1.2 V *vs*. Ag|AgCl) significantly affected the morphology, growth, and viability of HeLa cells cultured on bare indium oxide electrodes.[147] At potentials greater than +0.7 V *vs*. Ag|AgCl, cell membranes began to break down due to electrical lysis, and at +1.2 V, all cells were dead. Oni et al. developed electrode arrays functionalized with different electrocatalysts to detect NO from cultured HUVECs stimulated with bradykinin only to find no detectable NO release.[148] Comparison of cells cultured on the array with and without the +0.75 V *vs*. Ag|AgCl applied potential revealed that cells exposed to the working potential produced stress fibers and were significantly less viable. After modifying the design by culturing cells on Cellagen discs positioned ~0.1 μm above the electrodes, viability was retained, and bradykinin-stimulated NO release was measurable. Clearly, assurance of cell viability in the presence of the applied potential is critical to overall platform design. Cha et al. developed a microfluidic device in which macrophages were cultured in "soft-bottom" polyurethane microchannels modified with fibronectin for enhanced attachment.[52] The cells proliferated to a confluent monolayer within eight days of culture media perfusion. A downstream NO sensor based on a TeflonAF-modified gas-permeable membrane (described in Section 1.2.1) was able to detect NO released from macrophages stimulated with lipopolysaccharide (LPS) over the course of 16 h. Separation of the cells from the electrode surface eliminated viability concerns, but required deoxygenation of the perfusate solution to mitigate scavenging of NO by O_2 during passage to the electrode. Overall, in determining electrode placement, a potential trade-off

exists between the ability to measure the full flux of released NO and protection of the cell from potential-induced lysis.

New in vitro models are increasingly seeking to imitate complex native tissue environments. Electracellular matrix is comprised by a great variety of molecules (e.g., collagen, elastin, and proteoglycans) morphologies (e.g., pores, protrusions, and ridges 5 to 200 nm in scale), and Young's moduli, all of which impact the immobilization, spatial orientation, and function of cells.[149] As electrochemical NO sensors continue to develop, balancing electrochemical performance with biomimicry will be an important design consideration. Fortunately, the literature is rich with strategies developed for other electroactive analytes that are easily adaptable to the detection of NO.[149-153] Hu et al. recently developed a 3D graphene foam scaffold for the culturing of HeLa cells.[154] The graphene foam is better able to mimic the spatial arrangement of cells found in tissue while retaining conductivity. Electrochemical measurement of hydrogen sulfide with stimulation from cysteine was possible under a +0.5 V *vs*. Ag|AgCl working potential. With the application of a NO-selective modification (*see* Section 1.2.1) and a higher applied potential, the graphene foam scaffold could be customized for measurement of cellular NO release.

1.5 Conclusions and research aims

The transducer modifiers and techniques outlined here have the potential to improve analytical performance, although sometimes at a cost. Selectivity enhancements can come at the expense of reduced sensitivity; arrayed and multi-analyte detection platforms increase fabrication complexity; hydrophobic membranes improve NO diffusion but may be more susceptible to biofouling. What defines the ideal electrochemical NO sensor will ultimately depend on the application. Detection of the NO release of a therapeutic agent under tightly

controlled in vitro conditions will have a different set of requirements than detection in vivo or from cultured cells. From an arsenal of thirty years of platform development, modifiers may be used in countlessly different concentrations and combinations. Strict analytical characterization of individual modifications is therefore critical to an informed selection of appropriate modifiers for a certain application. Quantitative indicators of selectivity, sensitivity, sensocompatibility, and (if applicable) qualitative assurances of biocompatibility must be provided to demonstrate usability and encourage implementation. As electrochemical NO sensors are increasingly integrated into cell culture chambers, microfluidic devices, and tissue-emulating scaffolds, the characterization of long-term sensocompatibility, in particular, in relevant media will be necessary to assure measurement accuracy in the future.

My goal in writing this chapter was to provide an updated overview on the field of electrochemical NO detection, describe reports that specifically undertook rigorous analytical characterization, and suggest what kinds of future characterization would be beneficial. These goals are what informed the specific aims of my research, which included:

1) carrying out a comparative study of common electropolymerized films with individual optimizations of the deposition conditions for enhancing NO permselectivity (Chapter 2);
2) developing a novel, solid-type electrochemical NO sensor designed and evaluated for long-term sensocompatibility (Chapter 3);
3) applying said sensor to the measurement of NO release from inflammatory macrophages in terms of both temporal and spatial concentration profiles (Chapter 3);

4) comparing common metallophthalocyanine electrocatalysts and quantifying for the first time their selectivity benefits for electrochemical detection of NO (Chapter 4); and,
5) designing an electrochemical sensor for the detection of hydrogen sulfide, a gasotransmitter with biological roles similar to NO, for eventual integration into a dual-sensor platform (Chapter 5).

Electropolymerized films (EPFs) and metallophthalocyanines (MPcs) have been used in the construction of electrochemical NO sensors since the inception of this field. Because these modifiers are very often used in conjunction or with other membranes/modifiers, it can be difficult to determine their specific selectivity traits towards NO. Moreover, their mechanisms of imparted selectivity are vastly different, as EPFs rely on selective diffusion, and surface-confined MPc macrocycles depend on coordination with NO. By studying these modifiers in isolation (i.e., absent co-deposited modifiers), their selectivity traits were rigorously quantified. These comparative studies will inform future electrochemical NO sensor design, allowing selectivity performance (and therefore NO detection accuracy) to be maximized for the particular application.

For the design of our own electrochemical NO sensor for biological application, the comparative EPF study informed our selection of poly(5-amino-1-napthol) for its remarkable nitrite-rejecting ability and favorable performance in simulated wound fluid. Combined with a xerogel topcoat, the bilaminar-modified sensor was able to retain analytical performance with extended operation in proteinaceous media. Advantageous selectivity and sensocompatibility allowed for the continuous monitoring of iNOS-derived NO release from

pro-inflammatory stimulated macrophages for >24 h, and novel information regarding the spatial diffusion profile of NO release was obtained. Lastly, an amperometric and selective hydrogen sulfide (H_2S) sensor was designed based on an EPF-modified glassy carbon electrode. As NO and H_2S are suspected to experience biological crosstalk in a manner parallel to/or in conjunction with NO and CO, the construction of an accurate dual NO/H_2S sensor will be heavily informed by the findings presented here with respect to both analytes.

REFERENCES

(1) Ignarro, L. J.; Buga, G. M.; Wood, K. S.; Byrns, R. E.; Chaudhuri, G. Endothelium-derived relaxing factor produced and released from artery and vein is nitric oxide. *Proc. Natl. Acad. Sci. U. S. A.* **1987**, *84*, 9265-9269.

(2) Bogdan, C. Nitric oxide and the immune response. *Nature immunol.* **2001**, *2*, 907.

(3) Coleman, J. W. Nitric oxide in immunity and inflammation. *Int. immunopharmacol.* **2001**, *1*, 1397-1406.

(4) Isenberg, J. S.; Ridnour, L. A.; Espey, M. G.; Wink, D. A.; Roberts, D. D. Nitric oxide in wound-healing. *Microsurgery* **2005**, *25*, 442-451.

(5) Luo, J.-d.; Chen, A. F. Nitric oxide: a newly discovered function on wound healing. *Acta Pharmacol. Sin.* **2005**, *26*, 259-264.

(6) Loscalzo, J.; Welch, G. Nitric oxide and its role in the cardiovascular system. *Prog. Cardiovasc. Dis.* **1995**, *38*, 87-104.

(7) Wink, D. A.; Vodovotz, Y.; Laval, J.; Laval, F.; Dewhirst, M. W.; Mitchell, J. B. The multifaceted roles of nitric oxide in cancer. *Carcinogenesis* **1998**, *19*, 711-721.

(8) Calabrese, V.; Mancuso, C.; Calvani, M.; Rizzarelli, E.; Butterfield, D. A.; Stella, A. M. G. Nitric oxide in the central nervous system: neuroprotection versus neurotoxicity. *Nature Rev. Neurosci.* **2007**, *8*, 766.

(9) Bult, H.; Boeckxstaens, G.; Pelckmans, P.; Jordaens, F.; Van Maercke, Y.; Herman, A. Nitric oxide as an inhibitory non-adrenergic non-cholinergic neurotransmitter. *Nature* **1990**, *345*, 346.

(10) Liew, F. Y. Regulation of lymphocyte functions by nitric oxide. *Curr. Opin. Immunol.* **1995**, *7*, 396-399.

(11) Nathan, C. F.; Hibbs Jr, J. B. Role of nitric oxide synthesis in macrophage antimicrobial activity. *Curr. Opin. Immunol.* **1991**, *3*, 65-70.

(12) Aggarwal, B. B.; Mehta, K. Determination and regulation of nitric oxide production from macrophages by lipopolysaccharides, cytokines, and retinoids. *Methods Enzymol.* **1996**, *269*, 166-171.

(13) Yager, D. R.; Nwomeh, B. C. The proteolytic environment of chronic wounds. *Wound Repair Regen.* **1999**, *7*, 433-441.

(14) Bernatchez, S. F.; Menon, V.; Stoffel, J.; Walters, S. A.; Lindroos, W. E.; Crossland, M. C.; Shawler, L. G.; Crossland, S. P.; Boykin, J. V., Jr. Nitric oxide levels in wound fluid may reflect the healing trajectory. *Wound Repair Regen.* **2013**, *21*, 410-417.

(15) Li, J.; Chen, J.; Kirsner, R. Pathophysiology of acute wound healing. *Clin. Dermatol.* **2007**, *25*, 9-18.

(16) Morbidelli, L.; Donnini, S.; Ziche, M. Role of nitric oxide in the modulation of angiogenesis. *Curr. Pharm. Des.* **2003**, *9*, 521-530.

(17) Stearns-Kurosawa, D. J.; Osuchowski, M. F.; Valentine, C.; Kurosawa, S.; Remick, D. G. The pathogenesis of sepsis. *Annu. Rev. Pathol.: Mech. Dis.* **2011**, *6*, 19-48.

(18) Smith, M. A.; Harris, P. L. R.; Sayre, L. M.; Beckman, J. S.; Perry, G. Widespread peroxynitrite-mediated damage in Alzheimer's disease. *J. Neurosci.* **1997**, *17*, 2653-2657.

(19) Beal, M. F. Excitotoxicity and nitric oxide in Parkinson's disease pathogenesis. *Annu. Neurol.* **1998**, *44*, S110-S114.

(20) Valko, M.; Leibfritz, D.; Moncol, J.; Cronin, M. T. D.; Mazur, M.; Telser, J. Free radicals and antioxidants in normal physiological functions and human disease. *Int. J. Biochem. Cell Biol.* **2007**, *39*, 44-84.

(21) Naseem, K. M. The role of nitric oxide in cardiovascular diseases. *Mol. Aspects Med.* **2005**, *26*, 33-65.

(22) Rees, D.; Palmer, R.; Moncada, S. Role of endothelium-derived nitric oxide in the regulation of blood pressure. *Proc. Natl. Acad. Sci.* **1989**, *86*, 3375-3378.

(23) Webb, A.; Bond, R.; McLean, P.; Uppal, R.; Benjamin, N.; Ahluwalia, A. Reduction of nitrite to nitric oxide during ischemia protects against myocardial ischemia–reperfusion damage. *Proc. Natl. Acad. Sci.* **2004**, *101*, 13683-13688.

(24) Moorcroft, M. J.; Davis, J.; Compton, R. G. Detection and determination of nitrate and nitrite: a review. *Talanta* **2001**, *54*, 785-803.

(25) Knowles, R. G.; Moncada, S. Nitric oxide synthases in mammals. *Biochem. J.* **1994**, *298*, 249.

(26) Griess, J. P. XVIII. On a new series of bodies in which nitrogen substituted for hydrogen. *Philos. Trans. R. Soc. Lond.* **1864**, *154*, 667-731.

(27) Archer, S. Measurement of nitric oxide in biological models. *FASEB J.* **1993**, *7*, 349-360.

(28) Kalyanaraman, B.; Darley-Usmar, V.; Davies, K. J.; Dennery, P. A.; Forman, H. J.; Grisham, M. B.; Mann, G. E.; Moore, K.; Roberts II, L. J.; Ischiropoulos, H. Measuring reactive oxygen and nitrogen species with fluorescent probes: challenges and limitations. *Free Rad. Biol. Med.* **2012**, *52*, 1-6.

(29) Privett, B. J.; Shin, J. H.; Schoenfisch, M. H. Electrochemical nitric oxide sensors for physiological measurements. *Chem. Soc. Rev.* **2010**, *39*, 1925-1935.

(30) Bedioui, F.; Griveau, S. Electrochemical detection of nitric nxide: assessement of twenty years of strategies. *Electroanalysis* **2013**, *25*, 587-600.

(31) Xu, T.; Scafa, N.; Xu, L.-p.; Su, L.; Li, C.; Zhou, S.; Liu, Y.; Zhang, X. Electrochemical sensors for nitric oxide detection in biological applications. *Electroanalysis* **2014**, *26*, 449-468.

(32) Pryor, W. A.; Squadrito, G. L. The chemistry of peroxynitrite: a product from the reaction of nitric oxide with superoxide. *Am. J. Physiol. Lung Cell. Mol. Physiol.* **1995**, *268*, L699-L722.

(33) Griveau, S.; Dumézy, C.; Goldner, P.; Bedioui, F. Electrochemical analysis of the kinetics of nitric oxide release from two diazeniumdiolates in buffered aqueous solutions. *Electrochem. Commun.* **2007**, *9*, 2551-2556.

(34) Gow, A. J.; Stamler, J. S. Reactions between nitric oxide and haemoglobin under physiological conditions. *Nature* **1998**, *391*, 169.

(35) Lancaster, J. R. A Tutorial on the diffusibility and reactivity of free nitric oxide. *Nitric Oxide* **1997**, *1*, 18-30.

(36) Hall, C. N.; Garthwaite, J. What is the real physiological NO concentration in vivo? *Nitric Oxide* **2009**, *21*, 92-103.

(37) Shibuki, K. An electrochemical microprobe for detecting nitric oxide release in brain tissue. *Neurosci. Res.* **1990**, *9*, 69-76.

(38) Ciszewski, A.; Milczarek, G. Electrochemical detection of nitric oxide using polymer modified electrodes. *Talanta* **2003**, *61*, 11-26.

(39) Wang, J. Selectivity coefficients for amperometric sensors. *Talanta* **1994**, *41*, 857-863.

(40) Park, S. S.; Hong, M.; Song, C.-K.; Jhon, G.-J.; Lee, Y.; Suh, M. Real-time in vivo simultaneous measurements of nitric oxide and oxygen using an amperometric dual microsensor. *Anal. Chem.* **2010**, *82*, 7618-7624.

(41) Park, S. S.; Kim, J.; Lee, Y. Improved electrochemical microsensor for the Real-time simultaneous analysis of endogenous nitric oxide and carbon monoxide generation. *Anal. Chem.* **2012**, *84*, 1792-1796.

(42) Kang, S. W.; Kim, O. K.; Seo, B.; Lee, S. H.; Quan, F. S.; Shin, J. H.; Lee, G.-J.; Park, H.-K. Simultaneous, real-time measurement of nitric oxide and oxygen dynamics during cardiac ischemia-reperfusion of the rat utilizing sol-gel-derived electrochemical microsensors. *Anal. Chim. Acta* **2013**, *802*, 74-81.

(43) Jensen, G. C.; Zheng, Z.; Meyerhoff, M. E. Amperometric nitric oxide sensors with enhanced selectivity over carbon monoxide via platinum oxide formation under alkaline conditions. *Anal. Chem.* **2013**, *85*, 10057-10061.

(44) Dahlstrøm, P. K.; Harrington, D. A.; Seland, F. Kinetic study of CO oxidation on clean and oxidized Pt. *Electrochim. Acta* **2012**, *82*, 550-557.

(45) Malinski, T.; Taha, Z. Nitric oxide release from a single cell measured in situ by a porphyrinic-based microsensor. *Nature* **1992**, *358*, 676-678.

(46) Bedioui, F.; Trevin, S.; Devynck, J. The use of gold electrodes in the electrochemical detection of nitric oxide in aqueous solution. *J. Electroanal. Chem.* **1994**, *377*, 295-298.

(47) Lantoine, F.; Trevin, S.; Bedioui, F.; Devynck, J. Selective and sensitive electrochemical measurement of nitric oxide in aqueous solution: discussion and new results. *J. Electroanal. Chem.* **1995**, *392*, 85-89.

(48) Wynne, A. M.; Reid, C. H.; Finnerty, N. J. In vitro characterization of ortho phenylenediamine and Nafion-modified Pt electrodes for measuring brain nitric oxide. *J. Electroanal. Chem.* **2014**, *732*, 110-116.

(49) Kirwan, S. M.; Rocchitta, G.; McMahon, C. P.; Craig, J. D.; Killoran, S. J.; O'Brien, K. B.; Serra, P. A.; Lowry, J. P.; O'Neill, R. D. Modifications of poly (o-phenylenediamine) permselective layer on Pt-Ir for biosensor application in neurochemical monitoring. *Sensors* **2007**, *7*, 420-437.

(50) Pontié, M.; Gobin, C.; Pauporté, T.; Bedioui, F.; Devynck, J. Electrochemical nitric oxide microsensors: sensitivity and selectivity characterisation. *Anal. Chim. Acta* **2000**, *411*, 175-185.

(51) Mitchell, K. M.; Michaelis, E. K. Multimembrane carbon fiber electrodes for physiological measurements of nitric oxide. *Electroanalysis* **1998**, *10*, 81-88.

(52) Cha, W.; Tung, Y.-C.; Meyerhoff, M. E.; Takayama, S. Patterned electrode-based amperometric gas sensor for direct nitric oxide detection within microfluidic devices. *Anal. Chem.* **2010**, *82*, 3300-3305.

(53) Hunter, R. A.; Privett, B. J.; Henley, W. H.; Breed, E. R.; Liang, Z.; Mittal, R.; Yoseph, B. P.; McDunn, J. E.; Burd, E. M.; Coopersmith, C. M.; Ramsey, J. M.; Schoenfisch, M. H. Microfluidic amperometric sensor for analysis of nitric oxide in whole blood. *Anal. Chem.* **2013**, *85*, 6066-6072.

(54) Ha, Y.; Sim, J.; Lee, Y.; Suh, M. Insertable fast-response amperometric NO/CO dual microsensor: study of neurovascular coupling during acutely induced seizures of rat brain cortex. *Anal. Chem.* **2016**, *88*, 2563-2569.

(55) Shin, J. H.; Privett, B. J.; Kita, J. M.; Wightman, R. M.; Schoenfisch, M. H. Fluorinated xerogel-derived microelectrodes for amperometric nitric oxide sensing. *Anal. Chem.* **2008**, *80*, 6850-6859.

(56) Zhang, Z.; Liu, H.; Deng, J. A glucose biosensor based on immobilization of glucose oxidase in electropolymerized o-aminophenol film on platinized glassy carbon electrode. *Anal. Chem.* **1996**, *68*, 1632-1638.

(57) Dai, Y.-Q.; Zhou, D.-M.; Shiu, K.-K. Permeability and permselectivity of polyphenylenediamine films synthesized at a palladium disk electrode. *Electrochim. Acta* **2006**, *52*, 297-303.

(58) Killoran, S. J.; O'Neill, R. D. Characterization of permselective coatings electrosynthesized on Pt-Ir from the three phenylenediamine isomers for biosensor applications. *Electrochim. Acta* **2008**, *53*, 7303-7312.

(59) Rothwell, S. A.; McMahon, C. P.; O'Neill, R. D. Effects of polymerization potential on the permselectivity of poly(o-phenylenediamine) coatings deposited on Pt-Ir electrodes for biosensor applications. *Electrochim. Acta* **2009**, *55*, 1051-1060.

(60) Quinton, D.; Girard, A.; Kim, L. T. T.; Raimbault, V.; Griscom, L.; Razan, F.; Griveau, S.; Bedioui, F. On-chip multi-electrochemical sensor array platform for simultaneous screening of nitric oxide and peroxynitrite. *Lab Chip* **2011**, *11*, 1342-1350.

(61) Njagi, J.; Erlichman, J. S.; Aston, J. W.; Leiter, J. C.; Andreescu, S. A sensitive electrochemical sensor based on chitosan and electropolymerized Meldola blue for monitoring NO in brain slices. *Sens. Actuators, B* **2010**, *143*, 673-680.

(62) Huang, C.; Brisbois, E.; Meyerhoff, M. E. Flow injection measurements of S-nitrosothiols species in biological samples using amperometric nitric oxide sensor and soluble organoselenium catalyst reagent. *Anal. Bioanal. Chem.* **2011**, *400*, 1125-1135.

(63) Shim, J. H.; Do, H.; Lee, Y. Simple fabrication of amperometric nitric oxide microsensors based on electropolymerized membrane films. *Electroanalysis* **2010**, *22*, 359-366.

(64) Liu, Y.-L.; Wang, X.-Y.; Xu, J.-Q.; Xiao, C.; Liu, Y.-H.; Zhang, X.-W.; Liu, J.-T.; Huang, W.-H. Functionalized graphene-based biomimetic microsensor interfacing with living cells to sensitively monitor nitric oxide release. *Chem. Sci.* **2015**, *6*, 1853-1858.

(65) Zhao, L.; Zhu, S.; Zhou, J. A novel amperometric nitric oxide sensor based on imprinted microenvironments for controlling metal coordination. *Sens. Actuators, B* **2012**, *171-172*, 563-571.

(66) Derbyshire, E. R.; Marletta, M. A. Structure and regulation of soluble guanylate cyclase. *Annu Rev. Biochem.* **2012**, *81*, 533-559.

(67) Bredt, D. S.; Snyder, S. H. Nitric oxide: a physiologic messenger molecule. *Annu. Rev. Biochem.* **1994**, *63*, 175-195.

(68) Zhang, W.; Li, G. Third-generation biosensors based on the direct electron transfer of proteins. *Anal. Sci.* **2004**, *20*, 603-609.

(69) Léger, C.; Bertrand, P. Direct electrochemistry of redox enzymes as a tool for mechanistic studies. *Chem. Rev.* **2008**, *108*, 2379-2438.

(70) Fan, C.; Wagner, G.; Li, G. Effect of dimethyl sulfoxide on the electron transfer reactivity of hemoglobin. *Bioelectrochemistry* **2001**, *54*, 49-51.

(71) Li, P.; Ding, Y.; Lu, Z.; Li, Y.; Zhu, X.; Zhou, Y.; Tang, Y.; Chen, Y.; Cai, C.; Lu, T. Direct electrochemistry of hemoglobin immobilized on the water-soluble phosphonate

functionalized multi-walled carbon nanotubes and its application to nitric oxide biosensing. *Talanta* **2013**, *115*, 228-234.

(72) Laviron, E. General expression of the linear potential sweep voltammogram in the case of diffusionless electrochemical systems. *J. Electroanal. Chem. Interfacial Electrochem.* **1979**, *101*, 19-28.

(73) Wen, W.; Chen, W.; Ren, Q. Q.; Hu, X. Y.; Xiong, H. Y.; Zhang, X. H.; Wang, S. F.; Zhao, Y. D. A highly sensitive nitric oxide biosensor based on hemoglobin-chitosan/graphene-hexadecyltrimethylammonium bromide nanomatrix. *Sens. Actuators, B* **2012**, *166-167*, 444-450.

(74) Abdelwahab, A. A.; Koh, W. C. A.; Noh, H.-B.; Shim, Y.-B. A selective nitric oxide nanocomposite biosensor based on direct electron transfer of microperoxidase: Removal of interferences by co-immobilized enzymes. *Biosens. Bioelectron.* **2010**, *26*, 1080-1086.

(75) Jia, S.; Fei, J.; Zhou, J.; Chen, X.; Meng, J. Direct electrochemistry of hemoglobin entrapped in cyanoethyl cellulose film and its electrocatalysis to nitric oxide. *Biosens. Bioelectron.* **2009**, *24*, 3049-3054.

(76) Li, F.; Nie, M.; He, X.; Fei, J.; Ding, Y.; Feng, B. Direct electrochemistry and electrocatalysis of hemoglobin on a glassy carbon electrode modified with poly(ethylene glycol diglycidyl ether) and gold nanoparticles on a quaternized cellulose support. A sensor for hydrogen peroxide and nitric oxide. *Microchim. Acta* **2014**, *181*, 1541-1549.

(77) Kamin, R. A.; Wilson, G. S. Rotating ring-disk enzyme electrode for biocatalysis kinetic studies and characterization of the immobilized enzyme layer. *Anal. Chem.* **1980**, *52*, 1198-1205.

(78) Paul, D. W.; Stenken, J. A. A review of flux considerations for in vivo neurochemical measurements. *Analyst* **2015**, *140*, 3709-3730.

(79) Moore, A. N. J.; Katz, E.; Willner, I. Electrocatalytic reduction of organic peroxides in organic solvents by microperoxidase-11 immobilized as a monolayer on a gold electrode. *J. Electroanal. Chem.* **1996**, *417*, 189-192.

(80) Musameh, M. M.; Dunn, C. J.; Uddin, M. H.; Sutherland, T. D.; Rapson, T. D. Silk provides a new avenue for third generation biosensors: Sensitive, selective and stable electrochemical detection of nitric oxide. *Biosens. Bioelectron.* **2018**, *103*, 26-31.

(81) Yoon, J.; Shin, J.-W.; Lim, J.; Mohammadniaei, M.; Bharate Bapurao, G.; Lee, T.; Choi, J.-W. Electrochemical nitric oxide biosensor based on amine-modified MoS2/graphene oxide/myoglobin hybrid. *Colloids Surf., B* **2017**, *159*, 729-736.

(82) Marlinda, A. R.; Pandikumar, A.; Jayabal, S.; Yusoff, N.; Suriani, A. B.; Huang, N. M. Voltammetric determination of nitric oxide using a glassy carbon electrode modified with a nanohybrid consisting of myoglobin, gold nanorods, and reduced graphene oxide. *Microchim. Acta* **2016**, *183*, 3077-3085.

(83) Takahashi, S. H.; Cordoba de Torresi, S. I. Nitric oxide sensing by cytochrome c bonded to a conducting polymer modified glassy carbon electrode. *Synth. Met.* **2009**, *159*, 2159-2161.

(84) Bedioui, F.; Quinton, D.; Griveau, S.; Nyokong, T. Designing molecular materials and strategies for the electrochemical detection of nitric oxide, superoxide and peroxynitrite in biological systems. *Phys. Chem. Chem. Phys.* **2010**, *12*, 9976-9988.

(85) Griveau, S.; Bedioui, F. Overview of significant examples of electrochemical sensor arrays designed for detection of nitric oxide and relevant species in a biological environment. *Anal. Bioanal. Chem.* **2013**, *405*, 3475-3488.

(86) Calas-Blanchard, C.; Catanante, G.; Noguer, T. Electrochemical Sensor and Biosensor Strategies for ROS/RNS Detection in Biological Systems. *Electroanalysis* **2014**, *26*, 1277-1286.

(87) Amatore, C.; Arbault, S.; Koh, A. C. W. Simultaneous detection of reactive oxygen and nitrogen species released by a single macrophage by triple potential-step chronoamperometry. *Anal. Chem.* **2010**, *82*, 1411-1419.

(88) Li, Y.; Meunier, A.; Fulcrand, R.; Sella, C.; Amatore, C.; Thouin, L.; Lemaitre, F.; Guille-Collignon, M. Multi-chambers microsystem for simultaneous and direct electrochemical detection of reactive oxygen and nitrogen species released by cell populations. *Electroanalysis* **2016**, *28*, 1865-1872.

(89) Koppenol, W. H.; Moreno, J. J.; Pryor, W. A.; Ischiropoulos, H.; Beckman, J. S. Peroxynitrite, a cloaked oxidant formed by nitric oxide and superoxide. *Chem. Res. Toxicol.* **1992**, *5*, 834-842.

(90) Beckman, J. S.; Koppenol, W. H. Nitric oxide, superoxide, and peroxynitrite: the good, the bad, and ugly. *Am. J. Physiol. Cell Physiol.* **1996**, *271*, C1424-C1437.

(91) Amatore, C.; Arbault, S.; Guille, M.; Lemaitre, F. Electrochemical monitoring of single cell secretion: vesicular exocytosis and oxidative stress. *Chem. Rev.* **2008**, *108*, 2585-2621.

(92) Li, Y.; Sella, C.; Lemaitre, F.; Guille-Collignon, M.; Thouin, L.; Amatore, C. Electrochemical detection of nitric oxide and peroxynitrite anion in microchannels at highly sensitive platinum-black coated electrodes. Application to ROS and RNS mixtures prior to biological investigations. *Electrochim. Acta* **2014**, *144*, 111-118.

(93) Thi Kim, L. T. O.; Escriou, V.; Griveau, S.; Girard, A.; Griscom, L.; Razan, F.; Bedioui, F. Array of ultramicroelectrodes for the simultaneous detection of nitric oxide and peroxynitrite in biological systems. *Electrochim. Acta* **2014**, *140*, 33-36.

(94) Park, S. S.; Tatum, C. E.; Lee, Y. Dual electrochemical microsensor for simultaneous measurements of nitric oxide and oxygen: Fabrication and characterization. *Electrochem. Commun.* **2009**, *11*, 2040-2043.

(95) Kim, Y. S.; Ha, Y.; Sim, J.; Suh, M.; Lee, Y. Location-dependent sensing of nitric oxide and calcium ions in living rat kidney using an amperometric/potentiometric dual microsensor. *Analyst* **2016**, *141*, 297-304.

(96) Moon, J.; Ha, Y.; Kim, M.; Sim, J.; Lee, Y.; Suh, M. Dual electrochemical microsensor for real-time simultaneous monitoring of nitric oxide and potassium ion changes in a rat brain during spontaneous neocortical epileptic seizure. *Anal. Chem.* **2016**, *88*, 8942-8948.

(97) Kwon, N. S.; Nathan, C. F.; Gilker, C.; Griffith, O. W.; Matthews, D. E.; Stuehr, D. J. L-citrulline production from L-arginine by macrophage nitric oxide synthase. The ureido oxygen derives from dioxygen. *J. Biol. Chem.* **1990**, *265*, 13442-13445.

(98) Kajimura, M.; Fukuda, R.; Bateman, R. M.; Yamamoto, T.; Suematsu, M. Interactions of multiple gas-transducing systems: hallmarks and uncertainties of CO, NO, and H2S gas biology. *Antioxid. Redox Signal.* **2010**, *13*, 157-192.

(99) Dreyer, D. R.; Park, S.; Bielawski, C. W.; Ruoff, R. S. The chemistry of graphene oxide. *Chem. Soc. Rev.* **2010**, *39*, 228-240.

(100) Elliott, J.; Duay, J.; Simoska, O.; Shear, J. B.; Stevenson, K. J. Gold nanoparticle modified transparent carbon ultramicroelectrode arrays for the selective and sensitive electroanalytical detection of nitric oxide. *Anal. Chem.* **2017**, *89*, 1267-1274.

(101) Lee, Y.; Oh, B. K.; Meyerhoff, M. E. Improved planar amperometric nitric oxide sensor based on platinized platinum anode. 1. Experimental results and theory when applied for monitoring NO release from diazeniumdiolate-doped polymeric films. *Anal. Chem.* **2004**, *76*, 536-544.

(102) Liu, Z.; Nemec-Bakk, A.; Khaper, N.; Chen, A. Sensitive electrochemical detection of nitric oxide release from cardiac and cancer cells via a hierarchical nanoporous gold Microelectrode. *Anal. Chem.* **2017**, *89*, 8036-8043.

(103) Walcarius, A. Template-directed porous electrodes in electroanalysis. *Anal. Bioanal. Chem.* **2010**, *396*, 261-272.

(104) Nguyen, T. Q.; Padama, A. A. B.; Escano, M. C. S.; Kasai, H. Theoretical study on the adsorption of NO on metal macrocycles, metal = Mn, Fe, Co, Ni, Cu, Zn. *ECS Trans.* **2013**, *45*, 91-100.

(105) Nyokong, T.; Vilakazi, S. Phthalocyanines and related complexes as electrocatalysts for the detection of nitric oxide. *Talanta* **2003**, *61*, 27-35.

(106) Zagal, J. H.; Griveau, S.; Silva, J. F.; Nyokong, T.; Bedioui, F. Metallophthalocyanine-based molecular materials as catalysts for electrochemical reactions. *Coord. Chem. Rev.* **2010**, *254*, 2755-2791.

(107) Caro, C. A.; Zagal, J. H.; Bedioui, F. Electrocatalytic activity of substituted metallophthalocyanines adsorbed on vitreous carbon electrode for nitric oxide oxidation. *J. Electrochem. Soc.* **2003**, *150*, E95-E103.

(108) Liu, H.; Weng, L.; Yang, C. A review on nanomaterial-based electrochemical sensors for H2O2, H2S and NO inside cells or released by cells. *Microchim. Acta* **2017**, *184*, 1267-1283.

(109) Li, J.; Xie, J.; Gao, L.; Li, C. M. Au nanoparticles-3D graphene hydrogel nanocomposite to boost synergistically in situ detection sensitivity toward cell-released nitric oxide. *ACS Appl. Mater. Interfaces* **2015**, *7*, 2726-2734.

(110) Wang, F.; Deng, X.; Wang, W.; Chen, Z. Nitric oxide measurement in biological and pharmaceutical samples by an electrochemical sensor. *J. Solid State Electrochem.* **2011**, *15*, 829-836.

(111) Deng, X.-C.; Wang, F.; Chen, Z.-L. A novel electrochemical sensor based on nano-structured film electrode for monitoring nitric oxide in living tissues. *Talanta* **2010**, *82*, 1218-1224.

(112) Xu, H.; Liao, C.; Liu, Y.; Ye, B.-C.; Liu, B. Iron phthalocyanine decorated nitrogen-doped graphene biosensing platform for real-time detection of nitric oxide released from living cells. *Anal. Chem.* **2018**, *90*, 4438-4444.

(113) Nicholson, R. S. Theory and application of cyclic voltammetry for measurement of electrode reaction kinetics. *Anal. Chem.* **1965**, *37*, 1351-1355.

(114) Brown, A. P.; Anson, F. C. Cyclic and differential pulse voltammetric behavior of reactants confined to the electrode surface. *Anal. Chem.* **1977**, *49*, 1589-1595.

(115) González, V. J. Determination of standard rate constants for electrochemical irreversible processes from linear sweep voltammograms. *Electroanalysis* **1997**, *9*, 880-882.

(116) Sivanesan, A.; John, S. A. Highly sensitive electrochemical sensor for nitric oxide using the self-assembled monolayer of 1,8,15,22-tetraaminophthalocyanatocobalt(II) on glassy carbon electrode. *Electroanalysis* **2010**, *22*, 639-644.

(117) Bhat, S. A.; Pandit, S. A.; Rather, M. A.; Rather, G. M.; Rashid, N.; Ingole, P. P.; Bhat, M. A. Self-assembled AuNPs on sulphur-doped graphene: a dual and highly efficient electrochemical sensor for nitrite (NO2-) and nitric oxide (NO). *New J. Chem.* **2017**, *41*, 8347-8358.

(118) Liu, Z.; Chen, A.; Forsyth, H.; Khaper, N. Sensitive electrochemical detection of nitric oxide based on AuPt and reduced graphene oxide nanocomposites. *Analyst* **2016**, *141*, 4074-4083.

(119) Ikhsan, N. I.; Rameshkumar, P.; Huang, N. M. Electrochemical properties of silver nanoparticle-supported reduced graphene oxide in nitric oxide oxidation and detection. *RSC Adv.* **2016**, *6*, 107141-107150.

(120) Wang, Y.; Song, B.; Xu, J.; Hu, S. An amperometric sensor for nitric oxide based on a glassy carbon electrode modified with graphene, Nafion, and electrodeposited gold nanoparticles. *Microchim. Acta* **2015**, *182*, 711-718.

(121) Viswanathan, P.; Manivannan, S.; Ramaraj, R. Polyelectrolyte stabilized bi-metallic Au/Ag nanoclusters modified electrode for nitric oxide detection. *RSC Adv.* **2015**, *5*, 54735-54741.

(122) Shahid, M. M.; Rameshkumar, P.; Pandikumar, A.; Lim, H. N.; Ng, Y. H.; Huang, N. M. An electrochemical sensing platform based on a reduced graphene oxide-cobalt oxide nanocube@platinum nanocomposite for nitric oxide detection. *J. Mater. Chem. A* **2015**, *3*, 14458-14468.

(123) Hu, F. X.; Xie, J. L.; Bao, S. J.; Yu, L.; Li, C. M. Shape-controlled ceria-reduced graphene oxide nanocomposites toward high-sensitive in situ detection of nitric oxide. *Biosens. Bioelectron.* **2015**, *70*, 310-317.

(124) Vinu Mohan, A. M.; Aswini, K. K.; Biju, V. M. Electrochemical codeposition of gold particle-poly(2-(2-pyridyl) benzimidazole) hybrid film on glassy carbon electrode for the electrocatalytic oxidation of nitric oxide. *Sens. Actuators, B* **2014**, *196*, 406-412.

(125) Kim, S.-j.; Jung, H.; Lee, C.; Kim, M. H.; Lee, Y. Biological application of RuO2 nanorods grown on a single carbon fiber for the real-time direct nitric oxide sensing. *Sens. Actuators, B* **2014**, *191*, 298-304.

(126) Jayabal, S.; Viswanathan, P.; Ramaraj, R. Reduced graphene oxide-gold nanorod composite material stabilized in silicate sol-gel matrix for nitric oxide sensor. *RSC Adv.* **2014**, *4*, 33541-33548.

(127) Ting, S. L.; Guo, C. X.; Leong, K. C.; Kim, D.-H.; Li, C. M.; Chen, P. Gold nanoparticles decorated reduced graphene oxide for detecting the presence and cellular release of nitric oxide. *Electrochim. Acta* **2013**, *111*, 441-446.

(128) Zheng, D.; Liu, X.; Zhou, D.; Hu, S. Sensing of nitric oxide using a glassy carbon electrode modified with an electrocatalytic film composed of dihexadecyl hydrogen phosphate, platinum nanoparticles, and acetylene black. *Microchim. Acta* **2012**, *176*, 49-55.

(129) Ng, S. R.; Guo, C. X.; Li, C. M. Highly sensitive nitric oxide sensing using three-dimensional graphene/ionic liquid nanocomposite. *Electroanalysis* **2011**, *23*, 442-448.

(130) Penner, R. M.; Martin, C. R. Preparation and electrochemical characterization of ultramicroelectrode ensembles. *Anal. Chem.* **1987**, *59*, 2625-2630.

(131) Kim, L. T. T.; Girard, A.; Griscom, L.; Razan, F.; Griveau, S.; Bedioui, F. Micro-ring disc ultramicroelectrodes array for direct detection of NO-release from S-nitrosoglutathione. *Electrochem. Commun.* **2011**, *13*, 681-684.

(132) Trouillon, R.; Cheung, C.; Patel, B. A.; O'Hare, D. Electrochemical study of the intracellular transduction of vascular endothelial growth factor induced nitric oxide synthase activity using a multi-channel biocompatible microelectrode array. *Biochim. Biophys. Acta, Gen. Subj.* **2010**, *1800*, 929-936.

(133) Wisniewski, N.; Moussy, F.; Reichert, W. M. Characterization of implantable biosensor membrane biofouling. *Fresenius J. Anal. Chem.* **2000**, *366*, 611-621.

(134) Finnerty, N. J.; O'Riordan, S. L.; Brown, F. O.; Serra, P. A.; O'Neill, R. D.; Lowry, J. P. In vivo characterisation of a Nafion®-modified Pt electrode for real-time nitric oxide monitoring in brain extracellular fluid. *Anal. Methods* **2012**, *4*, 550-557.

(135) Hunter, R. A.; Storm, W. L.; Coneski, P. N.; Schoenfisch, M. H. Inaccuracies of nitric oxide measurement methods in biological media. *Anal. Chem.* **2013**, *85*, 1957-1963.

(136) Elbert, D. L.; Hubbell, J. A. Surface treatments of polymers for biocompatibility. *Annu. Rev. Mater. Sci.* **1996**, *26*, 365-394.

(137) Barfidokht, A.; Gooding, J. J. Approaches toward allowing electroanalytical devices to be used in biological fluids. *Electroanalysis* **2014**, *26*, 1182-1196.

(138) Frateur, I.; Lecoeur, J.; Zanna, S.; Olsson, C.-O.; Landolt, D.; Marcus, P. Adsorption of BSA on passivated chromium studied by a flow-cell EQCM and XPS. *Electrochim. Acta* **2007**, *52*, 7660-7669.

(139) Kruger, N. J.: The Bradford method for protein quantitation. In *The protein protocols handbook*; Springer, 2002; pp 15-21.

(140) Brown, F. O.; Finnerty, N. J.; Lowry, J. P. Nitric oxide monitoring in brain extracellular fluid: characterisation of Nafion-modified Pt electrodes in vitro and in vivo. *Analyst* **2009**, *134*, 2012-2020.

(141) Pekarova, M.; Kralova, J.; Kubala, L.; Ciz, M.; Lojek, A.; Gregor, C.; Hrbac, J. Continuous electrochemical monitoring of nitric oxide production in murine macrophage cell line RAW 264.7. *Anal. Bioanal. Chem.* **2009**, *394*, 1497-1504.

(142) Hunter, R. A.; Schoenfisch, M. H. S-Nitrosothiol analysis via photolysis and amperometric nitric oxide detection in a microfluidic device. *Anal. Chem.* **2015**, *87*, 3171-3176.

(143) Soto, R. J.; Hall, J. R.; Brown, M. D.; Taylor, J. B.; Schoenfisch, M. H. In vivo chemical sensors: role of biocompatibility on performance and utility. *Anal. Chem.* **2017**, *89*, 276-299.

(144) Pailleret, A.; Oni, J.; Reiter, S.; Isik, S.; Etienne, M.; Bedioui, F.; Schuhmann, W. In situ formation and scanning electrochemical microscopy assisted positioning of NO-sensors above human umbilical vein endothelial cells for the detection of nitric oxide release. *Electrochem. Commun.* **2003**, *5*, 847-852.

(145) Zhao, X.; Wang, K.; Li, B.; Wang, C.; Ding, Y.; Li, C.; Mao, L.; Lin, Y. Fabrication of a flexible and stretchable nanostructured gold electrode using a facile ultraviolet-irradiation approach for the detection of nitric oxide released from cells. *Anal. Chem.* **2018**, *90*, 7158-7163.

(146) Guo, C. X.; Ng, S. R.; Khoo, S. Y.; Zheng, X.; Chen, P.; Li, C. M. RGD-peptide functionalized graphene biomimetic live-cell sensor for real-time detection of nitric oxide molecules. *ACS Nano* **2012**, *6*, 6944-6951.

(147) Yaoita, M.; Ikariyama, Y.; Aizawa, M. Electrical effects on the proliferation of living HeLa cells cultured on optically transparent electrode surface. *J. Biotechnol.* **1990**, *14*, 321-332.

(148) Oni, J.; Pailleret, A.; Isik, S.; Diab, N.; Radtke, I.; Blöchl, A.; Jackson, M.; Bedioui, F.; Schuhmann, W. Functionalised electrode array for the detection of nitric oxide released by endothelial cells using different NO-sensing chemistries. *Anal. Bioanal. Chem.* **2004**, *378*, 1594-1600.

(149) Mendes, P. M. Cellular nanotechnology: making biological interfaces smarter. *Chem. Soc. Rev.* **2013**, *42*, 9207-9218.

(150) Robinson, J. T.; Jorgolli, M.; Shalek, A. K.; Yoon, M.-H.; Gertner, R. S.; Park, H. Vertical nanowire electrode arrays as a scalable platform for intracellular interfacing to neuronal circuits. *Nat. Nanotechnol.* **2012**, *7*, 180.

(151) Wang, J.; Trouillon, R.; Lin, Y.; Svensson, M. I.; Ewing, A. G. Individually addressable thin-film ultramicroelectrode array for spatial measurements of single vesicle release. *Anal. Chem.* **2013**, *85*, 5600-5608.

(152) Amato, L.; Heiskanen, A.; Caviglia, C.; Shah, F.; Zór, K.; Skolimowski, M.; Madou, M.; Gammelgaard, L.; Hansen, R.; Seiz, E. G. Pyrolysed 3D-carbon scaffolds induce spontaneous differentiation of human neural stem cells and facilitate real-time dopamine detection. *Adv. Funct. Mater.* **2014**, *24*, 7042-7052.

(153) Song, Q.; Jiang, Z.; Li, N.; Liu, P.; Liu, L.; Tang, M.; Cheng, G. Anti-inflammatory effects of three-dimensional graphene foams cultured with microglial cells. *Biomaterials* **2014**, *35*, 6930-6940.

(154) Hu, X.-B.; Liu, Y.-L.; Wang, W.-J.; Zhang, H.-W.; Qin, Y.; Guo, S.; Zhang, X.-W.; Fu, L.; Huang, W.-H. Biomimetic graphene-based 3D scaffold for long-term cell culture and real-time electrochemical monitoring. *Anal. Chem.* **2018**, *90*, 1136-1141.

CHAPTER 2: NITRIC OXIDE PERMSELECTIVITY IN ELECTROPOLYMERIZED FILMS FOR SENSING APPLICATIONS[2]

2.1 Introduction

Nitric oxide (NO) is a gaseous free radical endogenously produced from L-arginine by a group of isoenzymes called nitric oxide synthases (NOS).[1,2] Much prior work has revealed the importance of NO for essential physiological processes including wound healing,[3] angiogenesis,[4,5] platelet aggregation,[6] vasodilation, inflammation, and the immune response.[7] As the significance of this small molecule continues to be understood, the demand for accurate detection in biological systems grows as well. Due to its short half-life in the presence of various scavengers (oxygen, peroxides, free metals, and hemoglobin[8,9]), real-time measurements of NO in biological media are analytically challenging.[10] Although direct and sensitive detection can be achieved utilizing chemiluminescence or electron paramagnetic resonance spectroscopy (EPR), these techniques require complex, expensive instrumentation. Furthermore, these methods do not facilitate measurement in complex milieu such as blood or wound fluid.[11,12] In contrast, electrochemical strategies allow for real-time monitoring of NO in a simple, fast, and low-cost manner with superior spatial and temporal resolution.[13-15]

The sensitivity, dynamic range, and limit of detection (LOD) of an electrochemical sensor are important properties given the varied, but generally small concentrations of NO

[2] This chapter was adapted in part from an article that has already been published. The original citation is as follows: Brown, M. D.; Schoenfisch, M. H. Nitric oxide permselectivity in electropolymerized films for sensing applications. *ACS Sensors* **2016**, *1*, 1453-1461.

that exist physiologically. An equally important consideration is selectivity, particularly for amperometric measurements. Interfering species such as L-ascorbate, nitrite, acetaminophen, and dopamine are common in biological milieu and pose a significant obstacle to accurate NO measurement.[16,17] These interferents are oxidized at working potentials similar to or below those required to detect NO, and therefore contribute erroneously to the current response. In order to preserve sensor accuracy, the predominant strategy is to employ one or more membranes over the working electrode that selectively permit permeation of NO while reducing or eliminating the diffusion of interferents. Sensors that reduce interferent passage relative to that of the target analyte are said to have high permselectivity. Membranes used to fabricate NO sensors in this manner include Nafion,[18,19] Teflon,[20,21] nitrocellulose,[22] chloroprene,[23] and xerogel monoliths.[24] Greater hydrophobicity, size-exclusion, and/or charge-repulsion are often cited as the primary interferent exclusion mechanisms for these membranes. While enhanced NO selectivity is often observed, the depositions of these polymers necessitates dip-coating or solvent casting, resulting in undesirable variability in film thickness and, consequently, poor control over both NO sensitivity and selectivity.[25]

Self-terminating electropolymerized films represent a class of sensor membranes characterized by reproducible and straightforward depositions. Through electrooxidation-initiated radical coupling reactions, monomers polymerize and precipitate onto the working electrode surface. Growth of the film eventually creates an insulating layer that prohibits further monomer access to the electrode, resulting in depositions that are self-assembled and finite. The thickness of self-terminating films formed by electropolymerization spans 5-35 nm.[26-29] The films are deposited onto the electroactive surface with high specificity (i.e., without the need for masking) and uniformity regardless of electrode size or geometry,[30]

features that make electropolymerized films a compelling choice in fabricating sensors with consistent performance. A number of aromatic monomers have been used to create electropolymerized films for selective NO detection, often in conjunction with a secondary or tertiary membrane (e.g., Nafion).[31,32] Among the most frequently employed polymer films are those prepared from the three isomers of phenylenediamine (*o*-, *m*-, and *p*-PD), phenol, eugenol, and 5-amino-1-napthol (5A1N).[30,33] While prior work has largely investigated the potential of these films for hydrogen peroxide (H_2O_2) permselectivity,[25,27,34,35] a broad comparison with NO as the focus analyte has yet to be carried out.

Secondary to monomer selection, the electrochemical deposition technique may influence oligomer structure, and consequently the film morphology and permeability.[36,37] Indeed, the effects of monomer deposition conditions are often neglected with respect to permselectivity. Herein, we set out to evaluate the NO selectivity and analytical performance characteristics of sensors prepared using self-terminating electropolymerized films as a function of both monomer selection and deposition procedure. The objective of this work was to ascertain optimal electropolymerization methods for each monomer individually and then compare ensuing sensor performance as a function of monomer identity.

2.2 Experimental

2.2.1 Materials, reagents, and apparatus

Ortho-phenylenediamine (*o*-PD), *meta*-phenylenediamine (*m*-PD), *para*-phenylenediamine (*p*-PD), phenol, eugenol, 5-amino-1-naphthol (5A1N), hydrochloric acid (HCl), sodium nitrite, L-ascorbic acid, acetaminophen, dopamine hydrochloride, and fetal bovine serum (FBS) were purchased from Sigma (St. Louis, MO). Ammonium hydroxide, sodium hydroxide (NaOH), sulfuric acid, and hydrogen peroxide (30% w/v) were obtained

from Fisher Scientific (Hampton, NH). Nitric oxide gas (99.5%) was purchased from Praxair (Danbury, CT). Nitrogen (N_2) and argon (Ar) gases were purchased from National Welders Supply (Raleigh, NC). Other solvents and chemicals were analytical-reagent grade and used as received without further purification.

A Millipore Milli-Q UV Gradient A10 Water Purification System (Bedford, MA) was used to purify distilled water to a final resistivity of 18.2 MΩ·cm and a total organic content of ≤6 ppb. Saturated NO solutions (1.9 mM) were prepared by purging ~20 mL of phosphate buffered saline (PBS; 10 mM, pH 7.4) with Ar for 30 min, followed by NO gas for 20 min over ice. Solutions were used the day of preparation and stored at 4 °C. Electrochemical experiments were carried out using a CH Instruments 920D Scanning Electrochemical Microscope (Austin, TX). The four-electrode arrangement employed two inlaid 2 mm diameter polycrystalline platinum (Pt) disc working electrodes sealed in Kel-F (6 mm total diameter; CH Instruments), a silver-silver chloride (Ag|AgCl) reference electrode (3.0 M KCl; CH Instruments), and a coiled Pt wire counter electrode. All potentials herein are reported versus the Ag|AgCl reference electrode.

2.2.2 Preparation of the working electrode

Platinum disc working electrodes were mechanically polished on a microcloth with successively finer grades of deagglomerated alumina slurries down to 0.05 μm in particle size (Buehler; Lake Bluff, IL). Electrodes were rinsed with distilled water and ultrasonicated in ethanol to remove residual alumina loosely bound to the surface. The electrodes were then dried under a stream of N_2 and electrochemically polished in 1 N sulfuric acid by cycling between -0.4 and +1.8 V for 20 cycles (500 mV s^{-1}). Additional cycling in PBS between 0 and +1.0 V (100 mV s^{-1}) was applied until steady state cyclic voltammograms resulted. Prior

to deposition, Pt electrodes were calibrated using amperometry (+0.8 V) and injections of 1.9 μM saturated NO solution in deoxygenated PBS.

2.2.3 Electrodeposition of polymer films

The *o*-PD, *m*-PD, *p*-PD, and phenol monomers were dissolved in PBS at pH 7.4. For reasons of solubility, eugenol was dissolved in PBS titrated to pH 13 with NaOH. Likewise, 5A1N was dissolved in PBS titrated to pH 1 with HCl. The electropolymerization process was carried out through either cyclic voltammetry (CV) or constant potential amperometry (CPA). Cyclic voltammetric depositions were performed in either 10 or 100 mM solutions of monomer by sweeping the potential from 0 to +1.0 V (20 cycles; positive direction initial sweep) at a scan rate of either 10 or 100 mV s^{-1}. Electropolymerizations via constant potential amperometry were carried out for 15 min in either 10 or 100 mM solutions of monomer and an applied potential of +0.6, +0.75, or +0.9 V. In total, ten distinct electrodeposition procedures were evaluated for each monomer (with the exception of 5A1N, which was only soluble up to 10 mM). The resulting film-modified electrodes were then rinsed with distilled water to remove unbound oligomers prior to electrode testing.

2.2.4 Steady-state amperometric measurements

Film-modified Pt electrodes were polarized at +0.8 V in deoxygenated PBS for 10 min to achieve a constant background current prior to measurements. The change in electrooxidative current was then measured after injecting saturated NO solution aliquots (1.9 μM) to determine the change in sensitivity relative to bare Pt. Stock solutions of various interferents were initially prepared in PBS to test for selectivity to NO. The current responses to injections of sodium nitrite (1 mM), L-ascorbate (1 mM), acetaminophen (250 μM), dopamine hydrochloride (100 μM), ammonium hydroxide (1 mM), and hydrogen peroxide (1

mM) were measured and compared to the NO sensitivity. Selectivity coefficients were calculated using Eq. 1, where $\log k_{NO,j}$ is the selectivity coefficient for NO over interferent j, S_j is the sensitivity towards interferent j, and S_{NO} is the NO sensitivity of the film-modified electrode.

$$\log k_{NO,j} = \log\left(\frac{S_j}{S_{NO}}\right) \quad \text{(Eq. 1)}$$

2.2.5 Sensor performance in simulated wound fluid

Upon determining the optimal electrodeposition parameters for each monomer, the sensitivity of the film-modified electrodes was tested in simulated would fluid (SWF), a 10-fold dilution of FBS in deoxygenated PBS. After polarizing the electrode at +0.8 V for 10 min in SWF, the background current and responses to injections of saturated NO (1.9 μM) were measured and compared to trials in PBS. These measurements were repeated after 1 h immersion in the SWF without agitation.

2.2.6 Contact angle measurements

The 2 mm diameter Pt disc electrodes were too small for goniometric measurements, necessitating the fabrication of larger, planar electrodes. Briefly, silica microscope slides were masked with Kapton® polyimide tape to delineate an electrode geometry before oxygen plasma cleaning (100 W, 30 s). A 100 nm Pt layer with a 10 nm titanium (Ti) adhesion layer was deposited onto the silica substrate using a Kurt J. Lesker PVD 75 magnetron sputtering system (Clairton, PA). After removal of the mask, a band of epoxy-adhered silica was used to separate the working electrode area (~1 cm^2) from the potentiostat lead. Following electropolymerization, static contact angles were measured using a CAM 200 Optical Contact Angle Meter (KSV Instruments; Bridgeport, CT). Water droplets (~8 μL) were

placed in the center of the electrode plane, and measurements were averaged across four depositions of the same monomer to assess the hydrophobicity of the electropolymerized films.

2.2.7 Statistical analysis

The selectivity, NO permeability, limit of detection, and contact angle of the film-modified electrodes are presented as the mean ± standard error of the mean. Comparisons between groups of electrochemical deposition parameters were performed using a two-tailed *t*-test with $p < 0.05$ considered to be statistically significant.

2.3 Results and Discussion

The six monomers in this study undergo irreversible electrooxidation in aqueous media upon the application of a sufficiently positive potential. The phenylene diamine series is oxidized through one or both amine groups,[38] whereas phenol and eugenol are oxidized through the hydroxyl group. While 5A1N contains both amine and hydroxyl groups, previous work has indicated that electropolymerization occurs through the amine.[39] Both the electrolyte identity and concentration in the monomer solution have been shown to affect film permeability in electropolymerized films, presumably via ion entrapment during electropolymerization.[40] All monomers were therefore dissolved in 0.01 M phosphate buffered saline (PBS) solutions to maintain a constant electrolyte concentration and facilitate steady-state measurements. Platinum was chosen as the working electrode due to the ubiquity of its use and known sensitivity towards NO.[17,41]

2.3.1 Cyclic voltammetry of monomers

The shapes of the CV traces collected using a platinum working electrode in solutions of each monomer result from both the monomer redox activity and the insulating process that occurs during the electrodeposition of a film (Figure 2.1). Most film deposition occurs during the initial sweep, blocking further monomer access and causing the electrooxidative current to diminish rapidly. The CV traces become distorted as a result, obscuring higher potential wave features. This phenomenon was particularly evident in the traces of *o*-PD and eugenol (Figure 2.1A and E, respectively) with abrupt shoulders at +0.65 and +0.75 V, respectively. After the switching potential (+1.0 V), only minor reduction waves were observed in the return traces, indicative of irreversible oxidation of parent monomers. The cathodic feature in the return trace of poly(5A1N) (Figure 2.1F) is attributed to the film's conductive properties. However, the polymerization mechanism of poly(5A1N) is not autocatalytic and still proceeds to self-terminate, unlike other conducting films (e.g., poly(aniline)).[42] Monomer oxidation potentials were measured at the first peak present in the initial anodic sweep. The presence of multiple peaks in a given wave is attributed to secondary oxidations of radical cations and/or over-oxidation of the deposited film.[27,43] As evident in Figure 2.1C, *p*-PD had the lowest oxidation potential (+0.20 V), indicating that it is the most easily oxidized monomer and presumably the fastest to polymerize. The oxidation potential for phenol appeared at +0.62 V (Figure 2.1D), making this monomer the most difficult to oxidize. The oxidation potentials of other monomers fell in between *p*-PD and phenol in the following order: *p*-PD < eugenol < *o*-PD < *m*-PD < 5A1N < phenol. Increasing the monomer concentration to 100 mM and/or scan rate to 100 mV s^{-1} did not influence this order.

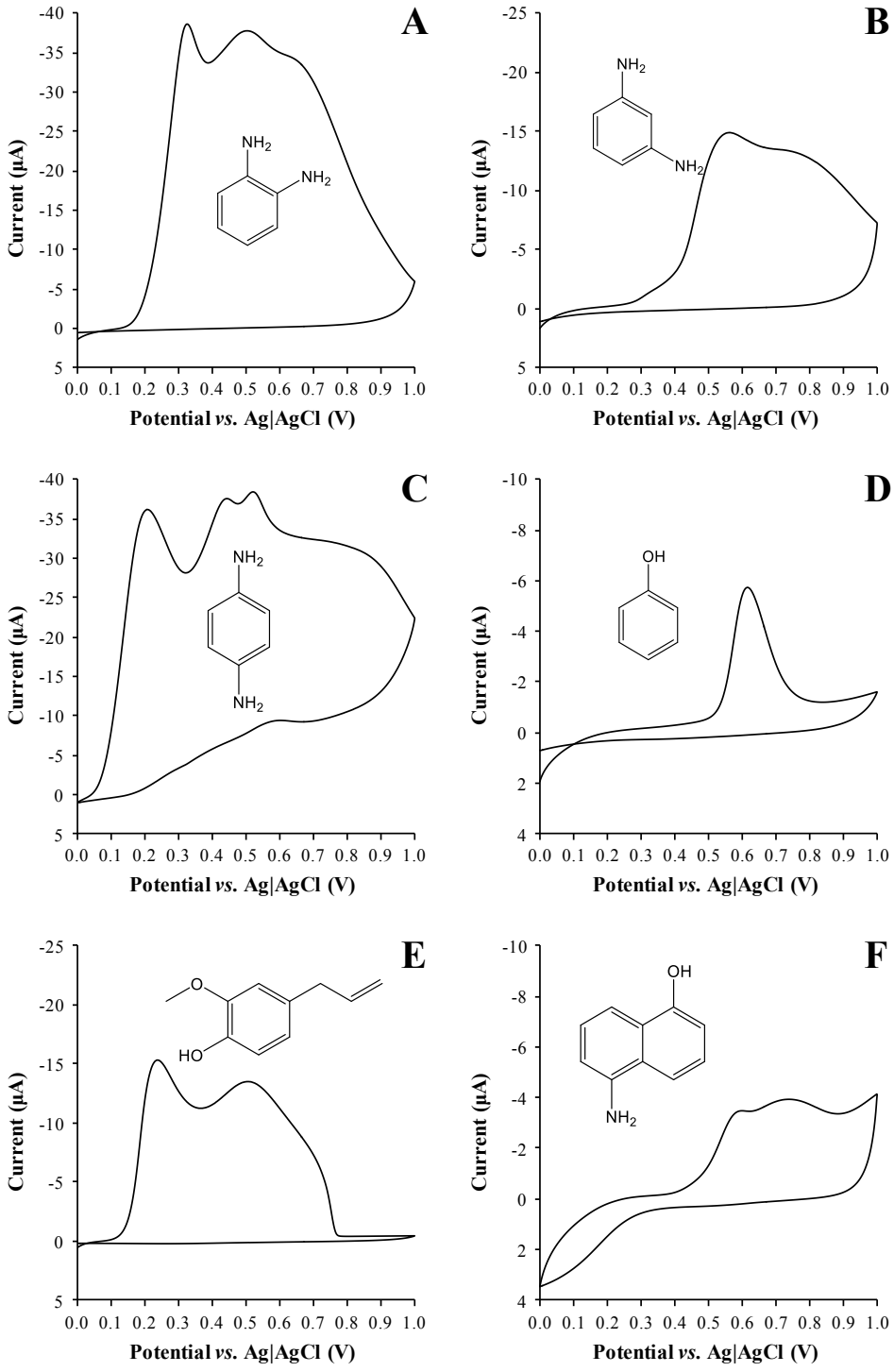

Figure 2.1 Cyclic voltammograms collected at 2 mm (dia.) Pt disk electrodes in 10 mM monomer solutions of (A) *o*-PD, (B) *m*-PD, (C) *p*-PD, (D) phenol, (E) eugenol, and (F) 5A1N in 0.01 M PBS. The pH of the *o*-PD, *m*-PD, *p*-PD, and phenol solutions was 7.4. The eugenol and 5A1N solutions were titrated to pH 13 and 1.0 with NaOH and HCl, respectively. Scan rate: 10 mV s^{-1}.

2.3.2 Electropolymerization of monomers via cyclic voltammetry

Twenty cycles of the same potential window (0 to +1.0 V) were applied to deposit a complete, self-terminating film on the surface of Pt disc electrodes. The switching potential at +1.0 V represented a significant overpotential to all monomers, allowing for cyclical generations of radical cations. While others have suggested that the switching potential can influence both the degree of oligomer conjugation and charge-state of the film,[34,43] we did not seek to study these parameters. Rather, we assessed the influence of scan rate (10 and 100 mV s^{-1}) and monomer concentration (10 and 100 mM) on the NO permselectivity, capturing the range of deposition variables reported previously.[27,30,44-47] The self-limiting behavior of these film depositions via CV is well understood. Briefly, growth of the insulating film effectively blocks monomer transport to the electrode surface, capping radical cation generation and the polymerization process. As a result, the anodic current decreases precipitously with successive cycles. For example, the oxidation peak for phenol at +0.62 V is reduced upon poly(phenol) film formation after the first cycle (Figure 2.2). The absence of anodic wave features in subsequent cycles indicates that the majority of the deposition/insulation process has occurred by the second cycle. Likewise, the switching potential current decreased rapidly during the first 10 cycles, converging to approximately −0.75 μA to mark film completion.

The above traits, characteristic of electrodeposition/insulation, were observed for each monomer studied. The rate at which the current diminished with each cycle, however, was distinct with respect to both the deposition procedure and monomer identity, signifying different rates of film formation. Based on the decrease in peak oxidation current between the first and second cycles, the rate of film formation trended as follows: eugenol > *o*-PD >

phenol > *m*-PD > 5A1N > *p*-PD. With the exception of phenol and *p*-PD, this order mirrored that of the oxidation peaks, presumably because lower oxidation potentials allow monomers to actively polymerize during a greater portion of each potential sweep. The fact that *p*-PD films were the slowest to form is likely the result of poor film formation, as CV tends to yield only low molecular weight oligomers of *p*-PD.[48] The loss of these soluble oligomers from the electrode surface also accounts for the deepening reddish-brown hue of the monomer solution as the deposition proceeded.[29]

Four different electropolymerization procedures were carried out for each monomer via CV by increasing the scan rate and/or monomer concentration by an order of magnitude. In theory, such changes should increase the rate of radical cation generation, affecting the organization and density of precipitated oligomers on the electrode surface. The initial cycle and resultant oxidation peak shifts for each of the four different deposition conditions carried out in phenol are provided in Figure 2.3. As expected for irreversible redox reactions, increasing the scan rate from 10 to 100 mV s^{-1} led to increased peak current and shifted the primary oxidation peak to more positive potentials. Similar results were observed for each of the other monomers upon increasing the scan rate. Increasing the phenol concentration from 10 to 100 mM shifted the peak potential negatively regardless of scan rate (Figure 2.3), demonstrating faster film formation and accompanying electronic insulation. While a positive correlation between peak height and redox agent concentration was anticipated, no such dependence was observed here. Convolution of the electronic properties of the monomer and the self-limiting nature of these depositions represent a likely explanation for these results (as previously noted in Figure 2.1). Solutions of *m*-PD demonstrated similar behavior to phenol. Depositions of 10 mM *o*-PD, *p*-PD, and eugenol resulted in peak

potentials and currents close or identical to those in 100 mM monomer solutions, indicating a negligible convolution effect. In this respect, the monomer concentration does not have an appreciable effect on the CV deposition rate for these monomers. Of note, monomer concentration was not studied for 5A1N due to limited solubility in the aqueous media.

2.3.3 Electropolymerization of monomers via CPA

Monomers were electropolymerized by CPA onto the surface of Pt electrodes as a function of monomer concentration (10 and 100 mM) and applied potential (+0.6, +0.75, and +0.9 V). Prior work suggests that a significant overpotential is required to yield optimally permselective films (with respect to H_2O_2).[34,36] Therefore, each of the applied potentials were chosen to exceed the first oxidation potential of each monomer, with the exception of phenol's oxidation peak at +0.62 V. The potential was applied to the working electrode for 15 min, a period that is typical for CPA depositions of electropolymerized films.[25,27,49] Due to the self-sealing nature of this process, longer amperometric polymerization times are generally not useful for further improving permselectivity.[50] A greater overpotential resulted in more easily oxidized phenol monomers at the electrode surface, with a concomitant increase in the initial current (Figure 2.4). This effect was most pronounced between +0.6 and +0.75 V, the former just below phenol's oxidation potential. Likewise, the initial current was elevated upon increasing the concentration from 10 to 100 mM phenol due to the greater flux of monomers to the electrode surface. This increase in initial current (with greater overpotentials and/or monomer concentration) was noted for each of the monomers investigated in our study.

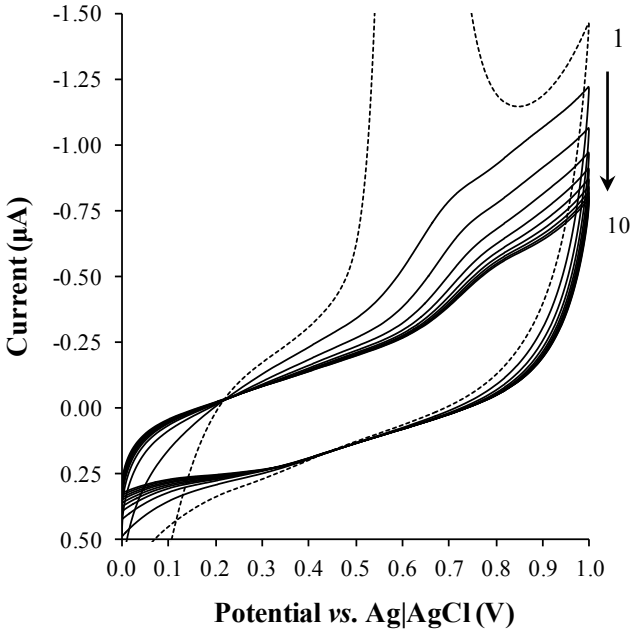

Figure 2.2 Cyclic voltammograms collected during the electrodeposition of 10 mM phenol in 0.01 M PBS (pH 7.4) using a 2 mm (dia) Pt disc electrode, with cycle numbers provided. The dashed line represents the first cycle (cut off for clarity of successive cycles). Scan rate: 10 mV s^{-1}.

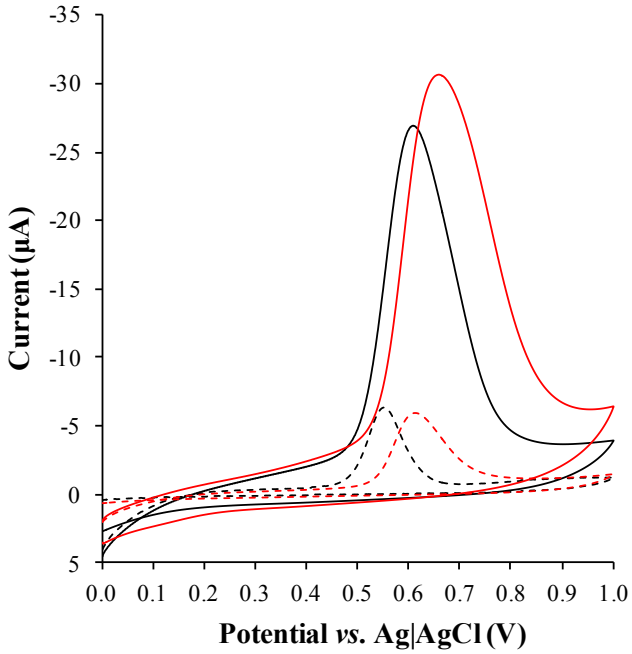

Figure 2.3 The initial cyclic voltammogram cycle collected during the electropolymerization of phenol from 10 and 100 mM monomer solutions (red and black lines, respectively) in 0.01 M PBS (pH 7.4) as a function of scan rate (10 and 100 mV s^{-1} depicted as dashed and solid lines, respectively).

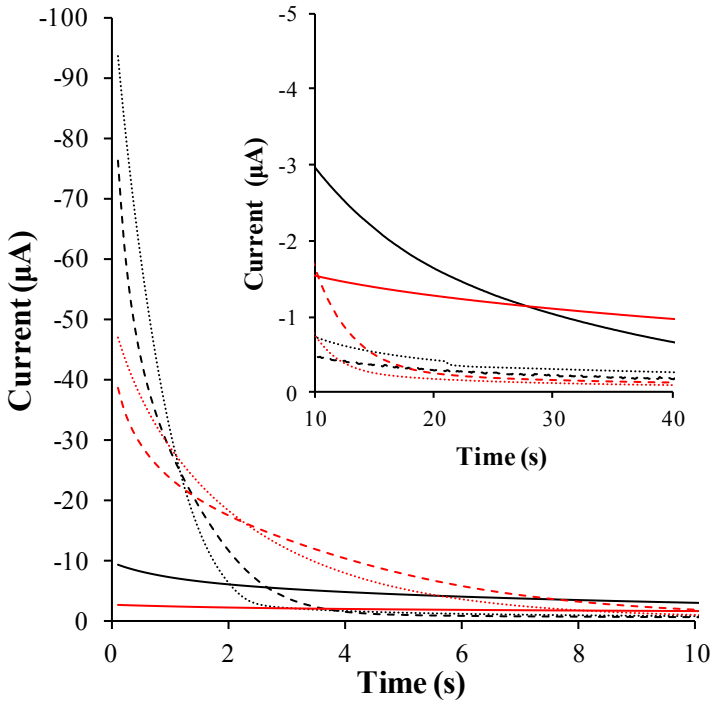

Figure 2.4 Amperograms of the initial 10 s of CPA electropolymerizations of phenol in 0.01 M PBS (pH 7.4) at +0.6, +0.75, and +0.9 V (solid, dashed, and dotted lines, respectively) in 10 and 100 mM monomer solutions (red and black lines, respectively). Inset: subsequent 30 s of electropolymerization. Curves are baseline corrected from the average current recorded in the last 10 s of electropolymerization (900 s deposition time).

Another feature of the amperograms was the rate of convergence to a steady current, marking when film-formation was nearly complete. In phenol, the rate of convergence increased with the applied potential, signifying faster film-formation at large overpotentials (i.e., +0.75 and +0.9 V; Figure 2.4). The same dependence was observed for *o*-PD, *p*-PD, and eugenol. However, this behavior was not observed with *m*-PD and 5A1N, in which the CPA depositions at +0.6 V converged most rapidly, followed by +0.9 and +0.75 V. In addition to facilitating monomer oxidation, the magnitude of the overpotential also impacts the size, charge-state, and solubility of resulting oligomers—factors that may, if not optimized appropriately, reduce packing efficiency and lower the rate of film formation, as may have been the case with *m*-PD and 5A1N. Constant potential amperometry depositions in 100 mM solutions of phenol were complete prior to those using 10 mM solutions (Figure 2.4). The greater flux of monomers to the electrode surface clearly impacted the rate of oligomer generation. This trend was also observed for *o*-PD and eugenol, but not *m*-PD and *p*-PD, which were characterized as having slower deposition rates at higher monomer concentration. Of note, the limited solubility of 5A1N precluded the study of its concentration on film-formation kinetics.

2.3.4 Analytical performance of film-modified electrodes

The electropolymerized film-modified electrodes were characterized with respect to NO selectivity over nitrite (NO_2^-) and L-ascorbate (AA), two biologically relevant interferents. At physiological pH, both molecules are negatively charged and coulombically drawn into positively charged films, such as those formed by oxidative electropolymerization.[27] Nitrite is a particularly challenging interferent because it is the primary oxidation product of NO and of a similar size. In contrast, AA is larger but has an

oxidation potential that is lower than NO. In serum, AA is present at larger concentrations (34-144 μM) than nitrite (<20 μM).[16,51] The amperometric response from film-modified electrodes was measured at +0.8 V following the addition of interferent and NO solutions into deoxygenated PBS. Selectivity coefficients were then calculated using this data (Figure 2.5). The optimal deposition procedure in each monomer was determined by the sum of anionic selectivity coefficients against nitrite and AA.

The best deposition procedures for each monomer and relevant analytical merits are provided in Table 2.1. For each monomer except phenol, the optimal CV deposition procedure yielded more selective films to NO than all CPA depositions tested. Of these monomers, all except *m*-PD formed more NO-selective films at the slower scan rate (10 mV s^{-1}), suggesting that slow, oscillatory generations and precipitations of oligomer units yield the most densely packed membranes. Of note, the cumulative anionic selectivity for NO under the optimal CPA deposition of phenol (100 mM, +0.9 V) was not statistically different than the optimal deposition by CV (10 mM, 100 mV s^{-1}). The fact that CV depositions of the phenylenediamine (PD) series yielded more selective films than via CPA depositions (Figure 2.5) stands in contrast to prior reports of PD film permselectivity.[27,29] Of note, the target analyte in these former studies was hydrogen peroxide and the comparison between CPA and CV was made without a tailored optimization of the CV deposition parameters. Potentiodynamic electropolymerization techniques (e.g., linear sweep, squarewave, and cyclic voltammetry) are thought to generate a greater density of nucleation sites on the electrode surface, improving both compactness and film adherence.[52,53]

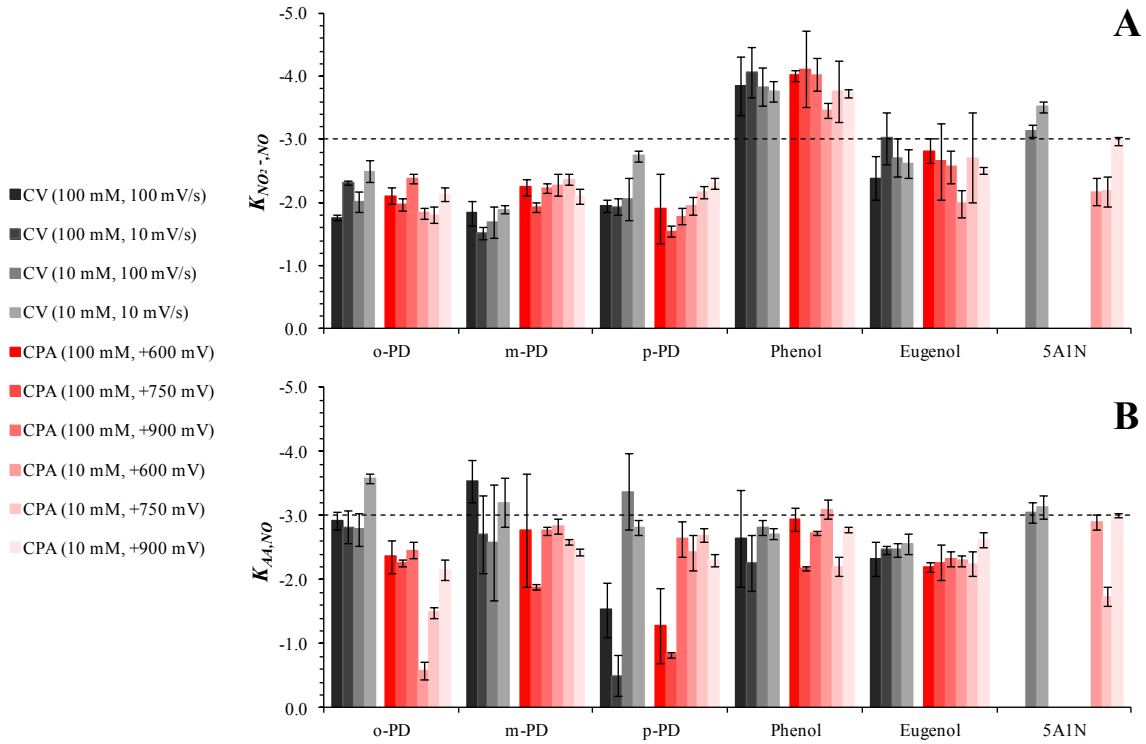

Figure 2.5 Selectivity coefficients for nitric oxide against interferents (A) nitrite and (B) L-ascorbate for electrodes modified by electropolymerized films of different compositions and different deposition procedures ($n \geq 4$). Selectivity coefficients were calculated from the current responses to injections of NO (1.9 μM) and the anionic interferents (1 mM). Error bars represent standard errors of the mean. Depositions were not conducted with 100 mM monomer in 5A1N due to limited solubility in aqueous solutions. The dashed lines mark a selectivity coefficient of −3.0, corresponding to 1000-fold greater sensor response to NO over the interferent under observation. The procedure deemed optimal for monomer deposition was determined by summing the selectivity coefficients versus nitrite and L-ascorbate and selecting the greatest value.

Table 2.1 Optimal electropolymerization deposition techniques observed in six self-terminating films and relevant analytical merits for selective nitric oxide detection (n ≥ 4).

Monomer	Technique	Optimized Parameters	LOD[a] (nM)	NO Permeability[b]	log $k_{NO,j}$ [c]					
					NO_2^-	AA	AP	DA	NH_4^+	H_2O_2
o-PD	CV	10 mM, 10 mV s^{-1}	16 ± 9	0.36 ± 0.08	-2.5 ± 0.2	-3.6 ± 0.1	-1.7 ± 0.4	-1.6 ± 0.1	-2.8 ± 0.0	-0.2 ± 0.1
m-PD	CV	100 mM, 100 mV s^{-1}	90 ± 40	0.13 ± 0.04	-1.8 ± 0.2	-3.5 ± 0.3	-3.7 ± 0.1	-1.9 ± 0.2	-1 ± 1	0.2 ± 0.1
p-PD	CV	10 mM, 10 mV s^{-1}	11 ± 6	0.50 ± 0.14	-2.7 ± 0.1	-2.8 ± 0.1	-2.7 ± 0.4	-2.6 ± 0.2	-2.9 ± 0.4	-0.5 ± 0.1
Phenol	CPA[d]	100 mM, +600 mV	6 ± 5	1.10 ± 0.29	-4.0 ± 0.1	-3.0 ± 0.2	-3.2 ± 0.2	-2.5 ± 0.1	-3.3 ± 0.2	-2.2 ± 0.1
Eugenol	CV	100 mM, 10 mV s^{-1}	130 ± 70	0.01 ± 0.00	-3.0 ± 0.4	-2.5 ± 0.1	-2.3 ± 0.5	-1.9 ± 1.0	-2.8 ± 0.3	-1.3 ± 0.2
5A1N	CV	10 mM, 10 mV s^{-1}	4 ± 3	1.72 ± 0.15	-3.5 ± 0.1	-3.1 ± 0.2	-3.4 ± 0.2	-2.4 ± 0.1	-3.1 ± 0.0	-0.8 ± 0.0
Bare Pt	---	---	10 ± 8	1	-1.2 ± 0.3	0.0 ± 0.1	0.3 ± 0.2	0.4 ± 0.2	-1.4 ± 0.1	-0.4 ± 0.1

[a] *S/N* = 3. [b] Ratio of film-modified and bare Pt electrode (2 mm dia.) NO sensitivities. [c] Selectivity coefficient against interferent *j* calculated from Eq. 1. Injections of nitrite (NO_2^-, 1 mM), L-ascorbate (AA, 1 mM), acetaminophen (AP, 250 μM), dopamine (DA, 100 μM), ammonium (NH_4^+, 1 mM), and hydrogen peroxide (H_2O_2, 1 mM) were made into deoxygenated 0.01 M PBS (pH 7.4; +0.8 V). [d] Not statistically superior to the optimal CV deposition (10 mM, 100 mV s^{-1}).

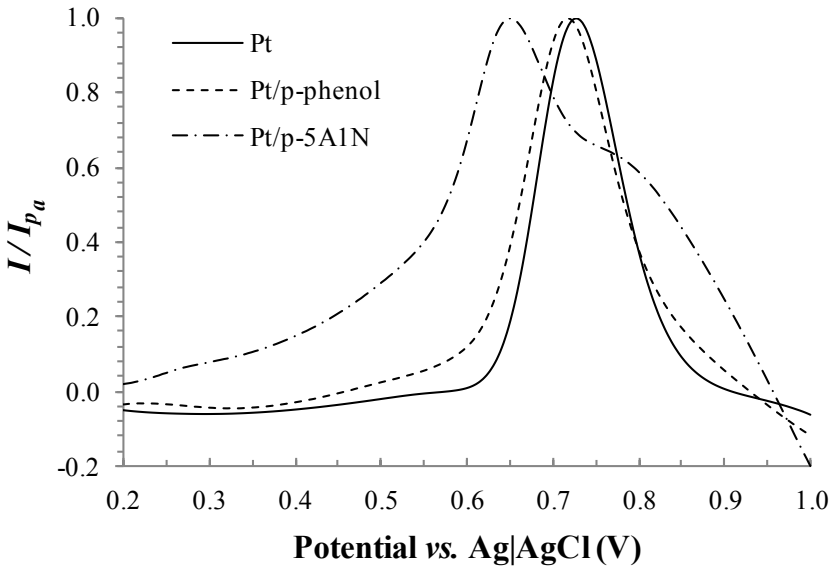

Figure 2.6 Differential pulse voltammograms of nitric oxide collected on bare Pt, poly-phenol-, and poly-5A1N-modified electrode (2 mm dia.) surfaces. Traces collected in deoxygenated phosphate buffered saline (0.01 M, pH 7.4) were subtracted from traces collected in the presence of 90 μM NO. Background-subtracted traces were then averaged over multiple runs (n = 8) and normalized to the peak oxidation current (I_{pa}). Peak potentials were determined to be 728 ± 2, 713 ± 2, and 649 ± 4 for bare Pt, poly-phenol-, and poly-5A1N-modified electrodes, respectively. Parameters: increased potential of 0.004 V, amplitude of 0.05 V, pulse width of 0.2 s, sampling width of 0.0167 s, and pulse period of 0.5 s.

Additional analytical performance metrics were measured for optimal film-modified electrodes, allowing for comparison on the basis of monomer identity. Many diverse physiological species are electroactive at the potentials required for NO oxidation, thus motivating testing selectivity against a broader panel of interferents. As analogs to the AA/nitrite anionic pair, dopamine (DA) and ammonium (NH_4^+) represent large and small cationic interferents, respectively. Likewise, acetaminophen (AP) and hydrogen peroxide (H_2O_2) are large and small neutral interferents, respectively. Poly(*o*-PD) and poly(*m*-PD) modifications led to the greatest selectivity coefficients against AA (selectivity coefficients ≤ −3.5; Table 2.1). Poly(*m*-PD) also provided the best selectivity against the large, hydrophobic molecule AP (−3.7 ± 0.1), indicative of superior interferent rejection on the basis of size-exclusion. Relative to the other monomers, however, the greater selectivity of *m*-PD films came at the expense of LOD (90 ± 40 nM) and NO permeability (0.13 ± 0.04). Poly(*p*-PD) was the best film for restricting DA (−2.6 ± 0.2), which suggests that it is more positively charged and capable of cationic repulsion. Within the PD isomer series as a whole, better selectivity coefficients against AA and AP versus the smaller interferents (nitrite and H_2O_2) verifies that size-exclusion plays a large role in restricting interferent diffusion to the electrode. While poly(eugenol)-modified electrodes had favorable selectivity regardless of the interferent identity, the accompanying reduced permeability to NO (0.01 ± 0.00) and concomitant increase in LOD (130 ± 70 nM) preclude use for sensor applications.

Poly(phenol)- and poly(5A1N)-modified sensors were the most sensitive to NO, yielding the lowest NO detection limits (6 ± 5 and 4 ± 3 nM, respectively). Of note, this sensitivity towards NO exceeded that observed for bare Pt. Electropolymerized films have been shown previously to aid in electron transport and enhance H_2O_2 detection without an

extraneous catalyst or mediator.[54] The oxidation potentials of NO measured via differential pulse voltammetry on bare Pt, poly(phenol)- and poly(5A1N)-modified working electrodes were found to be 728 ± 2, 713 ± 2, and 649 ± 4 mV, respectively (Figure 2.6). The reduced oxidation potential observed for poly(5A1N), in particular, strongly suggests an electrocatalytic mechanism facilitating electron transfer to the working electrode. The NO response amplification observed for poly(phenol) and poly(5A1N) modified electrodes represents a significant advantage over the other monomers, particularly when improvements in permselectivity so often come at the expense of sensitivity. Poly(phenol) films performed best against nitrite with a selectivity coefficient of −4.0 ± 0.1, representing a 10,000-fold greater current response to NO. To our knowledge, this selectivity against nitrite is unprecedented in the literature with respect to electrochemical NO-sensing electrodes modified solely by an electropolymerized film. Poly(phenol) films also exhibit unprecedented selectivity against H_2O_2 (−2.2 ± 0.1), a surprise given their extensive use in glucose biosensors. While the oxidation potential employed for glucose biosensors is often lower than that used for NO detection (+0.6 *vs*. +0.8 V), our findings indicate that poly(phenol) films are better suited for electrochemical NO detection. Poly(5A1N) modified sensors also demonstrated notable nitrite blocking with a selectivity coefficient of −3.5 ± 0.1. In terms of overall analytical performance, the poly(phenol) and poly(5A1N) modifications proved superior over the other monomers.

2.3.5 Performance in simulated wound fluid

Electropolymerized film-modified electrodes are favorable as NO sensors given their aforementioned reproducibility, high selectivity, and ease of fabrication. However, a key obstacle to in situ, biological NO measurements is biofouling, specifically the accumulation

of proteins on the transducer surface and concomitant degradation in analytical performance. While the anti-fouling properties of a sensor depend largely on the surface chemistry of the outermost coating, electropolymerized films (the PD isomers in particular) are most commonly utilized as inner coatings and have not been compared systematically for their biofouling resistance.[55] The analytical performance (i.e., LOD and sensitivity retention) of polymer-modified electrodes was therefore characterized in simulated wound fluid (SWF) in order to compare anti-fouling characteristics and assess potential application of electrodes modified by a single electropolymerized film to measurements in complex media.

The NO sensitivity of bare and film-modified Pt electrodes decreased upon exposure to SWF relative to measurements in PBS (Figure 2.7A). The reduction in sensitivity was attributed to both protein surface fouling (altering mass transfer of NO) and anticipated scavenging of NO in proteinacious media. It is worth noting that the NO sensitivity remained constant even after 1 h immersion in SWF (no stirring). Biofouling at the polymer film interface likely occurs quickly, allowing for short preconditioning times. Poly(*o*-PD) and poly(*m*-PD) retained sensitivity better than bare Pt with the lowest degree of uncertainty ($p < 0.01$). Poly(*m*-PD)-modified electrodes, in particular, displayed the greatest anti-fouling character, retaining 84% of the NO response (sensitivity) after 1 h SWF exposure relative to bare Pt (only 12%). Reynolds et al. reported similar sensitivity retention for poly(*m*-PD)-modified glucose biosensors (H_2O_2 measurement) upon SWF immersion (3% w/v FBS in pH 7.4 PBS).[35] Diminished NO sensitivity in SWF was often accompanied by an increase in background noise, resulting in elevated LODs (Figure 2.7B). Although changes in LOD from PBS to SWF trials were not statistically significant for the film-modified electrodes, a general increase in both LOD value and variability was observed (with the exception of

poly(eugenol), for which the LOD was already elevated in PBS). Poly(*o*-PD) and poly(5A1N)-modified electrodes were characterized as having the lowest LODs and changes in LOD in SWF relative to PBS, suggesting that these films would have the greatest utility for detection of NO in wound fluid.

The primary thermodynamic force driving protein and surface interaction is hydrophobicity. Due to the large release in entropic energy when an ordered water layer is disrupted by protein adsorption, hydrophilic surfaces are thought to have greater anti-fouling character than their hydrophobic counterparts.[56] The hydrophobicity of the electropolymerized films was assessed using static contact angle measurements. As shown in Figure 2.7B and C, poly(*o*-PD), poly(eugenol), and poly(5A1N) films proved to be less hydrophilic than the other films, but with LODs least impacted by biofouling. Furthermore, poly(*p*-PD) and poly(phenol) experienced large reductions in NO sensitivity and increases in LOD (Figures 2.7A and B, respectively) despite being the most hydrophilic. The greater hydrophilic character for electropolymerized films thus appears to be associated with biofouling-related performance degradation. Of note, the measured contact angles for each interface was between 45 and 75°. In this respect, all films studied could generally be described as hydrophilic. Expectations based on hydrophobicity alone are likely not sound given the coulombic interactions of net negatively-charged blood plasma proteins and the positively-charged electrooxidized films. The favorable selectivity, LOD, and NO permeability of poly(5A1N) and poly(phenol) modified electrodes in PBS motivate the use of an outer protective membrane—such as Nafion or a fluorinated xerogel—to further aid in maintaining analytical performance in proteinacious media.

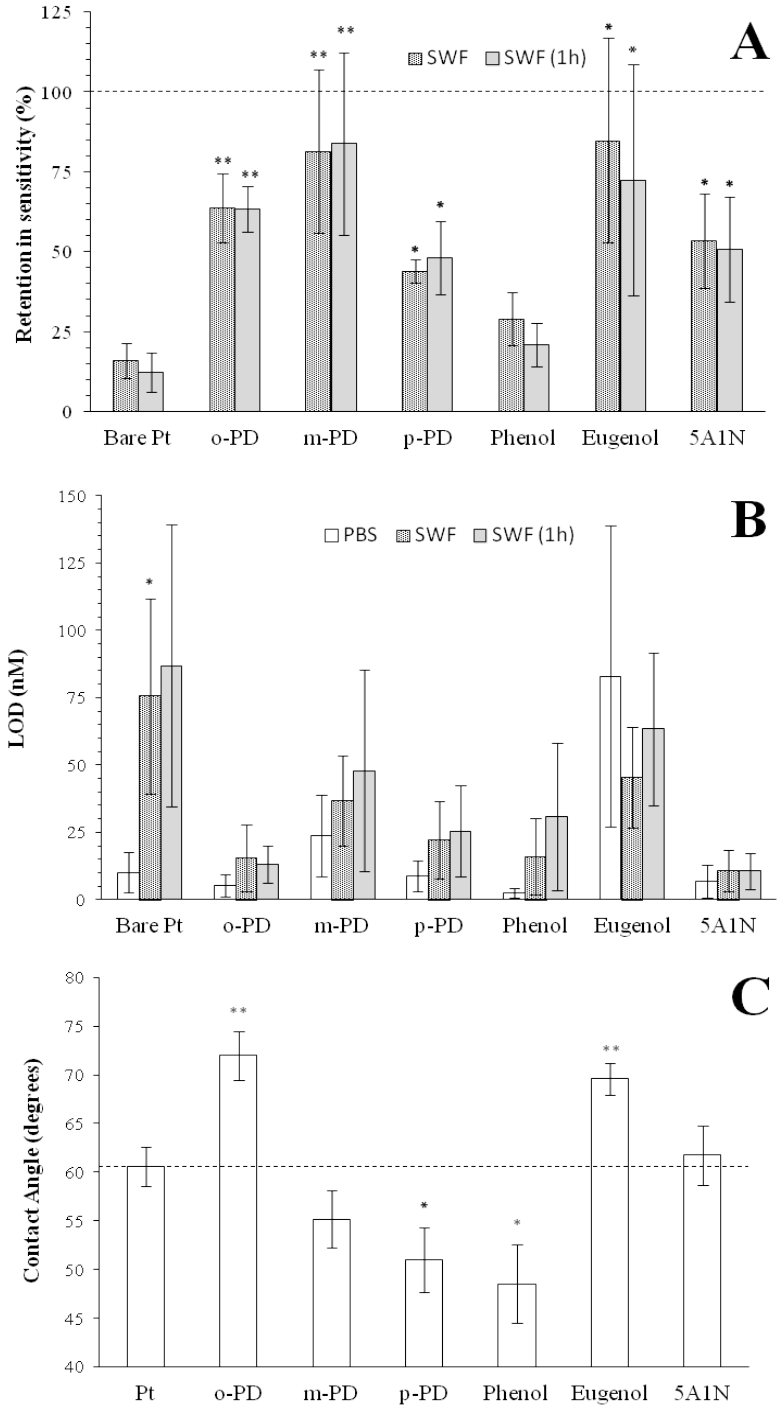

Figure 2.7 (A) Retention of NO sensitivity for polymer-modified Pt electrodes (2 mm dia.) in SWF relative to PBS (significance with respect to Pt; n ≥ 4). (B) Detection limit (*S/N* = 3) of electrodes in PBS, SWF, and after 1 h of SWF immersion (significance with respect to LOD in PBS; n ≥ 4). (C) Static contact angle measurements on polymer-modified planar Pt electrodes (significance with respect to Pt; n ≥ 4). * p <0.05; ** p <0.01.

2.4 Conclusions

Herein, we studied sensor performance (i.e., NO sensitivity and selectivity) as a function of both monomer identity and depositional protocol. Electrodeposition via CV proved superior to CPA in producing more selective films towards NO. While phenylenediamine monomers are more commonly employed to fabricate NO sensors, both poly(phenol)- and poly(5A1N)-modified electrodes proved to be superior with respect to NO sensitivity and selectivity. These analytical merits motivate future study and implementation of poly(phenol) and poly(5A1N) films for electrochemical NO-sensing platforms.

REFERENCES

(1) Dudzinski, D. M.; Igarashi, J.; Greif, D.; Michel, T. The regulation and pharmacology of endothelial nitric oxide synthase. *Annu. Rev. Pharmacol. Toxicol.* **2006**, *46*, 235-276, 232 plates.

(2) Wink, D. A.; Mitchell, J. B. Chemical biology of nitric oxide: insights into regulatory, cytotoxic, and cytoprotective mechanisms of nitric oxide. *Free Radical Biol. Med.* **1998**, *25*, 434-456.

(3) Luo, J.-d.; Chen, A. F. Nitric oxide: a newly discovered function on wound healing. *Acta Pharmacol. Sin.* **2005**, *26*, 259-264.

(4) Donnini, S.; Ziche, M. Constitutive and inducible nitric oxide synthase: Role in angiogenesis. *Antioxid. Redox Signaling* **2002**, *4*, 817-823.

(5) Morbidelli, L.; Donnini, S.; Ziche, M. Role of nitric oxide in the modulation of angiogenesis. *Curr. Pharm. Des.* **2003**, *9*, 521-530.

(6) van Goor, H.; Albrecht, E. W. J. A.; Heeringa, P.; Klok, P. A.; van der Horst, M. L. C.; de Jager-Krikken, A.; Bakker, W. W.; Moshage, H. Nitric oxide inhibition enhances platelet aggregation in experimental anti-Thy-1 nephritis. *Nitric Oxide* **2001**, *5*, 525-533.

(7) Fang, F. C. Perspectives series: host/pathogen interactions. Mechanisms of nitric oxide-related antimicrobial activity. *J. Clin. Invest.* **1997**, *99*, 2818-2825.

(8) Olbregts, J. Termolecular reaction of nitrogen monoxide and oxygen: a still unsolved problem. *Int. J. Chem. Kinet.* **1985**, *17*, 835-848.

(9) Wink, D. A.; Darbyshire, J. F.; Nims, R. W.; Saavedra, J. E.; Ford, P. C. Reactions of the bioregulatory agent nitric oxide in oxygenated aqueous media: determination of the kinetics for oxidation and nitrosation by intermediates generated in the NO/O2 reaction. *Chem. Res. Toxicol.* **1993**, *6*, 23-27.

(10) Hunter, R. A.; Storm, W. L.; Coneski, P. N.; Schoenfisch, M. H. Inaccuracies of nitric oxide measurement methods in biological media. *Anal. Chem.* **2013**, *85*, 1957-1963.

(11) Archer, S. Measurement of nitric oxide in biological models. *FASEB J* **1993**, *7*, 349-360.

(12) Hurst, R. D.; Clark, J. B. The utility of the nitric oxide electro-chemical sensor in biomedical research. *Sensors* **2003**, *3*, 321-329.

(13) Hetrick, E. M.; Schoenfisch, M. H. Analytical chemistry of nitric oxide. *Annu. Rev. Anal. Chem.* **2009**, *2*, 409-433.

(14) Davies, I. R.; Zheng, X. Nitric oxide selective electrodes. *Methods Enzymol.* **2008**, *436*, 63-95.

(15) Coneski, P. N.; Schoenfisch, M. H. Nitric oxide release: Part III. Measurement and reporting. *Chem. Soc. Rev.* **2012**, *41*, 3753-3758.

(16) Burtis, C.; Ashwood, E.; Bruns, D.: *Tietz Textbook of Clinical Chemistry and Molecular Diagnostics, Fifth Edition*; Elsevier, 2011.

(17) Privett, B. J.; Shin, J. H.; Schoenfisch, M. H. Electrochemical nitric oxide sensors for physiological measurements. *Chem. Soc. Rev.* **2010**, *39*, 1925-1935.

(18) Brown, F. O.; Finnerty, N. J.; Lowry, J. P. Nitric oxide monitoring in brain extracellular fluid: characterisation of Nafion-modified Pt electrodes in vitro and in vivo. **2009**, *134*, 2012-2020.

(19) Pariente, F.; Alonso, J. L.; Abruña, H. D. Chemically modified electrode for the selective and sensitive determination of nitric oxide (NO) in vitro and in biological systems. *J. Electroanal. Chem.* **1994**, *379*, 191-197.

(20) Cha, W.; Meyerhoff, M. E. Enhancing the selectivity of amperometric nitric oxide sensor over ammonia and nitrite by modifying gas-permeable membrane with Teflon AF. *Chem. Anal.* **2006**, *51*, 949-961.

(21) Do, J.-S.; Wu, K.-J.; Tsai, M.-L. Amperometric NO gas sensor in the presence of diffusion barrier: selectivity, mass transfer of NO and effect of temperature. *Sens. Actuators, B* **2002**, *86*, 98-105.

(22) Ichimori, K.; Ishida, H.; Fukahori, M.; Nakazawa, H.; Murakami, E. Practical nitric oxide measurement employing a nitric oxide-selective electrode. *Rev. Sci. Instrum.* **1994**, *65*, 2714-2718.

(23) Shibuki, K. An electrochemical microprobe for detecting nitric oxide release in brain tissue. *Neurosci. Res.* **1990**, *9*, 69-76.

(24) Shin, J. H.; Privett, B. J.; Kita, J. M.; Wightman, R. M.; Schoenfisch, M. H. Fluorinated xerogel-derived microelectrodes for amperometric nitric oxide sensing. *Anal. Chem.* **2008**, *80*, 6850-6859.

(25) Murphy, L. J. Reduction of interference response at a hydrogen peroxide detecting electrode using electropolymerized films of substituted naphthalenes. *Anal. Chem.* **1998**, *70*, 2928-2935.

(26) Ohnuki, Y.; Matsuda, H.; Ohsaka, T.; Oyama, N. Permselectivity of films prepared by electrochemical oxidation of phenol and amino-aromatic compounds. *J. Electroanal. Chem. Interfacial Electrochem.* **1983**, *158*, 55-67.

(27) Dai, Y.-Q.; Zhou, D.-M.; Shiu, K.-K. Permeability and permselectivity of polyphenylenediamine films synthesized at a palladium disk electrode. *Electrochimica Acta* **2006**, *52*, 297-303.

(28) Myler, S.; Eaton, S.; Higson, S. P. J. Poly(o-phenylenediamine) ultra-thin polymer-film composite membranes for enzyme electrodes. *Anal. Chim. Acta* **1997**, *357*, 55-61.

(29) Killoran, S. J.; O'Neill, R. D. Characterization of permselective coatings electrosynthesized on Pt-Ir from the three phenylenediamine isomers for biosensor applications. *Electrochim. Acta* **2008**, *53*, 7303-7312.

(30) Shim, J. H.; Do, H.; Lee, Y. Simple Fabrication of Amperometric Nitric Oxide Microsensors Based on Electropolymerized Membrane Films. *Electroanalysis* **2010**, *22*, 359-366.

(31) Friedemann, M. N.; Robinson, S. W.; Gerhardt, G. A. o-Phenylenediamine-modified carbon fiber electrodes for the detection of nitric oxide. *Anal. Chem.* **1996**, *68*, 2621-2628.

(32) Pontié, M.; Bedioui, F.; Devynck, J. New composite modified carbon microfibers for sensitive and selective determination of physiologically relevant concentrations of nitric oxide in solution. *Electroanalysis* **1999**, *11*, 845-850.

(33) Vidotti, M.; Dall'Antonia, L. H.; Cintra, E. P.; Cordoba de Torresi, S. I. Reduction of interference signal of ascorbate and urate in poly(pyrrole)-based ammonia sensors in aqueous solutions. *Electrochim. Acta* **2004**, *49*, 3665-3670.

(34) Calia, G.; Monti, P.; Marceddu, S.; Dettori, M. A.; Fabbri, D.; Jaoua, S.; O'Neill, R. D.; Serra, P. A.; Delogu, G.; Migheli, Q. Electropolymerized phenol derivatives as permselective polymers for biosensor applications. *Analyst* **2015**, *140*, 3607-3615.

(35) Reynolds, E. R.; Yacynych, A. M. Direct sensing platinum ultra-microbiosensors for glucose. *Biosens. Bioelectron.* **1994**, *9*, 283-293.

(36) Rothwell, S. A.; McMahon, C. P.; O'Neill, R. D. Effects of polymerization potential on the permselectivity of poly(o-phenylenediamine) coatings deposited on Pt-Ir electrodes for biosensor applications. *Electrochim. Acta* **2009**, *55*, 1051-1060.

(37) Rothwell, S. A.; O'Neill, R. D. Effects of applied potential on the mass of non-conducting poly(ortho-phenylenediamine) electro-deposited on EQCM electrodes: comparison with biosensor selectivity parameters. *Phys. Chem. Chem. Phys.* **2011**, *13*, 5413-5421.

(38) Oyama, N.; Sato, M.; Ohsaka, T. Preparation of thin polymeric films on electrode surfaces by electropolymerization of aromatic compounds with amino groups. *Synth. Met.* **1989**, *29*, E501-E506.

(39) Pham, M.-C.; Mostefai, M.; Simon, M.; Lacaze, P.-C. Electrochemical synthesis and study of poly(5-amino 1-naphthol) film in aqueous and organic media. *Synth. Met.* **1994**, *63*, 7-15.

(40) Rothwell, S. A.; Killoran, S. J.; Neville, E. M.; Crotty, A. M.; O'Neill, R. D. Poly(o-phenylenediamine) electrosynthesized in the absence of added background electrolyte provides a new permselectivity benchmark for biosensor applications. *Electrochem. Commun.* **2008**, *10*, 1078-1081.

(41) Bedioui, F.; Griveau, S. Electrochemical Detection of Nitric Oxide: Assessement of Twenty Years of Strategies. *Electroanalysis* **2013**, *25*, 587-600.

(42) Cintra, E. P.; Cordoba de Torresi, S. I. Resonant Raman spectroscopy as a tool for determining the formation of a ladder structure in electropolymerized poly(5-amino-1-naphthol). *J. Electroanal. Chem.* **2002**, *518*, 33-40.

(43) Losito, I.; Palmisano, F.; Zambonin, P. G. o-Phenylenediamine electropolymerization by cyclic voltammetry combined with electrospray ionization-ion trap mass spectrometry. *Anal. Chem.* **2003**, *75*, 4988-4995.

(44) Wang, J.; Chen, S.-P.; Lin, M. S. Use of different electropolymerization conditions for controlling the size-exclusion selectivity at polyaniline, polypyrrole and polyphenol films. *J. Electroanal. Chem. Interfacial Electrochem.* **1989**, *273*, 231-242.

(45) Ohsaka, T.; Ohba, M.; Sato, M.; Oyama, N. Formation of a novel electroactive film by electropolymerization of 5-amino-1-naphthol. *J. Electroanal. Chem. Interfacial Electrochem.* **1991**, *300*, 51-66.

(46) Ciszewski, A.; Milczarek, G. Preparation and general properties of chemically modified electrodes based on electrosynthesized thin polymeric films derived from eugenol. *Electroanalysis* **2001**, *13*, 860-867.

(47) Rothwell, S. A.; Killoran, S. J.; O'Neill, R. D. Enzyme immobilization strategies and electropolymerization conditions to control sensitivity and selectivity parameters of a polymer-enzyme composite glucose biosensor. *Sensors* **2010**, *10*, 6439-6462.

(48) Cataldo, F. On the polymerization of p-phenylenediamine. *Eur. Polym. J.* **1996**, *32*, 43-50.

(49) Malitesta, C.; Palmisano, F.; Torsi, L.; Zambonin, P. G. Glucose fast-response amperometric sensor based on glucose oxidase immobilized in an electropolymerized poly(o-phenylenediamine) film. *Anal. Chem.* **1990**, *62*, 2735-2740.

(50) Ryan, M. R.; Lowry, J. P.; O'Neill, R. D. Biosensor for neurotransmitter L-glutamic acid designed for efficient use of L-glutamate oxidase and effective rejection of interference. *Analyst* **1997**, *122*, 1419-1424.

(51) Pelletier, M. M.; Kleinbongard, P.; Ringwood, L.; Hito, R.; Hunter, C. J.; Schechter, A. N.; Gladwin, M. T.; Dejam, A. The measurement of blood and plasma nitrite by chemiluminescence: Pitfalls and solutions. *Free Radical Biol. Med.* **2006**, *41*, 541-548.

(52) Otero, T.; De Larreta, E. Electrochemical control of the morphology, adherence, appearance and growth of polypyrrole films. *Synth. Met.* **1988**, *26*, 79-88.

(53) Vreeland, R. F.; Atcherley, C. W.; Russell, W. S.; Xie, J. Y.; Lu, D.; Laude, N. D.; Porreca, F.; Heien, M. L. Biocompatible PEDOT: Nafion composite electrode coatings for selective detection of neurotransmitters in vivo. *Anal. Chem.* **2015**, *87*, 2600-2607.

(54) Treloar, P. H.; Christie, I. M.; Vadgama, P. M. Engineering the right membranes for electrodes at the biological interface; solvent cast and electropolymerised. *Biosens. Bioelectron.* **1995**, *10*, 195-201.

(55) Wisniewski, N.; Reichert, M. Methods for reducing biosensor membrane biofouling. *Colloids Surf., B* **2000**, *18*, 197-219.

(56) Barfidokht, A.; Gooding, J. J. Approaches toward allowing electroanalytical devices to be used in biological fluids. *Electroanalysis* **2014**, *26*, 1182-1196.

CHAPTER 3: PROFILING SPATIAL AND TEMPORAL RELEASE OF NITRIC OXIDE FROM IMMUNOSTIMULATED MACROPHAGES[3]

3.1 Introduction

Since its discovery as the endothelium-derived smooth muscle relaxation factor, nitric oxide (NO) has been implicated in an ever-growing collection of biological processes.[1,2] With its ability to freely permeate cell membranes, NO acts as an intercellular gasotransmitter, mediating such processes as wound healing,[3] vasodilation, angiogenesis,[4] platelet aggregation,[5] long-term memory potentiation,[6,7] and inflammation.[8] In order for one molecule to exert such varied, sometimes opposing effects, the biological activity of NO is necessarily concentration-dependent. Low concentrations of NO (pM-nM) are generated from endothelial and neuronal isoforms of the nitric oxide synthase enzyme (eNOS and nNOS, respectively), initiating enzymatic cascades through cyclic GMP.[9] High NO concentrations (nM-μM) are produced from inflammatory cells via the inducible isoform (iNOS) and create localized environments of nitrosative/oxidative stress to kill pathogens.[10] As a potential biomarker of inflammation state, measurements of NO from relevant biological fluids (e.g., blood, serum, wound fluid) demonstrate prognostic utility in cases of sepsis and chronic wounds.[11,12] Probing the concentration dynamics of this seemingly

[3] This chapter was adapted in part from an article that has been submitted for publication. The original citation is as follows: Brown, M. D.; Schoenfisch, M. H. Profiling the spatial and temporal release of nitric oxide from immunostimulated macrophages. *submitted.*

ubiquitous molecule is essential to understanding these and other yet undiscovered functions of NO in mammalian physiology.

The high reactivity and diffusibility of NO present challenges to in situ detection and quantification.[13] Nitric oxide's lifetime in biological milieu is limited to a few seconds due to scavenging by thiols, oxygen, free metal ions, and heme-containing proteins.[14-16] Indirect detection methods can measure NO's more stable oxidative byproducts, nitrite and nitrate (i.e., NO_x species, collectively). Although the effects of scavenging are largely circumvented, indirect methods fail to capture NO fluctuations in real time and generally require extensive sample preparation (e.g., the Griess assay).[17] Chemiluminescence and electron paramagnetic resonance spectroscopy offer direct and highly sensitive detection, but these techniques require complex instrumentation and are not well suited for real-time analysis in complex media.[18,19] Currently, electrochemical sensors offer the highest spatial and temporal resolution for in situ, real-time monitoring of NO in biological media.[20]

In the last thirty years, most biological applications of electrochemical NO sensors have involved measurement from either liver tissue (in the form of an excised organ or homogenate) or cultured cells.[21] For the latter, macrophages and human umbilical vein endothelial cells (HUVECs) are generally preferred given their well-known NO-release response to certain stimuli, including L-arginine,[22] acetylcholine,[23] bradykinin,[24] and calcium ionophore.[25] These stimuli activate the constitutively expressed (i.e., continually present in the cytoplasm) NOS isoforms, eNOS and nNOS, resulting in NO release within seconds. Negative control trials with competitive NOS inhibitors (e.g., *N*-nitroarginine methyl ester, aminoguanidine) or rapid NO scavengers (e.g., oxyhemoglobin) have been used to verify response accuracy. Detection of NO released from cultured cells is most often used as a

demonstration of a sensor's suitability for measurement in biological systems (i.e., sensocompatibility) rather than to furnish new biological information.

Though measurement of cellular NO release derived from eNOS or nNOS may demonstrate initial sensocompatibility, these experiments are generally conducted over the course of minutes, often without any indication that favorable sensor performance is maintained. A more analytically challenging biological application is the measurement of extended NO release (hours-days), specifically from iNOS. As part of the innate immune response, macrophages upregulate iNOS production in response to endotoxins and/or inflammatory cytokines, requiring 6-8 hours for complete enzyme expression.[26,27] Continuous electrochemical measurement of macrophage NO release on this time scale has been limited to two reports. Pekarova et al. demonstrated continuous NO measurement from lipopolysaccharide (LPS)-stimulated macrophages using a poly(porphyrin)- and Nafion-coated carbon fiber microelectrode (7 μm dia.) positioned above confluent cells.[28] The sensor's current response was converted to a rate of NO release (nmol NO h^{-1} 10^6 $cells^{-1}$) using Griess analysis of the supernatant at 20 h and assuming a 1:1 conversion of NO to nitrite (as opposed to calibration of the sensor with NO prior to the experiment). Although this study marked the longest continuous monitoring of macrophage-derived NO release at the time, the sensor selectivity against nitrite was low (1:609, NO_2^-:NO signal response; −2.8 selectivity coefficient), a troublesome characteristic particularly in an environment with continuously rising nitrite concentrations (≥20 μM NO_2^- at 20 h). In a different study, Cha et al. integrated an electrochemical NO senor within a microfluidic device to measure NO release from macrophages cultured in an upstream microchannel.[29] Using a TeflonAF gas permeable membrane, high selectivity was reported against both L-ascorbate and nitrite. The

evolution of NO release was monitored over the course of 16 h upon stimulation with LPS. Although the sensor possessed adequate selectivity, the microfluidic perfusate media did not contain serum, the primary source of proteins in standard culture media. Moreover, long response times (at most, 80 s) necessitated deoxygenation of the perfusate to prevent undesirable NO scavenging. While removing both oxygen and protein nutrients facilitated NO detection, such a configuration is unlikely to accurately model in vivo behavior of macrophages.

In order to meet both the selectivity and sensocompatibility challenges of long-term NO measurement from cells in proteinaceous media, we report the fabrication and characterization of a bilaminar sensor comprised of a platinum disk electrode modified by an electropolymerized 5-amino-1-naphthol (5A1N) film and a highly fluorinated xerogel (XG) topcoat. Previous studies have highlighted the benefits of poly(5A1N) for NO selectivity, particularly over nitrite.[30,31] Likewise, XG membranes have been shown to possess NO permselective characteristics based on size-exclusion and hydrophobicity.[32,33] We hypothesized that their combination would provide unequalled sensor performance characteristics for use over extended durations. The bilaminar sensor design was evaluated for selectivity for NO over a wide panel of biologically relevant interferents and for sensocompatibility (i.e., retention of NO sensitivity, selectivity, and LOD with extended use in proteinaceous media). Sensor utility was demonstrated by continuously monitoring NO release from pro-inflammatory macrophages stimulated with LPS and interferon-gamma (IFN-γ) over a 24 h period. Scanning electrochemical microscope approach curves were also collected to probe the NO diffusion profile emanating from confluent pro-inflammatory macrophages.

3.2 Experimental

3.2.1 Materials, reagents, and apparatus

Trimethoxymethylsilane (MTMOS), 5-amino-1-naphthol (5A1N), hydrochloric acid (HCl), sodium nitrite, sodium nitrite standard (0.1 M), L-ascorbic acid (AA), acetaminophen (AP), dopamine hydrochloride (DA), lipopolysaccharide (LPS), fetal bovine serum (FBS), lyophilized bovine oxyhemoglobin (Hb), *N*-(1-naphthyl)ethylenediamine dihydrochloride (NED), and sulfanilamide were purchased from Sigma Aldrich (St. Louis, MO). (Heptadecafluoro-1,1,2,2-tetrahydrodecyl)trimethoxysilane (17FTMS) was purchased from Gelest (Morrisvile, PA). Ethanol (200 proof), ammonium hydroxide, sodium hydroxide (NaOH), sodium chloride, sulfuric acid, phosphoric acid, and hydrogen peroxide (30 wt% H_2O_2) were obtained from Fisher Scientific (Hampton, NH). Dulbecco's modification of Eagle's medium (DMEM; 4.5 g/mL glucose; no phenol or L-glutamine) was purchased from Corning (Corning, NY). Interferon-gamma (IFN-γ) was obtained from BioLegend (San Diego, CA). Murine RAW 264.7 macrophages were obtained from the American Type Culture Collection (Manassas, VA). Nitric oxide (99.5%), carbon monoxide (99.3%), nitrogen (N_2), and argon (Ar) gases were purchased from National Welders Supply (Raleigh, NC). Platinum (75 μm) and tungsten (0.20 mm) wires were obtained from A-M Systems (Sequim, WA). Other solvents and chemicals were analytical-reagent grade and used as received without further purification.

A Millipore Milli-Q UV Gradient A10 System (Bedford, MA) was used to purify distilled water to a resistivity of 18.2 MΩ·cm and a total organic content of ≤6 ppb. Saturated NO (1.9 mM) and CO (0.9 mM) were made by purging ~20 mL of phosphate buffered saline (PBS; 0.01 M, pH 7.4) first with Ar for 25 min and then with NO or CO gas for 25 min over

ice. Saturated gas solutions were stored at 4 °C and used the day of preparation. Electrochemical experiments were carried out using either an 8-channel CH Instruments 1030C Electrochemical Analyzer or a CH Instruments 920D Scanning Electrochemical Microscope (SECM; Austin, TX). In total, eight inlaid 2 mm dia. polycrystalline platinum (Pt) disk working electrodes sealed in Kel-F (6 mm total diameter; CH Instruments), a silver-silver chloride (Ag|AgCl) reference electrode (3.0 M KCl; CH Instruments), and a coiled Pt wire counter electrode were employed for measurements on the 8-channel potentiostat. Platinum microelectrodes (75 μm dia.) were fabricated by hand for SECM measurements (detailed in Section 2.5.). All reported potentials hereafter are versus the Ag|AgCl reference electrode. Contact angle measurements were collected using a CAM 200 optical contact angle meter (KSV Instruments; Bridgeport, CT), and images were collected on a Hitachi S-4700 Scanning Electron Microscope (SEM; Tarrytown, NY).

3.2.2 Preparation of Pt/poly(5A1N)/XG sensors

Platinum working electrodes were mechanically polished with deagglomerated alumina slurries down to 0.05 μm in particle size (Buehler; Lake Bluff, IL) and ultrasonicated in ethanol to remove residual alumina. Electrodes were then electrochemically polished in 1 N hydrosulfuric acid by cycling between -0.4 and +1.8 V for 40 cycles (500 mV s^{-1}). Electrodes were rinsed with water and transferred to a monomer solution of 5A1N. To improve solubility, 10 mM 5A1N was dissolved in PBS solution titrated to pH 1 with HCl. Poly(5A1N) films were electropolymerized via cyclic voltammetry (CV), sweeping the potential from 0 to +1.0 V (20 cycles; positive direction initial sweep) at a scan rate of 10 mV s^{-1}. Film-modified electrodes were rinsed copiously with distilled water to remove unbound oligomer and allowed to dry for >1 h on the benchtop before spray-coating.

A fluoroalkoxysilane sol solution was prepared via acid-catalyzed hydrolysis and co-condensation of MTMOS and 17FTMS precursors (30% 17FTMS, v/v balance MTMOS). Ordered additions of 3.600 mL EtOH, 630 μL MTMOS, 270 μL 17FTMS, 960 μL H_2O, and 60 μL 0.5 M HCl constituted the sol solution, which was stirred vigorously for 1 h. The sol was spray-coated onto Pt disc electrodes (both bare and poly(5A1N)-modified) with an airbrush gun (Iwata HP-BC1 Plus; Yokohama, Japan) pressurized at 42 psi with a nozzle-target separation of 50 cm and 5 s of continuous dispersal. The sol-coated electrodes were then dried on the benchtop for >48 h to allow condensation of the xerogel matrix before further testing.

3.2.3 Steady-state amperometric measurements

Bare and modified electrodes were polarized at +0.8 V in deoxygenated PBS for 15 min to achieve a constant background current prior to measurements. Sensitivity for NO was determined with consecutive injections (475 nM each) of saturated NO solution into deoxygenated PBS. Calibrations were also done in FBS-supplemented DMEM to determine sensitivity retention relative to PBS trials. Limits of detection (LOD) were calculated with respect to 3 standard deviations of the noise (S/N = 3). The current responses to injections of sodium nitrite (1 mM), L-ascorbate (1 mM), acetaminophen (50 μM), dopamine hydrochloride (100 μM), carbon monoxide (0.9 μM), ammonium hydroxide (1 mM), and hydrogen peroxide (1 mM) were measured and compared to the NO sensitivity. Interferent concentrations well exceeded anticipated biological concentrations.[20] Selectivity coefficients were calculated using Eq. 1, where $\log k_{NO,j}$ is the selectivity coefficient for NO over interferent j, S_j is the sensor sensitivity towards interferent j, and S_{NO} is the NO sensitivity of the sensor.

$$\log k_{NO,j} = \log\left(\frac{S_j}{S_{NO}}\right) \quad \text{(Eq. 1)}$$

The long-term sensocompatibility of Pt/poly(5A1N)/XG, Pt/poly(5A1N), Pt/XG, and bare Pt electrodes were evaluated in PBS with 12 h of continuous operation (+0.8 V). Sensitivity towards NO, selectivity against nitrite, and the LOD were re-measured at the 12 h time-point and compared to initial measurements to assess performance maintenance. All sensor designs were also tested for sensitivity retention in DMEM. The Pt/poly(5A1N)/XG sensors were evaluated for long-term stability in FBS-supplemented (10% v/v) DMEM with 24 h of continuous operation (+0.8 V). Again, analytical metrics were re-measured at the 24 h time-point and compared to initial measurements to assess performance maintenance.

3.2.4 Continuous NO measurements from RAW 264.7 macrophages

The RAW 264.7 macrophages were seeded into a 12-well plate at a density of 1.0×10^6 cells/well (i.e., 2.5×10^5 cells cm^{-2}) and given 4 h to adhere to the plate. Each well contained 2.0 mL of phenol-free, FBS-supplemented DMEM. A custom 3D-printed well plate cover was designed to support a Pt/poly(5A1N)/XG working electrode and reference/counter electrodes in individual wells while the culture plate remained in an incubator at 37 °C and 5% CO_2 in air. Sensors were positioned using rubber O-rings and calipers such that the electrode surface was 200 ± 100 μm from the well bottom. Electrodes were given ~8 h to polarize at +0.8 V in solution before pro-inflammatory stimulants were injected into the cell (20 and 10 ng mL^{-1} LPS and IFN-γ, respectively). Continuous NO measurements were collected for 24 h post-stimulation. A least squares exponential regression was fit to the first 8 h pre-stimulation and used to background subtract the residual (i.e., non-analyte-specific) current from the entire trace. The current measured at t = 2 h post-stimulation (i.e., t = 10 h overall) was also background subtracted from all traces as a

reference point where no NO evolution from the cells was anticipated. Data collection was repeated for unstimulated macrophage cells with parameters and data processing kept the same.

After electrochemical experiments were completed, supernatant solutions were collected and stored at −20 °C. Endpoint Griess analysis was carried out on samples to quantitate nitrite totals from both stimulated and unstimulated cell runs as a measure of total NO production. Briefly, sulphanilic acid was reacted with nitrite in the sample to form a diazonium salt before reaction with NED to yield the characteristic pink azo dye detectable via absorbance spectroscopy at λ = 540 nm. Nitrite calibration standards were prepared in FBS-supplemented DMEM (the same matrix as the samples).

3.2.5 SECM measurements of NO from RAW 264.7 macrophages

Given the size constraints of the SECM probe positioner, Pt microelectrodes were fabricated by hand. Briefly, glass capillary tubes (0.68 mm internal dia.) were pulled and beaded at the tip before introducing a ~1.0 cm length of 75 μm dia. Pt wire. Passage over a propane blowtorch melted the capillary walls to encapsulate the Pt wire, which was then soldered to a tungsten lead. The distal end was sanded down to expose the Pt and sharpen the tip to a diameter of ~400 μm. The poly(5A1N) and XG modification of the Pt microelectrode proceeded exactly as with the disk macroelectrodes (*see* Section 3.2.2). Sensors were calibrated in DMEM immediately before use.

The RAW 264.7 macrophages were seeded into tissue culture dishes at a surface density of 2.5×10^5 cells cm^{-2} and given 4 h to adhere before stimulation with 20 and 10 ng mL^{-1} LPS and IFN-γ, respectively. In order to probe pro-inflammatory cells at their peak NO flux, 8 h of post-stimulation incubation were allotted for iNOS upregulation. Unstimulated

control cells were incubated for the same period. Approach curves to the cells in the z-direction were collected on the SECM with an approach rate of 1.0 μm s^{-1}. The background current measured at 600 μm was subtracted from all traces. Oxyhemoglobin (Hb; 160 μM) scavenging of NO from stimulated macrophage cells was used as a negative control.

3.2.6 Statistical analysis

The NO sensitivity, sensitivity retention, selectivity coefficients, and LOD of the bare and modified electrodes are presented (either numerically or with error bars) as the mean ± standard error of the mean.

3.3 Results and Discussion

3.3.1 Sensor fabrication

The electropolymerization of poly(5A1N) was carried out using a deposition procedure previously optimized for NO permselectivity against nitrite and AA.[31] As the potential is swept positively during electrodeposition, 5A1N monomers are oxidized through their amine groups to radical cations that dimerize, oligomerize, and ultimately precipitate out of solution onto the electroactive surface. The electrode surface is passivated against further monomer oxidation as the film grows with successive cycles. As a result, the process is self-terminating and results in thin (66-98 nm), reproducible (<5% relative error in total charge passed) films (Figure 3.1).[34] After deposition of poly(5A1N), the 17FTMS/MTMOS sol was spray-coated onto the electrode and allowed to dry/condense for at least 48 h. The poly(5A1N) film was predicted to improve xerogel compactness/adherence because amine functional groups have been reported to catalyze the condensation of alkoxysilane precursors in sol-gel systems.[35] The formation of a hydrophobic xerogel coating was confirmed by SEM

and contact angle measurements, the latter increasing from 62° to >90° after membrane deposition (Figure 3.1).

3.3.2 Sensor sensitivity and selectivity towards NO

As shown in Figure 3.2A, the analytical performance characterization of bilaminar Pt/poly(5A1N)/XG sensors included determining the NO sensitivity (12.4 ± 8.0 pA nM^{-1}), detection limit (~1 nM), and dynamic range (0.01-10 μM). The NO selectivity of the sensors was also evaluated against a range of biological interferents of different size and charge state (Figure 3.2B). Selectivity against a majority of interferents was markedly improved compared to the bare Pt electrode. In particular, selectivity improvements against larger interferents AA, AP, and DA (with net charges of -1, 0, and +1, respectively at physiological pH 7.4) demonstrated size-exclusion as a key selection mechanism. Among the smaller interferent species studied, cationic NH_4^+ and anionic NO_2^- were better rejected than uncharged CO and H_2O_2. The differential rejection of charged, water-solvated interferents over uncharged species demonstrates the membranes' combined hydrophobic character. Previous work has reported that hydrophobic membranes are better suited for selective NO diffusion versus membranes also containing hydrophilic domains, such as Nafion.[36] Of note, selectivity over CO was not improved for poly(5A1N)/XG-modified sensors compared to bare Pt electrodes (Figure 3.2B). The physicochemical properties of NO and CO, including size, lack of charge, and lipophilicity, are quite similar. These shared traits facilitate their roles as intercellular gasotransmitters and hemoprotein binders. As such, they regulate many of the same processes.[37,38] Lastly, the selectivity of the bilaminar sensor against nitrite was exceptional (selectivity coefficient of nearly −5) with ~80,000-fold greater sensitivity towards NO over nitrite.

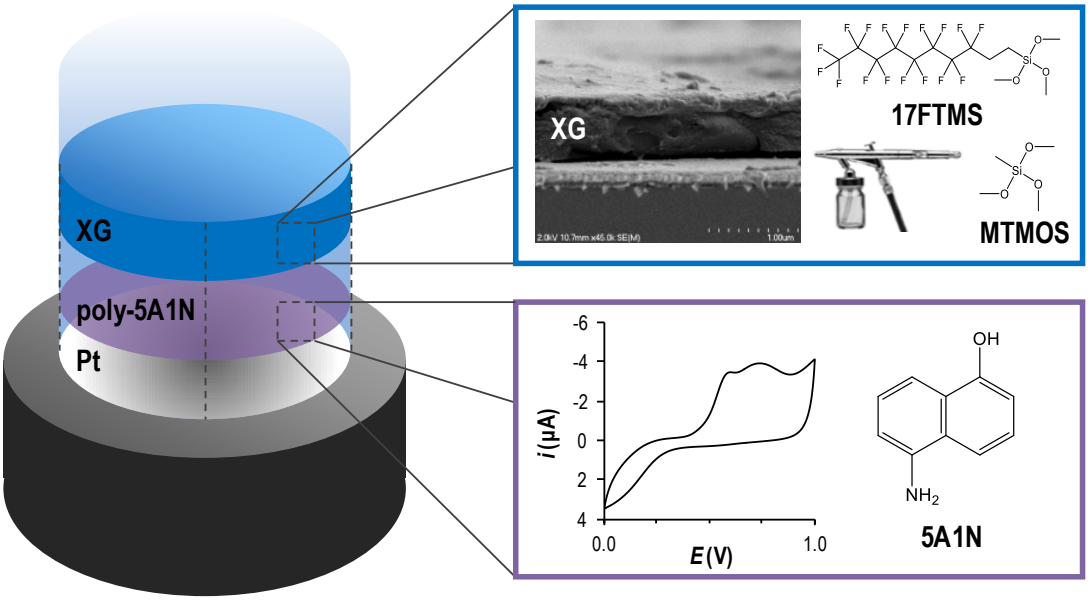

Figure 3.1 Schematic depiction of the Pt/poly(5A1N)/XG bilaminar sensor: (blue) xerogel deposition from condensed alkoxysilane precursors 17FTMS and MTMOS with SEM confirmation; (purple) electropolymerized film of poly(5A1N) and corresponding CV deposition trace.

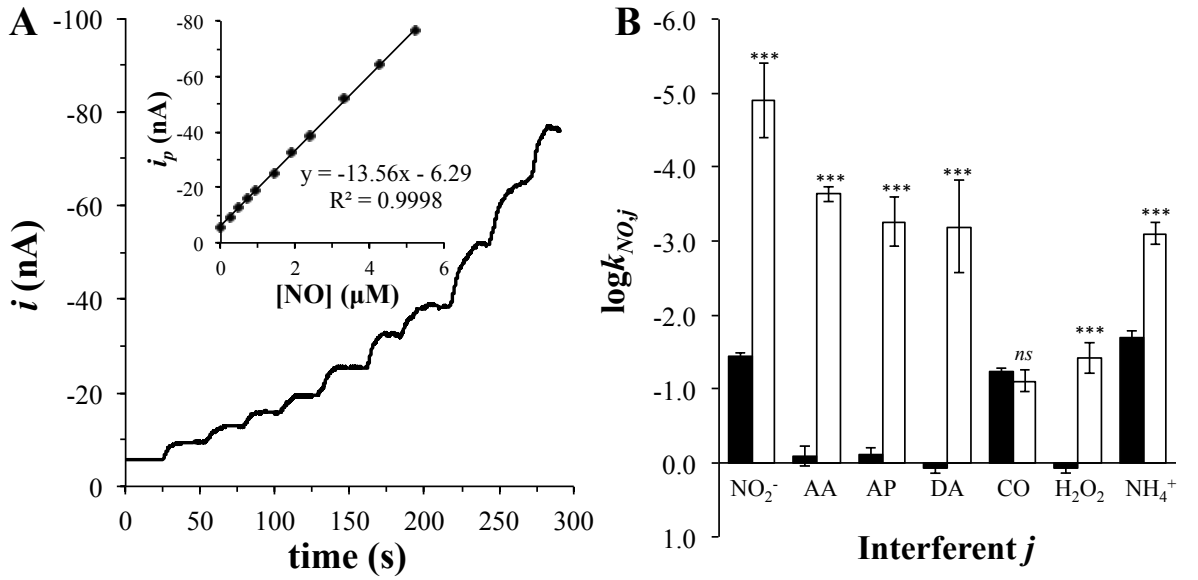

Figure 3.2 (A) Example staircase amperogram collected on a Pt/poly(5A1N)/XG electrode (2.0 mm dia.) in 10 mM PBS (pH 7.4) with 4 inj. of 0.25 μM, 3 inj. of 0.50 μM, and 3 inj. of 1.0 μM NO under CPA (applied potential: +0.8 V). Inset: corresponding calibration curve from plateau currents. (B) Selectivity coefficients of bare (black) and modified (white) Pt electrodes against common biological interferents nitrite (NO_2^-), L-ascorbic acid (AA), acetaminophen (AP), dopamine (DA), carbon monoxide (CO), hydrogen peroxide (H_2O_2), and ammonia (NH_3). For all selectivity measurements, $n \geq 8$.

3.3.3 Sensor performance with extended use in proteinaceous media

The long-term sensocompatibility (i.e., ability to maintain analytical performance) of a sensor is arguably more important than its optimal, initial performance, particularly with respect to biological utility. Bare Pt, Pt/poly(5A1N), Pt/XG, and bilaminar Pt/poly(5A1N)/XG sensors were thus characterized before and after extended use in buffer and biologically representative solutions. Sensors were polarized for 12 h continuously at +0.8 V *vs*. Ag|AgCl in PBS. Endpoint measurements of analytical metrics (NO sensitivity, LOD, and selectivity over nitrite) were calculated and compared to initial measurements (Table 3.1). Pt/poly(5A1N) sensors demonstrated good selectivity against nitrite initially (−3.8 ± 0.2) but could not maintain selectivity after extended use (−2.3 ± 0.2). Concomitantly, the NO sensitivity of these sensors increased. Previous work by Shim et al. characterized the operation stability of poly(5A1N)-modified microelectrodes with similar findings.[30] The authors attributed the selectivity reduction to hydration-induced membrane desorption, a gradual process delayed by the intrinsic hydrophobicity of compact poly(5A1N) films. The initial selectivity of Pt/XG sensors versus nitrite (−2.3 ± 0.3) was unfavorable compared to Pt/poly(5A1N); however, these sensors notably maintained all performance metrics over 12 h of operation (Table 3.1). We concluded that the XG membrane was more stable and capable of withstanding hydration and polarization effects during continuous operation relative to poly(5A1N) films alone.

The combination of poly(5A1N) and XG membranes yielded markedly greater selectivity over nitrite (−4.9 ± 0.5) than either film individually. The NO selectivity improvement suggests that XG deposition via spray-coating does not damage the poly(5A1N) film. After 12 h of continuous polarization in PBS, no change in LOD or nitrite

selectivity were observed for Pt/poly(5A1N)/XG sensors, with negligible deviation in sensor sensitivity, indicative of membrane durability. The bilaminar design thus benefits from both the high selectivity of the poly(5A1N) film and the performance stability imparted by the XG topcoat. In this manner, the XG membrane effectively shields the underlying poly(5A1N) film from hydration-induced desorption reported by Shim et al., thus helping retain the selectivity characteristics of the sensor.[30]

A critical challenge with in situ biological monitoring of NO is protein-related transducer biofouling. The effects of protein adsorption generally reduce sensor sensitivity and increase response time.[39,40] To study this potential effect, the NO sensitivity retention of bare and modified sensors was evaluated in FBS-supplemented DMEM solutions relative to PBS (Figure 3.3). Without transducer modification, bare Pt electrodes maintained <20% of their original NO sensitivity in the proteinaceous media. Such sensitivity reduction is the result of both biofouling and matrix effects, irrespective of protein-surface interactions. The presence of proteins, free metals, and thiol-containing residues in culture media are effective scavengers of NO. In addition, NO diffusion is diminished as a result of the greater viscosity of proteinaceous media.[41] In contrast, Pt/poly(5A1N) and Pt/XG sensors had improved sensitivity retention compared to bare Pt, but remained <70% relative to PBS trials. The bilaminar Pt/poly(5A1N)/XG sensors demonstrated ~80% sensitivity retention in DMEM. Clearly, sensors should be calibrated in the matrix of use after polarization pre-treatment. Of note, sensitivity retention returned to >95% when Pt/poly(5A1N)/XG sensors were re-calibrated in PBS, indicating that matrix effects play a greater role in sensitivity reduction relative to irreversible protein adsorption. This behavior is consistent with a previous report by Hunter et al.[14] The Pt/poly(5A1N)/XG sensors were also evaluated for long-term (24 h)

performance in FBS-supplemented DMEM under continuous operation (Table 3.1). The initial nitrite selectivity was slightly lower than in the PBS trials due to sensitivity reduction from matrix effects. However, the LOD, sensitivity, and selectivity each remained consistent over continuous operation in DMEM. To our knowledge, this demonstration of sensocompatibility for an electrochemical NO sensor has heretofore not been reported in the literature and strongly indicates the bilaminar sensor's capacity for use in biological samples.

3.3.4 Measurements of NO from RAW 264.7 macrophages

With the favorable sensocompatibility observed in proteinaceous media, the Pt/poly(5A1N)/XG sensor design was employed to measure long-term NO release from immunostimulated macrophages. Sensors were first polarized for 2 h and calibrated in FBS-supplemented DMEM before use to account for matrix effects and protein-related sensitivity reductions. The sensors were then positioned 200 ± 100 μm above confluent macrophages using a 3D-printed support, rubber O-rings, and calipers (Figure 3.4). In all trials, the background current decreased in the beginning due to adaptations of the electrode to the applied potential from double layer charging, formation of Pt oxides, membrane polarization, and redox reactions of impurities.[28] The sum of these processes, unrelated to analyte detection, constitutes the residual current, the trial-to-trial reproducibility of which is generally poor among electrochemical techniques.[42] In order to account for the residual current, least squares exponential regressions were fit to the first 8 h of polarization and subtracted from the remainder of the trace, a method comparable to other fit-based subtractions used to isolate the desired Faradaic current.[42-44]

Table 3.1 Analytical performance metrics of bare and modified Pt electrodes with extended use (n = 8).

Electrode [a]	Medium	t [b] (h)	S_{NO} [c] (pA nM^{-1})	LOD [d] (nM)	log$k_{NO,NO2-}$ [e]
Pt	PBS	---	18.3 ± 1.6	5 ± 2	-1.2 ± 0.0
Pt/poly(5A1N)	PBS	0	37.0 ± 6.4	1 ± 1	-3.8 ± 0.2
		12	81.5 ± 70.6	3 ± 3	-2.3 ± 0.2
Pt/XG	PBS	0	3.2 ± 1.3	4 ± 1	-2.3 ± 0.3
		12	2.7 ± 0.8	5 ± 5	-2.3 ± 0.1
Pt/poly(5A1N)/XG	PBS	0	12.4 ± 8.0	1 ± 1	-4.9 ± 0.5
		12	10.1 ± 4.9	1 ± 1	-4.8 ± 0.6
Pt/poly(5A1N)/XG	DMEM	0	7.6 ± 4.9	1.3 ± 0.4	-4.1 ± 0.4
		24	10.1 ± 4.0	0.8 ± 0.4	-4.2 ± 0.4

[a]Pt working electrodes (2 mm dia.). [b]Operation time under an applied potential of +0.8 V. [c]Sensitivity towards NO. [d]$S/N = 3$. [e]Calculated from Eq. 1.

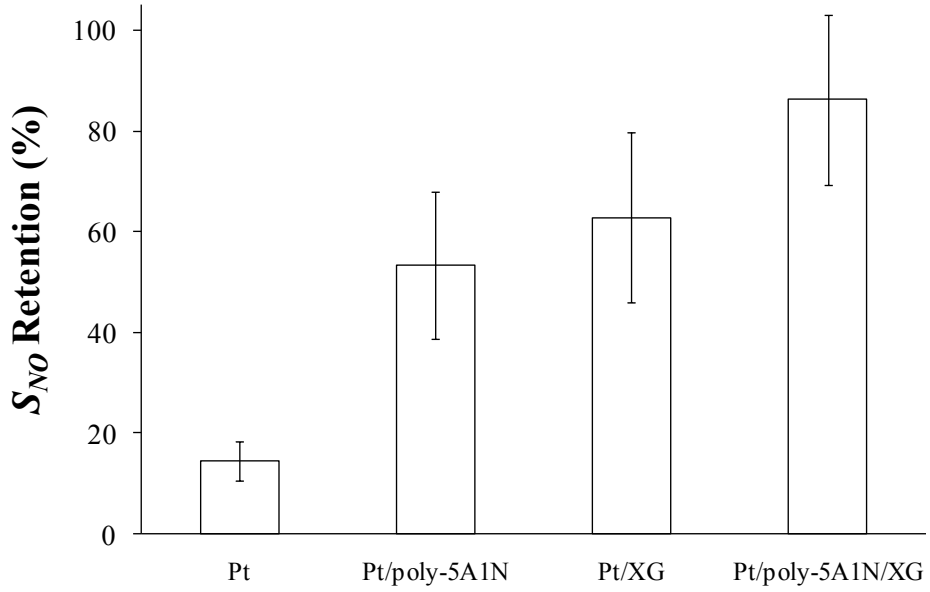

Figure 3.3 Retention of NO sensitivity of bare and modified Pt electrodes (2 mm dia.) in 10% FBS-supplemented DMEM relative to calibrations carried out in deoxygenated 10 mM PBS ($n \geq 8$).

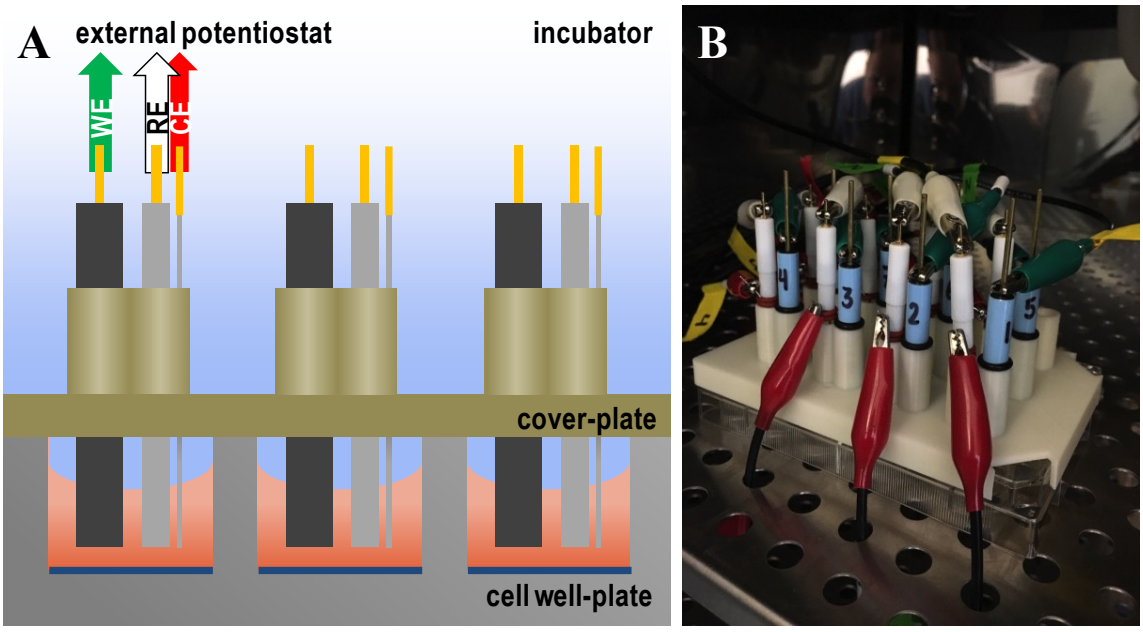

Figure 3.4 (A) Electrochemical setup for the measurement of NO from cultured macrophages with individually addressable Pt/poly-5A1N/XG working (WE), Ag|AgCl reference (RE), and Pt counter (CE) electrodes. (B) Setup inside an incubator with lead attachments to an external potentiostat.

At the 8-h time-point, 20 and 10 ng mL^{-1} lipopolysaccharide (LPS) and interferon-gamma (IFN-γ), respectively, were used to stimulate the macrophages. Lipopolysaccharide is recognized by macrophages as a structural element from the cell walls of *E. coli*. Interferon-γ is an inflammatory cytokine that, when combined with LPS, elicits a robust inflammatory response via iNOS upregulation.[10,45-47] As shown in Figure 3.5, the NO release increased gradually upon stimulation, plateauing to a steady flux approximately ~8 h post-stimulation. These results are in agreement with the reported rate of iNOS expression and work by Pekarova et al.[26-28] Approximately 14 h post-stimulation, the NO concentration began to decrease, indicative of total L-arginine consumption in solution. Cha et al. did not observe this reduction in NO concentration over the 16 h duration of their experiment, possibly due to perfusate replenishment of L-arginine compared to the static media used herein. The behavior of unstimulated macrophages was also monitored continuously over the same duration (Figure 3.5B). The lack of NO release indicates that an inflammatory response was not elicited in the unstimulated cells, as corroborated by endpoint Griess assay measurements (<2.5 μM LOD). The comparison between stimulated and unstimulated experiments verifies that NO was detected in the former and that the background subtraction methods employed did not artificially create nor enhance the NO-release profiles reported.

With repeated trials of macrophage stimulation, the temporal dynamics of NO release were similar. However, the concentrations measured varied from trial to trial, particularly in the region where the NO flux plateaued (50% relative error; Figure 3.5A). Griess measurements revealed that the total nitrite content in the supernatant of stimulated trials was 56 ± 3 μM, compared to sub-LOD (<2.5 μM) levels in unstimulated trials. As a stable oxidative byproduct of NO, the nitrite concentrations are a stoichiometric quantifier of the

total NO released from the cells. The small relative error in endpoint nitrite totals (5.4%) indicates that the macrophages were prepared and stimulated in a uniform fashion.

The possibility of a distance-dependence to the NO measured was investigated using scanning electrochemical microscopy (SECM) to identify the source of variation in plateau concentrations. In these experiments, the 2 mm dia. Pt electrode design was miniaturized to 75 μm and modified in exactly the same manner as macroelectrodes, thereby retaining analytical performance (7.03 pA μM^{-1} NO sensitivity in DMEM, $\log k_{NO,NO2^-} = -4.0$). Identically stimulated macrophages were profiled 8 h post-stimulation at their peak NO release (Figure 3.5A). As the SECM probe was moved from its location in bulk solution towards the confluent sheet of macrophages, the NO concentration sampled increased, beginning from baseline at ~500 μm and reaching a maximum (0.65 ± 0.11 μM) at the cell surface (Figure 3.6A). Control trials of unstimulated and oxyhemoglobin-scavenged cells were profiled for verification of accurate NO measurement (Figures 3.6B and 3.6C, respectively). The 17% relative error in the proximal NO is smaller than the ~50% error observed for long-term plateau measurements at the 8-h time-point (Figure 3.5A). Moreover, the range of NO concentrations measured as a function of sensor distance above the cell (0 – 0.65 μM) encapsulated the range of plateau values—evidence that electrode positioning accounted, at least partially, for variability in the latter.

Nitric oxide diffuses radially from cells, with the equilibrium between NO supply and solution scavengers resulting in a dissipating NO concentration gradient surrounding the cell (Figure 3.6A).[48] The NO concentration measured is therefore dependent on this gradient and subject to change in the synapse-like arrangement separating cell(s) and sensor. Careful consideration of this distance-dependence must be taken into account for any sensing

platform seeking to measure NO concentrations directly, particularly in efforts to examine the utility of NO as a biomarker. Our study represents the first application of SECM for continuously profiling the NO concentration gradient emanating from immunostimulated macrophages. Isik et al. previously reported variation in the peak NO response from bradykinin-stimulated HUVEC cells with SECM-guided electrode placement 5-30 μm above the cell surface (NO was not measurable at distances greater than 30 μm).[49] Comparatively, we observe dissipation of the NO concentration gradient at 500 μm above stimulated macrophages. The difference between spatial NO release profiles may be attributed to cell type and NOS expression. Macrophages are responsible for generating biocidal concentrations of NO during inflammation,[50] whereas HUVECs release lower, sustained NO fluxes to regulate vascular tone.[51] Once fully expressed, iNOS produces NO in 1000-fold larger quantities than the constitutive isoforms.[26]

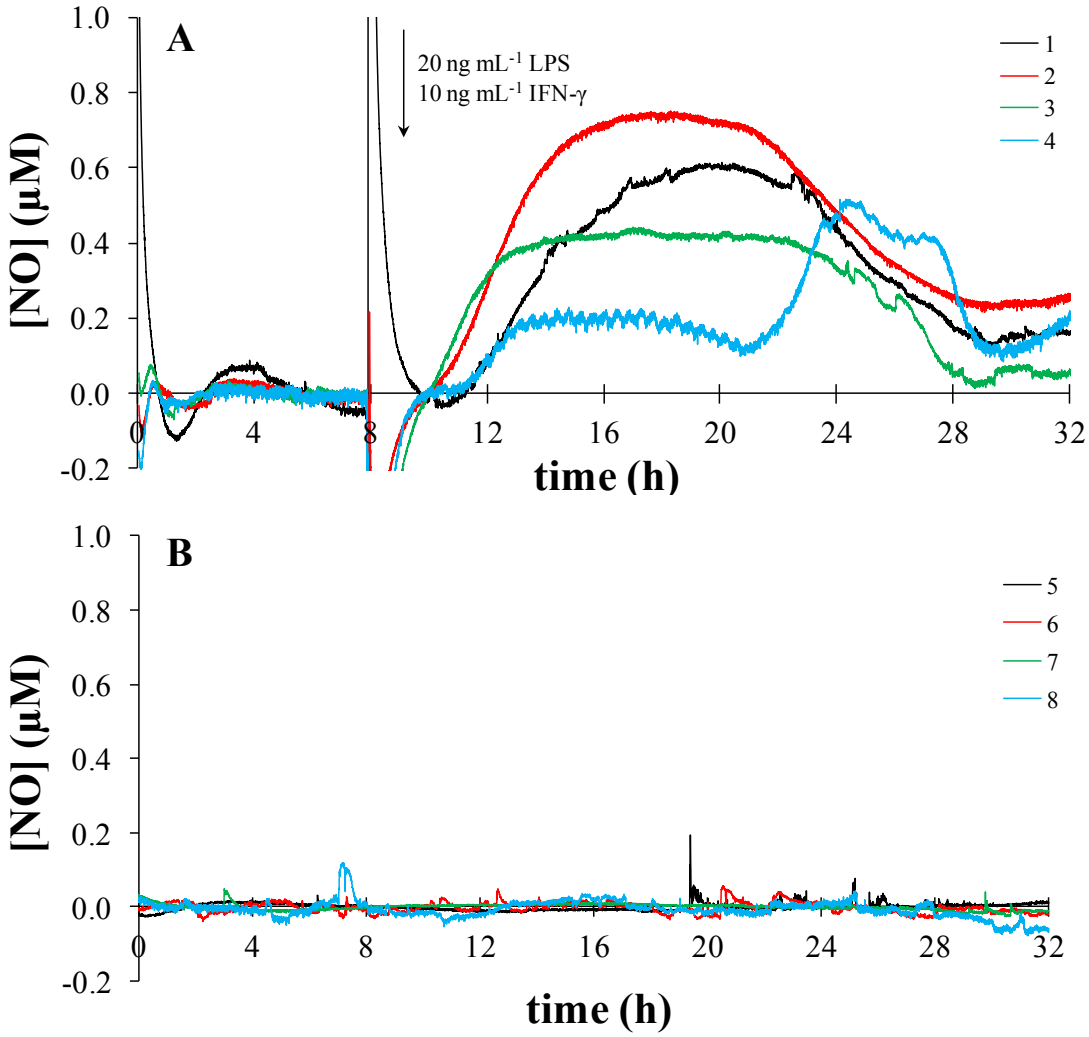

Figure 3.5 The NO-release profiles of (A) stimulated and (B) unstimulated RAW 264.7 macrophages measured using Pt/p(5A1N)/XG sensors (2.0 mm dia.) inside an incubator. The current collected from the first 8 h of each trace was fit to an least squares exponential regression, which was then background subtracted from the entire trace before conversion to NO concentration. The current measured at t = 10 h was also subtracted from the traces to address the effect of stimulant injection. Both stimulated (A) and unstimulated (B) received identical background current adjustments.

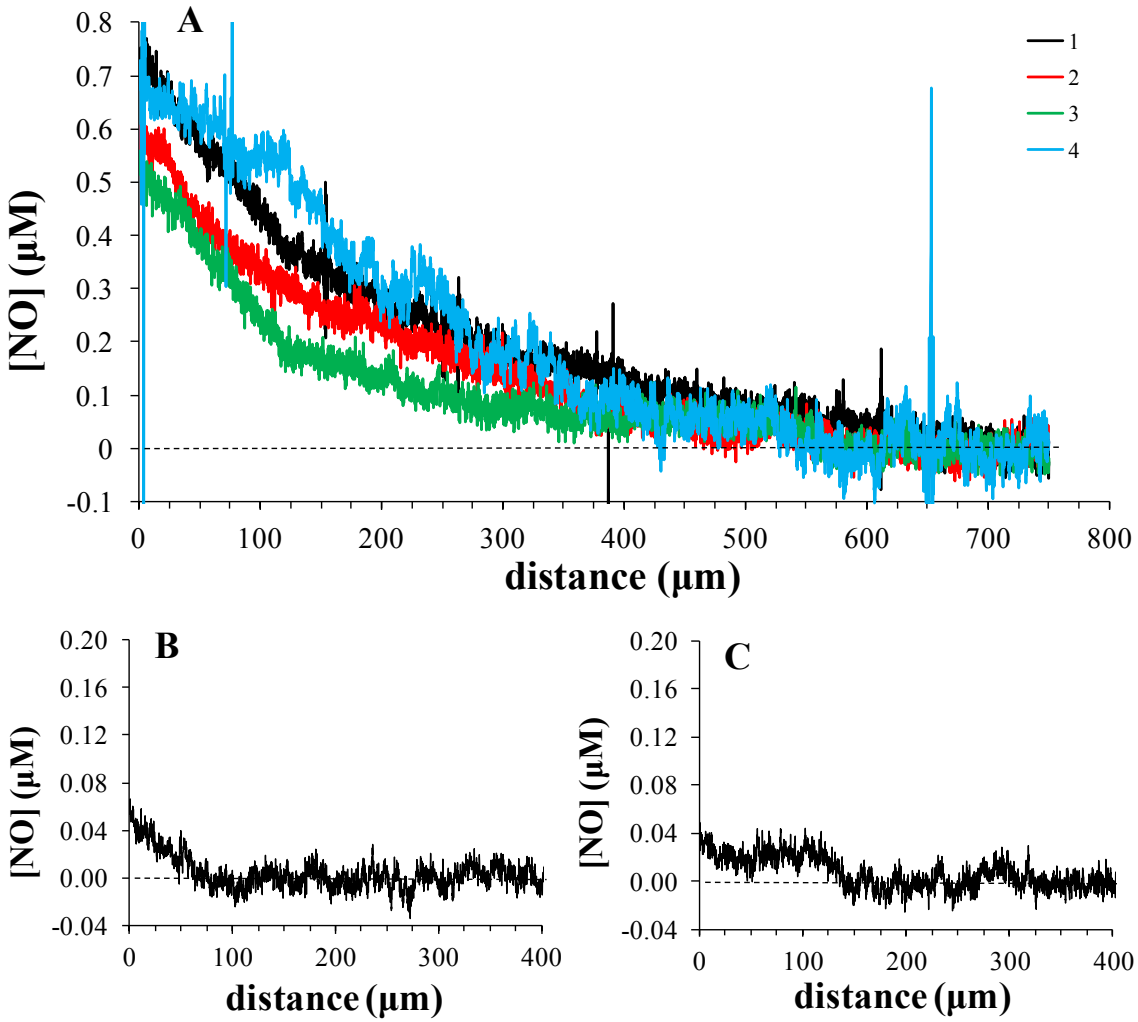

Figure 3.6 (A) The NO diffusion profiles of a confluent sheet of macrophages 8 h after stimulation with 20 ng mL^{-1} LPS and 10 ng mL^{-1} IFN-γ as measured by a Pt/poly(5A1N)/XG microelectrode approaching at a rate of 1 µm s^{-1} using a SECM (4 biological repetitions shown). The background current collected at 600 µm was subtracted from the entire trace. Repeated with (B) unstimulated cells and (C) stimulated cells in the presence of 160 µM hemoglobin, a potent NO scavenger. The background current collected at 400 µm was subtracted from both traces.

3.4 Conclusions

A bilaminar NO sensor was fabricated and evaluated for demanding use in biological media. The combination of a poly(5A1N) electropolymerized film and a xerogel topcoat significantly improved sensor selectivity over common biological interferents. The xerogel membrane also stabilized the sensor's analytical performance characteristics, enabling continuous operation over 24 h in proteinaceous media without reduction in the sensitivity or selectivity. These attributes facilitated the use of bilaminar sensors for monitoring long-term NO release from immunostimulated macrophages both temporally and spatially, the latter with SECM-assisted positioning. The proximal macrophage NO concentration at peak release was approximately 100× smaller than the concentration of accumulated nitrite (as measured by Griess), demonstrating the importance of imparting *and* maintaining selectivity towards NO. The accuracy of the bilaminar electrochemical NO sensor was assured by its sustained selectivity coefficient of −4.2 over nitrite. The distance-dependence of NO measurement from cells motivates the use of planar electrodes in future experiments, where direct culturing of cells on integrated electrode surfaces is anticipated to reduce sampling variability.

REFERENCES

(1) Ignarro, L. J.; Buga, G. M.; Wood, K. S.; Byrns, R. E.; Chaudhuri, G. Endothelium-derived relaxing factor produced and released from artery and vein is nitric oxide. *Proc. Natl. Acad. Sci. U.S.A.* **1987**, *84*, 9265-9269.

(2) Dudzinski, D. M.; Igarashi, J.; Greif, D.; Michel, T. The regulation and pharmacology of endothelial nitric oxide synthase. *Annu. Rev. Pharmacol. Toxicol.* **2006**, *46*, 235-276.

(3) Lee, R. H.; Efron, D.; Tantry, U.; Barbul, A. Nitric oxide in the healing wound: a time-course study. *J. Surg. Res.* **2001**, *101*, 104-108.

(4) Donnini, S.; Ziche, M. Constitutive and inducible nitric oxide synthase: Role in angiogenesis. *Antioxid. Redox Signal.* **2002**, *4*, 817-823.

(5) van Goor, H.; Albrecht, E. W. J. A.; Heeringa, P.; Klok, P. A.; van der Horst, M. L. C.; de Jager-Krikken, A.; Bakker, W. W.; Moshage, H. Nitric oxide inhibition enhances platelet aggregation in experimental anti-Thy-1 nephritis. *Nitric Oxide* **2001**, *5*, 525-533.

(6) Prast, H.; Philippu, A. Nitric oxide as modulator of neuronal function. *Prog. Neurobiol.* **2001**, *64*, 51-68.

(7) Garthwaite, J.; Boulton, C. L. Nitric oxide signaling in the central nervous system. *Annu. Rev. Physiol.* **1995**, *57*, 683-706.

(8) Fang, F. C. Mechanisms of nitric oxide-related antimicrobial activity. *J. Clin. Invest.* **1997**, *99*, 2818-2825.

(9) Knowles, R. G.; Moncada, S. Nitric oxide synthases in mammals. *Biochem. J.* **1994**, *298*, 249-258.

(10) Nathan, C. F.; Hibbs Jr, J. B. Role of nitric oxide synthesis in macrophage antimicrobial activity. *Curr. Opin. Immunol.* **1991**, *3*, 65-70.

(11) Ochoa, J. B.; Udekwu, A. O.; Billiar, T. R.; Curran, R. D.; Cerra, F. B.; Simmons, R. L.; Peitzman, A. B. Nitrogen oxide levels in patients after trauma and during sepsis. *Ann. Surg.* **1991**, *214*, 621-626.

(12) Bernatchez, S. F.; Menon, V.; Stoffel, J.; Walters, S. A.; Lindroos, W. E.; Crossland, M. C.; Shawler, L. G.; Crossland, S. P.; Boykin, J. V., Jr. Nitric oxide levels in wound fluid may reflect the healing trajectory. *Wound Repair Regen.* **2013**, *21*, 410-417.

(13) Hetrick, E. M.; Schoenfisch, M. H. Analytical chemistry of nitric oxide. *Annu. Rev. Anal. Chem.* **2009**, *2*, 409-433.

(14) Hunter, R. A.; Storm, W. L.; Coneski, P. N.; Schoenfisch, M. H. Inaccuracies of nitric oxide measurement methods in biological media. *Anal. Chem.* **2013**, *85*, 1957-1963.

(15) Archer, S. Measurement of nitric oxide in biological models. *FASEB J* **1993**, *7*, 349-360.

(16) Hurst, R. D.; Clark, J. B. The utility of the nitric oxide electrochemical sensor in biomedical research. *Sensors* **2003**, *3*, 321-329.

(17) McMurtry, M. S.; Kim, D. H.; Dinh-Xuan, T.; Archer, S. L. Measurement of nitric oxide, nitrite and nitrate using a chemiluminescence assay: an update for the year 2000. *Analysis* **2000**, *28*, 455-465.

(18) Pelletier, M. M.; Kleinbongard, P.; Ringwood, L.; Hito, R.; Hunter, C. J.; Schechter, A. N.; Gladwin, M. T.; Dejam, A. The measurement of blood and plasma nitrite by chemiluminescence: Pitfalls and solutions. *Free Rad. Biol. Med.* **2006**, *41*, 541-548.

(19) Coneski, P. N.; Schoenfisch, M. H. Nitric oxide release: Part III. Measurement and reporting. *Chem. Soc. Rev.* **2012**, *41*, 3753-3758.

(20) Privett, B. J.; Shin, J. H.; Schoenfisch, M. H. Electrochemical nitric oxide sensors for physiological measurements. *Chem. Soc. Rev.* **2010**, *39*, 1925-1935.

(21) Xu, T.; Scafa, N.; Xu, L.-p.; Su, L.; Li, C.; Zhou, S.; Liu, Y.; Zhang, X. Electrochemical sensors for nitric oxide detection in biological applications. *Electroanalysis* **2014**, *26*, 449-468.

(22) Zhao, X.; Wang, K.; Li, B.; Wang, C.; Ding, Y.; Li, C.; Mao, L.; Lin, Y. Fabrication of a flexible and stretchable nanostructured gold electrode using a facile ultraviolet-irradiation approach for the detection of nitric oxide released from cells. *Anal. Chem.* **2018**, *90*, 7158-7163.

(23) Li, J.; Xie, J.; Gao, L.; Li, C. M. Au nanoparticles-3D graphene hydrogel nanocomposite to boost synergistically in situ detection sensitivity toward cell-released nitric oxide. *ACS Appl. Mater. Interfaces* **2015**, *7*, 2726-2734.

(24) Oni, J.; Pailleret, A.; Isik, S.; Diab, N.; Radtke, I.; Blöchl, A.; Jackson, M.; Bedioui, F.; Schuhmann, W. Functionalised electrode array for the detection of nitric oxide released by endothelial cells using different NO-sensing chemistries. *Anal. Bioanal. Chem.* **2004**, *378*, 1594-1600.

(25) Liu, Z.; Chen, A.; Forsyth, H.; Khaper, N. Sensitive electrochemical detection of nitric oxide based on AuPt and reduced graphene oxide nanocomposites. *Analyst* **2016**, *141*, 4074-4083.

(26) Donnini, S.; Ziche, M. Constitutive and inducible nitric oxide synthase: role in angiogenesis. *Antioxid. Redox Signal.* **2002**, *4*, 817-823.

(27) Nakamura, Y.; Si, Q. S.; Kataoka, K. Lipopolysaccharide-induced microglial activation in culture: temporal profiles of morphological change and release of cytokines and nitric oxide. *Neurosci. Res.* **1999**, *35*, 95-100.

(28) Pekarova, M.; Kralova, J.; Kubala, L.; Ciz, M.; Lojek, A.; Gregor, C.; Hrbac, J. Continuous electrochemical monitoring of nitric oxide production in murine macrophage cell line RAW 264.7. *Anal. Bioanal. Chem.* **2009**, *394*, 1497-1504.

(29) Cha, W.; Tung, Y.-C.; Meyerhoff, M. E.; Takayama, S. Patterned electrode-based amperometric gas sensor for direct nitric oxide detection within microfluidic devices. *Anal. Chem.* **2010**, *82*, 3300-3305.

(30) Shim, J. H.; Do, H.; Lee, Y. Simple fabrication of amperometric nitric oxide microsensors based on electropolymerized membrane films. *Electroanalysis* **2010**, *22*, 359-366.

(31) Brown, M. D.; Schoenfisch, M. H. Nitric oxide permselectivity in electropolymerized films for sensing applications. *ACS Sensors* **2016**, *1*, 1453-1461.

(32) Hunter, R. A.; Privett, B. J.; Henley, W. H.; Breed, E. R.; Liang, Z.; Mittal, R.; Yoseph, B. P.; McDunn, J. E.; Burd, E. M.; Coopersmith, C. M.; Ramsey, J. M.; Schoenfisch, M. H. Microfluidic amperometric sensor for analysis of nitric oxide in whole blood. *Anal. Chem.* **2013**, *85*, 6066-6072.

(33) Shin, J. H.; Privett, B. J.; Kita, J. M.; Wightman, R. M.; Schoenfisch, M. H. Fluorinated xerogel-derived microelectrodes for amperometric nitric oxide sensing. *Anal. Chem.* **2008**, *80*, 6850-6859.

(34) Murphy, L. J. Reduction of interference response at a hydrogen peroxide detecting electrode using electropolymerized films of substituted naphthalenes. *Anal. Chem.* **1998**, *70*, 2928-2935.

(35) Delak, K. M.; Sahai, N. Amine-catalyzed biomimetic hydrolysis and condensation of organosilicate. *Chem. Mater.* **2005**, *17*, 3221-3227.

(36) Pontié, M.; Gobin, C.; Pauporté, T.; Bedioui, F.; Devynck, J. Electrochemical nitric oxide microsensors: sensitivity and selectivity characterisation. *Anal. Chim. Acta* **2000**, *411*, 175-185.

(37) Hughes, M. N. Chemistry of nitric oxide and related species. *Methods Enzymol.* **2008**, *436*, 3-19.

(38) Lee, Y.; Kim, J. Simultaneous electrochemical detection of nitric oxide and carbon monoxide generated from mouse kidney organ tissues. *Anal. Chem.* **2007**, *79*, 7669-7675.

(39) Wisniewski, N.; Moussy, F.; Reichert, W. M. Characterization of implantable biosensor membrane biofouling. *Fresenius J. Anal. Chem.* **2000**, *366*, 611-621.

(40) Wisniewski, N.; Reichert, M. Methods for reducing biosensor membrane biofouling. *Colloids Surf., B* **2000**, *18*, 197-219.

(41) Paul, D. W.; Stenken, J. A. A review of flux considerations for in vivo neurochemical measurements. *Analyst* **2015**, *140*, 3709-3730.

(42) Jakubowska, M. Signal processing in electrochemistry. *Electroanalysis* **2011**, *23*, 553-572.

(43) Bond, A. M.; Grabaric, B. S. Use of computerized instrumentation for pseudo-derivative direct current and normal pulse polarography with correction for charging current. *Anal. Chim. Acta* **1978**, *101*, 309-318.

(44) Tian, B.; Chen, H.; Xiao, Z. Subtraction of background current in polarographic curves. *Gaodeng Xuexiao Huaxue Xuebao* **1990**, *11*, 685-688.

(45) Hibbs, J. B., Jr.; Taintor, R. R.; Vavrin, Z.; Rachlin, E. M. Nitric oxide: a cytotoxic activated macrophage effector molecule. *Biochem. Biophys. Res. Commun.* **1988**, *157*, 87-94.

(46) Jorens, P. G.; Matthys, K. E.; Bult, H. Modulation of nitric oxide synthase activity in macrophages. *Mediators Inflamm.* **1995**, *4*, 75-89.

(47) Aggarwal, B. B.; Mehta, K. Determination and regulation of nitric oxide production from macrophages by lipopolysaccharides, cytokines, and retinoids. *Methods Enzymol.* **1996**, *269*, 166-171.

(48) Ye, X.; Rubakhin, S. S.; Sweedler, J. V. Detection of nitric oxide in single cells. *Analyst* **2008**, *133*, 423-433.

(49) Isik, S.; Etienne, M.; Oni, J.; Blöchl, A.; Reiter, S.; Schuhmann, W. Dual microelectrodes for distance control and detection of nitric oxide from endothelial cells by means of scanning electrochemical microscope. *Anal. Chem.* **2004**, *76*, 6389-6394.

(50) Coleman, J. W. Nitric oxide in immunity and inflammation. *Int. Immunopharmacol.* **2001**, *1*, 1397-1406.

(51) Loscalzo, J.; Welch, G. Nitric oxide and its role in the cardiovascular system. *Prog. Cardiovasc. Dis.* **1995**, *38*, 87-104.

CHAPTER 4: CATALYTIC SELECTIVITY OF METALLOPHTHALOCYANINES FOR ELECTROCHEMICAL NITRIC OXIDE SENSING[4]

4.1 Introduction

Nitric oxide (NO) is an endogenous free radical implicated in a number of essential physiological processes, including inflammation,[1] wound healing,[2] vasodilation,[3] and neurotransmission.[4] Despite a growing understanding of NO's roles, the ways in which endogenous levels of NO naturally fluctuate and the concentration-dependence of its activity are generally still not agreed upon. Unfortunately, dynamic detection of NO is constrained by NO's reactive nature and the presence of scavengers, greatly reducing its half-life in biological media.[5-7] Electrochemical sensors enable direct, real-time measurements of NO with fast response, high temporal resolution, low cost, and freedom from exogenous reagents.[8,9]

Selectivity remains perhaps the greatest challenge to accurate electrochemical detection of NO in situ.[5,10,11] While electrochemical oxidation of NO is thermodynamically favorable, formation of the initial nitrosyl cation (NO^+) is kinetically slow, requiring large overpotentials (Figure 4.1, adapted from reference 8) that are also capable of oxidizing interferent species present in biological milieu (e.g., nitrite, L-ascorbate, and carbon

[4] This chapter was adapted in part from an article that has already been published. The original citation is as follows: Brown, M. D.; Schoenfisch, M. H. Catalytic selectivity of metallophthalocyanines for electrochemical nitric oxide sensing. *Electrochim. Acta* **2018**, *273*, 98-104.

monoxide).[12] In this manner, sensor accuracy is diminished greatly. Working electrodes must therefore be chemically modified to differentially enhance the NO signal and/or impede interferent species' access to the electroactive surface.[11] Selective NO detection is traditionally achieved by the use of either selectively permeable (i.e., *permselective*) polymer membranes or electrocatalysts.[13] Permselective barriers confer NO selectivity through well-understood size-exclusion, hydrophobic interaction, or charge-repulsion sieving mechanisms—exploiting NO's small size, lipophilicity, and neutral charge, respectively.[14] In contrast, electrocatalysts do not physically obstruct interferents; rather they enhance the NO signal and/or reduce the overpotential required by facilitating electron transfer kinetics.

Metallophthalocyanines (MPc) represent the most common catalysts used in the fabrication of electrochemical NO sensors (Figure 4.2).[13,15] Belonging to the same class of transition metal-coordinated macrocycles as metalloporphyrins (MP), MPcs have extended π-systems, which allow them to undergo fast redox processes and thereby facilitate electron transfer to a variety of molecules.[16] Moreover, MPc catalysts are more chemically and thermally stable than their MP counterparts.[17] Coordination of NO with an electrode surface-confined MPc complex (chemisorptive or physisorptive) facilitates initial electron transfer from NO to the MPc, which then relays that electron to the electrode charge sink, generating the current response (Figure 4.3). The presence of certain MPc complexes is also believed to stabilize the transient NO^+ cation before further oxidation to nitrate.[16,18] It is through these stabilizing effects that the NO signal is amplified and voltammetric features are shifted to lower potentials.

The identity of the transition metal (M) has been reported to influence the site of NO coordination,[19] bond orientation,[20] electronic structure,[21] and oxidation potential.[12] While

separate studies have come to different conclusions as to the most catalytically active MPc complex towards NO,[12,18,22] no study has yet evaluated the concomitant effects on sensor selectivity. For instance, an electrocatalyst that enhances both the NO and interferent signals will not bear any improvement on sensor selectivity. Signal enhancement from such a catalyst is more likely the result of increased electroactive surface area rather than targeted ligation of NO. This hypothetical catalyst is significant in light of the fact that several MPc complexes do not specifically bind NO at the metal core.[19] For example, nickel-Pc is the most routinely used MPc for NO sensor fabrication due to its substantial NO signal sensitivity amplification, yet several studies have reiterated that the oxidation is not "metal-based" (i.e., mediated through the metal core).[13,18,22,23] First-principles density functional theory (DFT) calculations demonstrate that nickel- and zinc-Pc only weakly physisorb NO at the metal core, preferring instead to hybridize with the C atoms on the macrocycle's periphery (Figure 4.2).[19,20] Clearly, it is important to determine if these non-metal-based interactions actually furnish selectivity benefits to the detection of NO.

The findings above motivated us to systematically evaluate the selectivity benefits of MPc complexes in isolation (i.e., in the absence of a co-deposited permselective membrane). Based on independent studies carried out by Caro et al. and Vilakazi et al., iron-phthalocyanine (FePc), cobalt-phthalocyanine (CoPc), nickel-phthalocyanine (NiPc), and zinc-phthalocyanine (ZnPc) were identified as the most catalytically active MPc complexes.[18,22] These catalysts were drop-cast on glassy carbon (GC) electrode surfaces and evaluated for selectivity against: nitrite (NO_2^-), an oxidative product of NO oxidized at similarly high potentials; L-ascorbate (AA), a biologically ubiquitous, redox-active molecule;

Table 4.1 Interferents to electrochemical detection of nitric oxide.

Interferent	E_a (mV)	Concentration (nM)	Media	Reference
NO_2^-	800 - 1200	>20,000	Blood	25
AA	100 - 300	43,000	Serum	26
CO	200 - 500	500-1500	Kidney tissue	27

$$\cdot NO \rightarrow NO^+ + e^-$$
$$NO^+ + OH^- \rightarrow HNO_2$$
$$HNO_2 + H_2O \rightarrow NO_3^- + 3H^+ + 2e^-$$
$$\textbf{}\cdot\textbf{NO + H}_\textbf{2}\textbf{O + OH}^- \rightarrow \textbf{NO}_\textbf{3}^- \textbf{+ 3H}^+ \textbf{+ 3e}^-$$

Figure 4.1 Three-step electrochemical oxidation of nitric oxide.

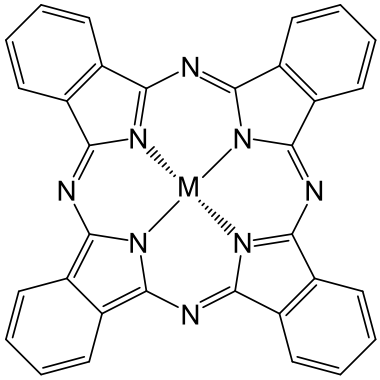

M = Fe, Co, Ni, Zn

Figure 4.2 Chemical structure of the metallophthalocyanines used in this study.

$$MPc + NO \rightarrow MPc^{\delta-}\text{-}NO^{\delta+}$$
$$MPc^{\delta-}\text{-}NO^{\delta+} \rightarrow MPc + NO^+ + e^-$$

Figure 4.3 Metallophthalocyanine-mediated oxidation of nitric oxide. The symbol δ^+ indicates a partial charge transfer to the MPc complex, not necessarily localized at the metal center.

evaluated for selectivity against: nitrite (NO_2^-), an oxidative product of NO oxidized at similarly high potentials; L-ascorbate (AA), a biologically ubiquitous, redox-active molecule; and carbon monoxide (CO), a molecule of similar size and structure that has been shown to exert similar physiological effects to NO through heme-coordination (e.g., with hemoglobin).[24] These properties are summarized in Table 4.1.

In addition to varying the interferent and MPc metal, selectivity was also monitored as a function of electrochemical technique. One of the ways MPcs purportedly improve selectivity is by lowering the required potential for NO oxidation, though actual selectivity benefits have never been rigorously quantified.[13] Herein, NO selectivity was measured using both differential pulse voltammetry (DPV) and constant potential amperometry (CPA). DPV was used to determine shifts, if any, in the NO oxidation potential ($E_{a,NO}$) relative to the bare glassy carbon electrode. Measured $E_{a,NO}$ values of the catalyst-modified electrode were then used as the working potentials for CPA measurements. Comparisons in selectivity when the working potential was set at either the $E_{a,NO}$ of the bare or MPc-modified electrode allowed for the determination of whether catalyst-enabled reductions of the working potential improved selectivity.

4.2 Experimental

4.2.1 Materials, reagents, and apparatus

Iron (II) phthalocyanine (FePc), cobalt (II) phthalocyanine (CoPc), nickel (II) phthalocyanine (NiPc), zinc (II) phthalocyanine (ZnPc), sodium nitrite ($NaNO_2$), and L-ascorbic acid (AA) were purchased from Sigma (St. Louis, MO). Pyridine was obtained from Fischer Scientific (Hampton, NH). Nitric oxide (99.5%), carbon monoxide (99.3%), nitrogen (N_2), and argon (Ar) gases were purchased from National Welders Supply (Raleigh, NC).

Chemicals and solvents were analytical-reagent grade and used as received without further purification.

Distilled water was purified to a final resistivity of 18.2 MΩ·cm and a total organic content of ≤6 ppb using a Millipore Milli-Q UV Gradient A10 System (Bedford, MA). Saturated solutions of gaseous NO (1.9 mM) and CO (0.9 mM) were prepared by purging ~20 mL of phosphate buffered saline (PBS; 10 mM, pH 7.4) on ice with Ar for 30 min to remove oxygen, followed by purging with NO or CO gas for 30 min.[28] Saturated solutions were prepared on the same day as use and stored at 4 °C between calibrations. All electrochemical experiments were carried out in 20 mL of deoxygenated PBS at room temperature (23 °C) using a CH Instruments 1030 8-channel Electrochemical Analyzer (Austin, TX). The electrode configuration consisted of glassy carbon (GC; 3 mm dia.) inlaid disc working electrodes sealed in Kel-F (6 mm total dia.; CH Instruments), a silver-silver chloride (Ag|AgCl) reference electrode (3.0 M KCl; CH Instruments), and a coiled Pt wire counter electrode. All potentials are reported versus the Ag|AgCl reference electrode.

4.2.2 Preparation of catalyst-modified glassy carbon electrodes

Glassy carbon disc working electrodes were sequentially polished with 1.0, 0.3, and 0.05 μm alumina slurries to achieve a mirror finish. To avoid surface cracking and loss of electrical contact, glassy carbon electrodes were wiped lightly with tissue and rinsed copiously with DI water (in place of sonication) to remove imbedded alumina. After drying under a N_2 stream, catalysts were drop-cast onto the GC electrode surface using 30 μL of 1.5 mM MPc solution dissolved in pyridine. After evaporation of the pyridine in ambient (~20 min), excess catalyst not physi- or chemisorbed to the surface was removed by rinsing with ethanol and then pyridine. Catalyst-modified electrodes were dried under a N_2 stream before

immediate use. Adsorption of the catalyst was confirmed by X-ray electron spectroscopy (XPS). Briefly, a Kratos Axis Ultra DLD X-ray photoelectron spectrometer with a monochromatic Al Kα X-ray source (base pressure = 6×10^{-9} torr) was used to collect both survey (80 eV pass energy) and high-resolution scans (20 eV pass energy) of the signature peaks of the transition metal centers. All data were corrected to the carbon 1*s* peak at 284.6 eV. Plates of glassy carbon (10 mm × 30 mm × 1 mm; SPI Supplies; West Chester, PA) were used in place of disk electrodes to facilitate surface analysis.

4.2.3 Electrochemical measurements via differential pulse voltammetry

Bare and MPc-modified GC electrodes were swept repetitively from 0 to +1100 mV for eight scans via differential pulse voltammetry (DPV) to achieve a constant background trace before measurements. Anodic peak potentials ($E_{a,NO}$) were measured and calibration curves collected for NO via DPV with aliquot concentrations ranging from 0.475 to 47.5 μM. Peak current trended linearly with NO concentration, the slope representing the sensitivity. Similar DPV calibration plots were generated for nitrite and AA over a concentration range between 0.1 – 3.0 mM. Carbon monoxide calibrations were generated over 9 – 180 μM. Of note, signal related to CO concentration was never observed, even at the saturation limit of 0.9 mM. All DPV traces were collected by sweeping from 0 to +1100 mV with an amplitude of 50 mV, step increase of 4 mV, period of 0.5 s, pulse width of 0.2 s, and sample width of 0.0167 s. Voltammograms herein are presented in the polarographic convention.

4.2.4 Electrochemical measurements via constant potential amperometry

The $E_{a,NO}$ peak potential measured for the bare GC electrodes under DPV was used as the working potential for constant potential amperometric (CPA) measurements ($E_{a,NO}$ = +1022 mV). For MPc-modified electrodes, the working potential was set at the $E_{a,NO}$ of the

bare electrode with measurements repeated at the specific $E_{a,NO}$ of the MPc-modified electrode for comparison. In all cases, electrodes were polarized for 10 min prior to measurement at the working potential being tested. Staircase calibration plots were collected with consecutive 0.475 μM injections of saturated NO solution. Similar plots were generated with 0.250 mM injections of nitrite and AA and 1.125 μM injections of saturated CO solution.

4.2.5 Calculations and statistical analysis

With the data collected from both DPV and CPA, selectivity coefficients for NO against interferent species were calculated according to Eq. 1, where S_j is the sensitivity towards interferent *j*, and S_{NO} is the NO sensitivity. Of note, more negative coefficients are indicative of greater selectivity.

$$\log k_{NO,j} = \log\left(\frac{S_j}{S_{NO}}\right) \qquad \text{(Eq. 1)}$$

Sensitivity amplification factors were calculated according to Eq. 2, where $S_{NO,MPc}$ represents the NO sensitivity of the MPc-modified electrode and $S_{NO,bare}$ that of the bare GC electrode.

$$A_{MPc} = \frac{S_{NO,MPc}}{S_{NO,bare}} \qquad \text{(Eq. 2)}$$

As a comparative metric for MPc-modified electrodes, theoretical selectivity coefficients were calculated according to Eq. 3, assuming perfectly selective amplification of solely the NO signal (i.e., no amplification of the interferent response), where $S_{j,bare}$ is the bare GC electrode sensitivity towards interferent *j*.

$$\log k_{NO,MPc,j} = \log\left(\frac{S_{j,bare}}{S_{NO,bare}A_{MPc}}\right) \qquad \text{(Eq. 3)}$$

An experimental selectivity coefficient (from Eq. 1) smaller (i.e., less negative) than its corresponding perfectly selective value (Eq. 3) was thus indicative of partial non-selective

catalytic behavior. Sensitivity to NO, NO oxidation potentials, sensitivity amplification factors, and selectivity coefficients are presented (either numerically or with error bars) as the mean ± the standard error of the mean. Comparisons between data sets were performed using two-tailed *t*-tests.

4.3 Results and Discussion

The outer aromatic ring of MPc macrocycles coordinates strongly with parallel carbon planes due to the overlap in π-orbitals, which facilitates functionalization of glassy carbon electrodes.[29-31] Drop-casting was selected as the method of surface modification due to its simplicity and reproducibility.[16,32] Although practically all NO sensors that incorporate MPc complexes do so in conjunction with a permselective membrane (either co-deposited or as a discrete secondary layer),[17,32-35] the GC electrodes herein were modified solely with the MPc complexes to observe their selectivity and catalytic effects in isolation.[12] Electrode surface modification was confirmed with XPS by identifying signature transition metal peaks (Figure 4.3). The metal/carbon ratio was calculated for relative comparisons of the extent of surface modification, though some literature suggests catalytic enhancements are not dependent on surface concentration.[36]

4.3.1 Differential pulse voltammetry

Metallophthalocyanines are known to exert catalytic effects by shifting voltammetric features to lower overpotentials and by amplifying current responses.[13] To observe both of these effects, differential pulse voltammograms were collected in the presence of NO on bare and MPc-modified GC electrodes. Incorporation of MPc catalyst elicited a marked shift in NO's anodic peak towards lower potentials ($\Delta E_{a,NO}$ = 100-200 mV), confirming successful

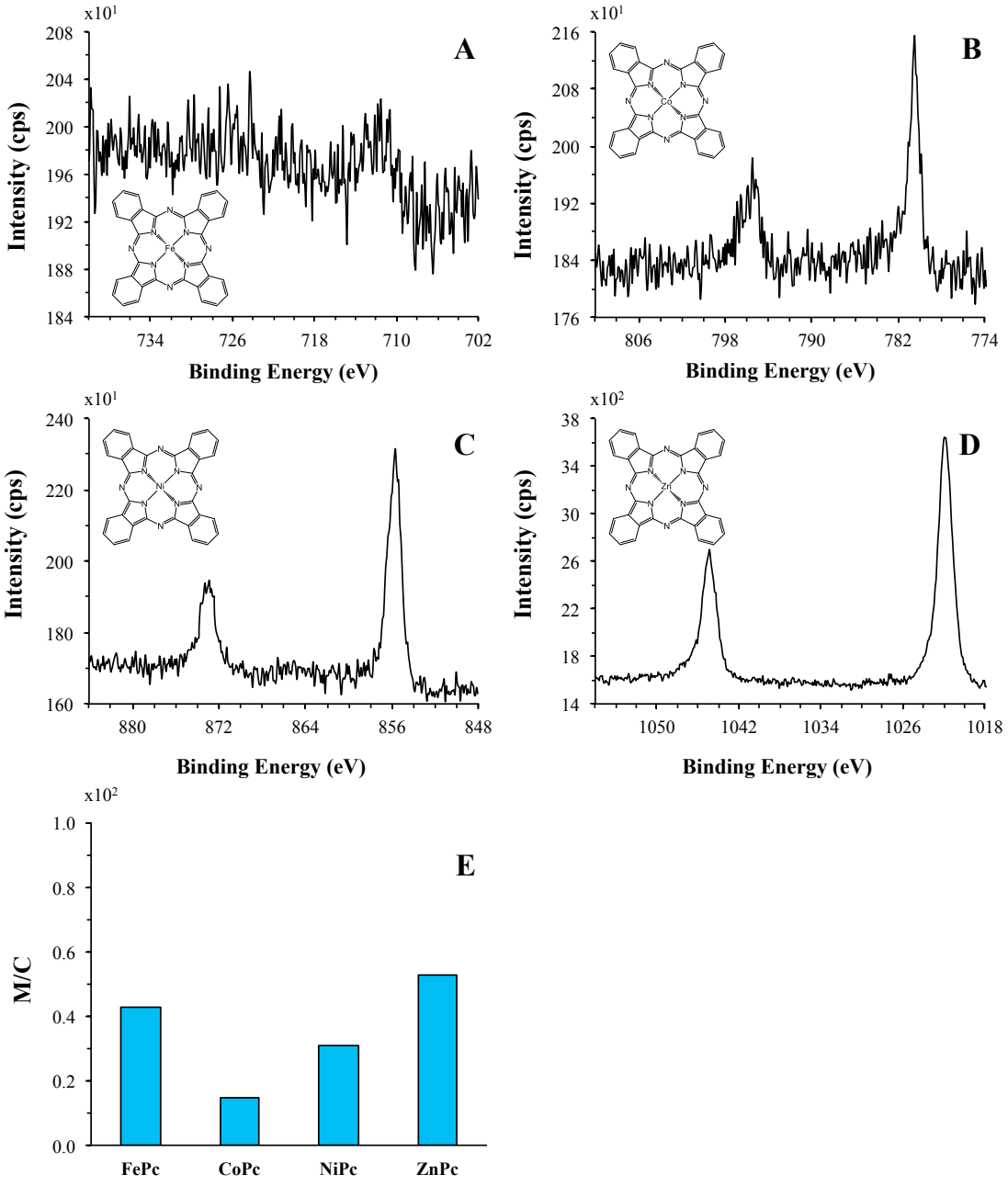

Figure 4.4 High-resolution scans of the signature 2*p* peaks of the transition metal centers of (A) iron-phthalocyanine (FePc), (B) cobalt-phthalocyanine (CoPc), (C) nickel-phthalocyanine (NiPc), and (D) zinc-phthalocyanine (ZnPc) deposited on glassy carbon (GC). (E) M/C atomic ratios of different MPc-modifications on GC calculated using Kratos Vision software.

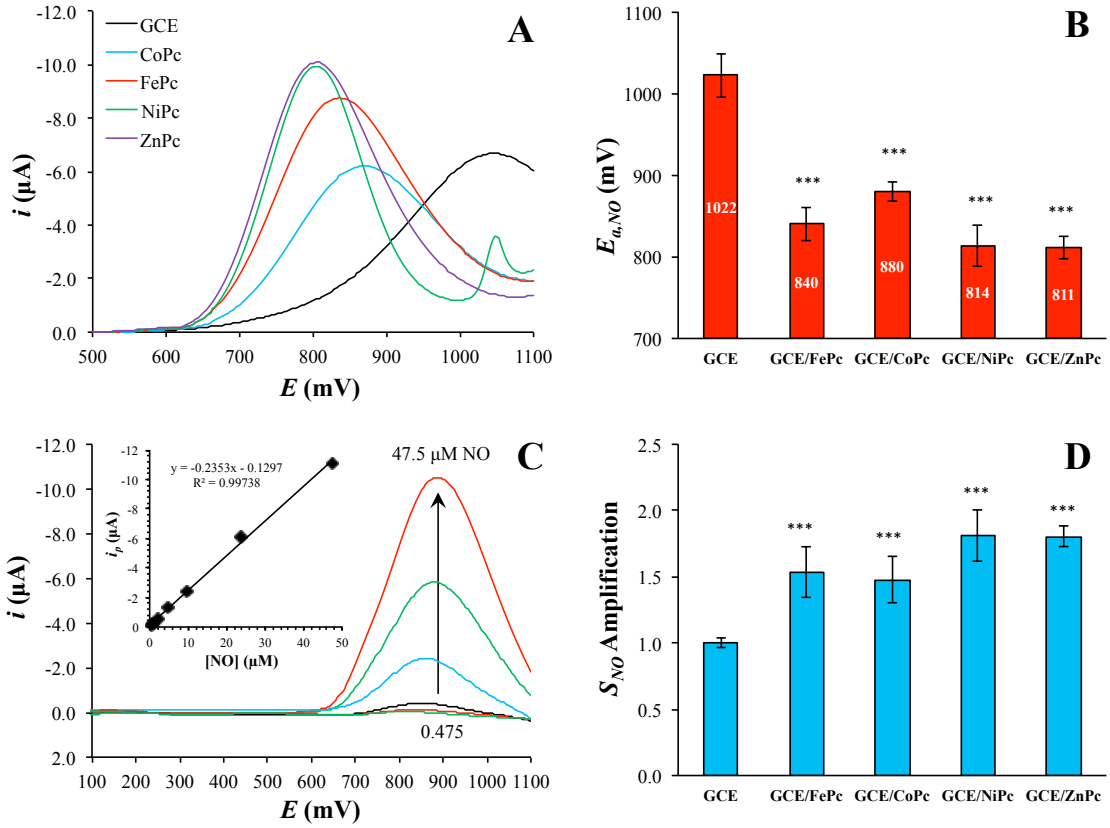

Figure 4.5 (A) Differential pulse voltammograms of bare and MPc-modified GC electrodes in the presence of 23.75 uM NO in pH 7.4 PBS with (B) corresponding peak potentials ($n \geq 3$). (C) Overlay of DPV traces collected in the presence of different NO concentrations on a FePc-modified GC electrode (Inset: calibration curve from the peak currents as a function of concentration). (D) Nitric oxide sensitivity amplification of MPc-modified electrodes relative to bare GC ($n \geq 3$). * = $p < 0.05$, ** = $p < 0.01$, and *** = $p < 0.001$ with respect to GCE.

facilitation of electron transfer (Figure 4.5A). Although the influence of the metal center identity was not strong, the order in peak shift was ZnPc ≈ NiPc > FePc > CoPc as shown in Figure 4.5B. This sequence is in agreement with the ordering of catalytic activity reported by Caro et al. based on the kinetic current measured on a rotating disc electrode.[18] The second peak feature in the trace of NiPc (ca. +1050 mV) was also observed in the absence of NO and was attributed to the Ni(III)|Ni(II) couple.[22,37] In order to precisely quantify amplifications to the current response, calibration curves were generated by plotting peak anodic current versus NO concentration (Figure 2C displays an example calibration for the FePc-modified GC electrode). Representative overlaid DPV traces and their corresponding calibration curves for modified and bare GC electrodes are provide in Figure 4.6. Signal sensitivity amplifications with MPc-incorporation were then calculated, normalized to the bare GC performance (Figure 4.5D; Eq. 2). In addition to lowering the peak anodic potential, all catalysts increased sensor sensitivity towards NO by a factor of ~1.5. Although the identity of the metal center did not significantly impact the degree of amplification, the same ordering as with respect to peak shifting persisted.

4.3.2 NO selectivity under DPV

Whereas permselective barriers impart selectivity by impeding interferent diffusion to the working electrode surface, a selective electrocatalyst (ideally) enhances the signal of solely the target analyte and not interferents. In order to assess the catalytic selectivity of different MPc complexes towards NO, potential off-target signal sensitivity amplifications were studied for relevant biological interferents: nitrite, L-ascorbate, and carbon monoxide (Table 4.1). Experimental selectivity coefficients were calculated for both MPc-modified and bare GC electrodes as a logarithmic ratio of sensitivities (Eq. 1). As a comparative metric to

the experimental selectivity coefficients, theoretical coefficients were calculated for each MPc complex assuming perfectly selective amplification of just the NO signal (Eq. 3). Any undesirable increases in the sensitivity towards an interferent will yield an experimental selectivity coefficient that is smaller (i.e., less negative) than the predicted coefficient that assumes perfectly selective sensitivity amplification.

As indicated by the discrepancies in experimental and theoretical selectivity coefficients in Figure 4.7A, it is clear that signal sensitivity amplifications from CoPc, NiPc, and ZnPc are not perfectly selective for NO against nitrite—most severely in the case of NiPc. Metallophthalocyanines have been shown to mediate electron transfers to/from a variety of molecules and ions, including nitrite.[16,36,38] Moreover, in the reaction to oxidize NO, nitrous acid (i.e., protonated nitrite) is formed before complete oxidation to nitrate (Figure 4.1). The considerable overlap in redox chemistry thus makes nitrite a potent interferent. Of all the MPc complexes investigated in this study, only FePc demonstrated a statistically insignificant difference between experimental and theoretical selectivity performance versus nitrite, indicating the most specific catalytic amplification of NO signal.

Density functional theory first-principles calculations of the optimized MPc-NO structures have demonstrated that NO binds strongly to FePc and CoPc at the metal center.[19,20] Iron-Pc in particular has the greatest theoretical change in adsorption energy upon hybridization, accounting for its high specificity towards NO.[39,40] Calculations via DFT carried out by Nguyen et al. have shown that MPc-NO adsorption energy decreases with *d*-orbital occupation, suggesting the need for unoccupied *d*-orbitals for proper interaction with the half-occupied π^*-orbital of NO (resulting from its unpaired electron).[19] The fact that FePc

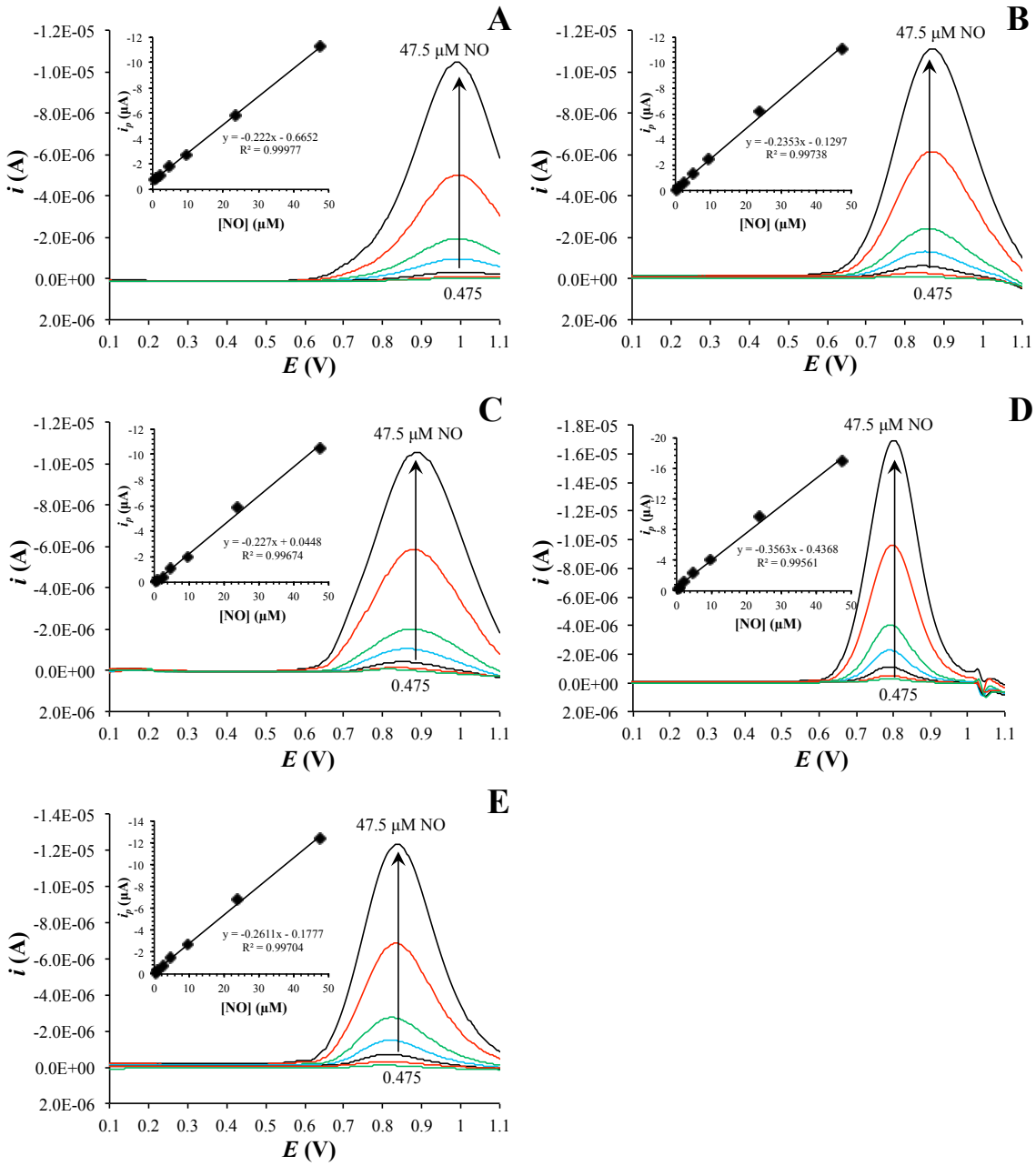

Figure 4.6 Representative overlays of the DPV traces collected in the presence of various concentrations of NO in PBS on (A) bare, (B) FePc-modified, (C) CoPc-modified, (D) NiPc-modified, and (E) ZnPc-modified GC electrodes (Insets: respective calibration curves from the peak currents as a function of NO concentration). Blank DPV scans collected over the same potential range in PBS were subtracted from all traces.

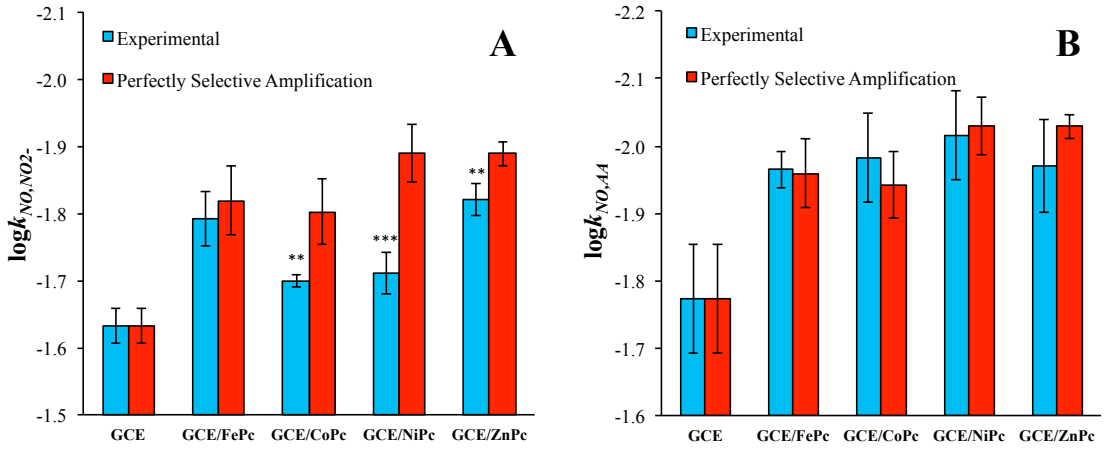

Figure 4.7 Experimental and theoretical (Eq. 3) selectivity coefficients for NO versus (A) nitrite and (B) L-ascorbate measured via DPV on MPc-modified and bare GC electrodes ($n \geq 3$). Statistical information is with respect to perfectly selective amplification. * = $p < 0.05$, ** = $p < 0.01$, and *** = $p < 0.001$.

Table 4.2 Summary of nitric oxide sensitivity amplification and selectivity performance of MPc-modified and bare GC electrodes measured by differential pulse voltammetry ($n \geq 3$).

Electrode	$E_{a,NO}$ (mV)	S_{NO} (pA/nM)	A_{MPc} [a]	$\log k_{NO,NO2-}$ [b]	$\log k_{NO,AA}$ [b]	$\log k_{NO,CO}$
GCE (bare)	1022 ± 27	-292 ± 10	1	-1.63 ± 0.03	-1.77 ± 0.08	< -4
GCE/FePc	840 ± 20	-448 ± 56	1.53 ± 0.19	-1.79 ± 0.04	-1.98 ± 0.07	< -4
GCE/CoPc	880 ± 12	-431 ± 52	1.48 ± 0.18	-1.70 ± 0.01	-1.97 ± 0.03	< -4
GCE/NiPc	814 ± 25	-527 ± 56	1.81 ± 0.19	-1.71 ± 0.03	-2.02 ± 0.07	< -4
GCE/ZnPc	811 ± 14	-526 ± 22	1.80 ± 0.08	-1.82 ± 0.02	-1.97 ± 0.07	< -4

[a] Calculated from Eq. 2. [b] Calculated from Eq. 1.

and CoPc strongly bind NO may also account for their higher NO oxidation potentials relative to NiPc and ZnPc (Figure 4.5B) as binding energy has been used as a reactivity descriptor to explain why Fe N4 macrocycles that strongly bind oxygen have lower catalytic activity.[41] Durable FePc-NO adduct formation may also lead to surface consumption of active electrocatalytic sites.[18]

Transition metals further across the periodic table have more highly occupied *d*-orbitals; thus NO only weakly physisorbs to aromatic carbons along the periphery of NiPc and ZnPc macrocycles. It has also long been understood that the catalytic effects observed for NiPc are distinctly not "metal-based,"[23] and lack of targeted ligation of NO may account for poorer selectivity against nitrite relative to the other MPc complexes studied herein (Figure 4.7A).

L-ascorbate (AA) is an equally relevant interferent capable of being oxidized at lower potentials than NO ($E_{a,AA}$ = 100-300 mV). Of note, AA is present at greater concentrations than nitrite physiologically (Table 4.1). Comparisons between experimental and theoretical selectivity coefficients for NO against AA revealed no statistically significant difference or off-target amplification of the AA signal occurring with MPc modification (Figure 4.7B). The specificity of all MPc catalysts for NO over AA is attributed to AA not sharing any part of its intrinsic redox chemistry with NO (in contrast to nitrite).[37] The lack of AA signal enhancement indicates that these MPc complexes do not amplify the NO signal through non-specific means (e.g., as with an increase in the electrode's electroactive surface area) regardless of M-NO binding ability.

Lastly, neither the bare nor MPc-modified GC electrodes exhibited measureable activity towards CO (Table 4.2). Heterogeneous electrochemical oxidation of CO requires

direct coordination with a transition metal electrode, such as tin or platinum.[27,42] As such, no activity was anticipated on bare GC. The continued lack of activity upon modification with the MPc catalysts suggests that either CO does not bind to the metal centers or such binding does not meaningfully facilitate electron transfer from CO to the GC electrode sink. Pre-treatment of MPc-modified electrodes in CO-spiked solution neither decreased sensitivity towards NO nor altered peak position, demonstrating that the catalytic effects towards NO are maintained even in the presence of CO.

4.3.3 Constant potential amperometry

Differential pulse voltammetry measures current across a range of potentials, the output of which may be used to ascertain electrochemical properties of the redox system under observation. Potentiodynamic techniques of this kind, however, are constrained by temporal resolution and the potentiostat's ability to apply complex waveforms. Potentiostatic techniques, such as CPA, are better suited for continuous measurement, since a constant potential is applied while sampling the current at a set rate. Though faster and simpler than potentiodynamic techniques, CPA suffers from an inherent lack of specificity.[11,33] For example, a DPV trace may show two peaks for two analytes, while CPA will return the sum of each analyte's contribution as a single current. We thus set out to determine if and how the selectivity benefits of MPc complexes observed with DPV could be transferred to CPA, a more widely employed technique.

With the potential set to the oxidation potential of NO on bare GC (+1022 mV), current response was measured with successive injections of NO to generate staircase calibration plots for bare and MPc-modified GC electrodes (Figure 4.8A). Catalyst inclusion increased the sensitivity 2-3-fold with the greatest amplifications observed for FePc and NiPc

(Figure 4.8B). Under DPV, by comparison, the MPc-derived signal increases were comparatively milder (~1.5×). The applied potential of +1022 mV under CPA represented a significant overpotential to MPc-catalyzed NO oxidation (Figure 4.5B). In order to determine if the resulting 2-3× signal sensitivity amplification was specific to NO, experimental and theoretical selectivity coefficients were compared (Figure 4.8C; Eq. 3). The large discrepancies observed across all MPcs point to off-target amplification of the nitrite signal, even in the case of FePc, the most selective catalyst under DPV. Of note, CPA and DPV experimental selectivity coefficients against nitrite were congruous (Figure 4.8C), revealing that only signal sensitivity amplification *in excess* of ~1.5× under CPA was non-specific to NO. The only exception was ZnPc, for which the NO sensitivity diminished with successive CPA trials, possibly indicative of breakdown/stripping at the continuously-maintained, high overpotential.

Due to the fact that the CPA current is the sum of all redox species' current contributions, increasing the applied potential extends the range of potential interferents included in the sum. Nitric oxide and nitrite share similar redox chemistry with oxidation potentials that closely mirror each other, even in the presence of an electrocatalyst (ΔE_a < 80 mV).[43] As a result, an excessive overpotential (e.g., +1022 mV compared with the reduced $E_{a,NO}$ values of MPc-modified electrodes) will amplify both signals as opposed to selectively amplifying NO. To potentially eliminate this non-specific signal sensitivity amplification, the CPA applied potential was reduced to the specific NO oxidation potential of each MPc catalyst (Figure 4.5B). Selectivity coefficients were then re-measured (Table 4.3). As anticipated, the NO sensitivity fell substantially without the large overpotential; however,

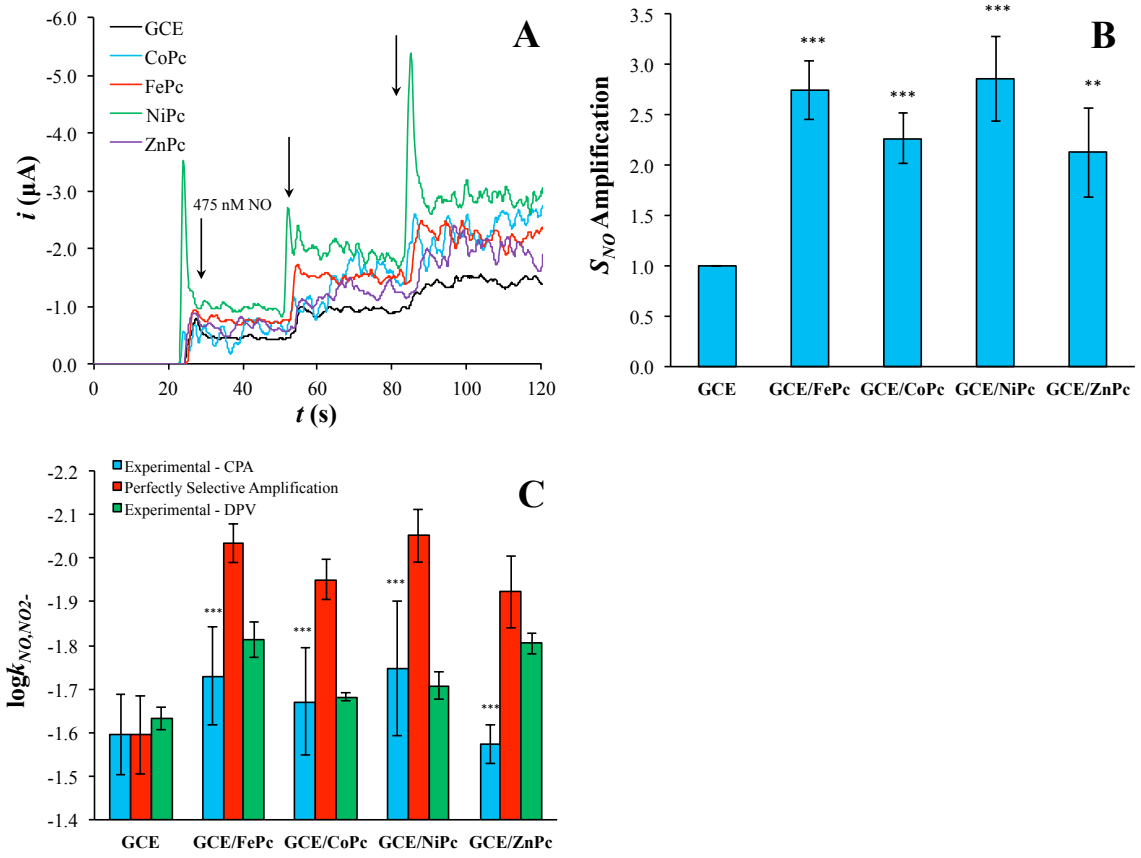

Figure 4.8 (A) Staircase amperograms of bare and MPc-modified GC electrodes with successive NO injections in pH 7.4 PBS and an applied potential of +1022 mV; (B) corresponding NO sensitivity amplifications relative to bare GC ($n \geq 3$). Statistical information is with respect to GCE. (C) Experimental and theoretical (Eq. 3) selectivity coefficients for NO versus nitrite ($n \geq 3$). Statistical information is with respect to perfectly selective amplification. * = $p < 0.05$, ** = $p < 0.01$, and *** = $p < 0.001$.

Table 4.3 Summary of nitric oxide sensitivity amplification and selectivity of MPc-modified and bare GC electrodes measured under constant potential amperometry with different applied potentials ($n \geq 3$).

$E_{applied}$ (mV)[a]	Electrode	S_{NO} (pA/nM)	A_{MPc}[b]	log$k_{NO,NO2-}$[c]	log$k_{NO,AA}$[c]	log$k_{NO,CO}$
1022	GCE (bare)	-895 ± 74	1	-1.60 ± 0.09	-1.61 ± 0.11	< -4
1022	GCE/FePc	-2453 ± 260	2.7 ± 0.3	-1.73 ± 0.11	-1.89 ± 0.12	< -4
1022	GCE/CoPc	-2026 ± 226	2.3 ± 0.3	-1.67 ± 0.12	-1.78 ± 0.07	< -4
1022	GCE/NiPc	-2556 ± 380	2.9 ± 0.4	-1.75 ± 0.15	-1.96 ± 0.04	< -4
1022	GCE/ZnPc	-1902 ± 398	2.1 ± 0.4	-1.57 ± 0.05	-1.84 ± 0.21	< -4
840	GCE/FePc	-1024 ± 66	1.1 ± 0.1	-1.79 ± 0.18	-1.57 ± 0.01	< -4
880	GCE/CoPc	-840 ± 173	0.9 ± 0.2	-1.75 ± 0.01	-1.41 ± 0.16	< -4
814	GCE/NiPc	-370 ± 151	0.4 ± 0.2	-1.57 ± 0.12	-1.09 ± 0.14	< -4
811	GCE/ZnPc	-812 ± 299	0.9 ± 0.3	-1.73 ± 0.07	-1.43 ± 0.10	< -4

[a] Applied via constant potential amperometry. [b] Calculated from Eq. 2. [c] Calculated from Eq. 1.

selectivity versus nitrite improved slightly (except for NiPc, for which the NO signal fell precipitously). Of note, amplifications were less than 1.1 for MPc-modified electrodes, indicating that selectivity improvements against nitrite were a result of reducing the nitrite signal to a greater degree than the NO signal (as opposed to selectively amplifying the NO signal).

While reducing the CPA applied potential benefitted or maintained selectivity against nitrite, the same could not be said for the selectivity versus AA. Even though the applied potential was reduced to the +800-900 mV range with MPc modification, these potentials still represent vast overpotentials to AA oxidation ($E_{a,AA}$ = 100-300 mV), precluding differential signal reduction over NO. As shown in Table 4.3, the selectivity coefficients against AA were diminished as a result. As with DPV measurements, no activity versus CO was observed, regardless of MPc modification or applied potential.

4.4 Conclusions

Metallophthalocyanines, and electrocatalysts more generally, exert their catalytic effects through two primary mechanisms: signal sensitivity amplification and reduction in the required overpotential. How these effects translate to NO sensor selectivity enhancements was explored using DPV and CPA. Signal sensitivity amplification (~1.5×) was perfectly specific to NO over AA for all MPc complexes studied herein, but only perfectly selective over nitrite in the case of FePc. The MPc catalysts greatly enhanced the NO signal under CPA (2-3×), but only a portion of that amplification was due to specific catalytic effects. The claim that MPc-enabled lowering of the applied potential improves selectivity is only true in the case of high potential interferents such as nitrite. The signal contributions of low potential interferents such as AA (and inferably others, including acetaminophen, dopamine, and uric

acid) remain largely unaffected and continue to pose a significant challenge to selective, continuous detection of NO. Therefore, signal sensitivity amplification (as opposed to peak shifting) is the only route by which MPc complexes may meaningfully improve NO selectivity. Compared to permselective membranes capable of mitigating interferent transport >1000-fold, the suggested selectivity benefits of MPc incorporation are real, but ultimately limited.

REFERENCES

(1) Fang, F. C. Perspectives series: host/pathogen interactions. Mechanisms of nitric oxide-related antimicrobial activity. *J. Clin. Invest.* **1997**, *99*, 2818-2825.

(2) Luo, J.-d.; Chen, A. F. Nitric oxide: a newly discovered function on wound healing. *Acta Pharmacol. Sin.* **2005**, *26*, 259-264.

(3) Ignarro, L. J.; Buga, G. M.; Wood, K. S.; Byrns, R. E.; Chaudhuri, G. Endothelium-derived relaxing factor produced and released from artery and vein is nitric oxide. *Proc. Natl. Acad. Sci. U. S. A.* **1987**, *84*, 9265-9269.

(4) Garthwaite, J.; Boulton, C. L. Nitric oxide signaling in the central nervous system. *Annu. Rev. Physiol.* **1995**, *57*, 683-706.

(5) Hunter, R. A.; Storm, W. L.; Coneski, P. N.; Schoenfisch, M. H. Inaccuracies of nitric oxide measurement methods in biological media. *Anal. Chem.* **2013**, *85*, 1957-1963.

(6) Archer, S. Measurement of nitric oxide in biological models. *FASEB J.* **1993**, *7*, 349-360.

(7) Hurst, R. D.; Clark, J. B. The utility of the nitric oxide electrochemical sensor in biomedical research. *Sensors* **2003**, *3*, 321-329.

(8) Privett, B. J.; Shin, J. H.; Schoenfisch, M. H. Electrochemical nitric oxide sensors for physiological measurements. *Chem. Soc. Rev.* **2010**, *39*, 1925-1935.

(9) Coneski, P. N.; Schoenfisch, M. H. Nitric oxide release: Part III. Measurement and reporting. *Chem. Soc. Rev.* **2012**, *41*, 3753-3758.

(10) Trouillon, R. Biological applications of the electrochemical sensing of nitric oxide: fundamentals and recent developments. *Biol. Chem.* **2013**, *394*, 17-33.

(11) Davies, I. R.; Zheng, X. Nitric oxide selective electrodes. *Methods Enzymol.* **2008**, *436*, 63-95.

(12) Nyokong, T.; Vilakazi, S. Phthalocyanines and related complexes as electrocatalysts for the detection of nitric oxide. *Talanta* **2003**, *61*, 27-35.

(13) Bedioui, F.; Griveau, S. Electrochemical detection of nitric oxide: assessement of twenty years of strategies. *Electroanalysis* **2013**, *25*, 587-600.

(14) Brown, M. D.; Schoenfisch, M. H. Nitric oxide permselectivity in electropolymerized films for sensing applications. *ACS Sensors* **2016**, *1*, 1453-1461.

(15) Xu, T.; Scafa, N.; Xu, L.-p.; Su, L.; Li, C.; Zhou, S.; Liu, Y.; Zhang, X. Electrochemical sensors for nitric oxide detection in biological applications. *Electroanalysis* **2014**, *26*, 449-468.

(16) Zagal, J. H.; Griveau, S.; Silva, J. F.; Nyokong, T.; Bedioui, F. Metallophthalocyanine-based molecular materials as catalysts for electrochemical reactions. *Coord. Chem. Rev.* **2010**, *254*, 2755-2791.

(17) Kim, I. K.; Chung, H. T.; Oh, G. S.; Bae, H. O.; Kim, S. H.; Chun, H. J. Integrated gold-disk microelectrode modified with iron(II)-phthalocyanine for nitric oxide detection in macrophages. *Microchem. J.* **2005**, *80*, 219-226.

(18) Caro, C. A.; Zagal, J. H.; Bedioui, F. Electrocatalytic activity of substituted metallophthalocyanines adsorbed on vitreous carbon electrode for nitric oxide oxidation. *J. Electrochem. Soc.* **2003**, *150*, E95-E103.

(19) Nguyen, T. Q.; Padama, A. A. B.; Escano, M. C. S.; Kasai, H. Theoretical study on the adsorption of NO on metal macrocycles, metal = Mn, Fe, Co, Ni, Cu, Zn. *ECS Trans.* **2013**, *45*, 91-100, 110 pp.

(20) Nguyen, T. Q.; Escano, M. C. S.; Kasai, H. Nitric oxide adsorption effects on metal phthalocyanines. *J. Phys. Chem. B* **2010**, *114*, 10017-10021.

(21) Liao, M.-S.; Scheiner, S. Electronic structure and bonding in metal phthalocyanines, Metal=Fe, Co, Ni, Cu, Zn, Mg. *J. Chem. Phys.* **2001**, *114*, 9780-9791.

(22) Vilakazi, S. L.; Nyokong, T. Voltammetric determination of nitric oxide on cobalt phthalocyanine modified microelectrodes. *J. Electroanal. Chem.* **2001**, *512*, 56-63.

(23) Cardenas-Jiron, G. I.; Gonzalez, C.; Benavides, J. Nitric oxide oxidation mediated by substituted nickel phthalocyanines: a theoretical viewpoint. *J. Phys. Chem. C* **2012**, *116*, 16979-16984.

(24) Kim-Shapiro, D. B.; Schechter, A. N.; Gladwin, M. T. Unraveling the reactions of nitric oxide, nitrite, and hemoglobin in physiology and therapeutics. *Arterioscler., Thromb., Vasc. Biol.* **2006**, *26*, 697-705.

(25) Pelletier, M. M.; Kleinbongard, P.; Ringwood, L.; Hito, R.; Hunter, C. J.; Schechter, A. N.; Gladwin, M. T.; Dejam, A. The measurement of blood and plasma nitrite by chemiluminescence: Pitfalls and solutions. *Free Rad. Biol. Med.* **2006**, *41*, 541-548.

(26) Reiber, H.; Ruff, M.; Uhr, M. Ascorbate concentration in human cerebrospinal fluid (CSF) and serum. Intrathecal accumulation and CSF flow rate. *Clin. Chim. Acta* **1993**, *217*, 163-173.

(27) Lee, Y.; Kim, J. Simultaneous electrochemical detection of nitric oxide and carbon monoxide generated from mouse kidney organ tissues. *Anal. Chem.* **2007**, *79*, 7669-7675.

(28) Park, S. S.; Kim, J.; Lee, Y. Improved electrochemical microsensor for the real-time simultaneous analysis of endogenous nitric oxide and carbon monoxide generation. *Anal. Chem.* **2012**, *84*, 1792-1796.

(29) Mho, S.-i.; Ortiz, B.; Park, S.-M.; Ingersoll, D.; Doddapaneni, N. Spectroelectro-chemical studies of metallophthalocyanines adsorbed on electrode surfaces. *J. Electrochem. Soc.* **1995**, *142*, 1436-1441.

(30) Zagal, J. H.; Griveau, S.; Santander-Nelli, M.; Granados, S. G.; Bedioui, F. Carbon nanotubes and metalloporphyrins and metallophthalocyanines-based materials for electroanalysis. *J. Porphyrins Phthalocyanines* **2012**, *16*, 713-740.

(31) Francisco Silva, J.; Griveau, S.; Richard, C.; Zagal, J. H.; Bedioui, F. Glassy carbon electrodes modified with single walled carbon nanotubes and cobalt phthalocyanine and nickel tetrasulfonated phthalocyanine: Highly stable new hybrids with enhanced electrocatalytic performances. *Electrochem. Commun.* **2007**, *9*, 1629-1634.

(32) Raveh, O.; Peleg, N.; Bettleheim, A.; Silberman, I.; Rishpon, J. Determination of NO production in melanoma cells using an amperometric nitric oxide sensor. *Bioelectrochem. Bioenerg.* **1997**, *43*, 19-25.

(33) Jin, J.; Miwa, T.; Mao, L.; Tu, H.; Jin, L. Determination of nitric oxide with ultramicrosensors based on electropolymerized films of metal tetraaminophthalocyanines. *Talanta* **1999**, *48*, 1005-1011.

(34) Bedioui, F.; Trevin, S.; Devynck, J.; Lantoine, F.; Brunet, A.; Devynck, M. A. Elaboration and use of nickel planar macrocyclic complex-based sensors for the direct electrochemical measurement of nitric oxide in biological media. *Biosens. Bioelectron.* **1997**, *12*, 205-212.

(35) Yu, F.; Niu, G.-x.; Huang, Y.; Huang, Y.-f.; Cheng, D.-s. Nickel (II) tetrasulfonated phthalocyanine modified glassy carbon electrode for nitric oxide sensor. *Fudan Xuebao, Ziran Kexueban* **2006**, *45*, 335-338, 343.

(36) Caro, C. A.; Bedioui, F.; Zagal, J. H. Electrocatalytic oxidation of nitrite on a vitreous carbon electrode modified with cobalt phthalocyanine. *Electrochim. Acta* **2002**, *47*, 1489-1494.

(37) Pereira-Rodrigues, N.; Albin, V.; Koudelka-Hep, M.; Auger, V.; Pailleret, A.; Bedioui, F. Nickel tetrasulfonated phthalocyanine based platinum microelectrode array for nitric oxide oxidation. *Electrochem. Commun.* **2002**, *4*, 922-927.

(38) Nyokong, T. Metallophthalocyanines as electrocatalysts for the detection of nitrate, nitrite and nitric oxide. *Curr. Top. Electrochem.* **2003**, *9*, 197-206.

(39) Tran, N. L.; Kummel, A. C. A density functional theory study on the binding of NO onto FePc films. *J. Chem. Phys.* **2007**, *127*, 214701/214701-214701/214707.

(40) Isvoranu, C.; Wang, B.; Ataman, E.; Knudsen, J.; Schulte, K.; Andersen, J. N.; Bocquet, M.-L.; Schnadt, J. Comparison of the carbonyl and nitrosyl complexes formed by adsorption of CO and NO on monolayers of iron phthalocyanine on Au(111). *J. Phys. Chem. C* **2011**, *115*, 24718-24727.

(41) Zagal, J. H.; Koper, M. T. M. Reactivity descriptors for the activity of molecular MN4 catalysts for the oxygen reduction reaction. *Angew. Chem., Int. Ed.* **2016**, *55*, 14510-14521.

(42) Gilman, S. The mechanism of electrochemical oxidation of carbon monoxide and methanol on platinum. II. The "reactant-pair" mechanism for electrochemical oxidation of carbon monoxide and methanol[1]. *J. Phys. Chem.* **1964**, *68*, 70-80.

(43) Pallini, M.; Curulli, A.; Amine, A.; Palleschi, G. Amperometric nitric oxide sensors: a comparative study. *Electroanalysis* **1998**, *10*, 1010-1016.

CHAPTER 5: A DIRECT AND SELECTIVE ELECTROCHEMICAL HYDROGEN SULFIDE SENSOR[5]

5.1 Introduction

Hydrogen sulfide (H_2S) was for a century only known as a noxious environmental pollutant—a product of decaying matter with a distinct smell of rotten eggs.[1-3] Only recently (i.e., the last few decades) was H_2S adopted into the family of endogenous gasotransmitters that regulate essential processes of mammalian physiology.[4,5] Nitric oxide (NO) and carbon monoxide (CO)—earlier members of this collection of gases—were also deemed poisonous gases at one point.[6-8] As the most recent addition, much attention around H_2S has been placed on interpreting its specific biological activity and related concentration-dependence.

Endogenous H_2S is either biosynthesized through enzymatic metabolism of cysteine or drawn from acid-labile/bound sulfide reservoirs.[9,10] It is now established that H_2S plays key roles in the cardiovascular, endocrine, gastrointestinal, and central nervous systems, as it has been identified in tissues associated with each function.[11,12] Like NO and CO, H_2S has been reported to modulate neuronal transmission,[13,14] relax smooth muscle,[15] heighten/suppress the inflammatory response,[7] and exert cardioprotective effects.[16] As a result, hydrogen sulfide-related research has grown to encompass therapeutic donors hoping to harness these effects.[16-22] Much investigation has also centered on the clinical utility of

[5] This chapter was adapted in part from an article that has been accepted for publication. The citation is as follows: Brown, M. D.; Hall, J. R.; Schoenfisch, M. H. A direct and selective electrochemical hydrogen sulfide sensor. *Anal. Chim. Acta* **2018**, *advance online publication*.

H_2S as a serum biomarker of cardiovascular disease, such as artherosclerosis,[23] hypertension,[24] coronary heart disease,[25] and chronic obstructive pulmonary disease.[12,26] Given the breadth of its activity (either defined or ambiguous), the ability to accurately detect and quantify H_2S in biological milieu is essential to further understanding the pharmacology and physiology of this pervasive molecule.

An ideal detection platform would be capable of sensing biologically relevant H_2S concentrations (100 nM – 10 μM) in situ, continuously, and with minimal sample preparation.[27-29] Traditionally, iodometric titration and methylene blue colorimetric assays have been the most common means of quantifying H_2S.[30,31] While relatively simple to execute, extensive sample preparation, high LODs (~1 μM), and potential sample damage (e.g., to cells, tissue) prevent the use of these assays for most biological applications.[32] Novel, but less conventional methods for H_2S measurement include chromatographic techniques, such as high pressure liquid chromatography (HPLC) and gas chromatography (GC).[9,33] However, column loading is not amenable to real-time measurement, and hypoxic/anoxic conditions are required to prevent conversion to sulfur oxides. Several fluorescent[34,35] and electrochemiluminescent[36,37] probes have been developed that are capable of highly sensitive and selective detection, but long incubation times and irreversible coordination of H_2S forgo the possibility of dynamic detection.[12]

In addition to their simple and low-cost fabrication, electrochemical platforms allow for highly sensitive, in situ detection without the need for exogenous reagents.[12] Ion sensitive electrodes (ISEs) are able to measure sulfide ions (S^{2-}) with near-perfect selectivity and low LODs (~100 nM); ISEs have thus been used extensively for serum measurements.[38,39] However, samples must undergo alkaline pre-treatment to shift proton dissociation equilibria

from H_2S towards S^{2-} (pK_{a1} = 6.6, pK_{a2} = 13.8), draining acid-labile sulfide pools and yielding concentrations representative of the total sulfide content instead of the freely available H_2S.[2] Alternatively, direct amperometric detection of H_2S and hydrosulfide (HS^-) is possible via a two-electron oxidation with elemental sulfur as a byproduct (Eq. 1 and 2, respectively).[40]

$$H_2S \rightarrow S^0 + 2e^- + 2H^+ \quad \text{(Eq. 1)}$$

$$HS^- \rightarrow S^0 + 2e^- + H^+ \quad \text{(Eq. 2)}$$

Of note, growth of an insulating sulfur layer passivates the electrode surface, causing sensitivity reduction and performance variability.[41-45] Clark-type amperometric sensors have attempted to resolve this problem by incorporating a gas-permeable membrane and alkaline internal solution with a redox mediator (e.g., ferrocyanide).[46,47] The redox mediator accepts electrons from H_2S/HS^- and is regenerated at the working electrode to create a measurable current (as low as 10 nM LOD).[11] Even with redox mediation, elemental sulfur is still produced, poisoning the internal solution and resulting in high background currents. Typical problems associated with internal solutions (i.e., leakage, evaporation, replacement, and poor miniaturizability) also remain as a concern.[12]

Herein, we report the development of a direct amperometric sensor based on the oxidation of H_2S/HS^- at a glassy carbon electrode (GCE). Previous work in our laboratory demonstrated the utility of a high potential cleaning pulse (+1.5 V) on a GCE to convert elemental sulfur to water-soluble sulfate, thereby mitigating surface passivation.[48] The use of such high potentials produced significant residual background currents, alter the chemical structure of the GCE surface, and potentially cause oxidative damage to any modifying films.[49] As a result, we have chosen to investigate the use of a surface conditioning procedure

to pre-poison the electrode surface with sulfur and stabilize sensor performance. To improve selectivity for H_2S over common biological interferents, we tested several common electropolymerized films previously used in the context of hydrogen peroxide (from glucose oxidase)[50-52] and NO[53,54] sensing. Polymers produced from the following monomers were studied: 5-amino-1-napthol, phenol, eugenol, and *ortho-, meta-*, and *para*-phenylenediamine. After extensive selectivity testing, film-modified electrodes were evaluated for anti-biofouling ability and long-term stability under continuous use in simulated wound fluid.

5.2 Experimental

5.2.1 Materials, reagents, and apparatus

5-Amino-1-naphthol (5A1N), phenol, eugenol, *ortho*-phenylenediamine (*o*-PD), *meta*-phenylenediamine (*m*-PD), *para*-phenylenediamine (*p*-PD), sodium sulfide nonahydrate ($Na_2S{\cdot}9H_2O$), hydrochloric acid (HCl), sodium nitrite, L-ascorbic acid, acetaminophen, dopamine hydrochloride, L-cysteine, ethylenediaminetetraacetic acid disodium salt dihydrate (EDTA), and fetal bovine serum (FBS), were acquired from Sigma-Aldrich (St. Louis, MO). Sodium hydroxide (NaOH) and hydrogen peroxide (H_2O_2; 30% w/v) were obtained from Fisher Scientific (Hampton, NH). Nitric oxide (99.5%), carbon monoxide (99.3%), and nitrogen (99.998%; N_2) gases were obtained from Airgas National Welders (Durham, NC). Other solvents and chemicals were analytical-reagent grade and used as received without further purification.

All solutions were prepared with distilled water purified to a resistivity of 18.2 MΩ·cm and a total organic content of ≤6 ppb with a Millipore Milli-Q UV Gradient A10 water purification system (Bedford, MA). Saturated solutions of NO (1.9 mM) and CO (0.9 mM) were prepared by purging ~20 mL of phosphate buffered saline (PBS; 10 mM, pH 7.4)

on ice with N_2 for 25 min to remove oxygen, followed by purging with NO or CO gas for an additional 25 min.[55] Saturated gaseous solutions were stored at 4 °C and used the same day as preparation. Fresh hydrogen sulfide (H_2S; 3.0 mM) stock was prepared the day of use by dissolving $Na_2S{\cdot}9H_2O$ in deoxygenated PBS with 150 μM EDTA, sealing the container with a rubber septum, and purging the headspace with N_2. Stock concentration was determined by iodometric titration.[30]

Electrochemical experiments were carried out on a CH Instruments 1030 8-channel Electrochemical Analyzer (Austin, TX). The multi-electrode configuration consisted of 8 glassy carbon inlaid disc working electrodes (GCE; 3.0 mm dia.) sealed in Kel-F (6.0 mm total dia.; CH Instruments), a silver-silver chloride (Ag|AgCl) reference electrode (3.0 M KCl; CH Instruments), and a platinum (Pt) wire counter electrode. All potentials cited are versus the Ag|AgCl reference electrode. Unless otherwise specified, electrochemical measurements were collected in 20 mL deoxygenated PBS (pH 7.4) at room temperature (23 °C).

5.2.2 Preparation of electropolymerized film-modified electrodes

Glassy carbon working electrodes were polished consecutively with 1.0, 0.3, and 0.05 μm particle size deagglomerated alumina slurries (Buehler; Lake Bluff, IL) dispersed on a microcloth. Electrodes were then copiously rinsed with water and wiped with tissue to remove residual alumina. To ensure a stable background, electrodes were cycled in PBS between 0 and +1.0 V using cyclic voltammetry (CV) eight times at a scan rate of 10 mV s^{-1} before being transferred to monomer solutions for electrodeposition. All monomers were dissolved at a concentration of 10 mM in PBS. To improve solubility, solutions of 5A1N were titrated to pH 1.0 with HCl, and eugenol to pH 13 with NaOH. Electropolymerized film

depositions were carried out using CV, sweeping the potential between 0 and +1.0 V at a scan rate of 10 mV s^{-1} for a total of 20 cycles. Film-modified electrodes were then rinsed with water to remove unbound oligomer from the surface.

5.2.3 Voltammetric measurements

The potential was scanned from −0.3 to +1.1 V in PBS eight times via differential pulse voltammetry (DPV) on bare glassy carbon electrodes to achieve a constant background. Differential pulse voltammograms were then collected in solutions of common, electroactive biological interferents by sweeping over the same potential window. The anodic peak potential(s) (E_a) of the following interferents were measured: L-ascorbate (AA; 1.0 mM), cysteine (CYS; 1.0 mM), dopamine (DA; 1.0 mM), acetaminophen (AP; 1.0 mM), hydrogen peroxide (H_2O_2; 1.0 mM), nitrite (NO_2^-; 1.0 mM), and nitric oxide (NO; 95 μM). Of note, voltammograms of carbon monoxide (CO) were indistinguishable from background at its saturation limit (0.9 mM) with no measured E_a value. All DPV traces were collected using the following parameters: 50 mV amplitude, 4 mV step increase, 0.5 s period, 0.2 s pulse width, and 0.0167 s sample width.

Bare glassy carbon electrodes were cycled between −0.3 and +1.1 V via CV (scan rate: 100 mV s^{-1}) in PBS eight times to achieve a constant background. Ten consecutive CV cycles were then collected over the same potential window in the presence of 30 μM H_2S (positive initial sweep; scan rate: 100 mV s^{-1}). All voltammetric data herein is presented in the polarographic convention after background subtraction.

5.2.4 Constant potential amperometric measurements

All electrodes (either bare or film-modified) were first polarized at the applied potential of measurement in PBS for 15 min via constant potential amperometry (CPA) to

achieve a stable background before use. Hydrogen sulfide sensitivity was measured on bare GCEs in a stirred solution of 20 mL deoxygenated PBS with five injections of 3.0 μM H_2S spaced 50-100 s apart. This procedure will hereafter be referred to as a "standard calibration." With the applied potential set to +0.1, +0.3, +0.5, or +0.7 V for these standard calibrations, the sensitivity and LOD were calculated and compared in order to determine the optimal applied potential for H_2S detection (+0.3 V in our evaluation). Once the optimal applied potential was determined, the effect of surface sulfur passivation was investigated to determine an appropriate surface conditioning procedure. With the applied potential set at +0.3 V, five consecutive standard calibrations were carried out. Analytical metrics, including H_2S sensitivity, LOD, and background current, were calculated and compared as a function of calibration number ($N_{calibration}$).

With the applied potential and surface conditioning procedure optimized (+0.3 V and $N_{calibration}$ = 3, respectively), standard calibrations were carried out on both bare and film-modified GCEs. Stock solutions of interferents were prepared in PBS to test for H_2S selectivity. Separate staircase amperograms were collected for each interferent with successive aliquot injections of AA (0.50 mM), AP (0.50 mM), DA (0.10 mM), CYS (0.50 mM), H_2O_2 (2.5 mM), NO_2^- (2.5 mM), or NO (0.475 mM). All selectivity measurements were carried out *after* surface preconditioning.

5.2.5 Measurements in simulated wound fluid

A simulated wound fluid (SWF) solution was prepared via a 10-fold dilution of FBS with PBS. Bare and film-modified GCEs were calibrated in PBS three times before being transferred and polarized at +0.3 V in SWF for 1 h. Standard calibrations were then repeated three times in SWF. Relative sensitivity retention, change in LOD, and response time (90%

max Δi) were evaluated to compare performance in SWF versus PBS. Based on these data, the best overall performing film modification (poly(*o*-PD)) was selected for long-term stability testing. Poly(*o*-PD)-modified electrodes were calibrated three times in PBS before polarizing for 24 h at a constantly held potential of +0.3 V in SWF. After this extended polarization, electrodes were calibrated in SWF, and selectivity coefficients versus AA, DA, and AP were measured in PBS.

5.2.6 Calculations and statistical analysis

Selectivity coefficients for H_2S against the interferent species were calculated according to Eq. 3, where S_j represents the sensitivity towards interferent *j*, and S_{H2S} the H_2S sensitivity.

$$\log k_{H2S,j} = \log\left(\frac{S_j}{S_{H2S}}\right) \qquad \text{(Eq. 3)}$$

The permeability of H_2S on film-modified GCEs was calculated according to Eq. 4, where P_{H2S} is the permeability of the film with respect to H_2S, and $S_{H2S,film}$ and $S_{H2S,bare}$ represent the sensitivities of the film-modified and bare GCEs, respectively.

$$P_{H2S} = \frac{S_{H2S,film}}{S_{H2S,bare}} \qquad \text{(Eq. 4)}$$

Sensitivities towards H_2S, LODs, sensitivity retentions, background currents, selectivity coefficients, permeabilities, and response times are all presented (either numerically or with error bars) as the mean ± the standard error of the mean. Comparisons between data sets were performed using two-tailed *t*-tests.

5.3 Results and Discussion

5.3.1 Voltammetry of H_2S and interferents

Cyclic voltammetry (CV) and differential pulse voltammetry (DPV) are useful techniques for determining the electrochemical properties of redox systems under observation. In the case of hydrogen sulfide (H_2S), interpretation of voltammetric data is confounded by elemental sulfur poisoning and resulting surface passivation. Low potentials give rise to sulfur production (E^0 = +0.171 V) while more positive potentials convert this sulfur to water-soluble sulfur oxides, including sulfate ($E^0 \geq$ +0.365 V).[40] The balance of these half-reactions depends upon the applied potential, and so the electrode surface is in a continuously changing state of passivation while the potential is swept. This phenomenon was evident in the CV traces collected in 30 μM H_2S cycling between −0.3 to +1.1 V (Figure 5.1). With the first sweep on a clean GCE, the low-potential oxidation wave feature at +0.16 V was easy to discern. By the second cycle, the surface had been poisoned with low-potential features noticeably suppressed. Higher-potential features (e.g., the initial peak at ca. +0.8 V) were also distorted and shifted positively, meaning higher potentials were needed to clear passivating sulfur and draw equivalent currents. With repeated cycling, these trends continued, erasing all readily identifiable redox features. The shape of the trace had stabilized by the tenth cycle.

The DPV traces of common, electroactive biological interferents were also collected on a clean GCE (Figure 5.2). Without the convoluting effects of surface passivation (as with

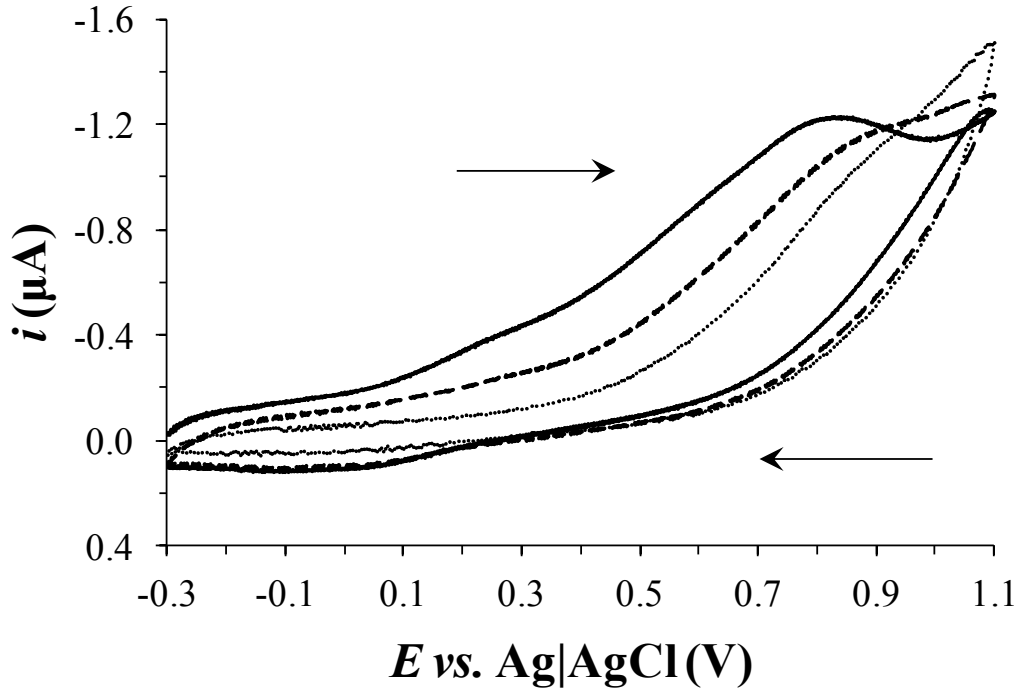

Figure 5.1 Representative cyclic voltammograms collected using a GCE (3.0 mm dia.) in the presence of 30 μM H_2S in 10 mM PBS (pH 7.4) with a positive initial sweep and a scan rate of 100 mV s^{-1}. Traces represent the first (solid), second (dash), and tenth (dot) cycles. Blank PBS backgrounds were subtracted from all traces.

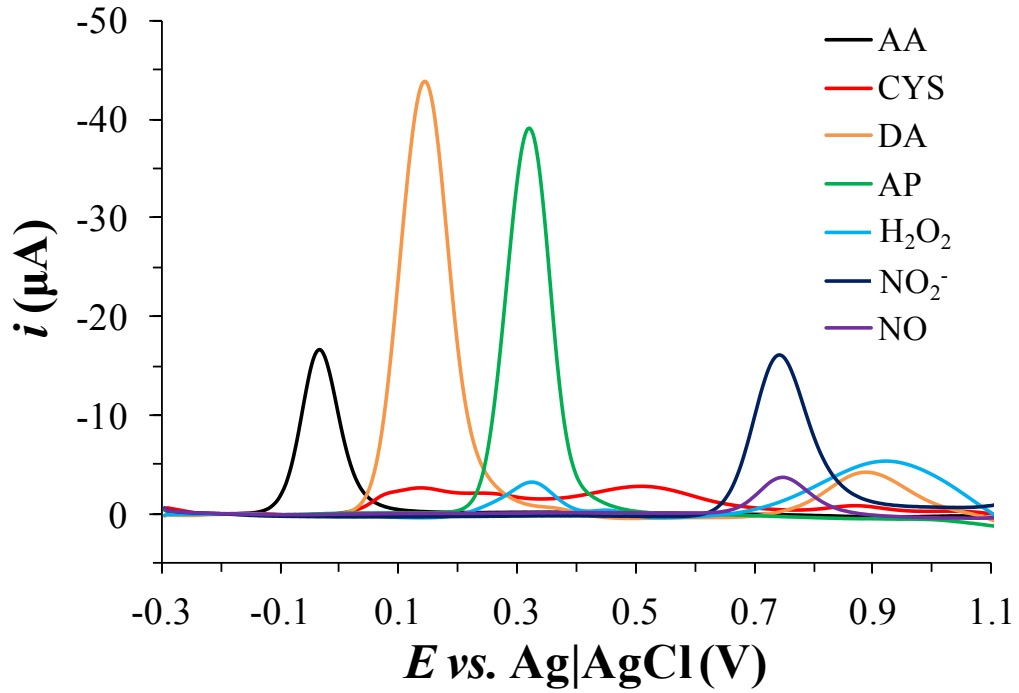

Figure 5.2 Representative differential pulse voltammograms collected on a GCE (3.0 mm dia.) in the presence of electroactive, biological interferents in 10 mM PBS (pH 7.4). L-ascorbate (AA), cysteine (CYS), dopamine (DA), acetaminophen (AP), hydrogen peroxide (H_2O_2), and nitrite (NO_2^-) were tested at a concentration of 1.0 mM, and nitric oxide (NO) at 95 µM. Parameters: 50 mV amplitude, 4 mV step increase, 0.5 s period, 0.2 s pulse width, and 0.0167 s sample width. Blank PBS backgrounds were subtracted from all traces.

Table 5.1 Anodic peak potentials of electroactive, biological interferents.

j [a]	$E_{a,1}$ (V) [b]	$E_{a,2}$ (V) [b]	$E_{a,3}$ (V) [b]
AA	-0.036 ± 0.004		
CYS	0.132 ± 0.003	0.507 ± 0.012	0.875 ± 0.008
DA	0.145 ± 0.003	0.894 ± 0.002	
AP	0.320 ± 0.003		
H_2O_2	0.323 ± 0.004	0.452 ± 0.001	0.934 ± 0.006
NO_2^-	0.742 ± 0.002		
NO	0.749 ± 0.002		

[a] Interferents: L-ascorbate (AA; 1.0 mM), cysteine (CYS; 1.0 mM), dopamine (DA; 1.0 mM), acetaminophen (AP; 1.0 mM), hydrogen peroxide (H_2O_2; 1.0 mM), nitrite (NO_2^-; 1.0 mM), and nitric oxide (NO; 95 µM). [b] Collected on a GCE (3 mm dia.) in 10 mM PBS (pH 7.4) under DPV ($n \geq 8$). Potentials given versus the Ag|AgCl reference (3.0 M KCl).

sulfur), anodic peak potentials (E_a) could be accurately measured (Table 5.1). Based on their relatively low E_a values and high signal response, it was evident that L-ascorbate and dopamine were the most problematic interferents to sensor selectivity on a GCE.

5.3.2 Surface conditioning for continuous electrochemical H_2S measurement

Continuous electrochemical techniques (e.g., constant potential amperometry, chronocoulometry) are simpler and allow for greater temporal resolution than voltammetry, but are no less susceptible to surface poisoning by H_2S. Deposition of an insulating sulfur layer on the electrochemical transducer reduces sensitivity and alters the analytical performance of the sensor. Although it may be possible to account for such changes with controlled H_2S exposure, continuous measurement from novel or unpredictable systems would remain unfeasible. It is therefore critical to ensure reproducible sensor performance while developing any continuous H_2S sensor for biological applications. Unlike other methods that seek to mitigate surface passivation (e.g., redox mediators, cleaning pulses), a surface conditioning procedure "pre-poisons" the electrode until a steady-state performance is reached.[46,48] While variability is greatly diminished, a repercussion is that the steady-state sensitivities may become so low that LODs are pushed to physiologically irrelevant levels (i.e., >100 nM).[28]

A suitable working potential was first determined to assess the utility of surface conditioning for a continuous electrochemical H_2S sensor. With the effects of poisoning, the only significant voltammetric feature of the H_2S trace was an increase in current with the increase in potential in the range of +0.1—1.1 V under CV (Fig. 1). As a direct result, the H_2S sensitivity increased with applied potential when measured at +0.1, +0.3, +0.5, and +0.7 V under constant potential amperometry (CPA; Figure 5.3A). While potentials greater than

+0.7 V are able to further oxidize deposited sulfur, a priori concerns with selectivity (particularly against NO and nitrite; Table 5.1) and electropolymerized film damage led to +0.7 V being selected as an upper bound to the applied potential. Increasing the applied potential also reduced the LOD significantly, particularly from +0.1 to +0.3 V (Figure 5.3B). Subsequent increases to +0.5 and +0.7 V did not greatly affect the LOD due to intensification of the background noise. The plateau in LOD, in addition to the goal of remaining below interferent peak anodic potentials (Table 5.1), motivated our selection of +0.3 V as a suitable working potential.

An appropriate surface conditioning procedure should provide enough exposure to the poisoning agent to ultimately elicit steady-state performance. In the context of electrochemical H_2S sensing, the target analyte and poisoning agent are the same molecule, so surface conditioning/exposure can simply be carried out with consecutive calibrations. The H_2S exposure within a single calibration will depend on the concentration range tested and duration of exposure. Based on these criteria, we have defined a "standard calibration" (*see* Section 5.2.4 and Figure 5.4) to convey key performance metrics as a function of calibration number ($N_{calibration}$). As shown in Figure 5.5, the H_2S sensitivity, LOD, and background current were each monitored and found to converge to values statistically insignificant from one another after three standard calibrations. More generally, the surface conditioning was completed upon the passage of 580 ± 110 μC cm^{-2} (background charge density subtracted). While the sensitivity fell to approximately 80% of its original value (Figure 5.5A) and the LOD increased slightly, both still allowed for measurement of biologically relevant concentrations of H_2S (Figure 5.5B).[28] An important clarification here is

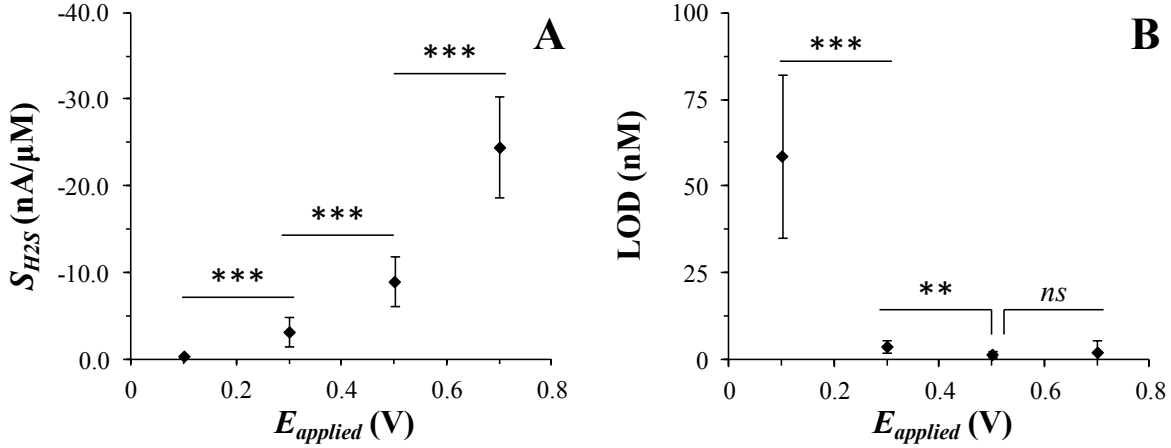

Figure 5.3 (A) Hydrogen sulfide sensitivity and (B) LOD of a bare GCE (3.0 mm dia.) as a function of the applied potential used under CPA ($n \geq 8$). *ns* = $p \geq 0.05$, * = $p < 0.05$, ** = $p < 0.01$, *** = $p < 0.001$.

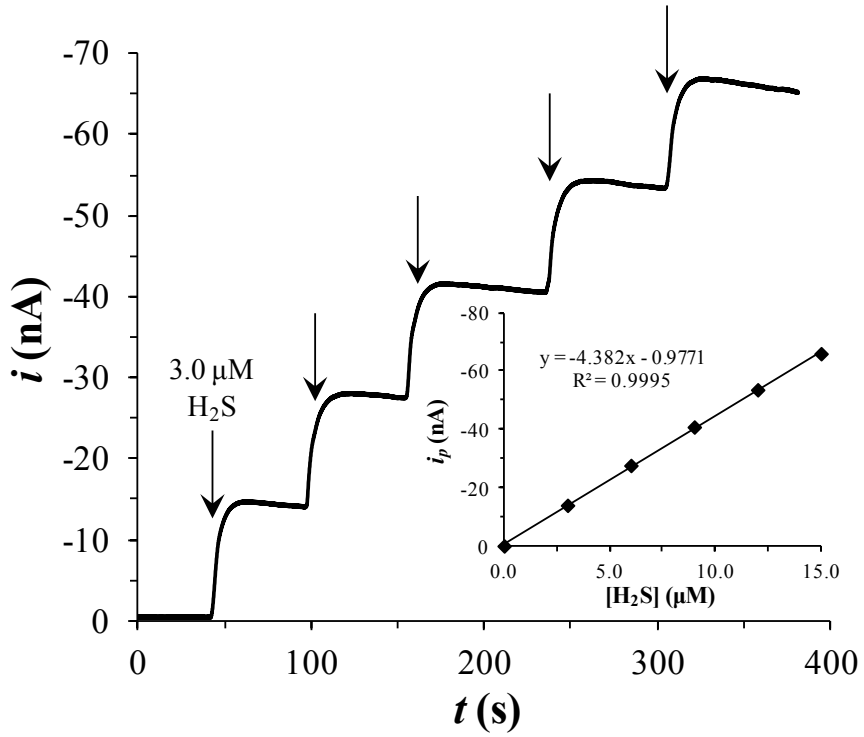

Figure 5.4 Example staircase amperogram collected on a bare GCE (3.0 mm dia.) in 10 mM PBS (pH 7.4) with successive injections of hydrogen sulfide under CPA (applied potential: +0.3 V). Inset: corresponding calibration curve from plateau currents.

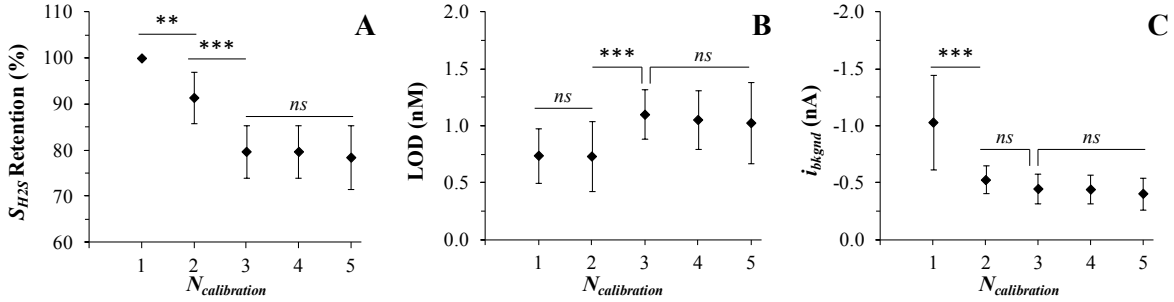

Figure 5.5 Analytical performance metrics of a GCE (3.0 mm dia.) as a function of the number of standard hydrogen sulfide calibrations carried out. (A) Sensitivity retention, (B) LODs, and (C) background currents measured under CPA with an applied potential of +0.3 V ($n \geq 8$). *ns* = $p \geq 0.05$, * = $p < 0.05$, ** = $p < 0.01$, *** = $p < 0.001$.

that while calibrations are discrete, poisoning occurs continuously throughout the calibration. The percent sensitivity retention will therefore depend upon the poisoning exposure (i.e., length and H_2S injection concentrations) occurring in the *first* calibration, to which all sensitivities are normalized. Abbreviated calibrations, though less accurate for measuring performance metrics, would foster greater resolution of poisoning dynamics and yield smaller retentions in sensitivity. For the purpose of surface conditioning an electrode quickly, the use of three standard calibrations was considered most favorable.

5.3.3 Analytical performance of film-modified electrodes

The performance of a surface-conditioned, but otherwise unmodified GCE affords high H_2S sensitivity (-4.03 ± 0.91 nA μM^{-1}) and a low LOD (1 nM) but does not sufficiently block nonspecific oxidation of key interferent species (Table 5.2). The choice of electrochemical technique and associated parameters does lend some control over selectivity. For instance, the use of a relatively low applied potential (e.g., +0.3 V) virtually eliminates the response to NO and nitrite oxidation (selectivity coefficients <-5). Furthermore, without coordination to surface-confined metals (e.g., Pt, Sn) CO cannot be readily oxidized at a GCE.[56] Aside from these interferents, AA, AP, DA, CYS, and H_2O_2 are each oxidized at potentials near or below +0.3 V and would thus distort H_2S measurements in biological milieu (Table 5.1).

In an effort to further enhance selectivity for H_2S, bare GCEs were modified with electropolymerized films via CV using a series of monomers known to undergo irreversible oxidation to cationic radicals in aqueous media under sufficiently positive potentials.[53] With radical coupling and secondary oxidations, oligomers whose size eventually exceeds solubility crash out from solution onto the electrode surface, building the electropolymerized

film. The CV traces of the monomers reveal that the majority of the deposition occurs within the first sweep, as subsequent cycles draw greatly diminished current (Figure 5.6). As the film approaches complete coverage, monomers in solution are blocked from the electrode surface, cutting off radical cation generation and self-terminating growth. Ultimately, the shapes of the CV traces are dictated by both the redox properties of the monomer and this insulating process, the latter capable of distorting higher-potential wave features. Nevertheless, peak oxidation potentials were measured from the first cycle with the 0 to +1.0 V window sufficient to oxidize all monomers (Table 5.3). The use of cyclic voltammetry at a slow scan rate (10 mV s^{-1}) creates more tightly packed films with greater adherence compared to CPA depositions.[53,57,58] The presence of multiple peaks in some cases (e.g., 5A1N and *o*-, *m*-, *p*-PD) was attributed to secondary/tertiary oxidations of soluble oligomers and/or over-oxidation of the film itself (which may retain a net positive charge).[51,59] The absence of reduction waves in the return traces is evidence of the insulating properties of these films, with the exception of 5A1N. The small, cathodic feature in the +0.3 to 0 V range demonstrates poly(5A1N)'s conductive properties. Unlike other conductive films (e.g., poly(aniline)), the polymerization mechanism of 5A1N is not autocatalytic and will proceed to self-terminate as would an insulating film.[53,54,60]

With film modification, the permeability and sensitivity towards H_2S decreased by roughly one order of magnitude for poly(5A1N), -(*o*-PD), and -(*m*-PD), and by two orders for poly(phenol) (Table 5.2). A previous comparison of these monomers in the context of NO sensing revealed that poly(5A1N) and poly(phenol) were more permeable towards NO than presently towards H_2S.[53] Although comparable in size to NO and H_2O in its undissociated

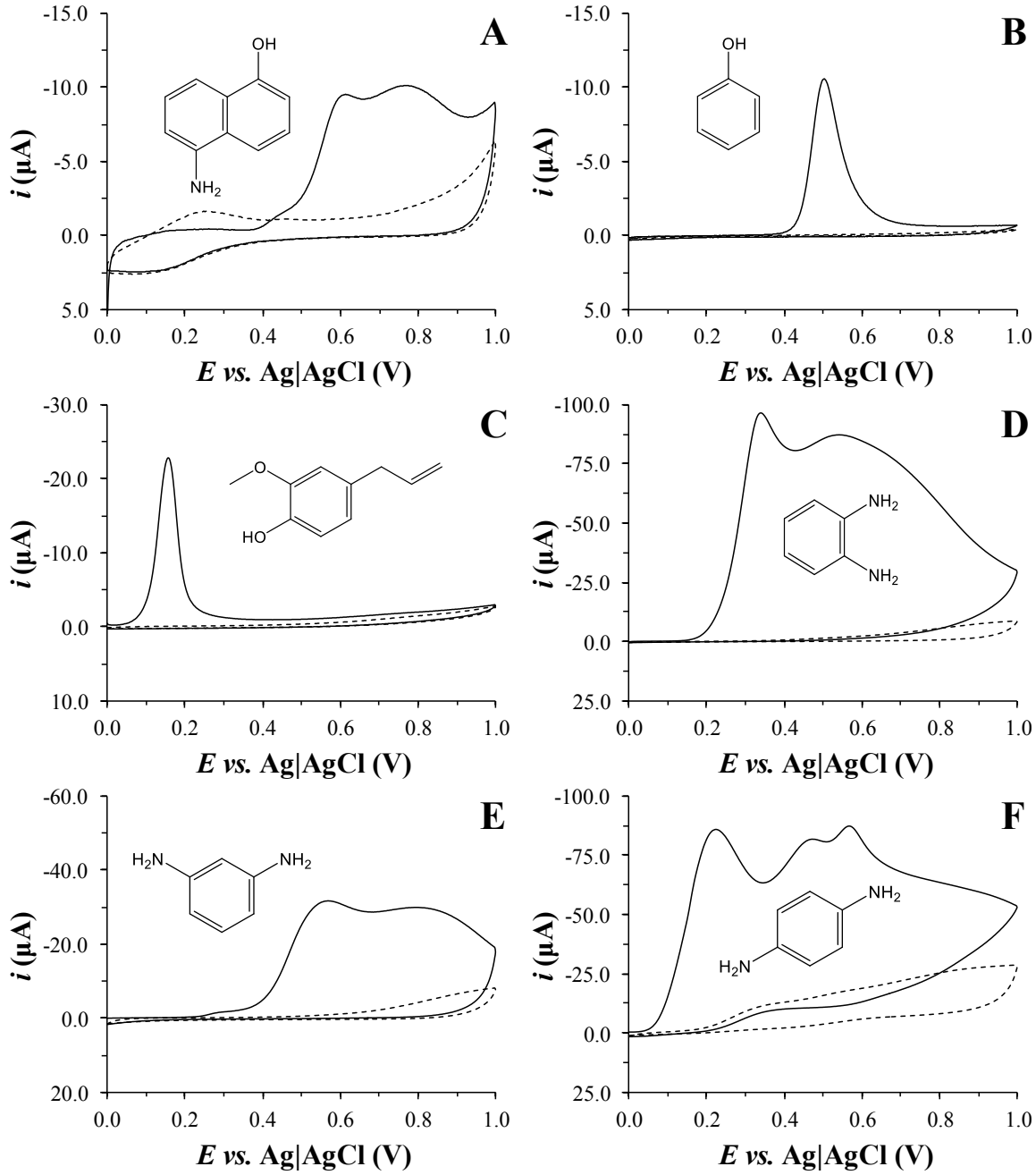

Figure 5.6 The first (solid) and second (dashed) cycle of electrodepositions carried out on a 3.0 mm dia. GCE in 10 mM monomer solutions of (A) 5A1N, (B) phenol, (C) eugenol, (D) *o*-PD, (E) *m*-PD, and (F) *p*-PD in 10 mM PBS via cyclic voltammetry (0 to +1.0 V positive sweep; scan rate: 10 mV s^{-1}). The pH of the phenol, *o*-PD, *m*-PD, and *p*-PD solutions was 7.4. Solutions of 5A1N and eugenol were titrated to pH 1.0 with HCl and pH 13 with NaOH, respectively. Insets: monomer chemical structures.

Table 5.2 Analytical merits of electropolymerized film-modified GCEs for hydrogen sulfide detection.

Electrode [a]	LOD [b] (nM)	S_{H2S} [c] (nA μM^{-1})	P_{H2S} [d]	$\log k_{H2S,j}$ [e]				
				AA	AP	DA	CYS	H_2O_2
GCE (bare)	1 ± 0	-4.03 ± 0.91	1.00 ± 0.23	-0.04 ± 0.11	-1.89 ± 0.14	0.76 ± 0.18	-1.77 ± 0.14	-4.58 ± 0.30
GCE/poly(5A1N)	9 ± 6	-0.42 ± 0.08	0.10 ± 0.02	-1.92 ± 0.10	-2.97 ± 0.33	-1.81 ± 0.30	-3.23 ± 0.19	-4.72 ± 0.49
GCE/poly(phenol)	79 ± 51	-0.05 ± 0.04	0.01 ± 0.01	-1.35 ± 0.34	-2.97 ± 0.52	-0.13 ± 0.42	-2.92 ± 0.46	-4.65 ± 0.62
GCE/poly(eugenol)	10 ± 5	-3.92 ± 1.42	0.97 ± 0.35	-0.76 ± 0.14	-1.24 ± 0.08	0.42 ± 0.22	-1.07 ± 0.08	-4.10 ± 0.16
GCE/poly(*o*-PD)	15 ± 12	-0.28 ± 0.06	0.07 ± 0.01	-2.39 ± 0.16	-4.49 ± 0.42	-2.50 ± 0.21	-2.78 ± 0.16	-5.01 ± 0.15
GCE/poly(*m*-PD)	73 ± 37	-0.42 ± 0.06	0.10 ± 0.01	-3.09 ± 0.06	-3.11 ± 0.16	-2.23 ± 0.32	-3.36 ± 0.10	-4.57 ± 0.22
GCE/poly(*p*-PD)	30 ± 10	-4.24 ± 0.58	1.05 ± 0.14	-2.40 ± 0.07	-4.28 ± 0.12	-3.09 ± 0.08	-2.28 ± 0.13	-4.79 ± 0.09

[a] Glassy carbon electrode (GCE; 3.0 mm dia.). [b] $S/N = 3$. [c] Sensitivity calculated from third standard calibration (applied potential: +0.3 V). [d] Permeability calculated using Eq. 4. [e] Selectivity coefficients calculated using Eq. 3 against interferent *j* as follows: L-ascorbate (AA; 0.25 mM), acetaminophen (AP; 0.50 mM), dopamine (DA; 0.10 mM), cysteine (CYS; 0.50 mM), hydrogen peroxide (H_2O_2; 2.5 mM). For all measurements, $n \geq 8$.

Table 5.3 Anodic peak potentials of monomers used in film electrodeposition.

Monomer	$E_{a,1}$ (V) [a]
5A1N	0.610 ± 0.005
Phenol	0.505 ± 0.005
Eugenol	0.156 ± 0.003
o-PD	0.346 ± 0.006
m-PD	0.571 ± 0.003
p-PD	0.225 ± 0.002

[a] Monomer solutions (10 mM) were dissolved in 10 mM PBS (pH 7.4 for phenol, *o*-, *m*-, and *p*-PD; pH 1.0 for 5A1N; pH 13 for eugenol). Peak anodic potentials were measured on a GCE under CV with a 0 to +1.0 V positive sweep and a scan rate of 10 mV s^{-1} ($n \geq 8$). Potentials given versus the Ag|AgCl reference (3.0 M KCl).

form, at pH 7.4 hydrogen sulfide exists primarily (~80%) as dissociated hydrosulfide (HS^-), whose hydration shell may impede film permeation in these films.[61] Both poly(eugenol) and poly(*p*-PD) retained H_2S permeability values close to unity (i.e., the bare GCE), suggesting that their polymeric structures may confer a unique advantage to H_2S detection (Table 5.2). As with bare GCEs, film-modified electrodes were surface conditioned with multiple H_2S calibrations ($N_{calibration}$ = 3) to ensure performance stability (Figure 5.7). Similar sensitivity reductions (20-30%) suggested that the presence of the film, regardless of monomer identity, did not greatly affect the surface conditioning process.

As a result of the reduced sensitivity, the LOD predictably increased (i.e., reciprocal changes in order of magnitude) for electrodes modified with poly(5A1N), -(*o*-PD), and -(phenol) (Table 5.2). An intensification in the background noise resulted in poly(eugenol), -(*m*-PD), and -(*p*-PD) to have LOD values higher than permeability alone would predict. From lowest (poly(5A1N), 9 ± 6 nM) to highest LOD (poly(phenol), 79 ± 51 nM), each film modification studied would still permit measurement of biologically relevant concentrations of H_2S. Though a permselective barrier may nonideally reduce the permeability of the target analyte, the membrane will still confer a selectivity advantage if greater obstruction occurs against interferent species.

The primary blocking mechanism of electropolymerized films is size-exclusion, particularly in the case of neutrally charged molecules (reducing solvation and charge-repulsion interactions).[51,52,62,63] With an applied potential of +0.3 V, the bare GCE confers inherent electrochemical selectivity for H_2S over neutrally charged interferents acetaminophen (AP), cysteine (CYS), and hydrogen peroxide (H_2O_2) at pH 7.4 (Table 5.2).

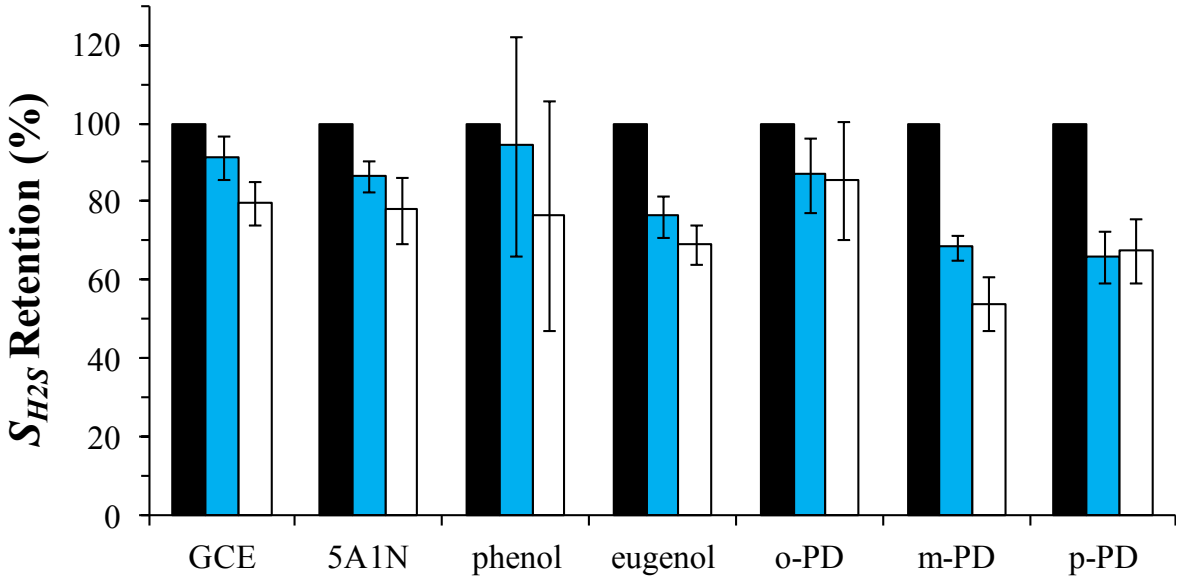

Figure 5.7 Hydrogen sulfide sensitivity retention on bare and electropolymerized film-modified GCEs (3.0 mm dia.) as a function of the number of standard calibrations ($N_{calibration}$) carried out via CPA under an applied potential of +0.3 V *vs*. Ag|AgCl ($n \geq 8$). Black, blue, and white bars represent $N_{calibration}$ = 1, 2, and 3, respectively (normalized to first calibration).

With film modification, the selectivity against H_2O_2 was maintained or marginally improved for each monomer studied, with the exception of eugenol, for which selectivity was slightly worse. In contrast to the larger interferents AP and CYS (against which selectivity was greatly improved over the bare GCE performance for each monomer except eugenol), the poor enhancement of H_2O_2 selectivity is rationalized by its comparatively small size. As each of these films has been studied previously with respect to H_2O_2 sensing (e.g., in the context of glucose biosensors), it was expected that H_2O_2 would be able to freely permeate.[50-52] The high overall H_2O_2 selectivity (coefficients <-4 for all films) is therefore chiefly attributed to the inherent electrochemistry for GCEs rather than differential permeation (Figure 5.2). Against AP, GCEs modified by films of any of the phenylenediamine series performed exceptionally well with selectivity coefficients all below −3; and CYS was best rejected by poly(5A1N) and poly(*m*-PD) films (both <-3).

Dopamine (DA) and L-ascorbate (AA) are comparable in size to AP and CYS but at pH 7.4 retain positive (+1) and negative (−1) charges, respectively. The bare GCE has poor selectivity for H_2S over DA and AA given their low oxidation potentials ($E_a < +0.3$ V) and large signal responses (Table 5.1, Figure 5.2). In fact, the bare GCE is even more responsive towards DA than H_2S, indicated by the positive selectivity coefficient (0.76 ± 0.18; Table 5.2). In order to isolate the selectivity benefits of the film modifications, changes in selectivity should be considered relative to the performance of the bare GCE. For each film modification investigated except poly(eugenol), selectivity for H_2S against both DA and AA was dramatically improved—most notably so with the phenylenediamine series (coefficients all <-2). Modifications with poly(5A1N), -(*o*-PD), and -(*p*-PD) all had greater improvements in electrode selectivity against DA than compared to similarly-sized AA, AP, and CYS,

suggesting that these films may retain a net positive charge for coulombic repulsion of DA. Improvements to selectivity against oppositely-charged DA and AA were within error of each other for poly(phenol) and poly(*m*-PD) films, indicating insignificant coulombic interactions.

Poly(eugenol) films did not perform well in any measure of selectivity. Given the large measured H_2S permeability, the pores are likely large and inadequate for sieving out larger interferents.[52,64] We have previously reported that poly(5A1N) and poly(phenol) have notable nitrite rejection capabilities;[53] given hydrosulfide's similar size and charge, these membranes proved nonideal for H_2S/HS^- sensing. Overall, the phenylenediamine series of films performed best in terms of improving selectivity against all interferents, and of this series, poly(*o*-PD) stood out for its low LOD (Table 5.2).

5.3.4 Performance in simulated wound fluid

In addition to interferents, a significant challenge for in situ biological H_2S measurements is biofouling. Protein accumulation on the transducer surface reduces sensitivity and degrades sensor performance.[65] Appropriate sensor characterization should be carried out in the media of measurement or closest simulant thereto to fully characterize utility. To this end, bare GCE and film-modified electrodes were polarized and calibrated in simulated wound fluid (SWF) to quantify any detrimental effects of biofouling (Figure 5.8). The bare GCE retained 36 ± 5 % of its initial sensitivity in SWF relative to PBS trials (Figure 5.8A) with an increase in LOD to 21 ± 9 nM (Figure 5.8B). Modification with electropolymerized films significantly improved sensitivity retention, regardless of the electropolymerized film employed. An unmodified, positively-polarized GCE will plausibly attract more protein than one modified with an insulating film since most blood plasma

proteins are negatively charged at pH 7.4 (e.g., albumin).[66] Poly(*o*-PD) performed better than all other film modifications with statistical significance ($p < 0.05$ *vs.* poly(5A1N); $p < 0.01$ *vs.* others), retaining 79 ± 6 % of its sensitivity in SWF. Previous studies have also highlighted poly(*o*-PD) for its anti-biofouling properties in proteinaceous media, possibly due to its greater compactness.[53]

Although having better sensitivity retention compared to bare GCEs, the majority of the film-modified electrodes predictably experienced an increase in LOD with the reduction in sensitivity (poly(eugenol) and poly(*p*-PD) being the exceptions; Figure 5.8B). Severely increased LODs for poly(5A1N) and poly(phenol) films resulted from an increase in the background noise. Along with poly(*m*-PD), the LOD values in SWF were too high to have any practical biological use. Of the remaining films with LOD < 100 nM, the H_2S response times of poly(eugenol)- and poly(*o*-PD)-modified electrodes were statistically insignificant from bare GCEs (15 ± 10 s; Figure 5.8C). Protein adsorption did not greatly affect response time overall, since the bare GCE responded in 12 ± 10 s in PBS trials (i.e., identically to SWF trials). The >100 s response times of poly(*m*-PD)- and poly(*p*-PD)-modified electrodes were deemed prohibitive to in situ measurement.

Combined with the data from selectivity measurements, the best overall performing film modification was determined to be poly(*o*-PD), which was selected for further testing of long-term stability. Continuous amperometric measurement in proteinaceous media may strain the electropolymerized film through protein adsorption and potential-induced degradation.[65,67] With partial or complete stripping of the poly(*o*-PD) film, the performance of the electrode would be expected to eventually approach that of the bare GCE. On one

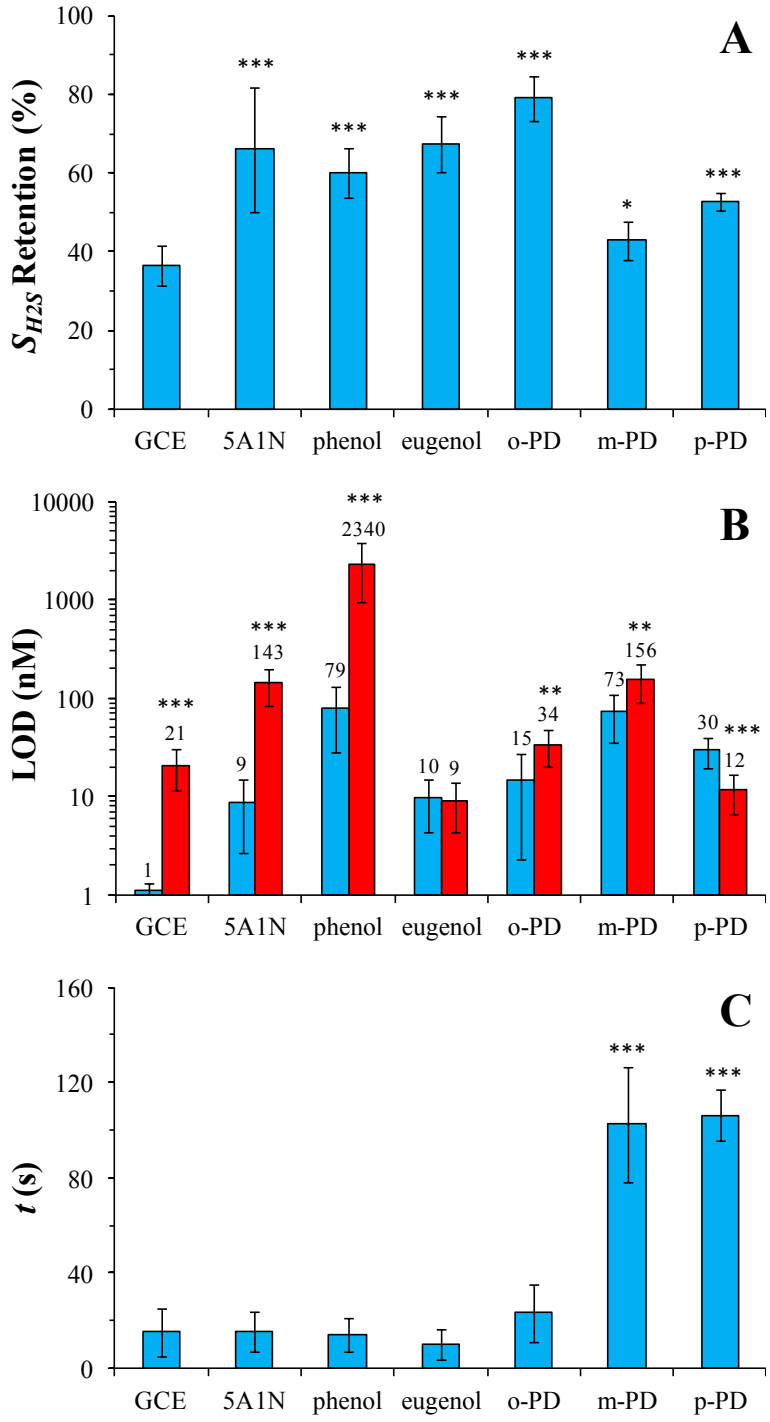

Figure 5.8 (A) H_2S sensitivity retention of bare and electropolymerized film-modified GCEs (3.0 mm dia.) in SWF relative to performance in PBS post-surface conditioning (significance with respect to the bare GCE). (B) Detection limit (S/N = 3) of electrodes in PBS (blue) and in SWF (red; significance with respect to corresponding PBS trials). (C) Response time (90% max Δi) of electrodes in SWF (significance with respect to the bare GCE). * = $p < 0.05$, ** = $p < 0.01$, *** = $p < 0.001$. For all measurements, $n \geq 8$.

Table 5.4 Selectivity characteristics of poly-*o*-PD-modified GCEs with long-term use in simulated wound fluid.

Electrode	Condition	$\log k_{H2S,\,j}$ [a]		
		AA	AP	DA
GCE (bare)	New	-0.04 ± 0.11	-1.89 ± 0.14	0.76 ± 0.18
GCE/poly-*o*-PD	New	-2.39 ± 0.16	-4.49 ± 0.42	-2.50 ± 0.21
GCE/poly-*o*-PD	After 24 h use in SWF [b]	-2.99 ± 0.12	-3.15 ± 0.08	-1.51 ± 0.03

[a] Selectivity coefficients calculated with Eq. 2 for H_2S against interferent *j* as follows: L-ascorbate (AA; 0.25 mM), acetaminophen (AP; 0.50 mM), dopamine (DA; 0.10 mM). [b] Under CPA with +0.3 V applied potential. For all measurements, $n \geq 8$.

hand, film destruction would increase the sensitivity towards H_2S in PBS (P_{H2S} = 0.07 ± 0.01 for poly(*o*-PD); Table 5.2), but the electrode would also be more susceptible to biofouling in SWF (Figure 5.8A). Combining these effects, an approximately 7-fold increase in sensitivity would be expected in the worst-case scenario of total membrane delamination. After 24 h continuous use (+0.3 V applied potential), the H_2S sensitivity of the poly(*o*-PD)-modified electrodes increased by a factor of 1.85 ± 0.16, indicative of partial film wear. As further evidence of damage, selectivity coefficients against DA and AP increased by one order; however, it is worth noting that the poly(*o*-PD) film still furnished significant selectivity benefits over the bare GCE (Table 5.4). Interestingly, the selectivity coefficient against AA improved slightly after long-term use. The adsorption of negatively-charged proteins on the surface may confer additional permselectivity characteristics, or in light of poorer coefficients against DA and AP, the protein layer may repel negatively-charged AA. Overall, the poly(*o*-PD)-modified electrode may be used for long-term continuous measurements without serious degradation in selectivity provided periodic recalibrations are used to account for changes in sensitivity.

5.4 Conclusions

Direct, continuous electrochemical measurement of hydrogen sulfide is possible without a redox mediator or integrated cleaning pulse provided that transducer sulfur poisoning is accounted for carefully. Front-end surface conditioning through repeated H_2S calibrations may be used to deposit a sulfur layer on the electrode before continuous measurement. Although this procedure reduces sensitivity, performance variability is practically eliminated while LODs remain biologically relevant (i.e., > 100 nM). Of the electropolymerized film modifications studied herein, poly(*o*-PD) best improved the overall

H_2S sensing performance of the modified GCEs when considering LOD, selectivity versus key interferent species, sensitivity retention in proteinaceous media, and response time. Future work should focus on miniaturizing poly(*o*-PD)-modified GCEs for continuous measurement in biological applications.

REFERENCES

(1) Lawrence, N. S.; Davis, J.; Compton, R. G. Analytical strategies for the detection of sulfide: a review. *Talanta* **2000**, *52*, 771-784.

(2) Olson, K. R. A Practical look at the chemistry and biology of hydrogen sulfide. *Antioxid. Redox Signal.* **2012**, *17*, 32-44.

(3) Lantto, V.; Mizsei, J. Hydrogen sulfide monitoring as an air pollutant with silver-doped tin dioxide thin-film sensors. *Sens. Actuators, B* **1991**, *5*, 21-25.

(4) Li, L.; Rose, P.; Moore, P. K. Hydrogen sulfide and cell signaling. *Annu. Rev. Pharmacol. Toxicol.* **2011**, *51*, 169-187.

(5) Garcia-Mata, C.; Lamattina, L. Hydrogen sulphide, a novel gasotransmitter involved in guard cell signalling. *New Phytol.* **2010**, *188*, 977-984.

(6) Wang, R. Two's company, three's a crowd: can H2S be the third endogenous gaseous transmitter? *FASEB J.* **2002**, *16*, 1792-1798.

(7) Li, L.; Hsu, A.; Moore, P. K. Actions and interactions of nitric oxide, carbon monoxide and hydrogen sulphide in the cardiovascular system and in inflammation - a tale of three gases. *Pharmacol. Ther.* **2009**, *123*, 386-400.

(8) Kolluru, G. K.; Shen, X.; Kevil, C. G. A tale of two gases: NO and H2S, foes or friends for life? *Redox Biol.* **2013**, *1*, 313-318.

(9) Shen, X.; Peter, E. A.; Bir, S.; Wang, R.; Kevil, C. G. Analytical measurement of discrete hydrogen sulfide pools in biological specimens. *Free Radical Biol. Med.* **2012**, *52*, 2276-2283.

(10) Paul, B. D.; Snyder, S. H. H2S signalling through protein sulfhydration and beyond. *Nat. Rev. Mol. Cell Biol.* **2012**, *13*, 499-507.

(11) Doeller, J. E.; Isbell, T. S.; Benavides, G.; Koenitzer, J.; Patel, H.; Patel, R. P.; Lancaster, J. R.; Darley-Usmar, V. M.; Kraus, D. W. Polarographic measurement of hydrogen sulfide production and consumption by mammalian tissues. *Anal. Biochem.* **2005**, *341*, 40-51.

(12) Xu, T.; Scafa, N.; Xu, L. P.; Zhou, S.; Abdullah Al-Ghanem, K.; Mahboob, S.; Fugetsu, B.; Zhang, X. Electrochemical hydrogen sulfide biosensors. *Analyst* **2016**, *141*, 1185-1195.

(13) Abe, K.; Kimura, H. The possible role of hydrogen sulfide as an endogenous neuromodulator. *J. Neurosci.* **1996**, *16*, 1066-1071.

(14) Boehning, D.; Snyder, S. H. Novel neural modulators. *Annu. Rev. Neurosci.* **2003**, *26*, 105-131.

(15) Hosoki, R.; Matsuki, N.; Kimura, H. The possible role of hydrogen sulfide as an endogenous smooth muscle relaxant in synergy with nitric oxide. *Biochem. Biophys. Res. Commun.* **1997**, *237*, 527-531.

(16) Lavu, M.; Bhushan, S.; Lefer, D. J. Hydrogen sulfide-mediated cardioprotection: mechanisms and therapeutic potential. *Clin. Sci.* **2011**, *120*, 219-229.

(17) Szabo, C. Hydrogen sulphide and its therapeutic potential. *Nat. Rev. Drug Discov.* **2007**, *6*, 917-935.

(18) Lee, Z. W.; Zhou, J.; Chen, C. S.; Zhao, Y.; Tan, C. H.; Li, L.; Moore, P. K.; Deng, L. W. The slow-releasing hydrogen sulfide donor, GYY4137, exhibits novel anti-cancer effects in vitro and in vivo. *PLoS One* **2011**, *6*, e21077.

(19) Kodela, R.; Chattopadhyay, M.; Kashfi, K. NOSH-Aspirin: a novel nitric oxide-hydrogen sulfide-releasing hybrid: a new class of anti-inflammatory pharmaceuticals. *ACS Med. Chem. Lett.* **2012**, *3*, 257-262.

(20) Guo, W.; Cheng, Z.; Zhu, Y. Hydrogen sulfide and translational medicine. *Acta Pharmacol. Sin.* **2013**, *34*, 1284-1291.

(21) Song, Z. J.; Ng, M. Y.; Lee, Z. W.; Dai, W.; Hagen, T.; Moore, P. K.; Huang, D.; Deng, L.-W.; Tan, C. H. Hydrogen sulfide donors in research and drug development. *Med. Chem. Comm.* **2014**, *5*, 557-570.

(22) Wallace, J. L.; Wang, R. Hydrogen sulfide-based therapeutics: exploiting a unique but ubiquitous gasotransmitter. *Nat. Rev. Drug Discov.* **2015**, *14*, 329-345.

(23) Wang, Y.; Zhao, X.; Jin, H.; Wei, H.; Li, W.; Bu, D.; Tang, X.; Ren, Y.; Tang, C.; Du, J. Role of hydrogen sulfide in the development of atherosclerotic lesions in apolipoprotein E knockout mice. *Arterioscler., Thromb., Vasc. Biol.* **2009**, *29*, 173-179.

(24) Chen, L.; Ingrid, S.; Ding, Y.; Liu, Y.; Qi, J.; Tang, C.; Du, J. Imbalance of endogenous homocysteine and hydrogen sulfide metabolic pathway in essential hypertensive children. *Chin. Med. J.* **2007**, *120*, 389-393.

(25) Jiang, H.-l.; Wu, H.; Li, Z.; Geng, B.; Tang, C. Changes of the new gaseous transmitter H2S in patients with coronary heart disease. *Diyi Junyi Daxue Xuebao* **2005**, *25*, 951-954.

(26) Chen, Y. H.; Yao, W. Z.; Geng, B.; Ding, Y. L.; Lu, M.; Zhao, M. W.; Tang, C. S. Endogenous hydrogen sulfide in patients with COPD. *Chest* **2005**, *128*, 3205-3211.

(27) Whitfield, N. L.; Kreimier, E. L.; Verdial, F. C.; Skovgaard, N.; Olson, K. R. Reappraisal of H2S/sulfide concentration in vertebrate blood and its potential significance in ischemic preconditioning and vascular signaling. *Am. J. Physiol.* **2008**, *294*, R1930-R1937.

(28) Olson, K. R. Is hydrogen sulfide a circulating "gasotransmitter" in vertebrate blood? *Biochim. Biophys. Acta, Bioenerg.* **2009**, *1787*, 856-863.

(29) Furne, J.; Saeed, A.; Levitt, M. D. Whole tissue hydrogen sulfide concentrations are orders of magnitude lower than presently accepted values. *Am. J. Physiol.* **2008**, *295*, R1479-R1485.

(30) Pawlak, Z.; Pawlak, A. S. Modification of iodometric determination of total and reactive sulfide in environmental samples. *Talanta* **1999**, *48*, 347-353.

(31) Ciesielski, W.; Zakrzewski, R. Iodometric titration of sulfur compounds in alkaline medium. *Chem. Anal.* **2006**, *51*, 653-678.

(32) Lawrence, N. S.; Davis, J.; Jiang, L.; Jones, T. G. J.; Davies, S. N.; Compton, R. G. The electrochemical analog of the methylene blue reaction: a novel amperometric approach to the detection of hydrogen sulfide. *Electroanalysis* **2000**, *12*, 1453-1460.

(33) Levitt, M. D.; Abdel-Rehim, M. S.; Furne, J. Free and acid-labile hydrogen sulfide concentrations in mouse tissues: anomalously high free hydrogen sulfide in aortic tissue. *Antioxid. Redox Signal.* **2011**, *15*, 373-378.

(34) Peng, H.; Cheng, Y.; Dai, C.; King, A. L.; Predmore, B. L.; Lefer, D. J.; Wang, B. A fluorescent probe for fast and quantitative detection of hydrogen sulfide in blood. *Angew. Chem., Int. Ed.* **2011**, *50*, 9672-9675.

(35) Nishida, M.; Sawa, T.; Kitajima, N.; Ono, K.; Inoue, H.; Ihara, H.; Motohashi, H.; Yamamoto, M.; Suematsu, M.; Kurose, H.; van der Vliet, A.; Freeman, B. A.; Shibata, T.; Uchida, K.; Kumagai, Y.; Akaike, T. Hydrogen sulfide anion regulates redox signaling via electrophile sulfhydration. *Nat. Chem. Biol.* **2012**, *8*, 714-724.

(36) Zhang, Y.-Y.; Zhou, H.; Wu, P.; Zhang, H.-R.; Xu, J.-J.; Chen, H.-Y. In situ activation of CdS electrochemiluminescence film and its application in H2S detection. *Anal. Chem.* **2014**, *86*, 8657-8664.

(37) Yue, X.; Zhu, Z.; Zhang, M.; Ye, Z. Reaction-based turn-on electrochemiluminescent sensor with a ruthenium(II) complex for selective detection of extracellular hydrogen sulfide in rat brain. *Anal. Chem.* **2015**, *87*, 1839-1845.

(38) Eckert, W. Electrochemical identification of the hydrogen sulfide system using a pH2S (glass/Ag°, Ag2S) electrode. *J. Electrochem. Soc.* **1998**, *145*, 77-79.

(39) Yang, G.; Wu, L.; Jiang, B.; Yang, W.; Qi, J.; Cao, K.; Meng, Q.; Mustafa, A. K.; Mu, W.; Zhang, S.; Snyder, S. H.; Wang, R. H2S as a physiologic vasorelaxant: hypertension in mice with deletion of systathionine γ-lyase. *Science* **2008**, *322*, 587-590.

(40) Kroll, A. V.; Smorchkov, V. I.; Nazarenko, A. Y. Electrochemical sensors for hydrogen and hydrogen sulfide determination. *Sens. Actuators, B* **1994**, *21*, 97-100.

(41) Kapusta, S.; Viehbeck, A.; Wilhelm, S. M.; Hackerman, N. The anodic oxidation of sulfide on platinum electrodes. *J. Electroanal. Chem. Interfacial Electrochem.* **1983**, *153*, 157-174.

(42) Buckley, A. N.; Hamilton, I. C.; Woods, R. An investigation of the sulfur(2-)/sulfur(0) system on gold electrodes. *J. Electroanal. Chem. Interfacial Electrochem.* **1987**, *216*, 213-227.

(43) Vandeberg, P. J.; Kowagoe, J. L.; Johnson, D. C. Pulsed amperometric detection of sulfur compounds: thiourea at gold electrodes. *Anal. Chim. Acta* **1992**, *260*, 1-11.

(44) Jeroschewski, P.; Haase, K.; Trommer, A.; Gruendler, P. Galvanic sensor for determination of hydrogen sulfide. *Electroanalysis* **1994**, *6*, 769-772.

(45) Szynkarczuk, J.; Komorowski, P. G.; Donini, J. C. Redox reactions of hydrosulfide ions on the platinum electrode-I. The presence of intermediate polysulfide ions and sulfur layers. *Electrochim. Acta* **1994**, *39*, 2285-2289.

(46) Jeroschewski, P.; Steuckart, C.; Kuehl, M. Amperometric microsensor for the determination of H2S in aquatic environments. *Anal. Chem.* **1996**, *68*, 4351-4357.

(47) Kraus, D. W.; Doeller, J. E. Sulfide consumption by mussel gill mitochondria is not strictly tied to oxygen reduction: measurements using a novel polarographic sulfide sensor. *J. Exp. Biol.* **2004**, *207*, 3667-3679.

(48) Hall, J. R.; Schoenfisch, M. H. Direct electrochemical sensing of hydrogen sulfide without sulfur poisoning. *Anal. Chem.* **2018**, *90*, 5194-5200.

(49) Engstrom, R. C.; Strasser, V. A. Characterization of electrochemically pretreated glassy carbon electrodes. *Anal. Chem.* **1984**, *56*, 136-141.

(50) Murphy, L. J. Reduction of interference response at a hydrogen peroxide detecting electrode using electropolymerized films of substituted naphthalenes. *Anal. Chem.* **1998**, *70*, 2928-2935.

(51) Dai, Y. Q.; Zhou, D. M.; Shiu, K. K. Permeability and permselectivity of polyphenylenediamine films synthesized at a palladium disk electrode. *Electrochim. Acta* **2006**, *52*, 297-303.

(52) Calia, G.; Monti, P.; Marceddu, S.; Dettori, M. A.; Fabbri, D.; Jaoua, S.; O'Neill, R. D.; Serra, P. A.; Delogu, G.; Migheli, Q. Electropolymerized phenol derivatives as permselective polymers for biosensor applications. *Analyst* **2015**, *140*, 3607-3615.

(53) Brown, M. D.; Schoenfisch, M. H. Nitric oxide permselectivity in electro-polymerized films for sensing applications. *ACS Sensors* **2016**, *1*, 1453-1461.

(54) Shim, J. H.; Do, H.; Lee, Y. Simple fabrication of amperometric nitric oxide microsensors based on electropolymerized membrane films. *Electroanalysis* **2010**, *22*, 359-366.

(55) Park, S. S.; Kim, J.; Lee, Y. Improved electrochemical microsensor for the real-time simultaneous analysis of endogenous nitric oxide and carbon monoxide generation. *Anal. Chem.* **2012**, *84*, 1792-1796.

(56) Brown, M. D.; Schoenfisch, M. H. Catalytic selectivity of metallophthalocyanines for electrochemical nitric oxide sensing. *Electrochim. Acta* **2018**, *273*, 98-104.

(57) Otero, T. F.; De Larreta, E. Electrochemical control of the morphology, adherence, appearance and growth of polypyrrole films. *Synth. Met.* **1988**, *26*, 79-88.

(58) Vreeland, R. F.; Atcherley, C. W.; Russell, W. S.; Xie, J. Y.; Lu, D.; Laude, N. D.; Porreca, F.; Heien, M. L. Biocompatible PEDOT:Nafion composite electrode coatings for selective detection of neurotransmitters in vivo. *Anal. Chem.* **2015**, *87*, 2600-2607.

(59) Losito, I.; Palmisano, F.; Zambonin, P. G. o-Phenylenediamine electropolymerization by cyclic voltammetry combined with electrospray ionization-ion trap mass spectrometry. *Anal. Chem.* **2003**, *75*, 4988-4995.

(60) Cintra, E. P.; Cordoba de Torresi, S. I. Resonant Raman spectroscopy as a tool for determining the formation of a ladder structure in electropolymerized poly(5-amino-1-naphthol). *J. Electroanal. Chem.* **2002**, *518*, 33-40.

(61) Hughes, M. N.; Centelles, M. N.; Moore, K. P. Making and working with hydrogen sulfide. The chemistry and generation of hydrogen sulfide in vitro and its measurement in vivo: A review. *Free Radical Biol. Med.* **2009**, *47*, 1346-1353.

(62) Ciszewski, A.; Milczarek, G. Preparation and general properties of chemically modified electrodes based on electrosynthesized thin polymeric films derived from eugenol. *Electroanalysis* **2001**, *13*, 860-867.

(63) Bedioui, F.; Griveau, S. Electrochemical detection of nitric oxide: assessement of twenty years of strategies. *Electroanalysis* **2013**, *25*, 587-600.

(64) Ciszewski, A.; Milczarek, G. Polyeugenol-modified platinum electrode for selective detection of dopamine in the presence of ascorbic acid. *Anal. Chem.* **1999**, *71*, 1055-1061.

(65) Barfidokht, A.; Gooding, J. J. Approaches toward allowing electroanalytical devices to be used in biological fluids. *Electroanalysis* **2014**, *26*, 1182-1196.

(66) O'Connell, T. X.; Horita, T. J.; Kasravi, B. Understanding and interpreting serum protein electrophoresis. *Am. Fam. Physician* **2005**, *71*, 105-112.

(67) K., P. K.; Chongdu, C. Stability of polymer electrolyte membranes in fuel cells: initial attempts to bridge physical and chemical degradation modes. *Fuel Cells* **2015**, *15*, 196-203.

CHAPTER 6: SUMMARY AND FUTURE DIRECTIONS

6.1 Summary of research

Ongoing research into the biological activity of nitric oxide (NO) is becoming increasingly dependent on accurate, quantitative indications of its in situ concentrations, particularly in consideration of the fact that many functions of NO are activated in a concentration-dependent manner. Once resolved, these concentrations could bare diagnostic/prognostic utility in various pathologies related to chronic inflammation.[1-3] Although electrochemical methods are best poised for detection of NO, measurement in biological milieu remains analytically challenging, requiring rigorous characterization of sensor performance to ensure accuracy. Thus, the primary goal of my research was to develop an electrochemical NO sensor of substantial selectivity and biological sensocompatibility to enable long-term monitoring of NO. A related, secondary goal was the comprehensive evaluation of two common categories of electrode modifiers—electropolymerized films (EPFs) and metallophthalocyanines (MPcs)—to provide a consolidated comparison of their selectivity performances.

The presence of electroactive biological interferents in physiological media necessitates modification of the working electrode with selective barriers. In Chapter 2, a series of self-terminating EPFs were electropolymerized onto the surfaces of platinum (Pt) electrodes from the following monomers: the three isomers of phenylenediamine (PD),

phenol, eugenol, and 5-amino-1-naphthol (5A1N). Deposition technique and related parameters (e.g., monomer concentration, applied potential, sweep rate, electrolyte) affect the rate of oligomer generation and precipitation, which dictates packing density and the permeability traits of the resulting film.[4] The deposition procedure for each monomer was individually tailored to maximize interferent rejection ability under cyclic voltammetry (CV) and constant potential amperometry (CPA). In general, depositions under CV with a slow scan rate (i.e., 10 mV s^{-1}) favored slower film formation and yielded improved selectivity for NO over nitrite and L-ascorbate (AA). Once depositions were optimized, EPF-modified electrodes were evaluated for selectivity against a larger panel of interferents and for additional performance metrics (i.e., sensitivity, permeability, and detection limit). Sensors prepared using poly(phenol) and poly(5A1N) demonstrated the most ideal analytical performance, particularly with respect to nitrite rejection ability. In proteinaceous simulated wound fluid, poly(5A1N) and poly(*o*-PD) films proved superior with respect to retention in NO sensitivity and detection limit relative to trials carried out in saline buffer.

Building off the findings of Chapter 2, a poly(5A1N)-modified Pt electrode was evaluated for long-term maintenance of NO sensitivity and selectivity against nitrite in Chapter 3. After continuous 12 h operation (+0.8 V *vs*. Ag|AgCl) in PBS, endpoint calibrations revealed that the sensitivity towards NO had increased while the selectivity against nitrite decreased, indicative of hydration-induced partial film desorption.[5] In order to reduce this effect, a protective fluorinated xerogel (XG) topcoat was spray-coated onto the base poly(5A1N) film. The resulting Pt/poly(5A1N)/XG bilaminar sensor maintained improved NO sensitivity and selectivity against nitrite with 24 h continuous operation in proteinaceous culture media (i.e., FBS-supplemented DMEM). The favorable selectivity and

sensocompatibility demonstrated by the sensor prompted application to cell measurement. Instantaneous release and measurement of NO can be achieved with stimuli to constitutive nitric oxide synthases (NOS) already present in the cell cytoplasm, but such demonstrations are heavily prevalent in the literature and only require data collection over the course of minutes. In order to exploit the long-term sensocompatibility of our sensor design, inducible NOS (iNOS) was stimulated with lipopolysaccharide (LPS) and interferon-gamma (IFN-γ) in macrophage cells. Requiring 6-8 h to become fully expressed, iNOS-derived NO release continues hours after activation, demanding high sensocompatibility.[6,7] Moreover, nitrite concentrations accumulate in static culture wells due to NO oxidation from oxygen, causing NO signal distortion if not appropriately rejected. As our bilaminar sensor was able to meet both of these requirements, the 24 h release profile was successfully resolved—the NO flux reaching a maximum at 8 h, plateauing for 6-8 h, and then gradually decreasing.

Because sensors were positioned in the "synapse-like" arrangement relative to the macrophages, variability in the vertical separation was hypothesized to cause differing plateau NO concentrations to be measured. The NO concentration gradient extending from a confluent sheet of macrophages was profiled with a scanning electrochemical microscope and a microelectrode probe with the same poly(5A1N)/XG modifiers. The proximal NO concentration was 0.65 ± 0.11 μM, and the concentration dissipated as the separation between the probe and cells increased (no NO measured at ~500 μm). Compared to previously reported work profiling bradykinin-simulated HUVECs,[8] the stimulated macrophage diffusion profile was at least an order of magnitude larger, in agreement with the much larger NO output of iNOS *vs*. constitutive isoforms. To our knowledge, this study represents the first spatial NO profiling of macrophage cells.

In Chapter 4, in a study comparable to the one described in Chapter 2, the NO selective properties of metallophthalocyanines were evaluated. The catalytic properties of MPc complexes have long been applied to electrochemical sensing of NO to amplify sensitivity and reduce the substantial overpotential required for NO oxidation. The latter point has significant ramifications for in situ amperometric detection, as large working potentials unfavorably oxidize interferents. Notably, there had been no previous attempts to isolate and quantify the selectivity benefits of MPc modification with respect to NO detection, despite electrocatalysis relying on specific chemical interaction between the surface-confined catalyst and target analyte.[9] To fill this gap, a series of the most catalytically active MPc complexes towards NO, including Fe(II)Pc, Co(II)Pc, Ni(II)Pc, and Zn(II)Pc, was selected and probed for NO sensing ability under both differential pulse voltammetry (DPV) and CPA.

Under DPV, sensitivity amplification (~1.5×) was perfectly specific to NO over AA for all MPc complexes studied, but only perfectly selective over nitrite in the case of FePc. The MPc catalysts greatly enhanced the NO signal under CPA (2-3×), but only a portion of that amplification was due to specific catalytic effects. The claim that MPc-enabled lowering of the applied potential improves selectivity was found to only be true in the case of high potential interferents such as nitrite. The signal contributions of low potential interferents such as AA (and inferably others, including acetaminophen, dopamine, and uric acid) remain largely unaffected and therefore continue to pose a significant challenge to selective, continuous detection of NO. It was concluded that signal sensitivity amplification (as opposed to peak shifting) is the only route by which MPc complexes may meaningfully improve NO selectivity. Compared to permselective membranes capable of mitigating

interferent transport >1000-fold, the suggested selectivity benefits of MPc incorporation existed, but were ultimately very limited. As a result, we did not seek to incorporate a MPc complex into the sensor design described in Chapter 3.

The significant similarities in the biochemistries of NO, carbon monoxide (CO), and hydrogen sulfide (H_2S)—all endogenous, electroactive gasotransmitters—motivates the design and fabrication of dual- and multi-analyte detection platforms.[10] The resolution of two or more concentration profiles not only furnishes novel biological information, but also improves selectivity by deconvoluting overlapping current responses (*see* Chapter 1, Section 1.2.3). As such, in Chapter 5, an electrochemical H_2S sensor was developed for eventual adaptation into a dual NO/H_2S sensor (*see* Section 6.2.1).

Continuous, in situ detection of H_2S in biological milieu is made possible with electrochemical methods, but direct amperometry is constrained by the generation of elemental sulfur as an oxidative byproduct. Deposition of a sulfur layer passivates the working electrode, reducing sensitivity and causing performance variability. A surface preconditioning procedure was therefore developed to deposit elemental sulfur on a glassy carbon electrode (GCE) prior to measurement and demonstrably stabilize analytical performance (i.e., sensitivity, detection limit, and background current). The lack of traditional anti-poisoning techniques (e.g. redox mediators, cleaning pulses) also allowed for facile surface modification with electropolymerized films. The same series of common EPFs evaluated in Chapter 2 were characterized for their H_2S permselective behavior against common biological interferents. Highly selective, film-modified electrodes were then evaluated for their anti-biofouling ability in simulated wound fluid. The final optimized

sensor comprised a poly(*o*-PD)-modified GCE and was capable of measuring H_2S with a low detection limit (i.e., <100 nM) and ~80% of its initial sensitivity in proteinaceous media.

6.2 Future directions

6.2.1 Dual-detection of NO and H_2S

Nitric oxide, H_2S, and CO share many attributes in common, beginning from their physiochemical properties and extending into their biological activities.[10] Most selectivity-enhancing barriers used to modify the surface of electrochemical NO sensors are unable to discriminate against H_2S and CO as wholly as other interferents. The shared ability of NO, H_2S, and CO to permeate membranes is critical to their functioning as intercellular gasotransmitters, and therefore, their migration traits are similar. Dual- and multi-analyte detection platforms are able to enhance a platform's selectivity towards an analyte through co-detection of interferents and correction of individual responses (*see* Section 1.2.3). A NO/CO dual-sensor has already been developed and put into use by Lee and colleagues, using tin- or gold- modifications of the CO-specific electrode to enhance the response.[11,12] With the development of a selective and biologically compatible H_2S sensor in Chapter 5, the fabrication of a novel NO/H_2S dual-sensor would ensure measurement accuracy of both species. Moreover, the resolution of two concentration profiles would be able to provide novel information about the real-time dynamics of NO-H_2S crosstalk. For example, in the cardiovascular system H_2S is a smooth muscle relaxant, and recent studies have suggested it is mutually required with NO to initiate angiogenesis and vasodilation.[13,14] One study observed that supply of exogenous H_2S from NaHS or L-cysteine substrate increased phosphorylation of eNOS in HUVEC cells, thereby stimulating NO production.[15] On the other hand, in the immune system, exogenous supply of H_2S or L-cysteine resulted in

inhibited expression of iNOS in macrophages stimulated by lipopolysaccharide (LPS).[16] Nitric oxide itself is also a known inhibitor of cystathionine beta synthase (CBS), an enzyme catalyzing H_2S production from cysteine/homocysteine condensation.[17] Whether inhibitory or enhancing, the co-regulation of these molecules is likely to occur in a concentration-dependent manner in order to exert such varied effects and warrants further investigation.

6.2.2 Measurement of NO from NO-releasing therapeutics

The antibacterial activity of NO-releasing therapeutics is likely to depend on both the concentration of the releasing agent and the kinetics of NO release.[18] The latter is very often characterized by a NO release half-life measured in vitro with chemiluminescent techniques, which require bubbling of a solution in which the NO-releasing therapeutic is placed. The released NO is then transported via an inert carrier gas to the detector, effectively consuming NO at the moment of generation. Parameters such as the total NO release, half-life, and peak flux can be obtained, but these properties are largely intrinsic to the scaffold and its stability within the particular milieu (typically pH 7.4 PBS). Although perhaps indicative of *when* the NO concentration is greatest at the site of application, these properties do not indicate *what* that specific concentration would be. Electrochemical methods are better suited to continuous measurement of NO concentrations and could be easily applied to NO-releasing scaffolds—in essence, replacing the macrophage cells of Chapter 3 with the scaffold of interest. Unlike chemiluminescent techniques, electrochemical sampling of the aqueous NO concentration does not require bulk consumption and is therefore able to monitor the buildup of NO in relevant media, in real time. Comparison of the resulting NO concentration profiles between different scaffolds, concentrations, and media would indicate which combination leads to the greatest temporally-confined buildup of NO for the purpose of bacterial killing. Preliminary

studies have already demonstrated the ability of Pt/poly(5A1N)/XG sensors to monitor the buildup of both NO and nitrite in culture well-plates with exposure to 160 and 500 ppm gaseous NO (Figure 6.1A and B, respectively).

6.2.3 Integration of planar NO sensors into culture wells

As demonstrated in Chapter 3, there is a critical dependence between the NO concentration measured and the distance between the source and probe. Unlike nitrite and other stable factors released by cells that homogenize into the bulk media, NO is by its nature transient and highly susceptible to scavenging, resulting in a unique concentration gradient emanating from the cell. The magnitude of the gradient will depend on the balance between the rate of NO production and the rate of scavenging, and its shape will be dictated by the physical conformation of the cell. Cells suspended in media or a 3D matrix are globular and will release NO radially. In the laboratory, 2D cultures are often more convenient but cause the cells to flatten.[19] At confluency, the NO concentration profile will extend linearly from the sheet of cells. The culturing of cells on planar electrodes eliminates undesirable variability in the probe-to-source distance, as the only separation to the transducer is any membrane modifier(s).

Preliminary studies are already underway to fabricate planar electrodes for integration into cell culture wells. Drawing from the same microfabrication techniques used by our laboratory previously to develop microfluidic devices,[20,21] the electrode geometry can be delineated with either adhesive masks or photolithographic techniques, followed by sputtering of an adhesive titanium coat and then Pt. Electropolymerization of the poly(5A1N) layer and spray-coating of the fluorinated XG may then be applied to planar electrodes just as

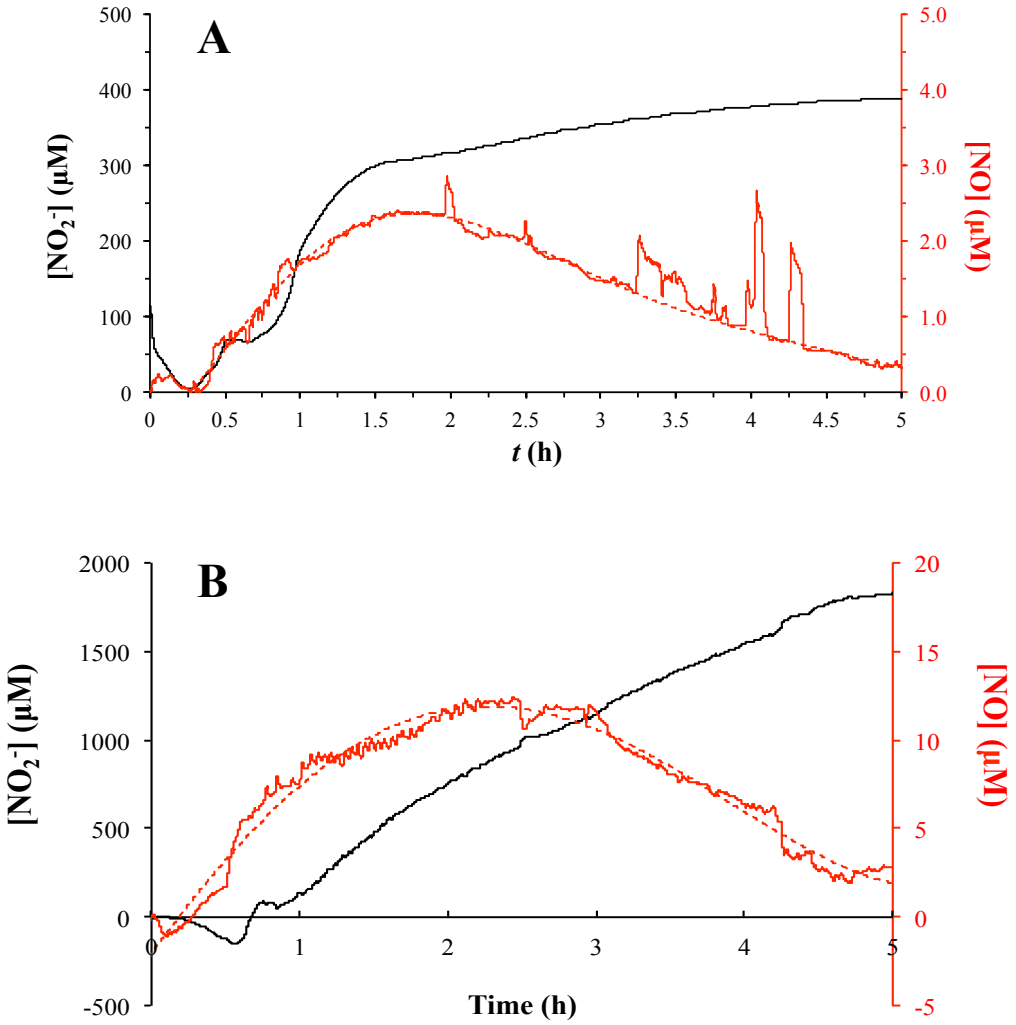

Figure 6.1 Temporal buildup of NO (red) and nitrite (black) concentrations in culture well-plates containing 1% tryptic soy broth-supplemented PBS with 5 h exposure to (A) 160 and (B) 500 ppm gaseous nitric oxide in air. Electrochemical measurements were collected on poly(5A1N)/XG-modified and bare Pt electrodes to resolve the concentration profiles of both analytes under CPA with an applied potential of +0.8 V *vs*. Ag|AgCl.

for the macroscopic disk-type electrodes used in Chapter 3, ensuring that part of the planar electrode is left unmodified to serve as a lead to the potentiostat. Once the electrodes are modified, poly(dimethylsiloxane) wells can be applied overtop and sealed to silica substrate under oxygen plasma treatment. Calibration of the device may be achieved with injections of saturated NO solution in PBS in a single well with an applied potential of +0.8 V *vs*. Ag|AgCl. In order to reduce calibration time for multiplexed platforms, a plate with multiple wells should be designed such that all potentiostat leads are condensed (e.g. for a rectangular platform, all leads are on one edge). Submersion of the multi-well device in a larger vessel would then allow for convenient simultaneous calibration with assistance from a multi-channel potentiostat.

Once fabricated, it would be necessary to characterize the biocompatibility of model cell lines as they were cultured overtop planar electrodes. Xerogels have been demonstrated to not adversely affect the morphology and propagation of macrophage cells;[22] however such assurances were made in the absence of an applied potential. Other studies have demonstrated that applied DC potentials can reduce the viability of cultured cells through potential-induced lysis.[23,24] A novel study characterizing the effect of applied potential on the viability and morphology of different cell lines (e.g., HUVECs and macrophages) would serve as an assurance of measurement biocompatibility or inform the design of a better platform. Increasing the electrode-cell distance has proven an adequate recourse in the past, but would need to be balanced against the response-time of the sensor.[24]

6.2.4 Translation to a microfluidic device for cell culture

Microfluidic devices confer several advantages to the culturing of cells, including: the application of flow-induced shear stress (better mimicking cells in native tissue),

replenishment of nutrients from flowing perfusate, and controlled exposure to the stimulants/inhibitors under study.[25,26] Cha et al. fabricated the only successful microfluidic device incorporating an electrochemical NO sensor for cellular measurement demonstrated in the literature.[27] However, placement of the electrode downstream from the cultured cells resulted in a (at most) 80 s response time, requiring the perfusate not to contain serum protein or oxygen. These factors are likely critical to emulating the native condition and response of cells. By developing a microfluidic device with cells cultured directly on integrated planar electrodes, NO release could be measured in real time with improved response times. For example, macrophage cells could be cultured and exposed to LPS and interferon-gamma (IFN-γ) to elicit an inflammatory response. Unlike in a static culture well (as with the measurements conducted in Chapter 3), novel information about the longevity of pro-inflammatory NO release could be obtained with changing media conditions. Some novel questions provoked by the ability to monitor NO from macrophages in real time *and* alter the perfusate media are listed below:

1) After initial stimulation with LPS/IFN-γ, how long does NO release last with continued L-arginine supplementation?
2) If LPS/IFN-γ are used to upregulate iNOS for 6-8 h, does NO release persist if LPS/IFN-γ are then removed from the perfusate?
3) How does pre-incubation with certain factors (e.g., anti-inflammatory cytokine interleukin-4, hemin, H_2S, etc.) affect the NO response to pro-inflammatory LPS/IFN-γ?
4) How does introduction of these same factors amid an already escalated pro-inflammatory response affect NO release?

Clearly, many fundamental questions regarding the nature of NO release in response to different pro- and anti-inflammatory agents exist, which are only answerable with real time monitoring of NO fluctuations. Perhaps in answering these questions, a reproducible model for the inflammatory response could be developed from macrophages cultured in microfluidic devices, thereby facilitating exploration of new anti-inflammatory agents.

6.3 Conclusions

As we continue to explore the biological significance of NO, indirect techniques monitoring either NOS expression or NO_x accumulation lack the temporal and spatial resolution required to ascertain the intricate concentration-dependence of NO's activity. Electrochemical platforms are best positioned for in situ, direct measurement of NO, but require rigorous evaluations of selectivity and performance maintenance in complex milieu to ensure measurement accuracy. Moving forward, quantitative indicators of these parameters will be critical to translating proposed sensor designs to biological contexts. My research presents a robust electrochemical NO sensor that can monitor real time evolution of NO with high selectivity and maintained sensitivity. Moreover, the use of an electropolymerized poly(5A1N) film in conjunction with a spray-coated XG enables facile modification of different electrode sizes and geometries than the ones studied herein. Future work will entail integration of this NO sensor in static culture wells and dynamic microfluidic devices for the culturing of macrophage cells. In time, testing of pro- and anti-inflammatory agents' effects on dynamic NO release will foster greater understanding of NO's roles in inflammation and may inform what therapeutic recourses can be taken to abate NO-mediated inflammation.

REFERENCES

(1) Kaur, H.; Halliwell, B. Evidence for nitric oxide‐mediated oxidative damage in chronic inflammation Nitrotyrosine in serum and synovial fluid from rheumatoid patients. *FEBS Lett.* **1994**, *350*, 9-12.

(2) Ying, L.; Hofseth, L. J. An emerging role for endothelial nitric oxide synthase in chronic inflammation and cancer. *Cancer Res.* **2007**, *67*, 1407-1410.

(3) Smith, K. J.; Lassmann, H. The role of nitric oxide in multiple sclerosis. *Lancet Neurol.* **2002**, *1*, 232-241.

(4) Ciszewski, A.; Milczarek, G. Electrochemical detection of nitric oxide using polymer modified electrodes. *Talanta* **2003**, *61*, 11-26.

(5) Shim, J. H.; Do, H.; Lee, Y. Simple fabrication of amperometric nitric oxide microsensors based on electropolymerized membrane films. *Electroanalysis* **2010**, *22*, 359-366.

(6) Donnini, S.; Ziche, M. Constitutive and inducible nitric oxide synthase: Role in angiogenesis. *Antioxid. Redox Signal.* **2002**, *4*, 817-823.

(7) Nakamura, Y.; Si, Q. S.; Kataoka, K. Lipopolysaccharide-induced microglial activation in culture: temporal profiles of morphological change and release of cytokines and nitric oxide. *Neurosci. Res.* **1999**, *35*, 95-100.

(8) Isik, S.; Schuhmann, W. Detection of nitric oxide release from single cells by using constant-distance-mode scanning electrochemical microscopy. *Angew. Chem., Int. Ed.* **2006**, *45*, 7451-7454.

(9) Bedioui, F.; Griveau, S. Electrochemical detection of nitric oxide: assessement of twenty years of strategies. *Electroanalysis* **2013**, *25*, 587-600.

(10) Li, L.; Hsu, A.; Moore, P. K. Actions and interactions of nitric oxide, carbon monoxide and hydrogen sulphide in the cardiovascular system and in inflammation—a tale of three gases! *Pharmacol. Ther.* **2009**, *123*, 386-400.

(11) Park, S. S.; Kim, J.; Lee, Y. Improved electrochemical microsensor for the real-time simultaneous analysis of endogenous nitric oxide and carbon monoxide generation. *Anal. Chem.* **2012**, *84*, 1792-1796.

(12) Ha, Y.; Sim, J.; Lee, Y.; Suh, M. Insertable fast-response amperometric NO/CO dual microsensor: study of neurovascular coupling during acutely induced seizures of rat brain cortex. *Anal. Chem.* **2016**, *88*, 2563-2569.

(13) Hosoki, R.; Matsuki, N.; Kimura, H. The possible role of hydrogen sulfide as an endogenous smooth muscle relaxant in synergy with nitric oxide. *Biochem. Biophys. Res. Commun.* **1997**, *237*, 527-531.

(14) Coletta, C.; Papapetropoulos, A.; Erdelyi, K.; Olah, G.; Módis, K.; Panopoulos, P.; Asimakopoulou, A.; Gerö, D.; Sharina, I.; Martin, E. Hydrogen sulfide and nitric oxide are mutually dependent in the regulation of angiogenesis and endothelium-dependent vasorelaxation. *Proc. Natl. Acad. Sci.* **2012**, *109*, 9161-9166.

(15) Altaany, Z.; Yang, G.; Wang, R. Crosstalk between hydrogen sulfide and nitric oxide in endothelial cells. *J. Cell. Mol. Med.* **2013**, *17*, 879-888.

(16) Oh, G.-S.; Pae, H.-O.; Lee, B.-S.; Kim, B.-N.; Kim, J.-M.; Kim, H.-R.; Jeon, S. B.; Jeon, W. K.; Chae, H.-J.; Chung, H.-T. Hydrogen sulfide inhibits nitric oxide production and nuclear factor-κB via heme oxygenase-1 expression in RAW264.7 macrophages stimulated with lipopolysaccharide. *Free Radic. Biol. Med.* **2006**, *41*, 106-119.

(17) Kamoun, P. Endogenous production of hydrogen sulfide in mammals. *Amino Acids* **2004**, *26*, 243-254.

(18) Carpenter, A. W.; Schoenfisch, M. H. Nitric oxide release: Part II. Therapeutic applications. *Chem. Soc. Rev.* **2012**, *41*, 3742-3752.

(19) Mendes, P. M. Cellular nanotechnology: making biological interfaces smarter. *Chem. Soc. Rev.* **2013**, *42*, 9207-9218.

(20) Hunter, R. A.; Privett, B. J.; Henley, W. H.; Breed, E. R.; Liang, Z.; Mittal, R.; Yoseph, B. P.; McDunn, J. E.; Burd, E. M.; Coopersmith, C. M.; Ramsey, J. M.; Schoenfisch, M. H. Microfluidic amperometric sensor for analysis of nitric oxide in whole blood. *Anal. Chem.* **2013**, *85*, 6066-6072.

(21) Hunter, R. A.; Schoenfisch, M. H. S-Nitrosothiol analysis via photolysis and amperometric nitric oxide detection in a microfluidic device. *Anal. Chem.* **2015**, *87*, 3171-3176.

(22) Kang, S. W.; Seo, B.; Kim, J.-H.; Kim, O.-K.; Shin, J. H.; Lee, G.-J.; Park, H.-K. Cell viability, adhesion and function of RAW 264.7 macrophages on fluorinated xerogel-derived nitric oxide permeable membrane for the application of cellular sensing. *J. Nanosci. Nanotechnol.* **2014**, *14*, 8398-8404.

(23) Yaoita, M.; Ikariyama, Y.; Aizawa, M. Electrical effects on the proliferation of living HeLa cells cultured on optically transparent electrode surface. *J. Biotechnol.* **1990**, *14*, 321-332.

(24) Oni, J.; Pailleret, A.; Isik, S.; Diab, N.; Radtke, I.; Blöchl, A.; Jackson, M.; Bedioui, F.; Schuhmann, W. Functionalised electrode array for the detection of nitric oxide released by endothelial cells using different NO-sensing chemistries. *Anal. Bioanal. Chem.* **2004**, *378*, 1594-1600.

(25) Hung, P. J.; Lee, P. J.; Sabounchi, P.; Lin, R.; Lee, L. P. Continuous perfusion microfluidic cell culture array for high‐throughput cell‐based assays. *Biotechnol. Bioeng.* **2005**, *89*, 1-8.

(26) Young, E. W.; Beebe, D. J. Fundamentals of microfluidic cell culture in controlled microenvironments. *Chem. Soc. Rev.* **2010**, *39*, 1036-1048.

(27) Cha, W.; Tung, Y.-C.; Meyerhoff, M. E.; Takayama, S. Patterned electrode-based amperometric gas sensor for direct nitric oxide detection within microfluidic devices. *Anal. Chem.* **2010**, *82*, 3300-3305.